Retrospective Theses and Dissertations

Iowa State University Capstones, Theses and Dissertations

1-1-2003

Laterally loaded intermediate cast-in-drilled-hole (CIDH) concrete piers: evaluation of scale and base shear effects

Longjie Hong
Iowa State University

Follow this and additional works at: https://lib.dr.iastate.edu/rtd

Laterally loaded intermediate Cast-In-Drilled-Hole (CIDH) concrete piers:

evaluation of scale and base shear effects

by

Longjie Hong

A thesis submitted to the graduate faculty

in partial fulfillment of the requirements for the degree of

MASTER OF SCIENCE

Major: Civil Engineering (Geotechnical Engineering)

Program of Study Committee:
David J. White, Major Professor
Vernon Schaefer
Neal R. Iverson

Iowa State University

Ames, Iowa

2003

Graduate College

Iowa State University

This is to certify that the master's thesis of

Longjie Hong

has met the thesis requirements of Iowa State University

Signatures have been redacted for privacy

TABLE OF CONTENTS

LIST OF FIGURES

LIST OF TABLES

ABSTRACT

Full-scale lateral load tests were conducted on twelve rigid piers constructed at the Iowa State University Spangler Geotechnical Experimentation Site (SGES) to evaluate the scale and base shear effects. The soil is glacial till with average undrained shear strength of 59 kPa from ground surface to 3 m deep. Results show that the load-displacement behavior of all piers at the SGES can be described by the simple power function: $s/s_f = (Q/Q_{ult})^{2.39}$. Also, a parametric study shows that the exponent of the power function ranges from 1.7 to 3, which depends on the undrained shear strength and e_{50} of the soil. The base shear effect becomes insignificant when the pier slenderness ratio (L/D) is about seven. Load displacement behavior of the pier can be well predicted by consolidated undrained (CU) triaxial test.

CHAPTER 1: INTRODUCTION

1.1 Background

Pile foundation systems are often designed to carry lateral loads for structures such as transmission towers, sign posts, power poles, bridges, mooring systems for ocean surface or submerged platforms, tall chimneys, and jetty structures. Sources of lateral load include: wind forces, earth pressures, seismic loads, eccentric vertical loads, wave action, water current, vessel impact and various other structural loading conditions. Intermediate and micropile foundation systems are becoming increasingly popular solutions to resist these lateral loads in lieu of traditional deep foundations – primarily because of cost effectiveness, high load-carrying capacity, and reduced disturbance (e.g. vibration and noise) to the surrounding environment. Intermediate and micropile foundation systems are especially suitable for foundations with difficult access, restricted clearance and poor ground conditions wherein minimal disturbance to the existing structure is required and for retrofitting and rehabilitation of existing foundations. Several recent reports have documented performance of traditional pile foundation systems with regard to: (1) improvement of bearing capacity and vertical settlement control (e.g. Mascardi 1982, Laefer 1999, Bruce *et al.* 1999 and IWM99 1999); and (2) control of structural deflections during an earthquake event (e.g. Taylor *et al.* 1998, Zelenko *et al.* 1998). However, limited data is available on lateral loaded behavior of intermediate and micropile foundation system (see Dearth 2002). Thus, design guidance is limited and needs further investigation. This study focuses on developing a better understanding of the behavior of intermediate cast-in-drilled-hole (CIDH) concrete piers under lateral load, with an emphasis on scale and base shear effects.

1.2 Objectives and Scope of Research

The primary objectives of this research are to: (1) investigate the influence of scale and base shear effects on the lateral load-displacement behavior of intermediate cast-in-drilled-hole (CIDH) concrete piers embedded in glacial till; (2) determine if the lateral load test results can be expressed in non-dimensional terms; and (3) determine if predictable load-displacement relations exist, thus facilitating a design approach. Ultimately, it is envisioned that load-displacement relationships developed from this research may be used in the design of intermediate CIDH concrete piers that conform to deflection and load-capacity performance criteria. Comparisons of results are made to several numerical methods previously developed for the analysis of laterally loaded soil-pile systems (see Broms 1964, Robertson *et al.* 1989, McClelland and Focht 1958, and Reese 2000).

Full-scale lateral load tests were conducted on twelve piers constructed at the Iowa State University Spangler Geotechnical Experimentation Site (SGES). All piers were constructed in pairs to serve as reactions to each other during load testing. The pier dimensions were 0.30, 0.61, 0.76, and 0.91 m (12, 18, 24 and 36 inches) diameters with lengths of 1.52, 2.29, and 3.05 m (5, 7.5 and 10 feet) for each diameter. The slenderness ratio (L/D) ranged from 1.67 to 10.

A laboratory and in situ testing program was implemented at the site to both characterize the subsurface conditions and determine design parameters for predicting pier behavior. The laboratory testing program included: water content, Atterberg limits, grain-size distribution, unconfined compression tests, consolidation tests, and consolidated-undrained triaxial (CU) tests. The in situ testing program included Dilatometer Tests (DMT), Standard Penetration Tests (SPT), and Cone Penetrometer Tests (CPT). Thermocouples and open

standpipe piezometers were installed at the site to monitor ground temperature and fluctuations in the ground water table (GWT) location.

1.3 Organization

The research described in this report is organized as the follows:

- Chapter 2 presents a literature review of the documented behavior of laterally loaded piers. This chapter also describes common methods for predicting the lateral load-displacement behavior of piers, various definitions of "ultimate" lateral capacity of piers, and the use of normalized load-displacement behavior of piers.

- Chapter 3 presents a parameteric study conducted to simulate and evaluate the lateral load-deflection behavior of intermediate CIDH concrete piers in typical soil conditions using available finite difference software programs: LPILE and LTBASE. A wide range of pier geometries and soil types was investigated.

- Chapter 4 presents the field investigation and discussion of in situ and laboratory test procedures and test results at the SGES.

- Chapter 5 presents and discusses the results of lateral load tests performed during this investigation. This chapter also includes predictions of load-displacement behavior and "ultimate" pier capacity using various methods, and a discussion of nondimensional expression of load-displacement curve.

- Chapter 6 presents conclusions based on the parametric study and lateral load test results.

CHAPTER 2: REVIEW OF LITERATURE

2.1 Introduction

Pile foundation systems can be designed to sustain vertical, uplift and lateral loading. This study focuses on the lateral load behavior. In recent years, researchers have developed methods to predict the load-displacement behavior and ultimate load of pile systems. Several of these methods are reviewed in this chapter.

2.2 Behavior of Laterally Loaded Piles

Pile foundations exhibit either flexible or rigid behavior under lateral loading conditions. A pile is defined as flexible when the deflection results in pile bending or as rigid when the pile rotates as a unit with respect to a point located close to its toe. Failure of a laterally loaded pile occurs either when the bending moment in the loaded pile reaches the ultimate or yield resistance of the pile section or when the lateral earth pressures reach the ultimate lateral resistance of the soil along the total length of the pile (Broms 1964), as shown in Figure 2.1. The behavior of a laterally loaded pile therefore involves pile-soil interaction, which is controlled by the flexural stiffness of the pile relative to the stiffness of surrounding soil. The load-deflection characteristics of a rigid pile are quite different from those of a flexible pile.
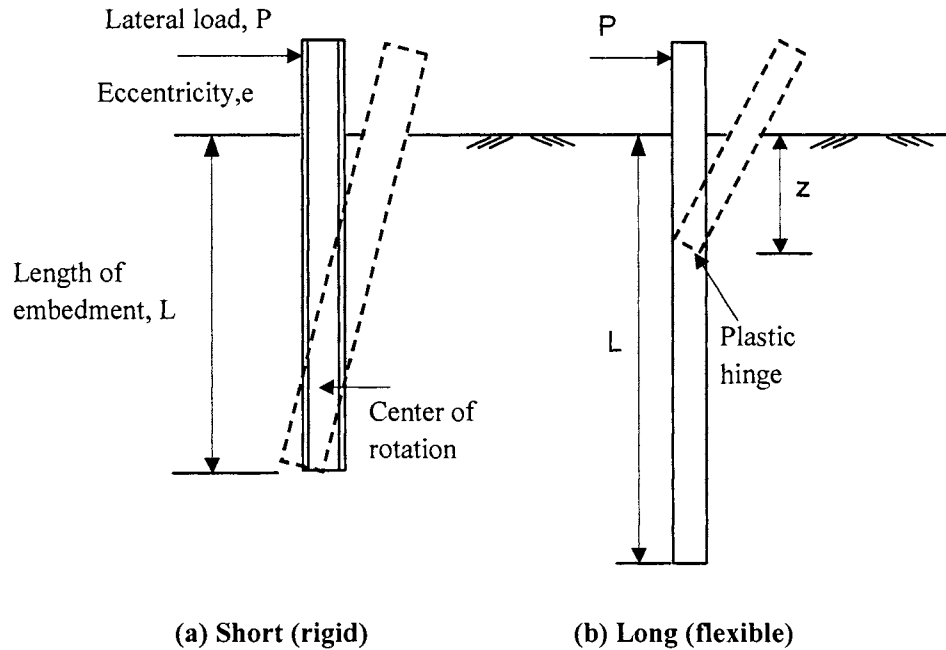
Figure 2.1 Failure Mode of Free-Headed Pile (after Broms 1964)

The demarcation between rigid and flexible pile can be determined in terms of a relative stiffness factor which expresses a relation between soil stiffness and pile flexural stiffness and is dependent on the soil modulus function assumed (Woodward *et al.* 1972). For a constant soil modulus assumption, the stiffness factor R is given by:

$$R = \sqrt[4]{\frac{E_p I_p}{K}}$$

[2.1]

in which:

R = stiffness factor (length)

E_p = modulus of elasticity of the pile material (force/length^2)

I_p = moment of inertia of the pile (length^4)

K = soil modulus (force/length^2)

Broms (1964), Woodward *et al.* (1972) and Briaud (1997) all proposed a pile lateral load behavior classification by comparing the pile length L with R, as summarized in Table 2.1. Although they used the same assumptions, they differed in the criteria.

McCorkle (1969) proposed that piles having ratios of L/D less than 10 would exhibit rigid behavior, independent of embedded soil type. However, Bierschwale *et al.* (1981) showed that the pile slenderness ratio (L/D) should be limited to approximately 6 to insure rigid behavior. Three drilled shafts with L/D of 5 (L=15ft, D=3ft), 6 (L=15ft, D=2.5ft), and 6.7 (L=20ft, D=3ft) were installed in a stiff clay stratum located at a test site near College Station, Texas. The undrained shear strength of the soil ranged from 127 kPa (0.6 tsf) to 422 kPa (2 tsf). It was found that a structural failure occurred in the shaft with L/D of 6.7, indicating that the shaft may have been experiencing flexural rather than rigid rotation (Bierschwale *et al.* 1981). Study by Bierschwale *et al.* (1981) indicates that, in addition to the pile geometry, the behavior of lateral loaded piles also depends on the soil stiffness.

It appears that there is no common criterion of lateral load behavior classification. In 2000, a computational technique was developed by Reese *et al.* (2000) based on the finite difference method, which is illustrated in Figure 2.2. Loads are applied at the top of the pile and a series of analyses are made with the length of the pile reduced in increments. Connecting the points for the deflection at the top of the pile yields the curve in Figure 2.2 (b). The curve shows that the value of y_t is unchanged above a pile length that is termed L_{crit}, but that the deflection increases for smaller values of pile length. Based on this method, the critical length L_{crit} can be determined graphically given the flexural stiffness of the pile and the soil type.
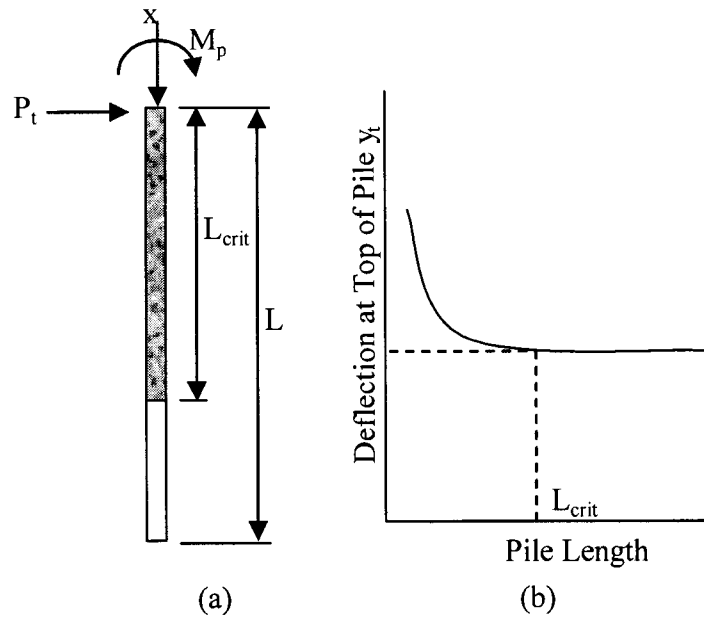
Figure 2.2 Solving for the Critical Length of a Pile (after Reese *et al.* 2000)

Table 2.1 Methods of Pile Lateral Load Behavior Classification

No.	Method	Rigid	Flexible	Assumptions and comments
1	Broms (1964)	L<1.5R	L>2.5R	Soil modulus K is constant along the entire depth
2	Woodward *et al.*(1972)	L<2R	L>3.5R	
3	Briaud (1997)	L<R	L>3R	
4	Bierschwale *et al.*(1981)	L/D<6	L/D>20	Based on failure mode of three drilled shafts in stiff clay
5	McCorkle(1969)	L/D<10	L/D>20	Independent of soil type
6	Reese *et al.* (2000)	L<l_{crit}	L >l_{crit}	Based on finite difference computational technique

Dearth (2002) compared the results produced by the aforementioned methods and found the various procedures yielded different results as expected. Eighteen drilled shafts were installed at Department of Energy Site (DOE) at the University of Massachusetts, Amherst campus and ten were installed at University of Massachusetts Agronomy Farm (UMAF) in South Deerfield, MA. The slenderness ratios of drilled shafts range from 2.5 to

10. This study concluded that the slenderness ratio ≤ 5 could ensure rigid behavior independent of embedment soil, whereas flexible behavior occurs at slenderness ratio ≥ 10.

2.3 Defining Ultimate Lateral Load Capacity

Generally, laterally loaded pile does not appear clear failure. Researchers have proposed different criteria to interpret the ultimate load capacity, such as the load when the displacement equals an absolute displacement of 0.5 inch (Rollins *et al.* 1994), absolute rotation of 2 degrees (Davidson *et al.* 1963) and fixed percentage of pile diameter, e.g., 20% (Broms 1964). Thus defining the ultimate load capacity from a lateral load test may not be simple and may be very subjective (Lutenegger *et al.* 1998). Lutenegger *et al.* (1998) presented four methods for approximating the ultimate bearing capacity of shallow footings on compacted sands. These methods are Tangent Intersection Method (Trautman and Kulhawy 1988), Log-Log Method (DeBeer 1970), Hyperbolic method (Chin 1983), and 10%D Method (Briaud and Gibbens 1994) and are summarized in Figure 2.3.
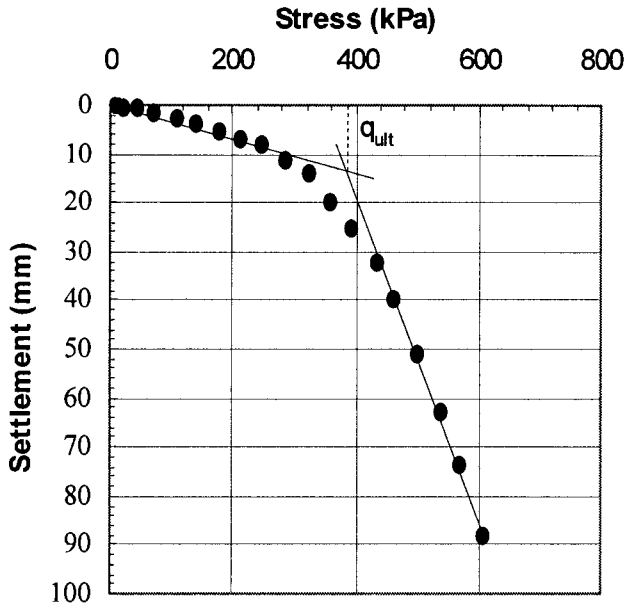
(a) Tangent Intersect Method
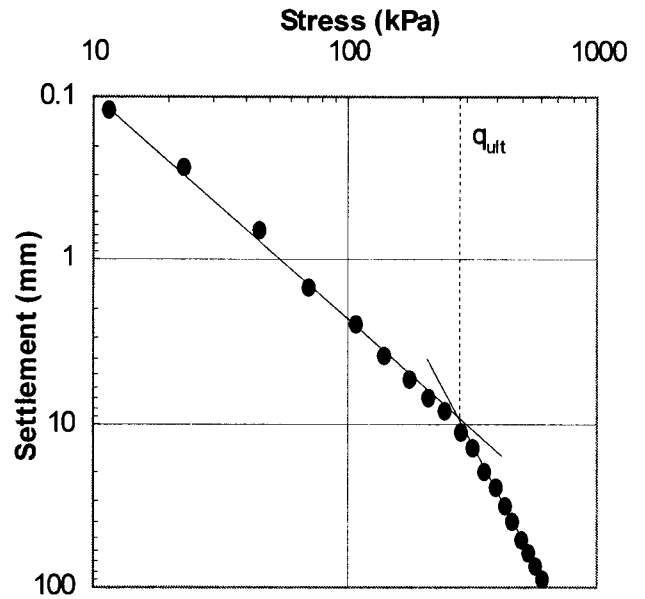
(b) Log-Log Method
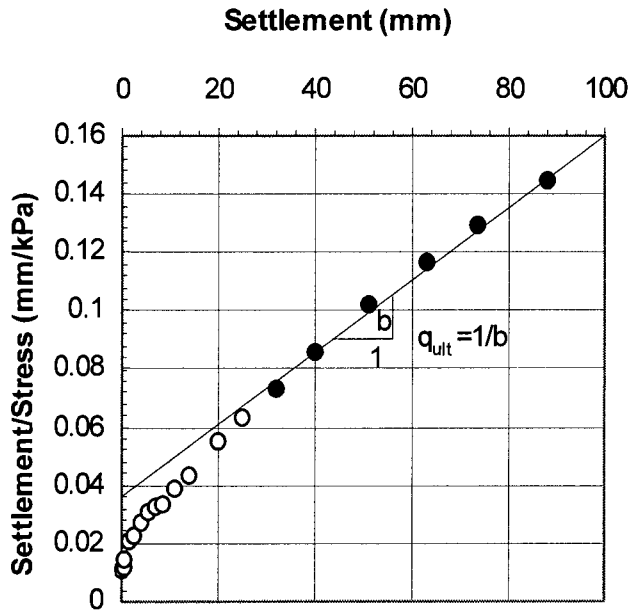
(c) Hyperbolic Method
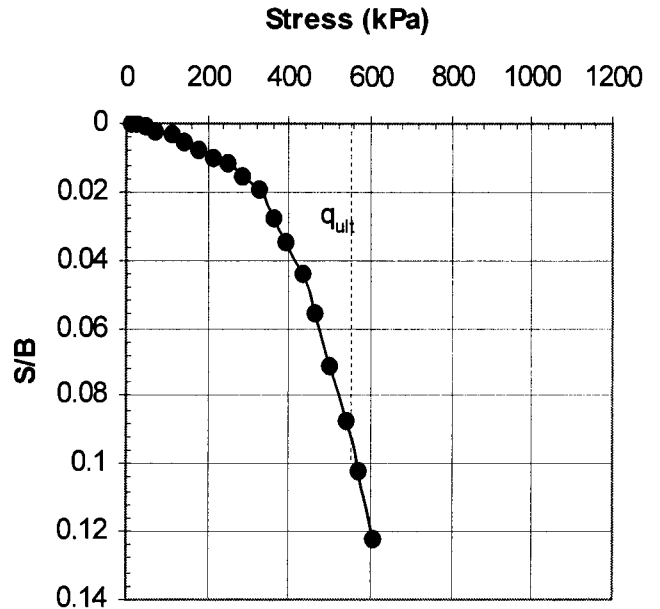
(d) 10%B Method

Figure 2.3 Methods of Defining Ultimate Bearing Capacity from a Load Test (after Lutenegger *et al.* 1998)

It was found that the ultimate load capacity (q_{ult}) determined by these four methods was different, which followed in the order of Log-Log method < Tangent Intersect Method < 0.1B Method < Hyperbolic Method. Lutenegger *et al.* (1998) proposed that the 10%B Method, although somewhat arbitrary, has the following advantages:

- Convenient and easy to remember,

- It may actually be close to the average soil strain at failure (especially in granular soils),

- It forces a fixed value at Q_{ult}, and

- It treats the displacement of all footings the same.

2.4 Methods for Predicting Load-Displacement Behavior

One of the primary objectives of this research is to investigate various methods for predicting the load-displacement behavior of laterally loaded piles. Methods used by previous researchers for predicting load-deflection behavior of a laterally loaded pile include the ultimate strength method and the nonlinear subgrade reaction method (p-y method).

2.4.1 Ultimate Strength Method

Broms (1964) proposed a method for the analysis of piles in cohesive and cohesionless soils. Figures 2.4 and 2.5 present soil reaction distributions with depth for both rigid and flexible piles in cohesive and cohesionless soils.
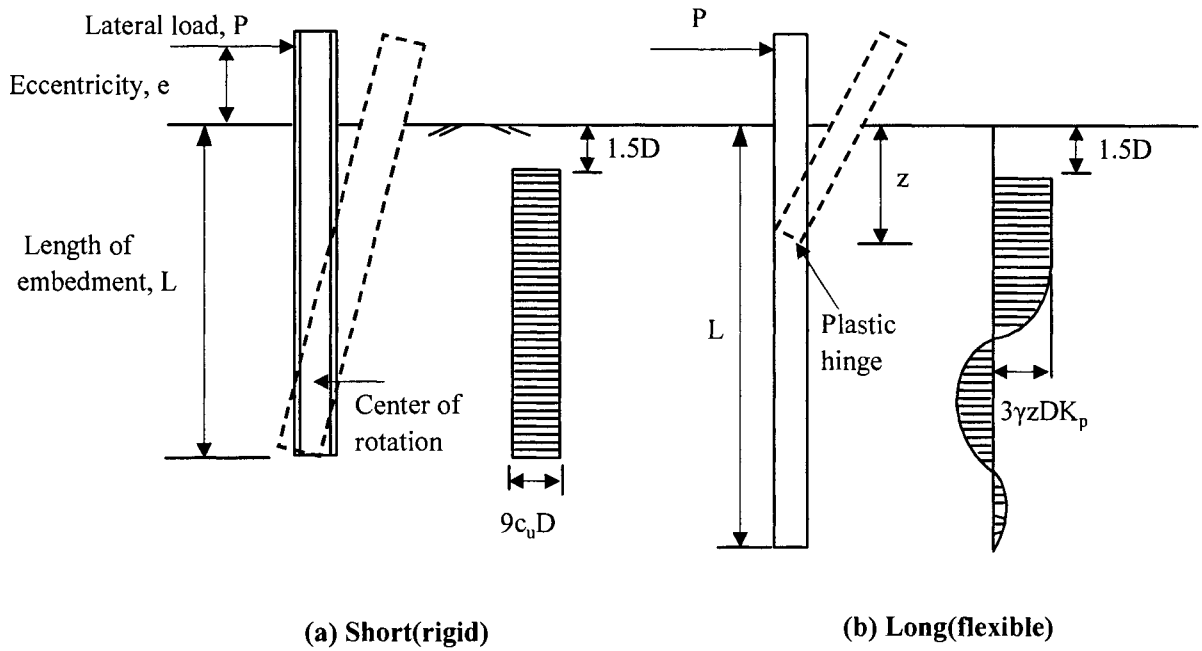
Figure 2.4 Failure Mode of Free-Head Pile in Cohesive Soil (after Broms 1964)
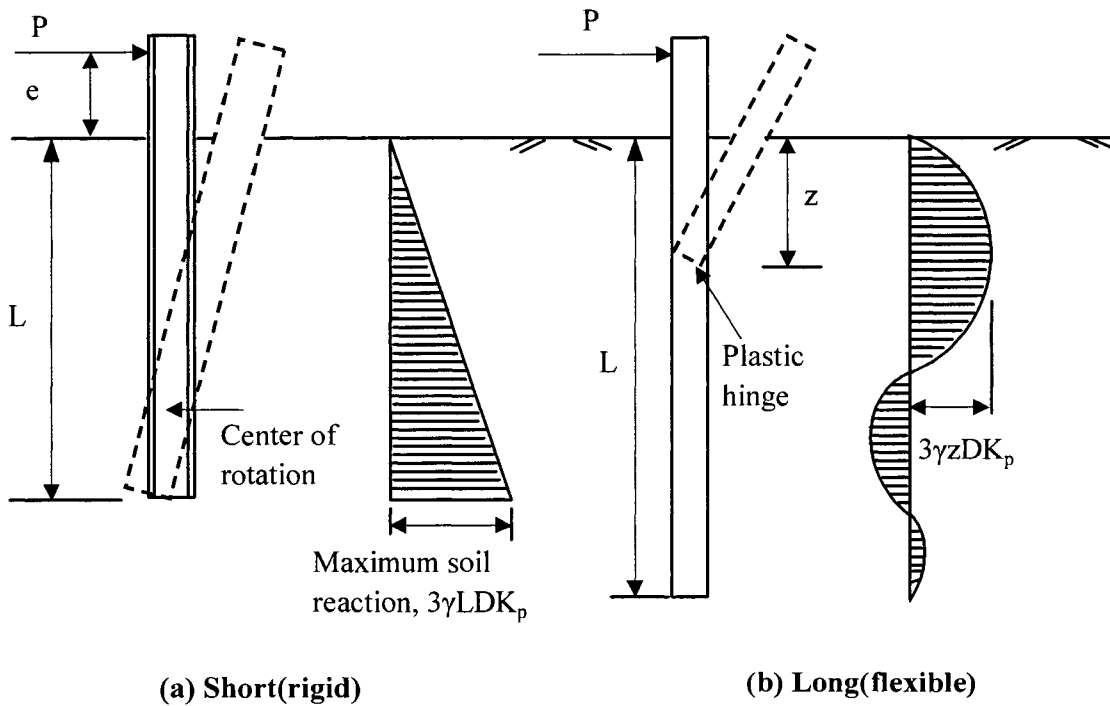
Figure 2.5 Failure Mode of Free-Head Pile in Cohesionless Soil (after Broms 1964)

For cohesive soil, the soil is assumed to reach an ultimate capacity of $9c_uD$ at depth below 1.5D, where c_u is the average undrained shear strength of soil and D is the pile diameter (Brom 1964). For a conservative design for large pile foundations, the top length of 1.5D is ignored.

For cohesionless soil, Broms (1964) made the assumptions as below:

- As a result of three-dimensional earth pressure effects, the net difference between the passive and active earth pressure at depth, z, is $3\gamma DK_p$, where K_p is the Rankine passive earth pressure coefficient.

- The point of rotation is at the bottom of the pile.

Broms' (1964) method is simple and has been accepted by many foundation engineers for design of simple pile foundations.

2.4.2 Nonlinear Subgrade Reaction Method (p-y Method)

The nonlinear subgrade reaction method is based on the concept of p-y curve, which relates soil reaction and pile deflection at points along the pile length. This method was first proposed by McClelland and Focht (1956) for the analysis of lateral loaded piles, and later advanced by Matlock (1970), using the principle of beam on elastic foundation and the finite difference method. A fourth order differential equation of a beam on elastic foundation is used in the analysis. It was later extended by Reese (1975) for the analysis of laterally loaded piles in different types of soils. This concept yields nonlinear predictions that approximate the actual behavior of piles under lateral loading conditions.

2.4.2.1 The Numerical Equation of P-y Curve

General nonlinear lateral load-displacement behavior is commonly expressed as a series of Winkler springs which can be described by a differential equation:

$$EI \frac{d^4 y}{dx^4} + P_x \frac{d^2 y}{dx^2} - p = 0 \qquad [2.2]$$

and

$$p = E_s(x, y)y \qquad [2.3]$$

in which:

P_x = axial load

y = lateral deflection of pile

x = length along the pile

EI = flexural stiffness of the pile

p = soil reaction

E_s = soil lateral elastic modulus

This approach has many limitations, especially that the lateral elastic modulus of soil E_s is not only a soil parameter but also depends on the geometry and flexural rigidity of the pile as well as the boundary conditions (Jamiolkowski and Garassino 1977). Also, it is difficult to define the p-y relationship. However, this method remains popular because of its simplicity and its capability to handle nonlinear p-y relationships.

A finite difference program COM622 was developed by Reese et al. (1977) to solve Equation [2.2]. Various boundary conditions can be considered at the top of the pile. Soil properties are defined by a set of p-y curves.

2.4.2.2 P-y Curve of Soft Clay

Matlock (1970) proposed the use of a cubic parabola to predict p-y curves, which is valid for short-term static loading and has the form

$$\frac{p}{p_u} = 0.5(\frac{y}{y_{50}})^{\frac{1}{3}}$$

[2.4]

in which:

p_u = ultimate soil resistance per unit length of pile (force/length)

y_{50} = deflection at one-half the ultimate soil resistance (length)

The cubic parabolic p-y curve is shown in Figure 2.6, in which p remains constant beyond $y = 8y_{50}$.

The ultimate soil resistance p_u is determined from the smaller value given by the following two equations (Reese *et al.* 2000):

$$p_u = [3 + \frac{\gamma'}{c_u}x + \frac{J}{b}x]c_u b$$

[2.5]

$$p_u = 9c_u b$$

[2.6]

in which:

γ' = average effective unit weight from ground surface to p-y curve,

x = depth from the ground surface to p-y curve,

c_u = undrained shear strength of soil at depth x,

b = width of pile, and

J = empirical coefficient (0.25 for soft clay, 0.5 for medium and stiff clay).

The y_{50} is determined by the following equation

$$y_{50} = 2.5\varepsilon_{50}b$$

[2.7]
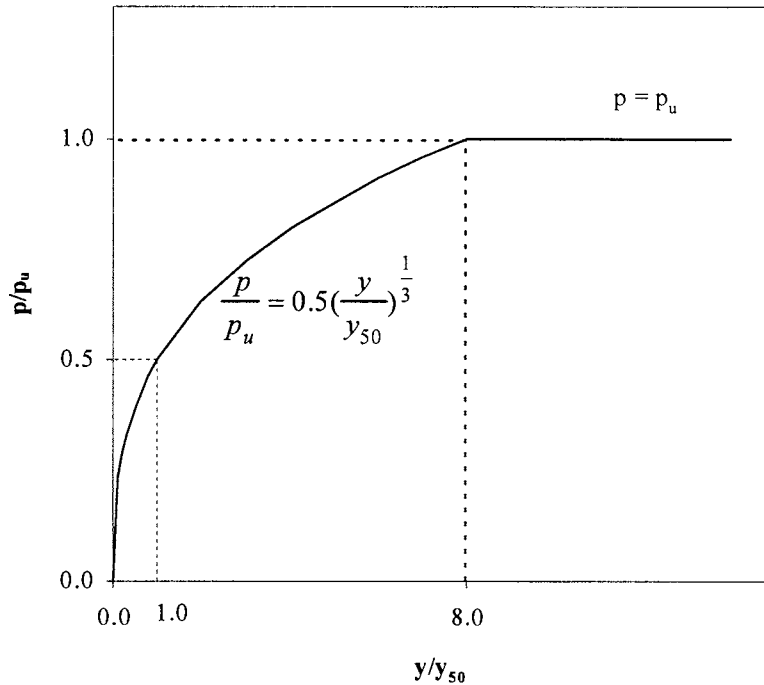
Figure 2.6 P-y Curve for Soft Clay (after Matlock, 1970)

2.4.2.3 P-y Curve of Stiff Clay with No Free Water

For stiff clay, Reese and Welch (1975) proposed the p-y curve to have the form

$$\frac{p}{p_u} = 0.5(\frac{y}{y_{50}})^{\frac{1}{4}}$$ [2.8]

It is valid for static loading in stiff clay with no free water. As shown in Figure 2.7, p

remains constant beyond y = 16y_{50}. The curve is similar to soft clay except that the exponent

is 1/4. Reese and Welch (1975) also stated that y_{50} and p_u could be determined using the

same equations (Equations [2.5], [2.6], [2.7]) as previously discussed for soft clay.
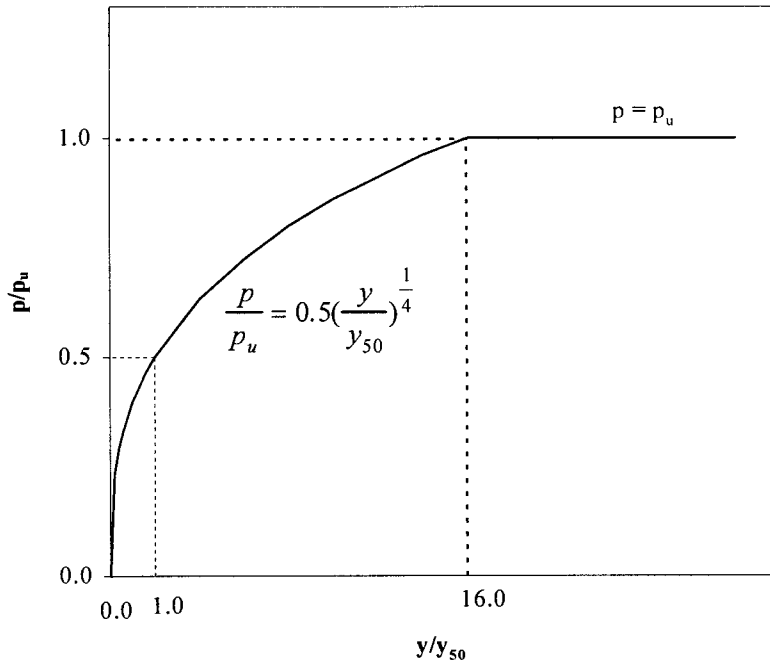
Figure 2.7 P-y Curve for Stiff Clay (Reese and Welch, 1975)

2.4.2.4 P-y Curves for Sands

Reese *et al.* (1974) proposed the p-y curve for sand to be composed by four portions: three straight lines and one parabolic section, which is shown in Figure 2.8.

The initial straight-line portion of the p-y curve represents "elastic" behavior of the sand and the horizontal portion of the curve represents "plastic" behavior. These two straight lines are joined with a parabola and a sloping straight line. The parabola and the intermediate straight line were selected empirically to yield a shape consistent with experimental p-y curves.

Reese *et al.* (1974) proposed the following procedures to establish the p-y curves.

1. Obtain values for soil properties and pile dimensions, ϕ, γ, b.

2. Make the following preliminary computations.

$$\alpha = \frac{\phi}{2}; \beta = 45 + \frac{\phi}{2}, k_0 = 0.4, and$$

$$K_A = \tan^2 (45 - \frac{\phi}{2})$$

[2.9]

3. Compute the ultimate soil resistance per unit length of pile using the smaller of the values given by the following equations.

$$p_{st} = \gamma x [\frac{K_o \tan \phi \sin \beta}{\tan(\beta - \phi) \cos \alpha} + \frac{\tan \beta}{\tan(\beta - \phi)} (b + x \tan \beta \tan \alpha)$$

$$+ K_0 x \tan \beta (\tan \phi \sin \beta - \tan \alpha) - K_A b]$$

[2.10]

$$p_{sd} = K_A b \gamma x (\tan^8 \beta - 1) + K_0 b \gamma x \tan \phi \tan^4 \beta$$

[2.11]

4. In making the computation in Step 3, find the depth x_t at which there is an intersection at Equations [2.10] and [2.11]. Above this depth use Equation [2.10]. Below this depth use Equation [2.11].
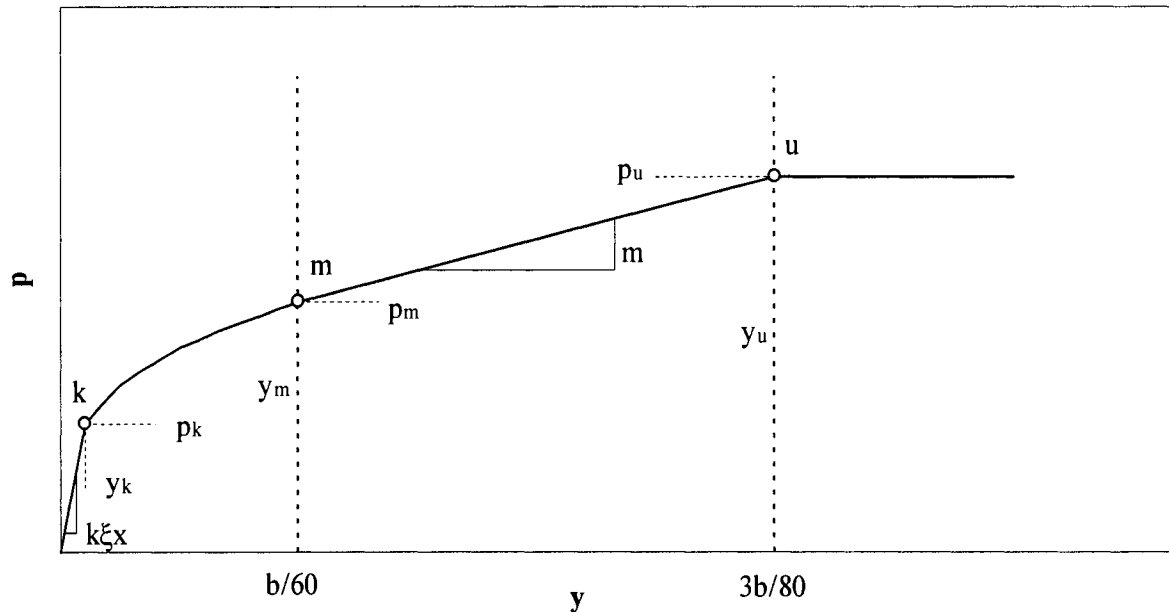
Figure 2.8 Characteristic Shape of a Family of p-y Curves for Static and Cyclic Loading in Sand (Reese *et al.* 1974)

5. Select a depth at which a p-y curve is desired.

6. Establish y_u as 3b/80. Compute p_u by the following equation:

$$p_u = Ap_s$$ [2.12]

Use the appropriate value of A from Figure 2.9 for the particular nondimensional depth for the static case. Use the appropriate equation for p_s, Equation [2.10] or Equation [2.11], by referring to the computation in Step 4.
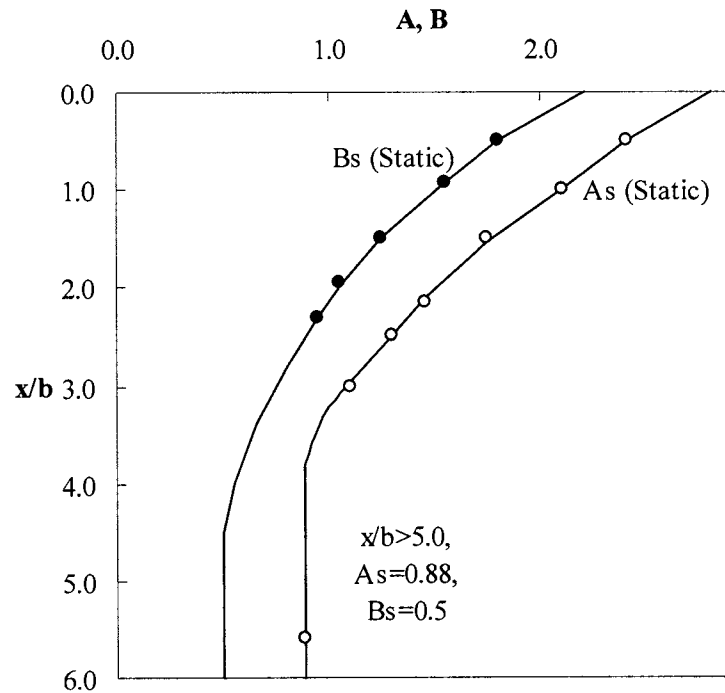
Figure 2.9 Values of Coefficients As and Bs (after Reese *et al.* 1974)

7. Establish y_m as b/60. Compute p_m by the following equation:

$$p_m = Bp_s$$ [2.13]

Use the appropriate value of B from Figure 2.9 for the particular nondimensional depth for the static case. Use the appropriate equation for p_s. The two straight-line

portions of the p-y curve, beyond the point where y is equal to b/60, can now be established.

8. Establish the initial straight-line portion of the p-y curve,

$$p = (kx)y \qquad [2.14]$$

Use the appropriate value of k from Table 2.2.

Table 2.2 Representative Values of k for Submerged Sand (Reese, *et al.*, 1974)

Recommended k	Relative Density		
	Loose	Medium	Dense
MN/m^3	5.4	16.3	34
(pci)	(20.0)	(60.0)	(125.0)

9. Establish the parabolic section of the p-y curve,

$$p = Cy^{\frac{1}{n}} \qquad [2.15]$$

Fit the parabola between points k and m as follows:

a. Get the slope of the line between points m and u by,

$$m = \frac{p_u - p_m}{y_u - y_m} \qquad [2.16]$$

b. Obtain the power of the parabolic section by,

$$n = \frac{p_m}{m y_m} \qquad [2.17]$$

c. Obtain the coefficient C as follows:

$$C = \frac{p_m}{y_m^{\frac{1}{n}}} \qquad [2.18]$$

d. Determine point k as,

$$y_k = \left(\frac{C}{kx}\right)^{\frac{n}{n+1}} \qquad [2.19]$$

e. Compute appropriate number of points on the parabola by using equation [2.15].

2.4.2.5 P-y Curve by In Situ Testing

P-y curves estimated from in situ tests provide a promising model for analyses of piles under lateral loading. Continuous profiles can be obtained from in situ tests to estimate the necessary parameters for predicting p-y curves. In situ tests include the Pressuremeter Test (PMT), Dilatometer Test (DMT), Field Vane Test (FVT), Standard Penetration Test (SPT), and Cone Penetrometer Test (CPT). Both the PMT and DMT have received increased attention in recent literature (e.g. Briaud 1997, Huang *et al.* 1989, Lutenegger and Miller 1993, Gabr and Borden 1988, Robertson *et al.* 1989). The reason is that p-y curves determined directly from PMT and DMT tests have the advantage of being based on lateral deformation properties of the soil. However, all in situ test methods are limited because they are based on empirical correlations.

2.4.2.5.1 Dilatometer Test (DMT)

The use of DMT to produce p-y curves has many advantages including:

- Membrane expansion in the horizontal direction.

- Ability to produce a relatively continuous profile.

- Simple, high repeatability of results and economic.

- The small size of the dilatometer blade enables data to be collected close to the ground surface where the lateral response of piles is most influenced.

- The dilatometer blade is pushed into the soil, thus it can be considered a model of a driven pile.

As mentioned in previous section 2.4.2.2, Matlock (1970) proposed the use of a cubic parabola to predict p-y curves, which has the form as Equation [2.4]. This approach requires an evaluation of the ultimate soil resistance p_u and the deflection y_{50}.

Robertson *et al.* (1989) proposed a method to determine p_u and y_{50} by using the DMT test results. For cohesive soils, Robertson *et al.* (1989) stated that y_{50} is evaluated by means of the following equation:

$$y_{50} = \frac{23.67 C_u D^{0.5}}{F_c E_D} \qquad [2.20]$$

in which:

F_c = empirical factor (suggested value F_c=10)

E_D = dilatometer modulus

C_u = undrained shear strength (from DMT)

D = pile diameter

The initial tangent modulus of soil E_i is given by

$$E_i = F_c E_D \qquad [2.21]$$

P_u is determined by equations [2.5], [2.6] as proposed by Matlock (1970), in which c_u is the undrained shear strength from DMT tests.

For Cohesionless soils, y_{50} is given by the following equation:

$$y_{50} = \frac{4.17 \sin\phi' \sigma_{vo}' D}{E_D F_s (1 - \sin\phi')} \qquad [2.22]$$

in which:

F_s = empirical stiffness factor

E_D = dilatometer modulus.

Both y_{50} and D are in cm.

The initial tangent modulus of soil E_i is given by

$$E_i = F_s E_D$$ [2.23]

P_u is the minimum value calculated using Equations [2.24], [2.25]:

$$P_u = \sigma'_{vo}[D(K_p - K_a) + xK_p \tan\phi' \tan\beta]$$ [2.24]

$$P_u = \sigma'_{vo}D[K_p^3 + 2K_oK_p^2 \tan\phi' + \tan\phi' - K_a]$$ [2.25]

in which:

σ'_{vo} = vertical effective stress at depth x,

D = pile diameter,

ϕ' = angle of internal friction,

K_a = Rankine active coefficient = $\dfrac{1 - \sin\phi'}{1 + \sin\phi'}$,

K_p = Rankine passive coefficient = $1/K_a$,

K_0 = coefficient of earth pressure at-rest, and

$\beta = 45^0 + \phi/2$.

This method relies on many empirical correlations. In clays the major soil parameters are C_u and E_i. In sands the parameters are ϕ', K_0, and E_i. At working lateral loads where pile deflections are small, the most important parameter is the soil stiffness E_i. The proposed analysis is therefore sensitive to changes in E_i. For both clays and sands the pile deflection y_{50} is inversely proportional to E_i. Therefore, the major variables in the proposed method are the empirical stiffness factors F_c and F_s. The values suggested for F_c and F_s are a preliminary attempt to enable an evaluation of the method to be made (Robertson *et al.* 1989).

The Robertson *et al.* (1989) method took into account, in addition, the effects of pile installation by reducing C_u as a function of overconsolidation ratio (OCR). The reduction factor, as suggested by Gabr (1988), may be assumed equal to 2/3 for OCR $\geq$ 2 and ranging from 1 to 2/3 for $1 \leq OCR \leq 2$.

2.4.2.5.2 Pressuremeter Test (PMT)

The PMT, a test of lateral expansion in a prebored hole, closely replicates important characteristics of a laterally loaded pile. Unlike the dilatometer test, which produces 1mm of lateral deformation, the pressuremeter test can produce large lateral deformations. Because of this, there are increments of pressure with which to develop a load-deformation curve.

The PMT methods have the advantage that the cylindrical expansion can be considered a reasonable model of the lateral movement of the soil during lateral loading of piles. However, several problems still exist. Some of the major difficulties relate to the following:

- Pressuremeter tests are often difficult and expensive to conduct and usually only a limited number of tests are performed, and

- The large size of most pressuremeters makes it difficult to obtain data close to the ground surface where the lateral response of piles is most influenced.

Robertson *et al.* (1985) suggested a method that uses the results of a pushed-in pressuremeter to evaluate p-y curves of a driven displacement pile. They multiplied the pressure component of the PMT curve by an α factor to obtain the correct p-y curve. The critical depth was assumed to be four pile diameters as shown in Figure 2.10.
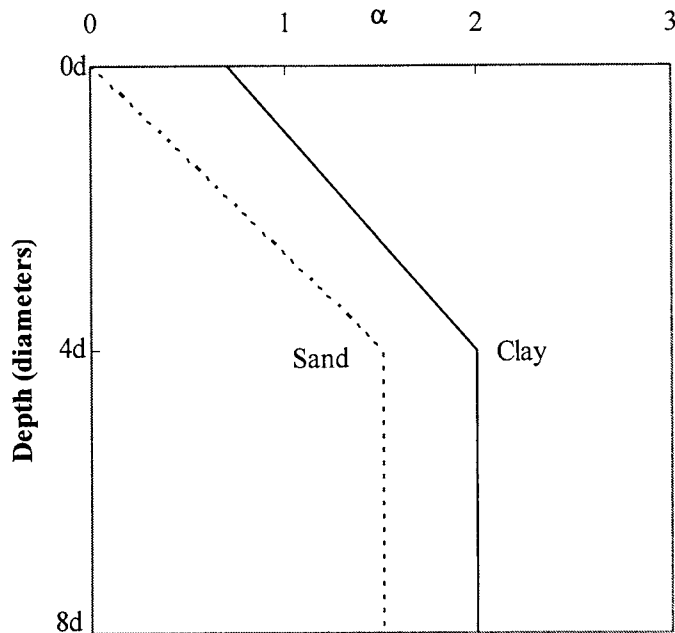
Figure 2.10 Correction Factor α Versus Depth (after Robertson *et al.* 1985)

Robertson *et al.* (1985) reduced α near the surface assuming that the response is affected by the reduced vertical stress. To obtain the p-y curve, the pressuremeter curve is translated to the lift off pressure that is equivalent to the initial lateral stress around the pile. The stress is multiplied by the pile width and the strain component (ΔR/R) is multiplied by the pile half width. For small strain conditions (ΔR/R) is equal to (ΔV/2V).

Since the installation of the pushed-in pressuremeter results in an initial pressure on the probe, an unload/reload sequence is often used. For this method, the portion of the corrected pressuremeter curve from the beginning of reload through the maximum volume was used to determine the p-y curves. The following equations outline the Robertson *et al.* (1985) method for determination of p-y curves from pressuremeter data:

1. Determine the initial radius of the probe:

   R_p = Initial Circumference of Probe/(2π)

2. Calculate the initial volume of the probe:

$$V_p = \pi * R_p^2 * \text{Length of Membrane}$$

3. Determine P in units of force/length:

A reduction factor, α, is applied to the P.

If DCM/Pile Diameter > 4

Then $\alpha = 1.5$ for sand or 2 for clay

Else $\alpha = 1.5 * \text{DCM}/(4 * \text{Pile Diameter})$ for sand

Or $\alpha = 0.67 + 2 * \text{DCM}/(4 * \text{Pile Diameter})$ for clay

Thus P = (Corrected Pressure from PMT)*(Pile Diameter)*(Reduction Factor)

4. Determine Y in units of Length

$Y = [(\text{Corrected Volume from PMT})/(2 * \text{Initial Volume})] * (\text{Pile Diameter}/2)$

in which:

DCM = Depth from the ground surface to the center of the pressuremeter membrane.

In addition, Briaud *et al.* (1997) proposed a Pressuremeter-based method for the design of both long flexible and short rigid laterally loaded piles. He suggested a "Rule of Thumb" to estimate horizontal shaft behavior which was later refined and presented as SALLOP: Simple Approach for Lateral Loads on Piles. The important assumption made by this method is that soil resistance p alternates direction and essentially cancels itself out except for a shallow zone close to the surface, which contributes most to the lateral resistance. More specifically, there is a depth close to the ground surface where the shear force in the pile is zero as shown in Figure 2.11. This depth is called the zero-shear depth D_v. The horizontal equilibrium of this relatively shallow segment of pile is the basis for SALLOP. One key element is to determine the depth of this shallow segment of pile.
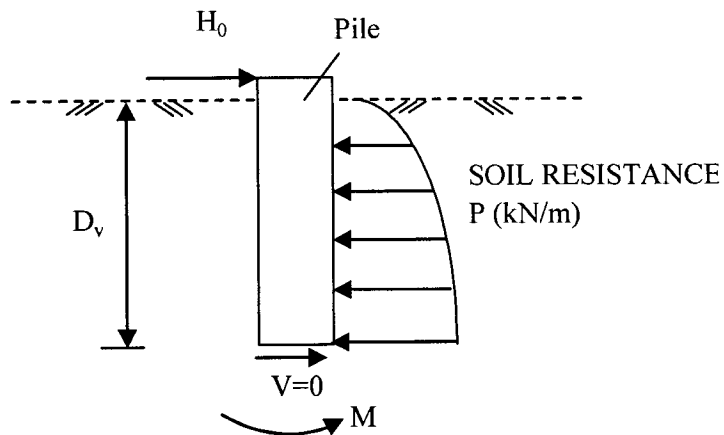
Figure 2.11 Free Body Diagram of Pile Down to Zero-Shear Depth (after Briaud 1997)

SALLOP utilizes the transfer length, l_0, as defined previously as R in Equation [2.1], to determine the zero-shear depth, D_v, for both flexible and rigid piles, respectively, as:

$$D_v = \frac{\pi}{4} l_0 \quad \text{if } L \geq 3l_0 \text{ flexible} \tag{2.26}$$

$$D_v = \frac{L}{3} \quad \text{if } L \leq l_0 \text{ rigid} \tag{2.27}$$

A linear interpolation between the two values will be used if the pile length is between l_0 and $3l_0$ as shown in Figure 2.12.
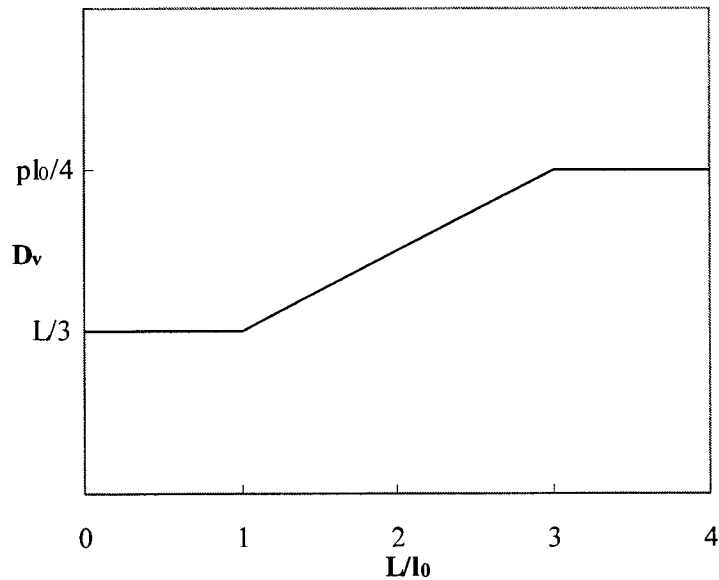
Figure 2.12 Linear Interpolation for Zero-Shear Depth Dv (after Briaud 1997)

The lateral capacity H_{ou} was defined as:

$$H_{ou} = \int_0^{D_v} P_u dz \qquad \text{[2.28]}$$

in which:

P_u = soil resistance (kN/m)

H_{ou} = horizontal pile capacity (kN)

D_v = zero-shear depth (m).

Horizontal pile capacity is defined as the load corresponding to a pile head deflection equal to one tenth of the pile diameter. The SALLOP method quantifies lateral capacity as:

$$H_{ou} = \frac{3}{4} p_L B D_v \qquad \text{[2.29]}$$

in which:

p_L = pressure against the soil when the pressuremeter probe reaches a volume corresponding to a cavity volume equal to twice the initial cavity volume (Briaud 1992),

B = pile diameter or width (m).

If the SPT blow count N, the CPT point resistance q_c, or the undrained shear strength s_u are available instead of p_L, Briaud (1992) proposed the correlations between N, q_c, s_u, and p_L to estimate p_L. However, the reliability of the predictions is decreased because of the scatter in the correlations (Briaud 1997).

2.4.2.5.3 Standard Penetration Test (SPT) and Cone Penetration Test (CPT)

The p-y models require soil parameters such as friction angle ϕ', undrained shear strength s_u, p-y modulus k, and strain corresponding to 50% or 100% maximum stress, i.e., ε_{50} or ε_{100}. However, these parameters are not readily apparent from SPT and CPT measurements without using empirical relationships.

The sand p-y curves require ϕ', k, and γ'. Similarly, the clay curves require s_u, ε_{50}, ε_{100}, γ', and k. These parameters are used to develop p-y curves required by current design software LPILE and LTBASE.

Table 2.3 summarizes the necessary input parameters used for the "default" p-y models used in LPILE.

Table 2.3 Summary of Input Parameters

Soil type	Soil stiffness	Soil location	Parameters	Model (reference)
Sand	Loose-dense	Above/below GWT	ϕ, k, γ	Murchison and O'Neill (1984)
			ϕ, k, γ	Reese et al. (1974)
Clay	Soft/medium stiff	Above GWT	s_u, ε_{50}, ε_{100}	Gazioglu and O'Neill (1984)
		Below GWT	s_u, ε_{50}, γ	Matlock(1970)
	Stiff	Above GWT	s_u, ε_{50}, γ	Welch and Reese(1972); Reese and Welch (1975)
		Below GWT	s_u, ε_{50}, γ, k	Reese et al. (1975)

The following equation is from Peck et al. (1974), using uncorrected N-values from SPT to obtain ϕ value:

$$\phi' = 53.881 - 27.6034e^{-0.0147N} \qquad [2.30]$$

Subgrade reaction modulus k is obtained from Terzaghi (1955).

A correlation by Robertson and Campanella (1983) can be used to estimate the friction angle ϕ' values from the CPT tip resistances q_c. Correlations have been attempted for estimating s_u from SPT values, even though it is known that these correlations may not be very reliable. The most common of these is from Terzaghi and Peck (1968), which was developed primarily using unconfined compression tests. From the results of this correlation, s_u can be approximated by s_u/P_a=0.06N where P_a is the atmospheric pressure. The relationship for estimating undrained shear strength from the cone tip resistance in clay is given by:

$$s_u = \frac{q_c - \sigma_{vo}}{N_{kk}} \qquad [2.31]$$

in which:

q_c = cone tip resistance;

σ_{vo} = total overburden stress;

N_{kk} = an empirical constant.

The value of N_{kk} ranges between 10 and 20 and depends on the overconsolidation ratio and plasticity index (Aas *et al.* 1986). Typically N_{kk} = 15 is used [Electrical Power Research Institute (EPRI) 1990].

Although empirical correlations between SPT blow count, N, CPT tip resistance, q_c, with the undrained shear strength, s_u, and friction angle, ϕ, do exist, the reliability of predictions is increased by eliminating dependence on such correlations as such correlations are not based on soil mechanics theory.

2.4.2.5.4 Field Vane Test (FVT)

Reese and Allen (1977) recommended that for submerged clays, the p-y curves be established based on a profile of s_u and ε_{50}. For soft clay soils that are normally or lightly overconsolidated, Matlock (1970) recommended the FVT as the preferable method to determine the in situ undrained shear strength. Although this is not exactly the case for the clay crust, undrained shear strengths from FVT were used in establishing the p-y curves. This is primarily due to the lack of good-quality samples for laboratory testing, as is usually the case for clay crusts.

The p-y relationships were established according to the "integrated clay method" proposed by Gazioglu and O'Neill (1984). This semi-empirical method considers the effects of soil ductility, nonlinear dependence on pile diameter, and relative stiffness of soil and pile. It is applicable to both soft and stiff clays, as the name implies. A critical pile length (L_c) is computed first as

$$L_c = 3(EI / E_s D^{0.5})^{0.286} \tag{2.32}$$

in which:

D = diameter of the pile,

EI = flexural stiffness of the pile, and

E_s = average soil modulus.

The lateral load-deflection relationships are unaffected by penetration beyond L_c according to Gazioglu and O'Neill. The critical depth (x_{cr}) is related to L_c by the following equation:

$$x_{cr} = L_c/4 \tag{2.33}$$

A reference deflection (y_c) is defined as follows:

$$y_c = 0.8\varepsilon_{50}D^{0.5}(EI/E_s)^{0.125} \tag{2.34}$$

$$p_u = 0.75 \, N_p s_u D \tag{2.35}$$

and

$$N_p = 3 + 6(x/x_{cr}) \leq 9 \tag{2.36}$$

in which:

x = Depth below ground surface.

The lateral reaction (p) at depth x is then computed as

$$p = 0.5\left(\frac{y}{y_c}\right)^{0.387} p_u \tag{2.37}$$

Figure 2.13 shows the typical shape of a p-y curve established on the basis of this method.

The figure shows a P-y curve with the following annotations:

$p = p_u$ for $x > x_{cr}$

$p = 0.5 \left(\dfrac{y}{y_c} \right)^{0.387} p_u$

Vertical axis: p/p_u (with values 1.0 and 0.0)

Horizontal axis: y/y_c, with x_{cr} marked.
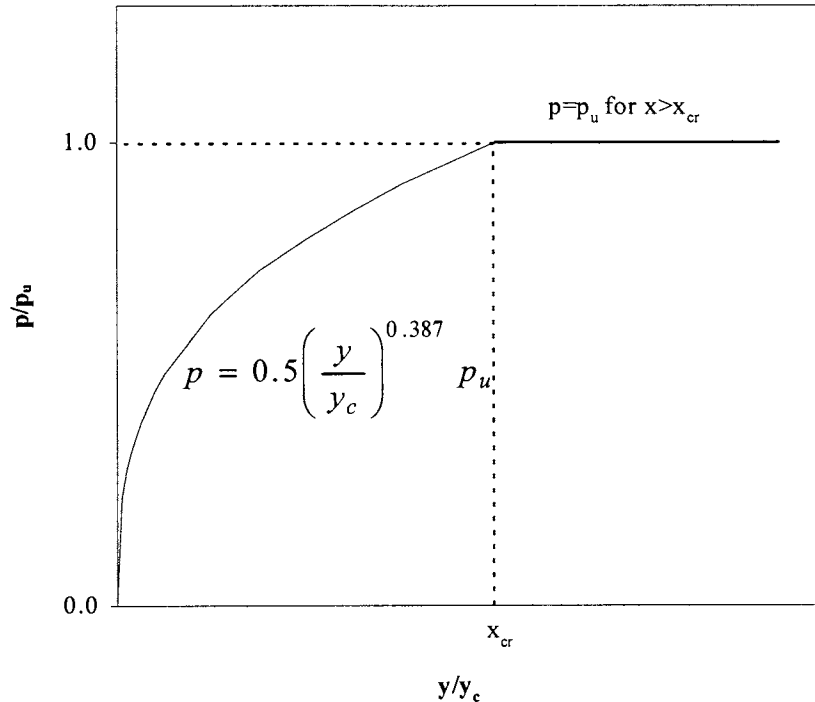
Figure 2.13 P-y Curve Using the "Integrated Clay Method" (after Huang _et al._, 1989)

2.4.2.5.5 P-y Curves from Triaxial Tests

P-y curves can also be obtained from the triaxial tests. Early in 1951, Skempton (1951) developed a method to predict load-settlement curves. The theory can be used to obtain p-y curves if the assumptions below are made (Skempton 1951):

- the ground surface does not affect the results,

- the state of stress is the same in the horizontal and vertical directions, and

- the soil is isotopic.

For the same ratio of applied stress to ultimate stress, the settlement and soil resistance in the footing test (or pile under lateral loading) is related to the strain and stress in the laboratory compression test by the following equations.

$$y = 2\varepsilon b \qquad\qquad [2.38]$$

$$p = 4.5\sigma_D b \tag{2.39}$$

Skempton (1951) stated that the failure stress for a footing reaches a maximum value of 9c. If one assumes the same value for a pile in saturated clay under lateral loading, p_u becomes 9cb. A p-y curve can be obtained by taking points from a laboratory stress-strain curve and using Equation [2.38] to obtain deflection and Equation [2.39] to obtain soil resistance. The procedure would presumably be valid at depths beyond where the presence of the ground surface would not reduce the soil resistance.

Skempton (1951) presented information about laboratory stress-strain curves to indicate that ε_{50}, the strain corresponding to a stress of 50 percent of the ultimate stress, ranges from about 0.005 to 0.02. That information, and information about the general shape of a stress-strain curve, allows an approximate curve to be developed if only the strength of the soil is available.

Soon after Skempton, McClelland and Focht (1958) presented the first paper giving the concept of p-y curves, and they presented the first experimental curves from a full-scale, instrumented, pile-load test. The paper shows conclusively that soil modulus is not a soil property but is a function of pile deflection and depth below the mudline, as well as of soil properties.

The paper recommends the performance of consolidated-undrained triaxial tests with the confining pressure equal to the overburden pressure. The full curve of deviator stress σ_D and the corresponding strain ε is plotted. The following equation is recommended for obtaining the soil resistance p:

$$p = 5.5\sigma_D b \tag{2.40}$$

To obtain values of pile deflection y from stress-strain curves, the authors proposed the following equation.

$$y = 0.5\varepsilon b \qquad\qquad\qquad [2.41]$$

These equations are similar in form but have different constants from those derived by Skempton (1951).

2.4.3 Estimating Load-Displacement Behavior from Computer Software LPILE and LTBASE

Piles and drilled shafts are structural members used to transfer loads to deep strata through skin friction and end bearing. These deep foundations are necessary when the upper soil layers are too weak to prevent excessive settlement of the structure, when the structure is subject to large lateral forces, or when the foundation is subject to scour. Ship impact, wind, earth pressure, and water pressure are all sources of lateral load on deep foundations. Lateral loading of a single pile is a soil-structure interaction problem. The problem does not have a simple solution and is often attacked by Finite Difference or Finite Element techniques. Thus, "by hand" lateral analyses are very time consuming, and may not be reasonable due to the number of assumptions necessary.

2.4.3.1 LPILE

The computer program, LPILE, commercially available from Ensoft, Inc. developed by Reese *et al.* (2000), is designed to analyze a single pile subjected to lateral loading. Embedment soil behavior is modeled with p-y curves developed internally from specified soil characteristics or with manually inputted p-y curves created using in situ testing methods described in the previous sections. The program uses rational procedures to compute

deflection, shear, bending moment, and soil response with respect to depth in nonlinear soils. Estimates of "ultimate" lateral pile capacity can be made from the output data file and graphics.

2.4.3.2 LTBASE

In general, the load-deflection analysis of laterally loaded piles is conducted without consideration for the influence of base resistance. Although it can be shown that this assumption is valid for piles with relatively large length/diameter (L/D) ratios, for the case of short rigid piles, the influence of base resistance can be significant.

Two theoretical approaches have generally been employed for predicting the lateral movement of piles. The elastic approach, which assumes the soil to be an ideal elastic continuum, and the subgrade reaction approach, in which the soil reaction at a point is related to the pile deflection at that point through a constant of subgrade reaction referred to as K_{ho}. Using the subgrade reaction approach, the soil-pile interaction mechanism is modeled by treating the pile as a linear elastic beam and the soil reaction as a line load. Using a finite number of elements in a numerical solution, the interaction is represented by discrete nonlinear springs, with the spring stiffness varying as a nonlinear function of pile lateral deformation. The subgrade reaction concept provides a rational approach that permits the description of the nonlinear behavior of the soil-pile interaction system readily, if only approximately.

The computer program, LTBASE (Borden and Gabr 1987), *La*Teral pier analysis including *B*ase *A*nd *S*lope *E*ffect, is a program for the load-deflection analysis of laterally loaded piles. Developed by North Carolina State University, the program utilizes the finite

difference technique to solve the non-linear simulation model formulated using the subgrade reaction approach. The program is coded in Fortran77 computer language, and is well documented internally. The source code is compiled using Microsoft FORTRAN77 version 3.2 compiler. The compiled code is linked to MS-FORTRAN runtime library, FORTRAN . L87, which supports an 8087 coprocessor. The Microsoft 8086 object linker version 3.02 is used in the linking process. Double precision arithmetic is used through out the program to enhance the accuracy of the solution.

The purpose of this program is to evaluate the non-linear lateral load-deflection response of laterally loaded piers. A procedure to account for the influence of the mobilized resistance at the base of the drilled piers on the predicted lateral response is incorporated in the program. A comparison of the shear and moment distribution of pile between LPILE and LTBASE is shown in Figure 2.14. The LPILE algorithm assumes no shear or moment at the base, whereas in LTBASE, the base shear and moment are not neglected.
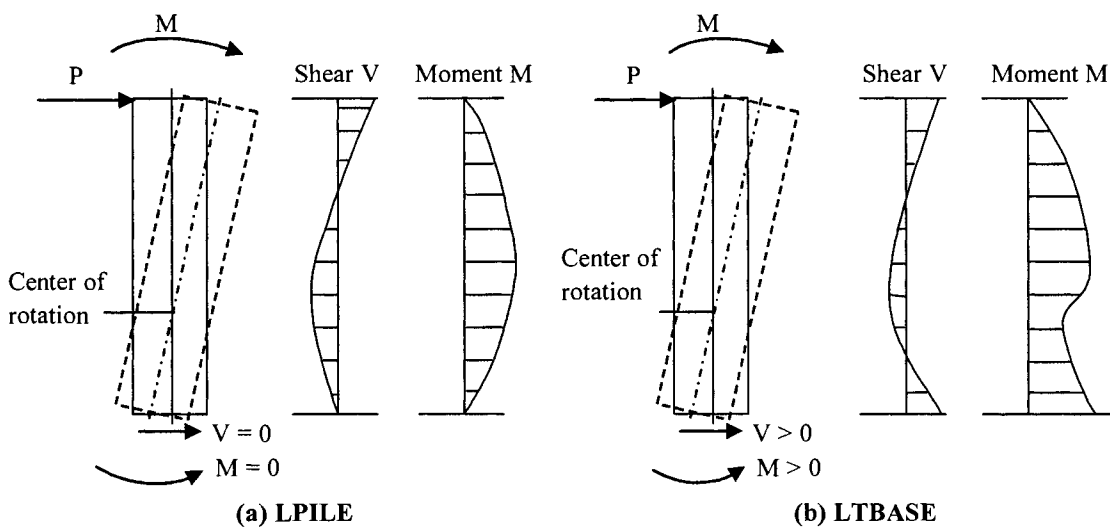
Figure 2.14 Comparison of Shear, Moment Distribution of Pile in LPILE and LTBASE

2.5 Normalized Load-Displacement Behavior of Foundation

To investigate the scale effects of the foundation, the load-displacement is generally transformed into nondimensional terms. This procedure involves normalizing the applied load (or pressure) by ultimate capacity (or pressure) and displacement by diameter/width (or settlement by depth of embedment). Lutenneger *et al.* (1998) applied the technique of normalizing to the experimental data on shallow foundation in fine-grained soil presented by Housel (1927). As shown in Figure 2.15, the relative load and relative settlement was followed on one curve, indicating it is independent of the foundation size. Dearth (2002) used this technique on drilled shaft foundations - nine rigid drilled shafts installed at DOE Site at the University of Massachusetts, Amherst campus as shown in Figure 2.16. A fitting curve was plotted and it was found that the relative load and relative settlement can be expressed in a single power function:

$$\frac{s}{s_f} = (\frac{Q}{Q_{ult}})^x \qquad\qquad [2.42]$$

in which:

Q = applied load

Q_{ult} = load at specified failure

s = settlement at any load, Q

s_f = 10%D, and

x = exponent determined for curve fitting.

The 10%B method was used to define ultimate footing capacity as the load corresponding to the settlement equal to 10% of the footing width.

"These results suggest that nondimensional behavior is not unique to shallow foundations. It appears that any foundation whose load-deformation behavior is dominated by a single component may be described in this way" (Luttenegger 2003).
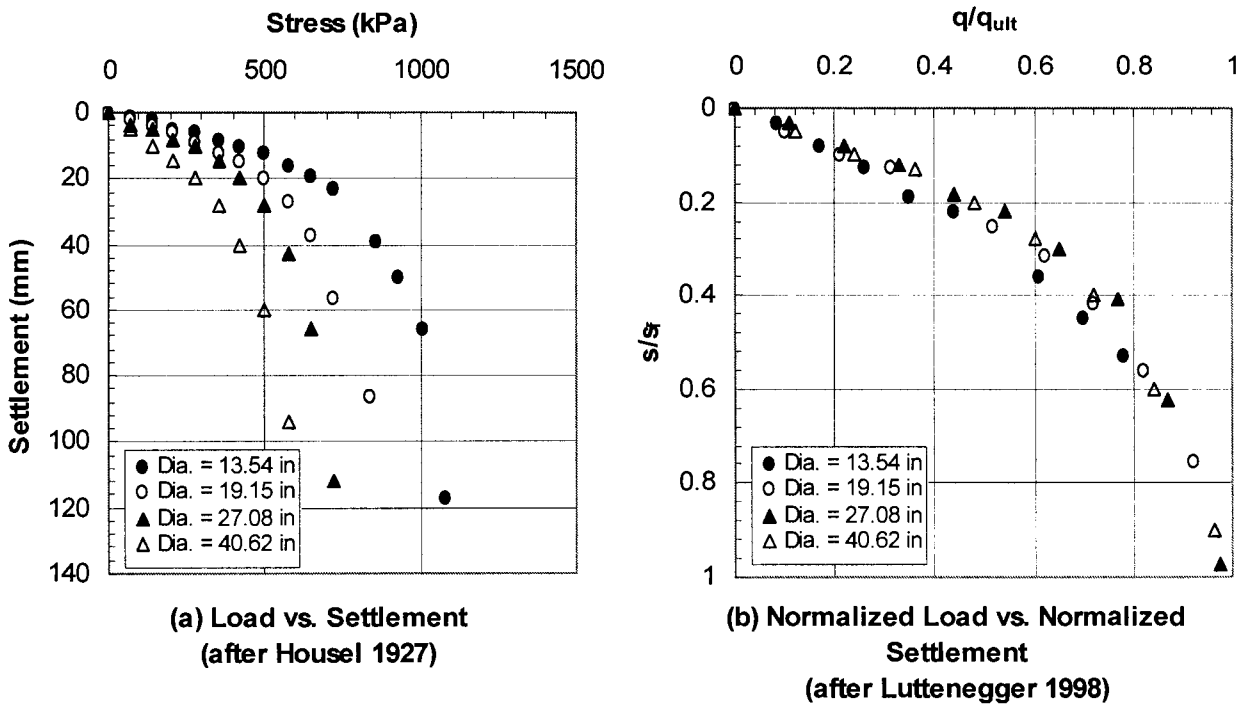
Figure 2.15 Normalized Load vs. Normalized Settlement for Shallow Foundation (after Luttenegger _et al._ 1998)
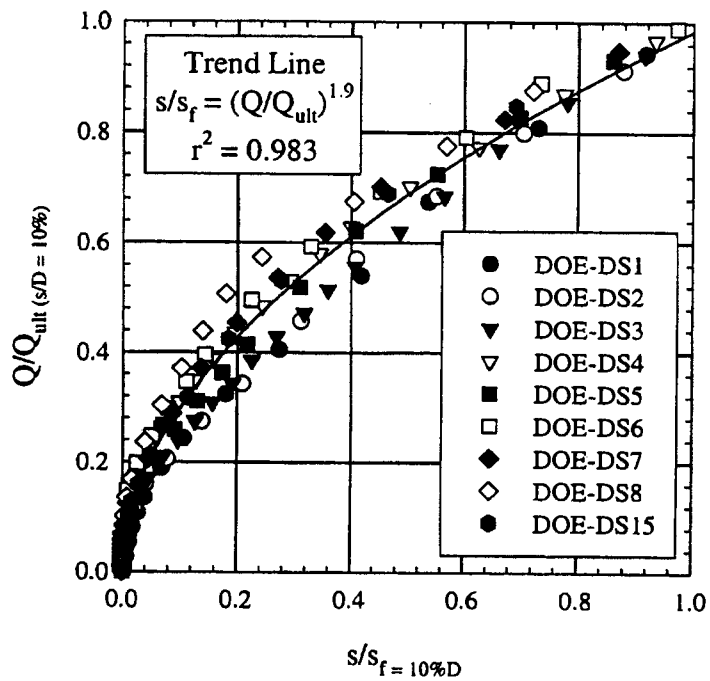
Figure 2.16 Normalized Lateral Load-Displacement Behavior Series DOE-A at DOE Site (from Dearth 2002)

CHAPTER 3: PARAMETRIC STUDY

3.1 Introduction

The design of foundation systems to sustain lateral loading is an important problem and one that is encountered frequently in engineering practice. It involves many considerations, among which the most important aspects are: (1) the computation of the loading at which a particular pile will fail as a structure or the loading that will cause an unacceptable deflection; and (2) the computation of deflection, bending moment, and shear stress along the length of a pile under service loading conditions. If the load-deflection behavior of different pile geometries in a particular soil type is known, the appropriate pile length and diameter can be selected to achieve the aforementioned design criteria.

LPILE is a special purpose program developed by Reese *et al.* (2000) based on rational procedures for analyzing a pile or drilled shaft under lateral loading conditions. The program computes deflection, shear, bending moment, and soil response with respect to depth in nonlinear soil, and offers an extensive graphic capability for presenting the results, including a user-friendly preprocessor module for data entry. LTBASE (VERSION F1.5) is a program developed by Borden and Gabr (1987) to evaluate the non-linear lateral load-deflection response of laterally load piles. The program includes the influence of the mobilized resistance at the base of the drilled piers on the predicted lateral response. Also, the program is capable of analyzing cases where the laterally loaded piers are constructed on slopes. Such cases are common for piers supporting light poles or overhead signs and constructed on the sides of a highway embankment.

A parameteric study was conducted to simulate and evaluate the lateral load-deflection behavior of intermediate CIDH concrete piers in typical soil condition using

available finite difference software programs: LPILE and LTBASE. A wide range of

intermediate pier geometries were investigated whose dimensions are listed in Table 3.1. The

properties of the soils simulated in the analyses are listed in Table 3.2.

Table 3.1 Pier Dimensions and L/D Value

		Length m(ft.)					
		1.52(5)	1.83(6)	2.13(7)	2.44(8)	2.74(9)	3.05(10)
		L/D					
	0.30(12)	5	6	7	8	9	10
Diameter m(in.)	0.46(18)	3.33	4	4.67	5.33	6	6.67
	0.61(24)	2.5	3	3.5	4	4.5	5
	0.76(30)	2	2.4	2.8	3.2	3.6	4
	0.91(36)	1.67	2	2.33	2.67	3	3.33

Table 3.2 Soil Parameter Values for Analysis

Parameters	LPILE			LTBASE	
	Soft Clay	Stiff Clay	Sand	Soft Clay	Sand
Undrained shear strength c_u kPa(psi)	28(4)	104(15)	0	28(4)	0
Friction angle ϕ^0	--	--	32	--	32
Initial p-y modulus K kN/m^3(pci)	--	135700(500)	16300(60)	--	16300(60)
Effective unit weight γ' kN/m^3(pcf)	6.3(40)	19(121)	9.2(58.5)	6.3(40)	9.2(58.5)
Strain at one-half maximum deviator stress ε_{50}	0.02	0.005	--	0.02	--

Note: -- not required

As shown in Table 3.2, the undrained shear strength was assumed to be 28 kPa (4 psi)

for soft clay and 104 kPa (15 psi) for stiff clay, as suggested by Reese *et al.* (2000). Further,

for soft clay, the assumption is made that high ground water table (GWT) conditions exist

and the submerged unit weight is 6.3 kN/m^3 (40 pcf); while for stiff clay, it is assumed that

high GWT conditions do not exist and the total unit weight is 19 kN/m^3 (121 pcf). The sand was assumed to be medium dense with an internal friction angle of 32 degrees and a submerged unit weight of 9.2 kN/m^3 (58.5 pcf). For all soils, the ε_{50} and k values were based on recommended values proposed by Reese *et al.* (2000).

LPILE and LTBASE results were compared for sand and soft clay only. The same p-y curves were used in comparisons. LTBASE does not include user input p-y curves and generates the p-y curves by the program itself. In this parametric study, p-y curves created by LTBASE were used as input in LPILE.

3.2 P-y Curves

Three types of soils were used in the analyses: soft clay, stiff clay, and sand. In LTBASE, p-y curves for soft clay were created using the unified methods proposed by Reese and Allen (1977), while in LPILE, methods suggested by Matlock (1970) for soft clay, and Reese *et al.* (1975) for stiff clay were used for construction of p-y curves. For sand, both programs use p-y curves proposed by Reese, *et al.* (1974). The procedures of developing p-y curves are described in section 2.4.2.

Examples of p-y curves at depth 0.61 m are presented in Figure 3.1 for soft clay, stiff clay and sand. The pile used in the calculation has a diameter of 0.61 m with length of 3.05 m. Figure 3.1 shows that the p-y modulus follows in the order: stiff clay > sand > soft clay.
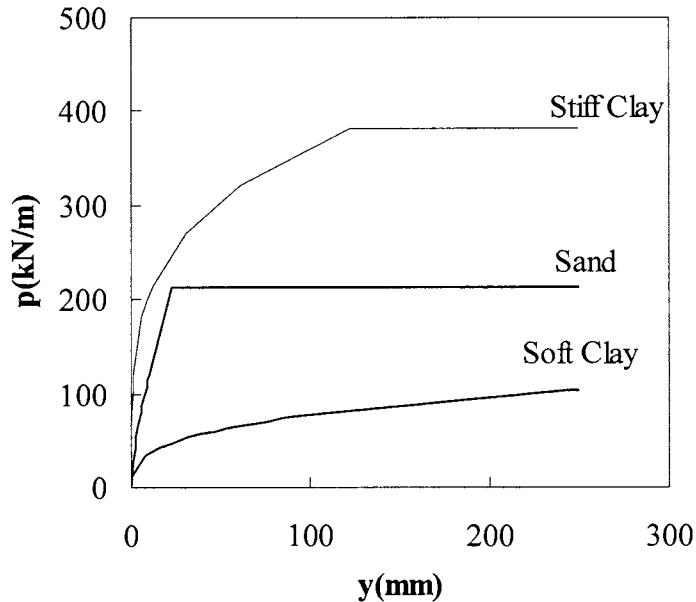
Figure 3.1 P-y Curves at Depth=0.61 m (D=0.61 m, L=3.05 m.)

3.3 Displacement, Moment, Shear Curves

Using the p-y curves created by previously mentioned methods, two piers with diameter of 0.3 m, length of 3 m and diameter of 0.91 m, length of 1.52 m placed in sand were analyzed under lateral loading using LPILE and LTBASE. The displacement, shear, and moment curves with depth are presented in Figures 3.2 and 3.3. Results are shown for pier head deflection equals to 10%D.

As shown in Figure 3.2, for a length-diameter ratio (L/D) equal to 10, LPILE and LTBASE provided similar displacement, moment and shear curves. The pier exhibits flexible bending behavior and both the base shear and moment calculated by LTBASE is equal to approximately zero. When the L/D decreases to 1.7, as shown in Figure 3.3, it exhibits rigid rotation. The base shear effect is significant, which results a large moment and shear force (about 2 times as the top shear) at the base. The difference of shear and moment curves

between LPILE and LTBASE becomes obvious. Displacement, shear, and moment curves

for all 30 piers analyzed in both sand and clay are included in Appendix A.
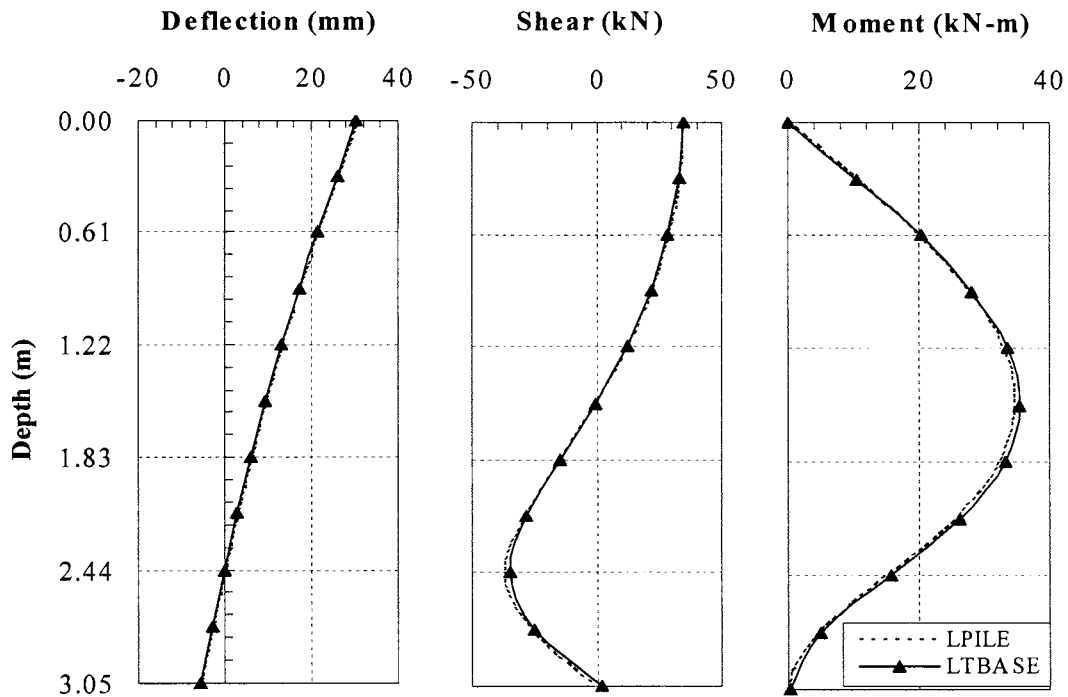
Figure 3.2 Displacement, Shear, Moment Curves when Pier Head Displacement Equals to 10%D (D = 0.3 m, L = 3 m. L/D=10)
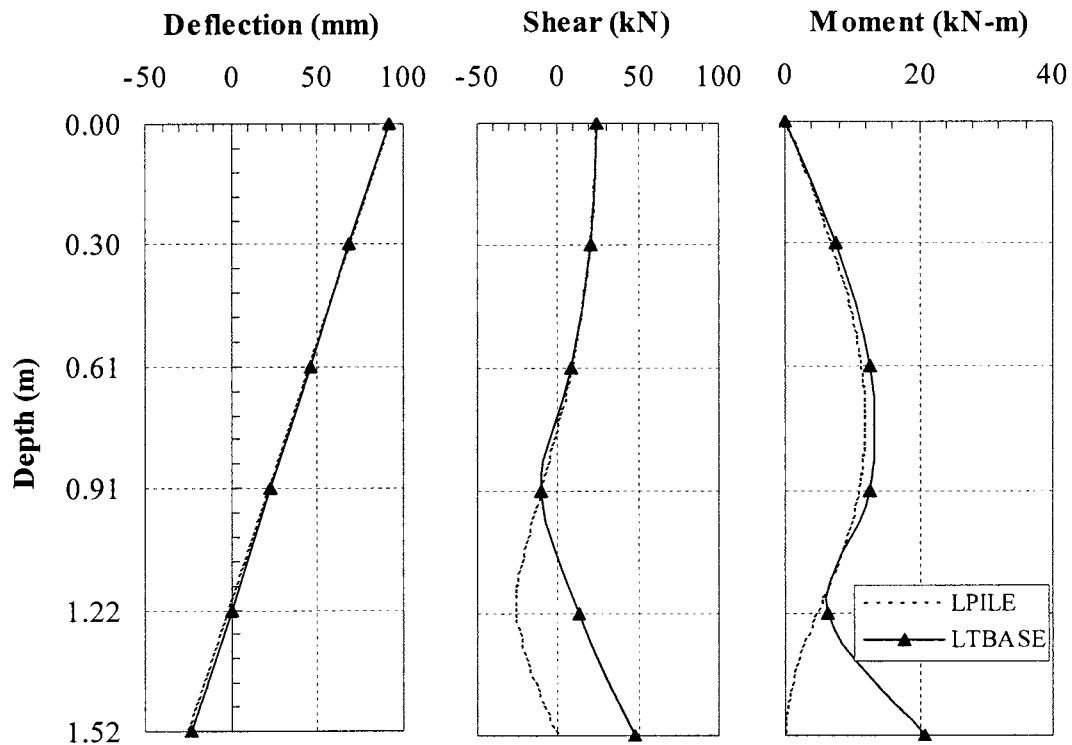
Figure 3.3 Displacement, Shear, Moment Curves when Pier Head Displacement Equals to 10%D (D = 0.91 m, L = 1.52 m. L/D = 1.7)

3.4 Classification of Load-Deflection Behavior

As mentioned previously in section 2.2 and presented in Table 2.1, there are six methods that can be used to classify pier behavior. Thirty piers were classified and summarized in Figure 3.4.

Figure 3.4 indicates that a pier may have different behavior in different soils. Even in the same soil, a pier may have different classification by different methods. For example, a pier with L/D equals to 10 is classified by method 1 as rigid in soft clay, as semi-rigid in sand, and as flexible in stiff clay. In soft clay, a pier with L/D equals to 8 is classified as rigid by method 1, while it is classified as semi-rigid by method 4. When L/D is less than or equals to 4, a pier is classified as rigid by all methods and it is independent of embedment soil. The behavior of 30 piers in this study is tabulated and presented in Tables 3.3 to 3.5.
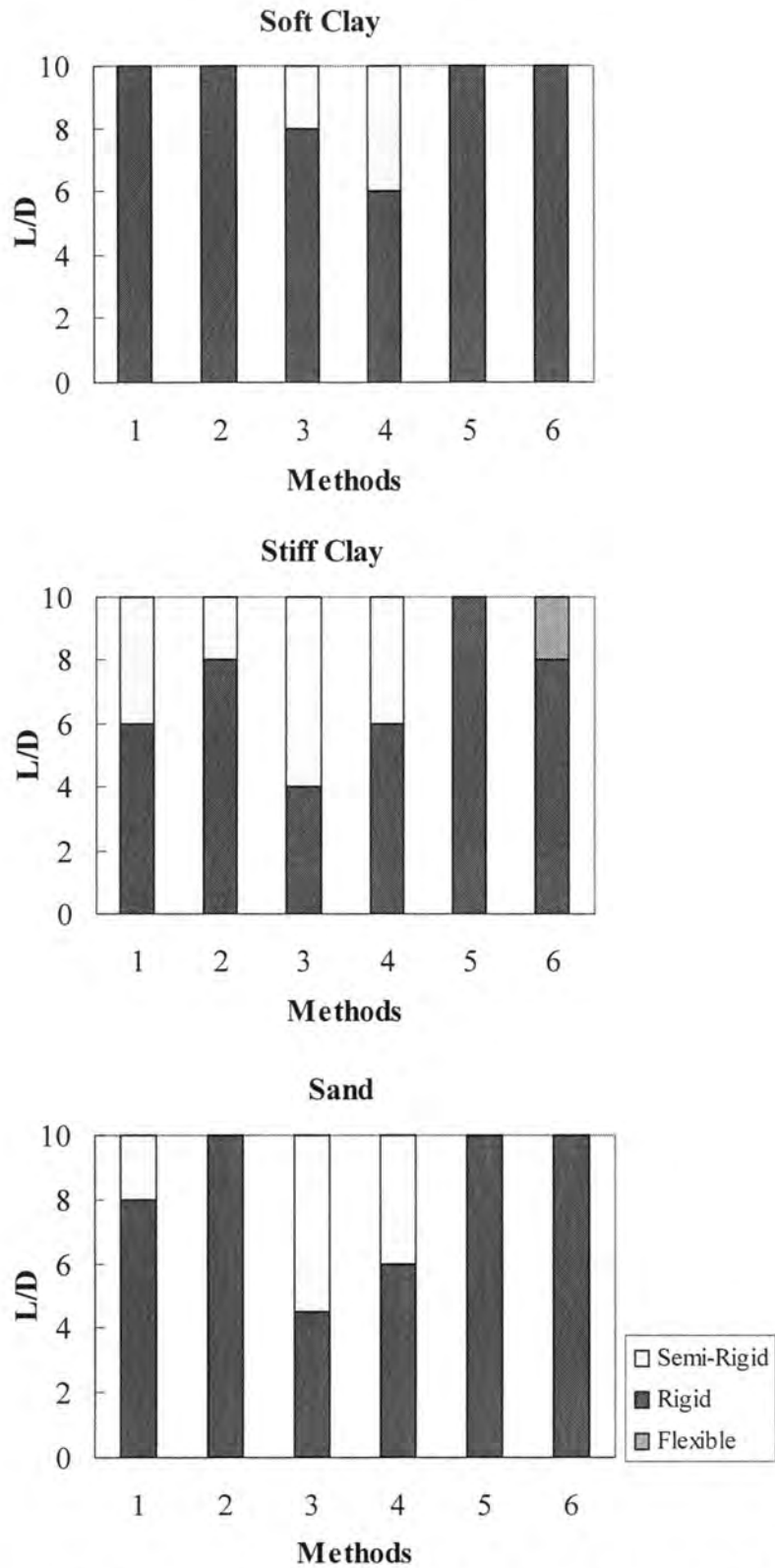
Figure 3.4 Summary of Rigidity Classification by Different Methods (a) Soft Clay (b) Stiff Clay (c) Sand

Table 3.3 Classification of Rigidity in Soft Clay

L(m)	D(m)	L/D	I (m⁴)	K(kPa)	R (m)	Methods					
						1	2	3	4	5	6
3.05	0.91	3.33	0.034	1154	7.37	R	R	R	R	R	R
2.74	0.91	3	0.034	1119	7.43	R	R	R	R	R	R
2.44	0.91	2.67	0.034	1089	7.48	R	R	R	R	R	R
2.13	0.91	2.33	0.034	1054	7.54	R	R	R	R	R	R
1.83	0.91	2	0.034	1024	7.60	R	R	R	R	R	R
1.52	0.91	1.67	0.034	989	7.66	R	R	R	R	R	R
3.05	0.76	4	0.017	1201	6.08	R	R	R	R	R	R
2.74	0.76	3.6	0.017	1164	6.13	R	R	R	R	R	R
2.44	0.76	3.2	0.017	1127	6.18	R	R	R	R	R	R
2.13	0.76	2.8	0.017	1090	6.23	R	R	R	R	R	R
1.83	0.76	2.4	0.017	1053	6.29	R	R	R	R	R	R
1.52	0.76	2	0.017	1012	6.35	R	R	R	R	R	R
3.05	0.61	5	0.007	1271	4.80	R	R	R	R	R	R
2.74	0.61	4.5	0.007	1225	4.84	R	R	R	R	R	R
2.44	0.61	4	0.007	1179	4.89	R	R	R	R	R	R
2.13	0.61	3.5	0.007	1139	4.93	R	R	R	R	R	R
1.83	0.61	3	0.007	1093	4.98	R	R	R	R	R	R
1.52	0.61	2.5	0.007	1052	5.03	R	R	R	R	R	R
3.05	0.46	6.67	0.002	1388	3.52	R	R	R	S	R	R
2.74	0.46	6	0.002	1334	3.56	R	R	R	S	R	R
2.44	0.46	5.33	0.002	1273	3.60	R	R	R	R	R	R
2.13	0.46	4.67	0.002	1219	3.64	R	R	R	R	R	R
1.83	0.46	4	0.002	1165	3.68	R	R	R	R	R	R
1.52	0.46	3.33	0.002	1104	3.73	R	R	R	R	R	R
3.05	0.30	10	4E-04	1610	2.26	R	R	S	S	S	R
2.74	0.30	9	4E-04	1530	2.29	R	R	S	S	R	R
2.44	0.30	8	4E-04	1461	2.32	R	R	S	S	R	R
2.13	0.30	7	4E-04	1380	2.35	R	R	R	S	R	R
1.83	0.30	6	4E-04	1300	2.39	R	R	R	S	R	R
1.52	0.30	5	4E-04	1219	2.42	R	R	R	R	R	R

Table 3.4 Classification of Rigidity in Stiff Clay

L(m)	D(m)	L/D	I (m^4)	K(kPa)	R (m)	Methods					
						1	2	3	4	5	6
3.05	0.91	3.33	0.034	20125	3.61	R	R	R	R	R	R
2.74	0.91	3	0.034	19588	3.63	R	R	R	R	R	R
2.44	0.91	2.67	0.034	19033	3.66	R	R	R	R	R	R
2.13	0.91	2.33	0.034	18496	3.68	R	R	R	R	R	R
1.83	0.91	2	0.034	17959	3.71	R	R	R	R	R	R
1.52	0.91	1.67	0.034	17403	3.74	R	R	R	R	R	R
3.05	0.76	4	0.017	20953	2.98	R	R	S	R	R	R
2.74	0.76	3.6	0.017	20309	3.00	R	R	R	R	R	R
2.44	0.76	3.2	0.017	19688	3.02	R	R	R	R	R	R
2.13	0.76	2.8	0.017	19067	3.05	R	R	R	R	R	R
1.83	0.76	2.4	0.017	18446	3.07	R	R	R	R	R	R
1.52	0.76	2	0.017	17802	3.10	R	R	R	R	R	R
3.05	0.61	5	0.007	22166	2.35	R	R	S	R	R	R
2.74	0.61	4.5	0.007	21419	2.37	R	R	S	R	R	R
2.44	0.61	4	0.007	20671	2.39	R	R	S	R	R	R
2.13	0.61	3.5	0.007	19924	2.41	R	R	R	R	R	R
1.83	0.61	3	0.007	19176	2.43	R	R	R	R	R	R
1.52	0.61	2.5	0.007	18429	2.46	R	R	R	R	R	R
3.05	0.46	6.67	0.002	24227	1.72	S	R	S	S	R	R
2.74	0.46	6	0.002	23268	1.74	S	R	S	S	R	R
2.44	0.46	5.33	0.002	22310	1.76	R	R	S	R	R	R
2.13	0.46	4.67	0.002	21352	1.78	R	R	S	R	R	R
1.83	0.46	4	0.002	20393	1.80	R	R	S	R	R	R
1.52	0.46	3.33	0.002	19435	1.82	R	R	R	R	R	R
3.05	0.30	10	4E-04	28290	1.10	F	S	S	S	S	F
2.74	0.30	9	4E-04	26910	1.12	S	S	S	S	R	F
2.44	0.30	8	4E-04	25530	1.13	S	S	S	S	R	F
2.13	0.30	7	4E-04	24150	1.15	S	R	S	S	R	R
1.83	0.30	6	4E-04	22828	1.17	S	R	S	S	R	R
1.52	0.30	5	4E-04	21505	1.18	R	R	S	R	R	R

Table 3.5 Classification of Rigidity in Sand

L(m)	D(m)	L/D	I (m⁴)	K(kPa)	R (m)	Methods					
						1	2	3	4	5	6
3.05	0.91	3.33	0.034	14180	3.94	R	R	R	R	R	R
2.74	0.91	3	0.034	12834	4.04	R	R	R	R	R	R
2.44	0.91	2.67	0.034	11523	4.15	R	R	R	R	R	R
2.13	0.91	2.33	0.034	10005	4.30	R	R	R	R	R	R
1.83	0.91	2	0.034	8522	4.47	R	R	R	R	R	R
1.52	0.91	1.67	0.034	6969	4.70	R	R	R	R	R	R
3.05	0.76	4	0.017	13701	3.31	R	R	R	R	R	R
2.74	0.76	3.6	0.017	12542	3.38	R	R	R	R	R	R
2.44	0.76	3.2	0.017	11341	3.47	R	R	R	R	R	R
2.13	0.76	2.8	0.017	9975	3.58	R	R	R	R	R	R
1.83	0.76	2.4	0.017	8609	3.72	R	R	R	R	R	R
1.52	0.76	2	0.017	6995	3.92	R	R	R	R	R	R
3.05	0.61	5	0.007	12785	2.69	R	R	S	R	R	R
2.74	0.61	4.5	0.007	11854	2.75	R	R	S	R	R	R
2.44	0.61	4	0.007	10974	2.80	R	R	R	R	R	R
2.13	0.61	3.5	0.007	9783	2.88	R	R	R	R	R	R
1.83	0.61	3	0.007	8593	2.98	R	R	R	R	R	R
1.52	0.61	2.5	0.007	7143	3.12	R	R	R	R	R	R
3.05	0.46	6.67	0.002	7767	2.29	R	R	S	S	R	R
2.74	0.46	6	0.002	7334	2.32	R	R	S	S	R	R
2.44	0.46	5.33	0.002	6900	2.36	R	R	S	R	R	R
2.13	0.46	4.67	0.002	6269	2.41	R	R	R	R	R	R
1.83	0.46	4	0.002	5678	2.48	R	R	R	R	R	R
1.52	0.46	3.33	0.002	4810	2.58	R	R	R	R	R	R
3.05	0.30	10	4E-04	6416	1.60	S	R	S	S	S	R
2.74	0.30	9	4E-04	5546	1.66	S	R	S	S	R	R
2.44	0.30	8	4E-04	4677	1.73	S	R	S	S	R	R
2.13	0.30	7	4E-04	4263	1.77	R	R	S	S	R	R
1.83	0.30	6	4E-04	3891	1.81	R	R	S	S	R	R
1.52	0.30	5	4E-04	3436	1.87	R	R	R	R	R	R

Note: R=Rigid, S=Semi-Rigid, F=Flexible.

For method 6, Reese *et al.* (2000) did not provide the load used in the determination of critical length. In this parametric study, different loads were used to examine the critical length. The critical length/diameter as a function of loading is presented in Figures 3.5 to 3.9.

As shown in Figures 3.5 to 3.9, when the diameter D is constant, the critical length depends on the loading in soft clay, but almost independent of loading in sand and stiff clay. In soft clay, the critical length increases as load increases. In stiff clay and sand, the loads used in the study are not large enough to have an effect on the critical length. However, there is a general trend of increasing because as the load increases, the deeper soil may begin to exert resistance to the pier, thus the critical length increases. Figures 3.5 to 3.9 also show that critical length is largest in soft clay, intermediate in sand and smallest in stiff clay. The reason is that a pier may become flexible at a small L/D ratio in stiff clay, while in soft clay and sand, pier should have a larger L/D to behave flexible. In this parametric study, the average values of critical length/diameter (L_{crit}/D) were used in the classification of pier behavior as summarized in Table 3.6.
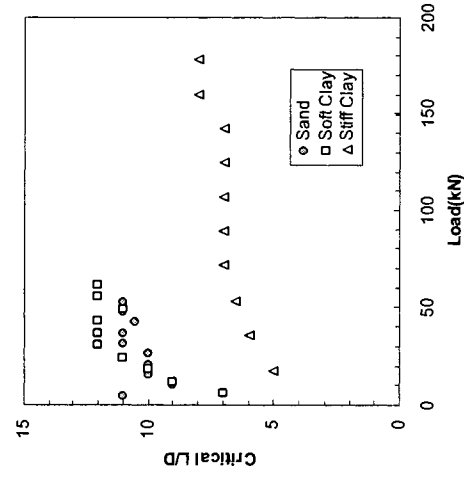
Figure 3.5 Critical L/D as a Function of Load (D = 0.91 m)
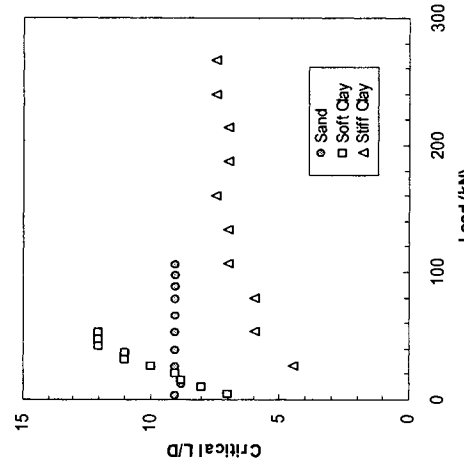
Figure 3.6 Critical L/D as a Function of Load (D = 0.76 m)

Figure 3.7 Critical L/D as a Function of Load (D = 0.61 m)
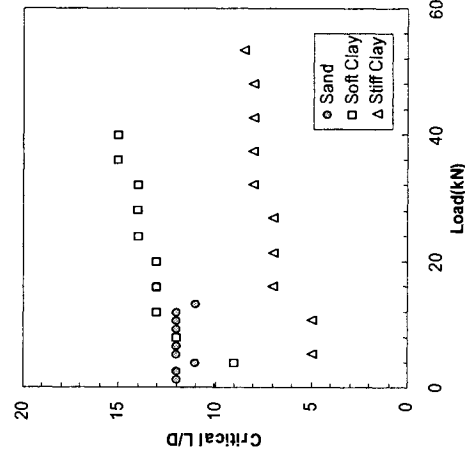
Figure 3.8 Critical L/D as a Function of Load (D = 0.46 m)
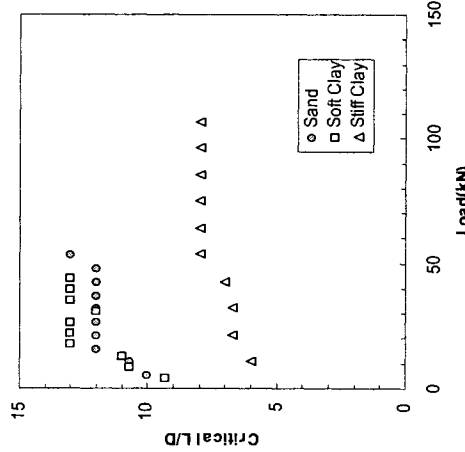
Figure 3.9 Critical L/D as a Function of Load (D = 0.3 m)

Table 3.6 Critical Length-Diameter Ratio (Average) in Different Soils

Diameter (m)	L_{crit}/D		
	Sand	Stiff Clay	Soft Clay
0.30	11.8	7.2	13.2
0.46	11.8	7.4	12.1
0.61	10.5	6.8	10.8
0.76	9	6.7	10.1
0.91	8.8	6.3	9.5

3.5 Determination of Q_{ult}

In this parametric study, lateral load capacity Q_{ult} was determined by absolute displacement of 0.25 inch, 0.5 inch, and 1 inch, absolute rotation of 1 degree and 2 degrees, fixed percentage of pile diameter of 1%, 2%, 5%, 10%, and 20%. Q_{ult} determined by each method in different soils, is summarized in Tables 3.7 to 3.9.

Table 3.7 Lateral Load Capacity in Soft Clay

Length m	Diameter m	Q_{ult} (kN)									
		s=6.35 mm	s=12.7 mm	s=25.4 mm	s= 1%D	s= 2%D	s= 5%D	s= 10%D	s= 20%D	$R=1^0$	$R=2^0$
1.52	0.30	6	8	10	5	6	8	11	13	10	13
1.83	0.30	8	10	12	6	8	10	13	17	13	17
2.13	0.30	9	12	15	7	9	13	16	20	17	21
2.44	0.30	11	14	18	9	11	15	19	24	21	26
2.74	0.30	13	16	20	10	13	17	21	27	25	32
3.05	0.30	14	17	22	11	14	19	24	31	29	38
1.52	0.46	8	10	12	7	9	12	15	19	12	16
1.83	0.46	10	12	15	9	11	15	18	23	16	21
2.13	0.46	11	14	18	10	13	18	22	28	21	26
2.44	0.46	13	17	21	12	15	21	26	33	25	32
2.74	0.46	15	20	25	14	18	24	30	38	31	38
3.05	0.46	18	22	28	16	20	27	34	43	36	45
1.52	0.61	9	11	14	9	11	15	19	24	14	18
1.83	0.61	11	14	18	11	14	19	24	30	19	24
2.13	0.61	13	17	21	13	16	22	28	35	24	30
2.44	0.61	16	20	25	15	19	26	33	42	29	37
2.74	0.61	18	23	28	18	22	30	38	48	35	44
3.05	0.61	20	26	32	20	25	34	43	54	41	52
1.52	0.76	10	13	16	11	14	19	23	29	16	21
1.83	0.76	13	16	20	13	17	23	29	36	21	27
2.13	0.76	15	19	24	16	20	27	34	43	27	34
2.44	0.76	17	22	28	19	23	32	40	50	33	41
2.74	0.76	20	25	32	21	27	36	46	58	39	50
3.05	0.76	23	29	36	24	30	41	52	66	46	58
1.52	0.91	11	14	18	13	16	22	28	35	18	23
1.83	0.91	14	18	22	16	20	27	34	43	24	30
2.13	0.91	17	21	26	19	24	32	40	51	30	38
2.44	0.91	19	24	31	22	27	37	47	59	36	46
2.74	0.91	22	28	35	25	31	43	54	68	43	55
3.05	0.91	25	32	40	28	36	48	61	77	51	64

Table 3.8 Lateral Load Capacity in Stiff Clay

Length m	Diameter m	Q_{ult} (kN)									
		s=6.35 mm	s=12.7 mm	s=25.4 mm	s= 1%D	s= 2%D	s= 5%D	s= 10%D	s= 20%D	$R=1^0$	$R=2^0$
1.52	0.30	36	43	52	30	36	46	55	65	53	63
1.83	0.30	43	53	64	34	42	55	67	81	68	82
2.13	0.30	46	60	74	34	45	63	79	96	83	101
2.44	0.30	47	63	82	35	46	68	88	103	97	106
2.74	0.30	47	63	85	35	46	68	90	103	100	105
3.05	0.30	47	63	85	35	46	68	90	103	101	106
1.52	0.46	47	56	67	44	52	65	78	92	68	81
1.83	0.46	58	69	82	54	64	80	96	114	87	104
2.13	0.46	69	82	98	63	75	95	114	136	108	129
2.44	0.46	77	94	114	70	86	111	133	160	131	157
2.74	0.46	83	104	128	74	94	124	151	182	153	184
3.05	0.46	86	112	142	76	99	137	170	202	177	205
1.52	0.61	57	67	80	56	67	84	100	119	81	97
1.83	0.61	70	83	99	69	82	103	123	146	104	124
2.13	0.61	83	99	118	82	98	123	146	174	130	154
2.44	0.61	97	116	137	96	114	143	171	204	156	186
2.74	0.61	109	129	155	108	128	163	195	233	183	219
3.05	0.61	118	144	175	117	143	184	222	265	214	256
1.52	0.76	66	78	93	69	82	103	122	145	94	112
1.83	0.76	80	96	114	84	100	126	150	178	120	143
2.13	0.76	96	114	135	100	119	150	178	212	149	177
2.44	0.76	112	133	158	117	139	175	208	248	180	214
2.74	0.76	127	152	181	133	159	200	238	283	212	252
3.05	0.76	145	173	206	152	181	228	270	322	247	294
1.52	0.91	74	88	105	81	97	122	144	172	106	126
1.83	0.91	91	108	128	99	118	149	177	210	136	161
2.13	0.91	108	128	152	118	140	176	210	250	168	199
2.44	0.91	125	149	177	137	163	206	244	291	202	240
2.74	0.91	143	170	203	157	186	235	279	332	237	282
3.05	0.91	162	193	230	178	212	266	316	377	276	329

Table 3.9 Lateral Load Capacity in Sand

Length m	Diameter m	Q_{ult} (kN)								$R=1^0$	$R=2^0$
		s=6.35 mm	s=12.7 mm	s=25.4 mm	s= 1%D	s= 2%D	s= 5%D	s= 10%D	s= 20%D		
1.52	0.30	5	6	8	4	5	7	8	9	8	9
1.83	0.30	6	9	11	5	6	9	12	13	12	13
2.13	0.30	9	12	15	6	8	13	16	18	17	18
2.44	0.30	11	15	20	8	11	16	21	25	23	25
2.74	0.30	13	18	25	9	13	20	27	32	30	33
3.05	0.30	15	23	32	10	15	25	34	42	40	45
1.52	0.46	6	8	10	6	7	10	12	13	11	12
1.83	0.46	9	11	15	8	10	14	17	19	16	18
2.13	0.46	12	15	20	10	13	19	23	26	22	25
2.44	0.46	15	20	26	13	17	25	30	34	30	34
2.74	0.46	18	24	32	16	21	31	38	43	38	43
3.05	0.46	22	30	40	19	26	38	48	55	50	56
1.52	0.61	8	10	13	8	10	13	16	17	13	15
1.83	0.61	11	14	18	11	14	19	23	25	20	23
2.13	0.61	15	19	24	15	19	26	31	34	28	32
2.44	0.61	19	24	31	19	24	34	40	44	37	43
2.74	0.61	23	30	39	23	29	41	50	55	48	54
3.05	0.61	28	37	48	28	36	52	63	70	61	69
1.52	0.76	9	12	15	10	12	17	19	21	15	18
1.83	0.76	13	17	21	14	18	24	28	31	23	27
2.13	0.76	17	23	28	19	24	33	38	42	32	38
2.44	0.76	23	29	37	24	31	42	50	55	44	51
2.74	0.76	28	36	45	30	38	53	63	69	57	65
3.05	0.76	34	44	56	36	47	65	79	87	73	84
1.52	0.91	10	13	16	12	15	20	23	25	17	21
1.83	0.91	14	19	24	17	21	29	34	37	26	32
2.13	0.91	19	26	32	23	29	39	46	50	37	45
2.44	0.91	25	34	42	30	38	52	61	66	50	60
2.74	0.91	32	42	52	37	47	64	76	83	65	77
3.05	0.91	39	51	65	46	58	80	95	104	84	98

Table 3.10 presents the comparison of different ultimate load as defined by a fixed percentage of pier diameter. For example, the average ratio of $Q_{1\%}$, $Q_{2\%}$, $Q_{5\%}$, $Q_{20\%}$ to $Q_{10\%}$ is about 0.53, 0.64, 0.83, and 1.19 for stiff clay, with small deviations (0.02-0.06). For soft clay and sand, those values are close to stiff clay. The load increases about 100% when

displacement increases from 1%D to 10%D, but only increases about 20% from 10%D to 20%D.

Table 3.10 Comparison of Different Ultimate Lateral Load

	Stiff Clay				Soft Clay				Sand			
	$Q_{1\%}/$ $Q_{10\%}$	$Q_{2\%}/$ $Q_{10\%}$	$Q_{5\%}/$ $Q_{10\%}$	$Q_{20\%}/$ $Q_{10\%}$	$Q_{1\%}/$ $Q_{10\%}$	$Q_{2\%}/$ $Q_{10\%}$	$Q_{5\%}/$ $Q_{10\%}$	$Q_{20\%}/$ $Q_{10\%}$	$Q_{1\%}/$ $Q_{10\%}$	$Q_{2\%}/$ $Q_{10\%}$	$Q_{5\%}/$ $Q_{10\%}$	$Q_{20\%}/$ $Q_{10\%}$
Average	0.53	0.64	0.83	1.19	0.46	0.58	0.79	1.26	0.45	0.58	0.83	1.11
Standard Deviation	0.06	0.05	0.03	0.02	0	0	0	0.01	0.05	0.05	0.03	0.03

Analyses were conducted on piers constructed at the SGES to investigate pier ultimate load capacity. The computer software MCURV was used in the analyses to obtain the pier yielding moment M_n, which is the transitional moment between elastic and plastic behavior, and breaking moment M_u, which is the maximum moment, as shown in Table 3.11. Figure 3.10 presents the moment as a function of pier diameter. From Figure 3.10 it can be seen that M_n and M_u are proportionally related to diameter. Given the values of M_n and M_u, the yielding and breaking displacement of a pier can be determined using LPILE program, which is summarized in Table 3.12.

Table 3.12 shows that a pier may yield or break at different displacement in sand, soft clay, and stiff clay. For example, a pier with diameter of 0.91m yields at displacement-diameter ratio (s_f/D) equals to 6.3% in sand, 13.2% in soft clay, and only 4.8% in stiff clay. It is reasonable because in soft clay the pier exhibits rigid behavior and the soil may fail first. While in stiff clay the pier may become flexible and yields at smaller displacement. Table 3.12 also shows that even in the same soil, different pier diameter has different s_f/D at yielding or breaking. For example in sand, piers with diameters of 0.91, 0.76, 0.61, 0.46, and

0.3 m yield at s_f/D=6.3%, 7.7%, 16.6%, 19.1%, and 32.1%, respectively. The pier with larger diameter may yield or break at smaller displacement.

Table 3.11 Summary of M_u, M_n for Different Pier Diameters

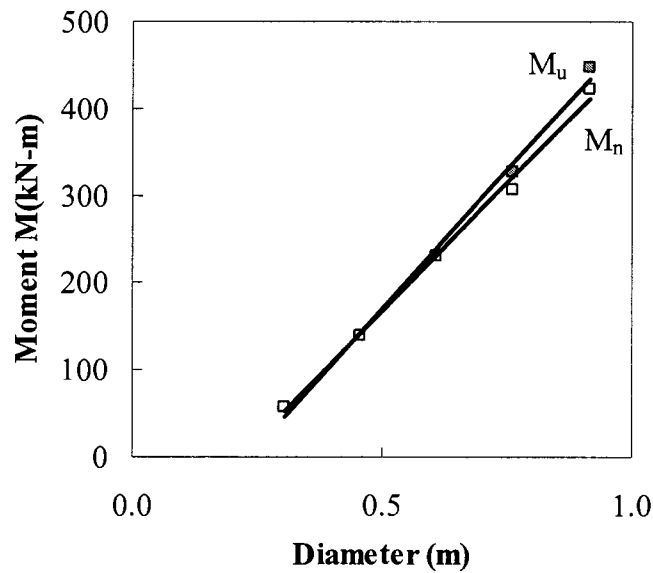| Diameter m	M_u kN-m	ε_s'	M_y' kN-m	ϕ_y' 1/m	M_n kN-m	ϕ_n 1/m
0.91	448	0.00207	291	0.00308	422	0.0045
0.76	326	0.00207	207	0.00388	305	0.0057
0.61	232	0.00207	159	0.00532	231	0.0078
0.46	140	0.00207	97	0.00803	139	0.0115
0.30	57	0.00207	43	0.01566	57	0.0206

Figure 3.10 Breaking Moment and Yielding Moment as A Function of Diameter

Table 3.12 Displacement-Diameter Ratio (s/D) at Which Piles Yield or Break

Sand					
D(m)	0.91	0.76	0.61	0.46	0.3
s/D (M_u)	10.5%	10.5%	16.6%	19.1%	32.1%
s/D (M_n)	6.3%	7.7%	16.6%	19.1%	32.1%
Soft Clay					
D(m)	0.91	0.76	0.61	0.46	0.3
s/D (M_u)	23.5%	33.3%	17.5%	37.2%	NA
s/D (M_n)	13.2%	17%	17.5%	37.2%	NA
Stiff Clay					
D(m)	0.91	0.76	0.61	0.46	0.3
s/D (M_u)	8.5%	6.5%	8.2%	12.9%	18.9%
s/D (M_n)	4.8%	6%	8.2%	12.9%	18.9%

Note: NA = Not Available

3.6 Nondimensional Expression of Load-Displacement Results

The load-displacement behavior of piles may be expressed in nondimensional terms by normalizing the load by the interpreted ultimate lateral load capacity, Q_{ult} (Q at s/D = 1%, 2%, 5%, 10%, and 20%), and normalizing the displacement, s, by s_f (s_f/D = 1%, 2%, 5%, 10%, and 20%). Figures 3.11 to 3.16 present the normalized results for all piers except those didn't reach 10%D or 20%D displacement at M_u.
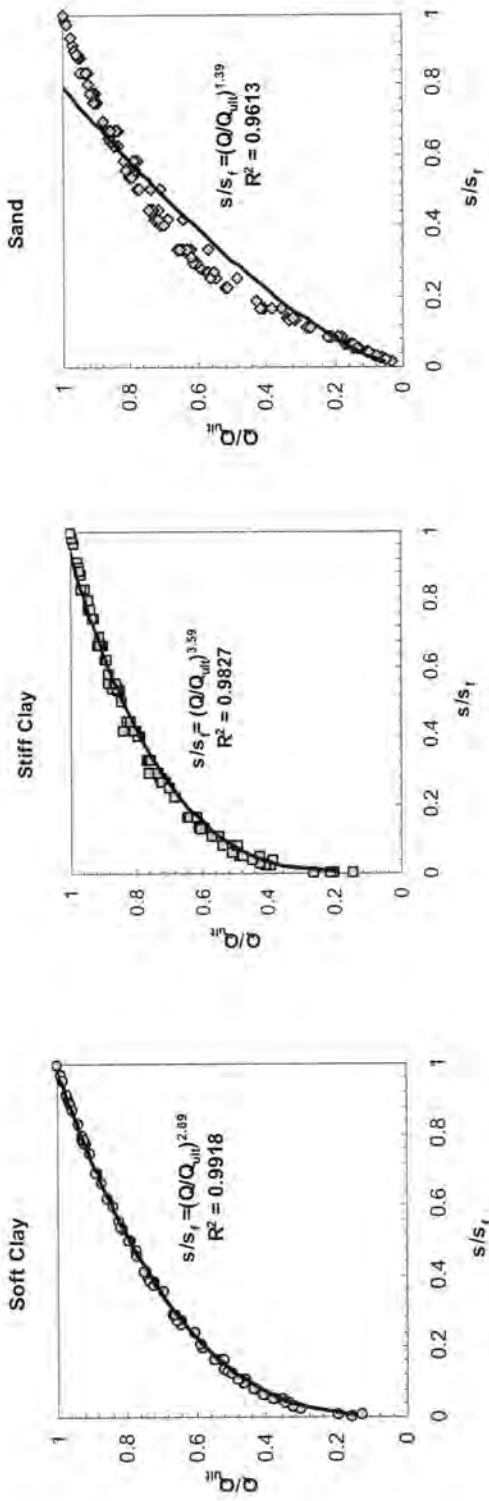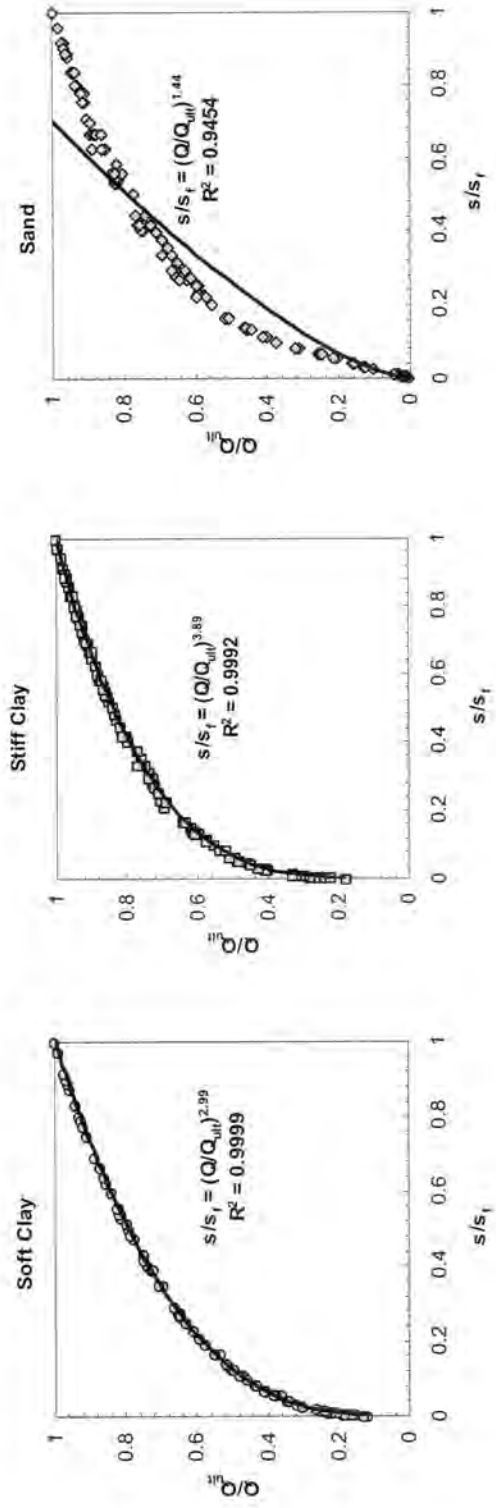
Figure 3.11 Normalized Results sf/D= 1% (LPILE)

Figure 3.12 Normalized Results sf/D= 2% (LPILE)

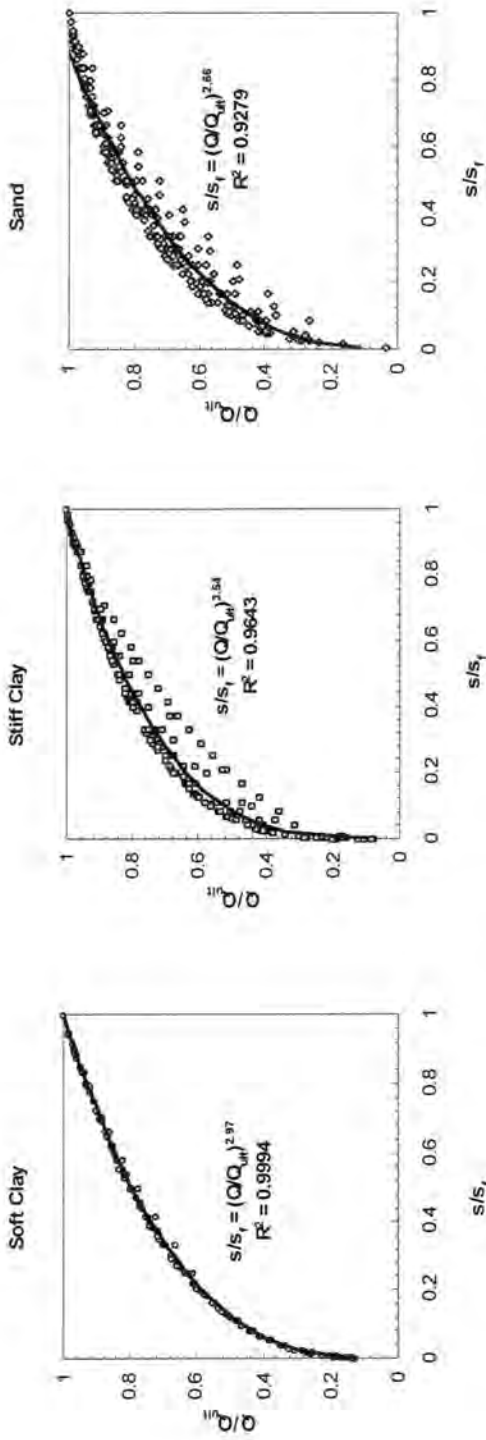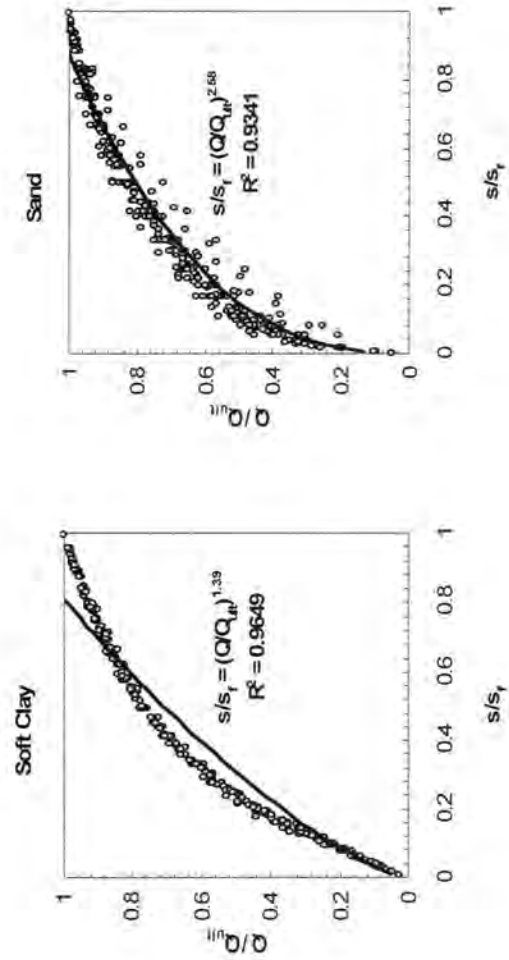**Figure 3.13 Normalized Results sf/D= 10% (LPILE)**

Figure 3.14 Normalized Results sf/D= 10% (LTBASE)
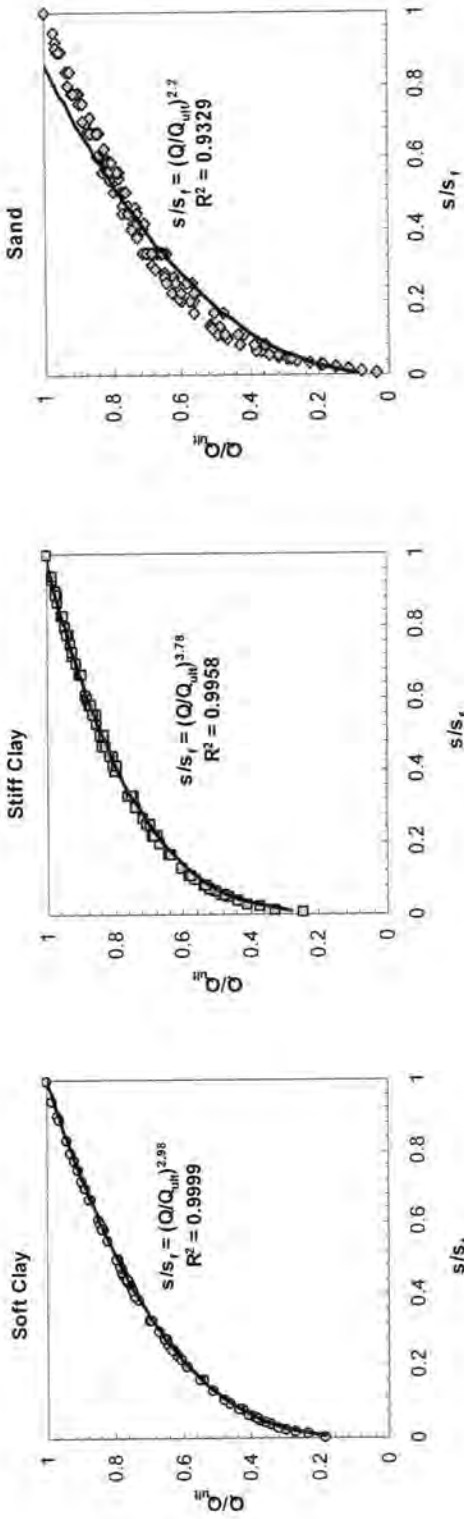
Figure 3.15 Normalized Results sf/D= 5% (LPILE)
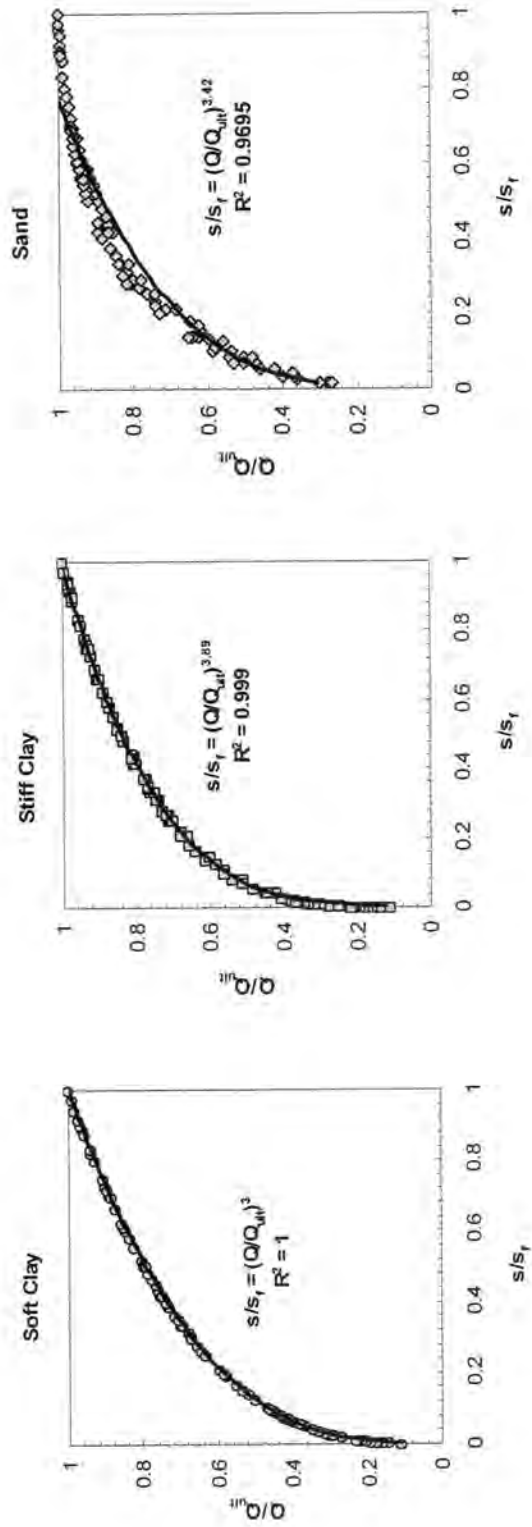
Figure 3.16 Normalized Results sf/D= 20% (LPILE)

The normalized model parameters: exponent, coefficient, and R^2 values for each soil are summarized in Table 3.13. R^2 values range from 0.93 to 1, which indicates nondimensional load-displacement curve can be expressed by a power function. The exponent ranges from 2.89 to 3 for soft clay, 3.54 for 3.89 for stiff clay, and 1.39 to 3.42 for sand. The variation is very small in stiff and soft clay, while in sand, it is very large because p-y curves for soft clay and stiff clay used in this study are power functioned, which have the exponents of 1/3, and 1/4, respectively; while for sand, the p-y curve consists of four portions: three straight lines and one parabolic curve.

The normalized results of LPILE and LTBASE were compared at $s_f/D=10\%$ in sand and soft clay. For soft clay, p-y curves proposed by Reese and Allen (1977) are used in both LPILE and LTBASE for comparison. It can be seen from Table 3.13 that LPILE and LTBASE have very similar R^2, coefficients, and exponents because the same p-y curves were used.

Table 3.13 Normalized Model Parameters (Q_{ult} at s/D=1%, 2%, 5%, 10%, 20%)

Soil Type	R^2				
	1%	2%	5%	10%	20%
Soft Clay (Matlock 1970)	0.99	1	1	1	--	1
Stiff Clay (Reese and Welch 1975)	0.98	1	1	0.96	--	1
Sand (Reese et al. 1974)	0.96	0.95	0.93	0.93	0.93*	0.97
Soft Clay (Reese and Allen 1977)	--	--	--	0.96	0.96*	--

	Coefficients				
	1%	2%	5%	10%	20%
Soft Clay (Matlock 1970)	1.01	1	1	1	--	1
Stiff Clay (Reese and Welch 1975)	1.02	1	1.01	1.01	--	1
Sand (Reese et al. 1974)	1.18	1.28	1.07	1.05	1.05*	1.08
Soft Clay (Reese and Allen 1977)	--	--	--	1.14	1.17*	--

	Exponents				
	1%	2%	5%	10%	20%
Soft Clay (Matlock 1970)	2.89	2.99	2.98	2.97	--	3
Stiff Clay (Reese and Welch 1975)	3.59	3.89	3.78	3.54	--	3.89
Sand (Reese et al. 1974)	1.39	1.44	2.2	2.66	2.58*	3.42
Soft Clay (Reese and Allen 1977)	--	--	--	1.47	1.39*	--

Note: * values obtained by LTBASE; others are by LPILE.
-- Analyses not conducted.

3.7 Normalized Results of Base Shear Using LTBASE

By using the LTBASE program, the base shear was calculated for each pier and compared with the ultimate pier capacity. Figure 3.17 presents the normalized results of pier base shear in both sand and soft clay. The base shear is normalized by Q_{ult} (s_f=10%D). Base shear/Q_{ult} decreases dramatically with increasing L/D and approaches to zero. From Figure 3.17 it can be seen that, base shear is less than 10%Q_{ult} when L/D is greater than about 5 for sand, and 13 for soft clay.
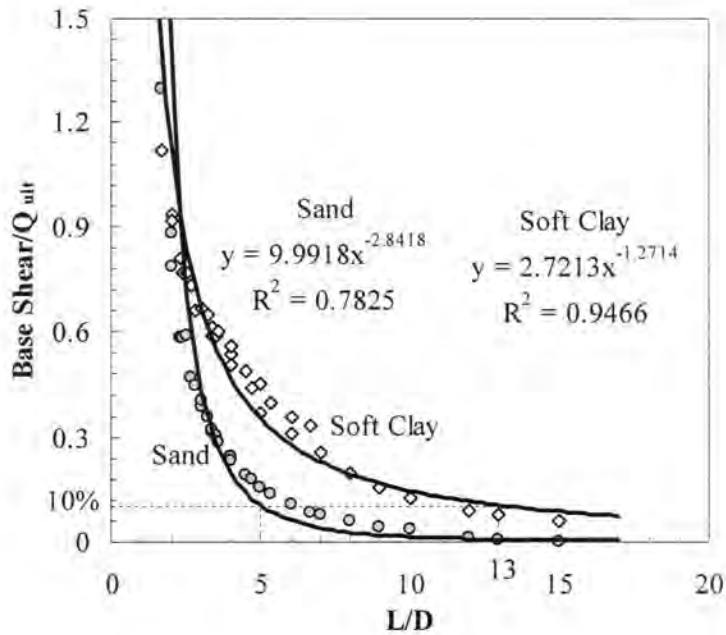
Figure 3.17 Normalized Results of Base Shear for Sand and Soft Clay

3.8 Comparison of Q_{ult} between LPILE and LTBASE

In LPILE, the load-deflection analysis of laterally loaded piers is conducted without consideration of the influence of base shear. Although this assumption is valid for piers with relatively large L/D ratios, for the case of short rigid piers, the effect of base shear is significant.

Due to the base shear effect, Q_{ult} calculated by LTBASE should be larger than that calculated by LPILE. Piers with L/D ranging from 0.25 to 15 embedded in sand were investigated and Q_{ult} were compared between LPILE and LTBASE, as shown in Figure 3.18. With all other parameters constant, Figure 3.18 shows that there is significant difference in Q_{ult} between LPILE and LTBASE when L/D ≤ 2. When L/D is 2, Q_{ult} by LPILE is about

90% of that by LTBASE; when L/D is 4, it is about 95% and that base shear effect is negligible.
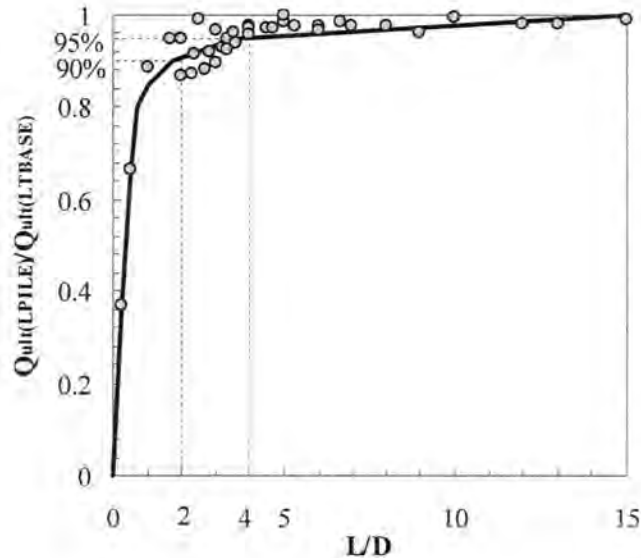
Figure 3.18 Comparison of Qult from LPILE and LTBASE

3.9 Problems in the Parametric Study

- ✓ In soft clay, piers always appear as rigid and it is hard to reach breaking moment. Hence, it is difficult to find the displacement at which the pier yields or breaks.

- ✓ LTBASE does not include user-input p-y curves in the analysis. The p-y curves are generated by the program itself. There are three types of p-y curves in LTBASE program. For sand, p-y curves are generated using the procedure developed by Reese *et al.* (1974). For clay, p-y curves are generated using the unified method developed by Reese and Allen (1977) or by Parker *et al.* (1971).

✓ In LTBASE, the number of increments into which a pier is divided influences the load-deflection curves. When the number of increments increases, Q_{ult} also increases and base shear decreases. This problem is shown in Figure 3.19. A pier with length of 1.52 m, diameter of 0.61 m was investigated, and the pier length was divided into 5, 10, 20, 40, and 80 increments, respectively. Figure 3.19 shows that the top shear calculated by LTBASE varies from 23 kN to 30 kN, and the base shear varies from 14 kN to 2 kN. While the shear calculated by LPILE is independent of number of increments. It is also shown in Figure 3.19 that when the number of increments equals 5, the shear calculated by LPILE and LTBASE is very close. Hence, 5 was taken as number of increments in the calculation. In this parametric study, it is assumed that 0.3 m (1ft) is one increment length for all piers analyzed by LTBASE.
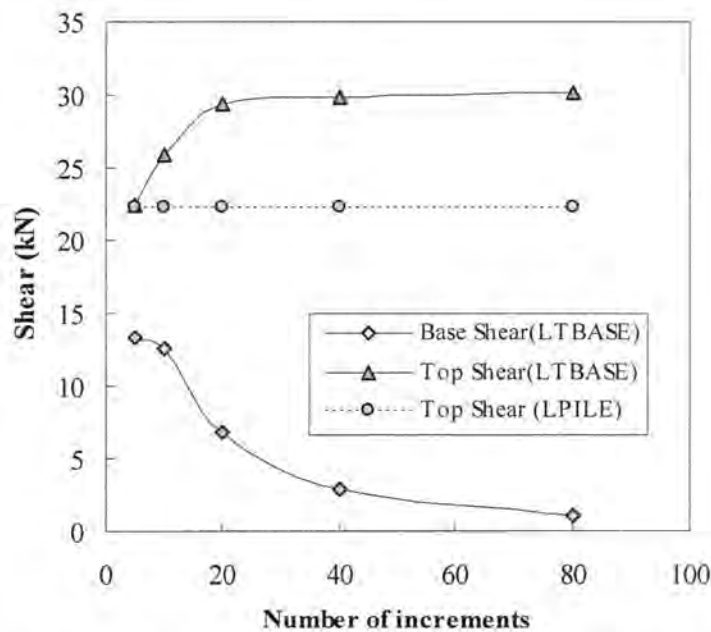

Figure 3.19 Effect of Number of Increments on Shear (LTBASE) (D=0.61 m, L=1.52 m)

CHAPTER 4: FIELD INVESTIGATION AND DISCUSSION

4.1 Introduction

A field investigation was carried out at the SGES to evaluate the soil characteristics and subsurface conditions. The investigation includes laboratory tests and in situ tests. Laboratory tests included: determination of water content, Atterberg limits, grain-size distribution, unconfined compression tests, consolidation tests and consolidated-undrained triaxial tests. The in situ testing consisted of Flat Dilatometer Tests (DMT), Standard Penetration tests (SPT) and Cone Penetration Tests (CPT). Both thermocouples and piezometers were also installed and monitored at the site. The investigation procedures and test results are presented in the following sections.

4.2 Laboratory Tests

Laboratory tests were performed during November, 2002 and July, 2003. 0.76 m (2.5 feet) long, 71 mm (2.8 inch) inside diameter Shelby tubes were pushed with the drill rig to obtain relatively undisturbed samples. Two boring holes were drilled to a depth of 3.81 m (12.5 ft) from ground surface and each has five Shelby tube samples, with which moisture content, grain-size distribution, Atterberg limits, unconfined compressive strength, and consolidation tests were performed. CU triaxial tests samples were obtained from another three boring holes, each to a depth of 1.52 m (5 feet), below which the soil is sandy and samples could not be obtained. Figure 4.1 shows the plan view of SGES Site.
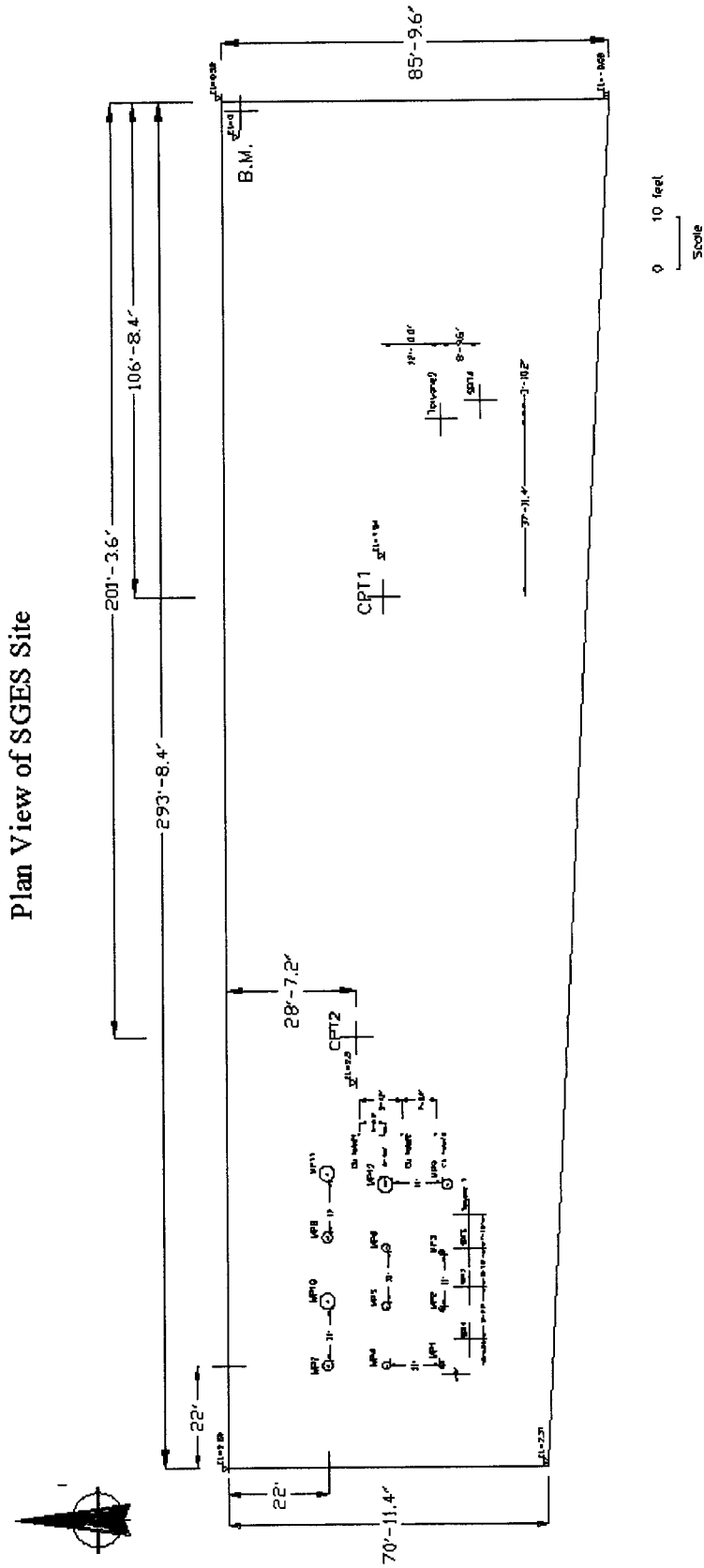
69

Plan View of SGES Site

Figure 4.1 Plan View of SGES

4.2.1 Moisture Content Determination

The natural moisture content of collected soil samples was performed in general accordance with American Society for Testing and Materials (ASTM) Standard D2216-92 (ASTM 1994) Standard Test Method for *Laboratory Determination of Water (Moisture) Content of Soil and Rock*. A specimen from each sample was oven dried at 110^0C for 24 hours for the water content determination.

Figure 4.2 presents the water content of two borings. Samples were taken from ground surface to 3.81 m (12.5 feet) below the ground surface. The water contents ranged from approximately 12% to 27%, with a general trend of decreasing water content with increasing depth, possibly because the upper soils are more affected by infiltration of rainwater and snow. The results of the water content determinations are presented in Appendix B.
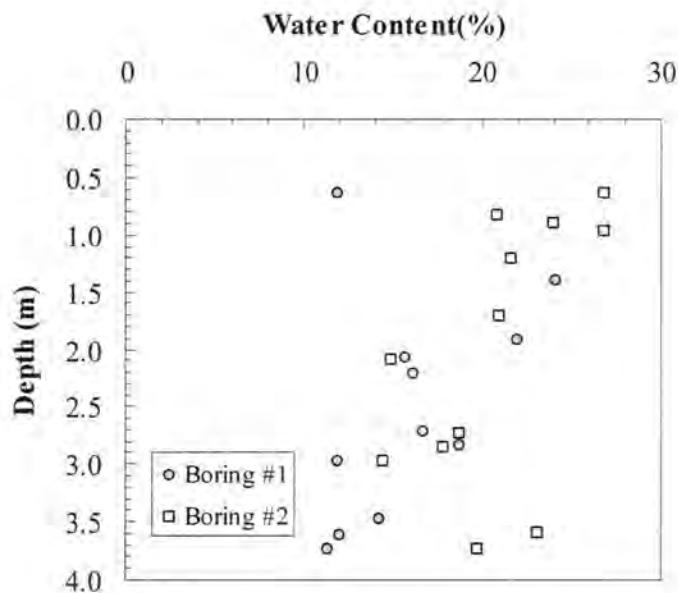

Figure 4.2 Water Content Variations at SGES

4.2.2 Atterberg Liquid and Plastic Limits

The Atterberg Limits of the soil samples were conducted according to ASTM D4318-93(ASTM 1994) *Liquid Limit, Plastic Limit, and Plasticity Index of Soils.* Before the test, the soil was air-dried, pulverized with a rubber tipped pestle, and passed through the No. 40 sieve. Approximately 150 grams of soil was mixed with distilled water to a 15-drop consistency and subsequently placed in the humid room to cure for a minimum of 24 hours. The plastic limits (PL) and liquid limits (LL) of the soil samples were then determined.

A summary of Atterberg Limits are presented along with grain-size distribution results in Table 4.1. Figure 4.3 illustrates the range of natural water content and plasticity over the depth of sampling at the site. From the ground surface to approximately 3.81 m (12.5 feet) the in situ natural water content is below the liquid limit, which is typical for overconsolidated clays.

Figure 4.4 presents the plasticity data plotted on the Casagrande Plasticity Chart. In boring 1, from the ground surface down to approximately 3.05 m (10 feet), the soil samples are in the zone of CL (inorganic clays with low plasticity) or OL (organic silts and organic silty clays with low plasticity); from 3.05 to 3.81 m (10 to 12.5 feet), the soil is in the hatched zone, which is classified as CL-ML (inorganic clays, silts and very fine sands with low plasticity). In boring 2, from ground surface to 0.76 m (2.5 feet) is located below "A" line in the zone of ML (inorganic silts and very fine sands with slight plasticity) or OL; both soil samples from 0.76 to 1.52 m (2.5 to 5 feet) and from 3.05 to 3.81 m (10 to 12.5 feet) are in the hatched zone (CL-ML); while from 1.52 m to 3.05 m (5 feet to 10 feet), the soil is classified as SC (clayey sand) and because the coarse grain (sand and gravel) is greater than

50% it is not plotted in this chart. The Atterberg limits test results are included in Appendix

B.

Table 4.1 Atterberg Limit and Grain-Size Test Results

Boring #1

Depth (m)	w (%)	LL (%)	PL (%)	PI (%)	% Fines	% Clay	% Silt	% Sand	% Gravel	Unified Soil Classification
0-0.76	11.9	31.6	22.7	8.8	77.2	22.1	55.1	22.8	0	CL
0.76-1.52	24.1	31.4	20	11.4	72	15.5	56.5	24.9	3.1	CL
1.52-2.29	18	25	18	7	51.4	26	25.4	45.1	3.5	CL
2.29-3.05	16	26	17	9	52	23	29	40.9	7.2	CL
3.05-3.81	12.5	24.4	19	5.4	50.4	15	35.4	45.1	4.5	CL-ML

Boring #2

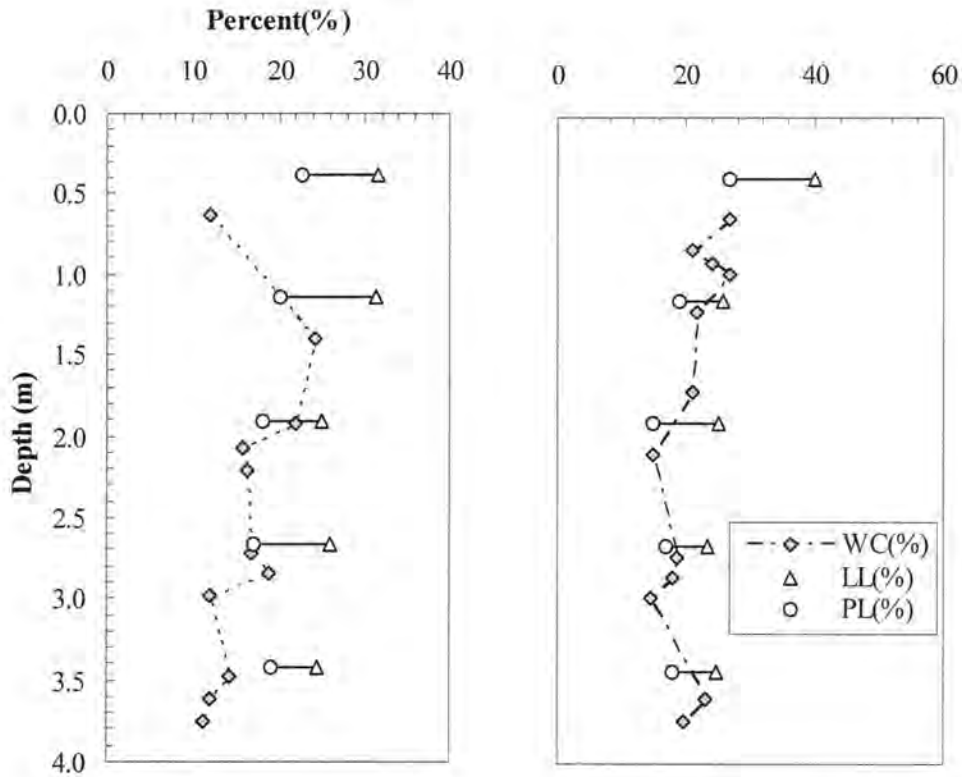| Depth (m)	w (%)	LL (%)	PL (%)	PI (%)	% Fines	% Clay	% Silt	% Sand	% Gravel	Unified Soil Classification
0-0.76	26.9	40	26.7	13.3	75.9	37.3	38.6	24.2	0	ML
0.76-1.52	23.4	25.6	19	6.6	64.6	17	47.6	31.8	3.7	CL-ML
1.52-2.29	18	25	15	10	44.3	23	21.3	52.2	3.5	SC
2.29-3.05	17	23.4	17	6.4	33.1	21	12.1	64.3	2.7	SC
3.05-3.81	22	24.6	18	6.6	56	20	36	41.3	2.7	CL-ML

Figure 4.3 Summary of Atterberg Limits (a) Boring #1 (b) Boring #2
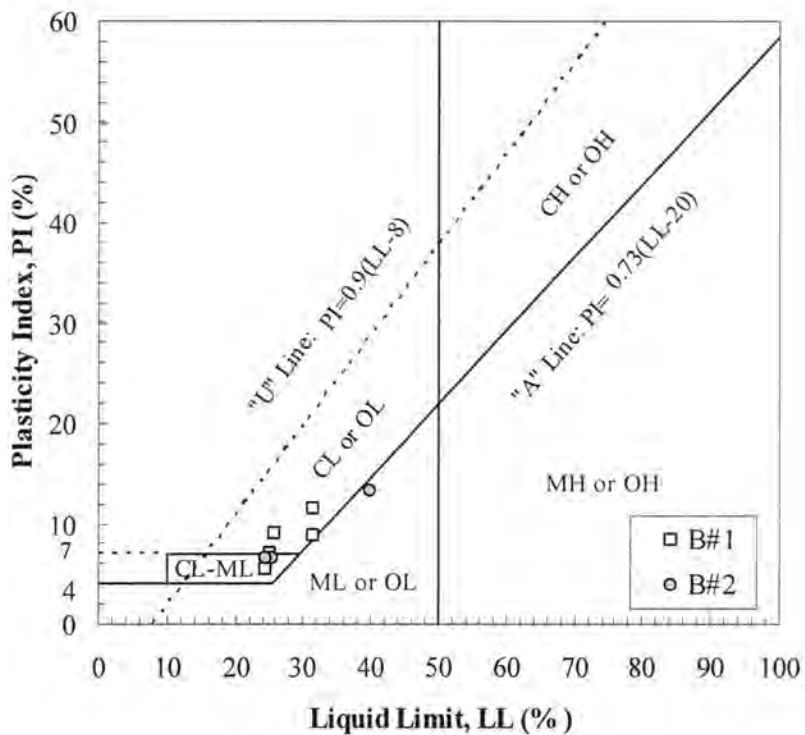

Figure 4.4 Casagrande Plasticity Chart for Soils at SGES

4.2.3 Grain-Size Distribution

Hydrometer Analysis

The grain-size analysis of fine-grained soils conducted according to ASTM Standard D422-63 (ASTM 1994) *Standard Test Method for Particle Size Analysis of soils.* Hydrometer testing was used to determine the corresponding percentages by weight of clay, silt, and sand present in collected samples. Soils were air dried, pulverized with a rubber tipped pestle, and passed through a No.10 sieve prior to testing. Solutions of test soil and dispersing agent (40g/l of sodium hexametaphosphate) were let to soak for 16 hours prior to testing. A 152H hydrometer was used for all hydrometer tests. Following each test, the test soil was wet sieved through a No.200 sieve. The retained soil was oven dried and weighted to determine the percent sand by weight.

Sieve Analysis

The grain-size analysis of soils greater than the No.200 sieve was conducted in general accordance to ASTM Standard D422-63 (ASTM 1994) *Standard Test Method for Particle Size Analysis of Soils.* The distribution of particle sizes was determined for air dried sample using No. 10, 20, 40, 60, 80, 100, and 200 sieves. Grain-size distribution curves were plotted as cumulative percent finer by weight versus the particle diameter. The coefficient of uniformity, C_u, coefficient of gradation, C_c, and the percent fines were determined to complete the grain-size analysis.

A summary of the grain-size distribution results is tabulated in Table 4.2 and presented graphically as grain-size distribution curve in Figure 4.5. Based on the results of the hydrometer analyses and sieve analyses, an indication of the distribution of clay, silt and sand with depth is provided. The plot indicates that the soil is composed of mostly silt and

clay from the surface to about 1.52 m (5 feet) deep. From 1.52 m (5 feet) to 3.81 m (12.5 feet)

is a layer of soil consisting of high percentage of sand, which varies from 21.5% at the

surface to 58.0% at 3.81 m (12.5 feet). The grain size distribution curves are included in

Appendix B.
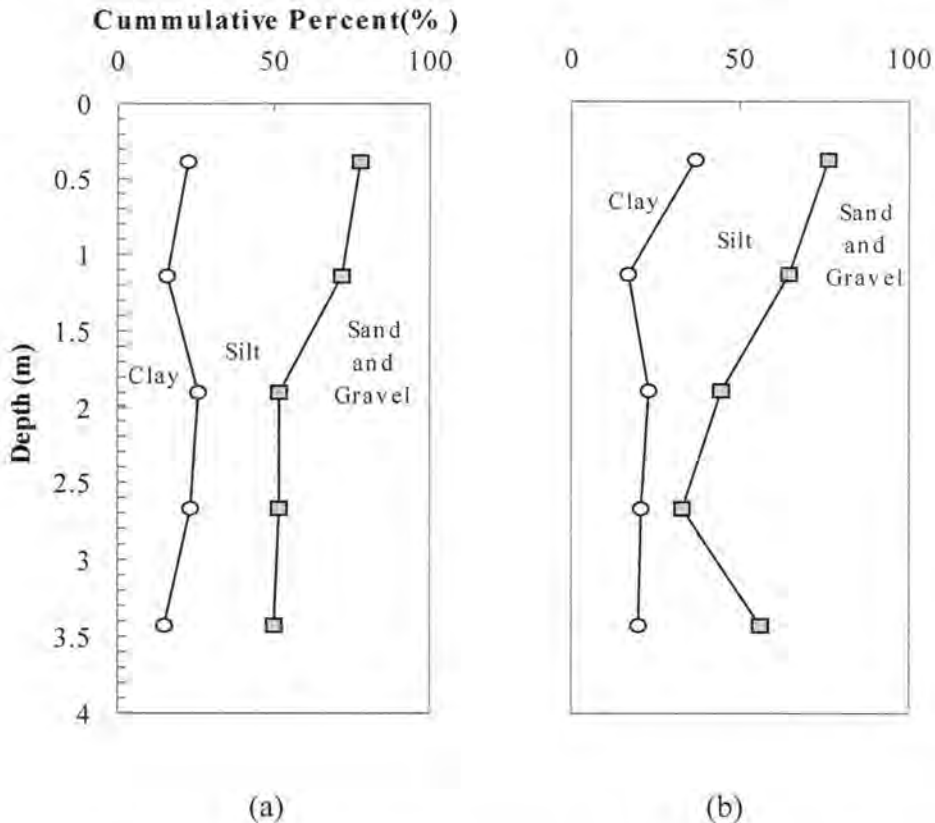
Figure 4.5 Grain-Size Distribution (a) Borehole #1 (b) Borehole #2

4.2.4 Unconfined Compression Tests

The unconfined compression tests were conducted according to ASTM standard

D2166-00 *Test Method for Unconfined Compressive Strength of Cohesive Soils.* A loading

rate of 0.05 inch per minute was used in performing the tests until the stress went down and

the sample failed. The unconfined compression strength, q_u, is presented in Figure 4.6, which

shows a general trend of increasing with depth. The values of q_u range from 31.5 kPa (658 psf) to 280.2 kPa (5853 psf). According to the consistency of cohesive soil listed in Table 4.2, the soils vary from soft clay to very stiff clay in the upper 3.81 m (12.5 feet). The stress-strain curves of unconfined compression tests are included in Appendix B.
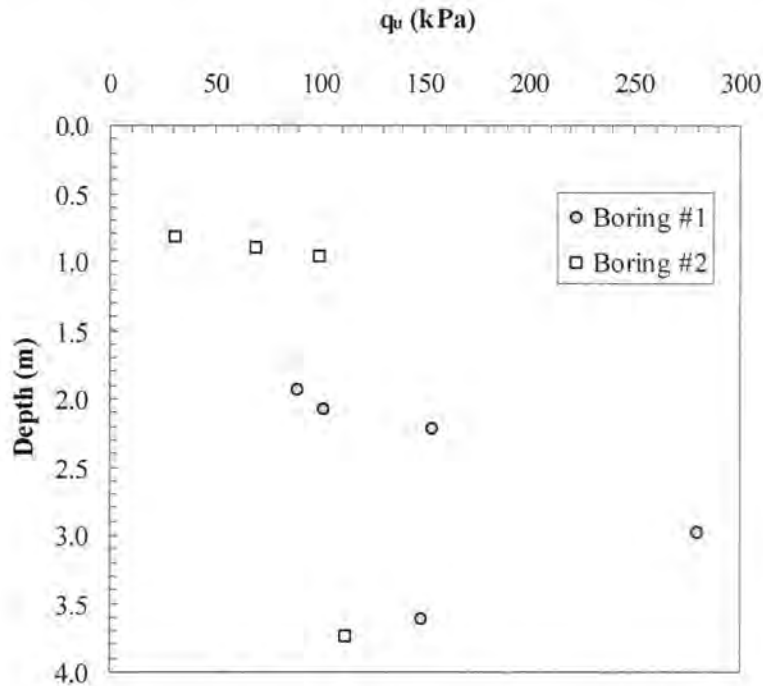
Figure 4.6 Unconfined Compression Tests

Table 4.2 Consistency of Cohesive Soil (Terzaghi and Peck 1968)

Consistency	q_u (psf)
Very soft	0-500
Soft	500-1000
Medium	1000-2000
Stiff	2000-4000
Very stiff	4000-8000

4.2.5 Reinforcing Steel Strength tests

The reinforcing steel strength tests were conducted at normal temperature and the stress-strain curve of No.6 steel is presented in Figure 4.7. As shown in Figure 4.7, the steel

started to yield at approximately 3.6×10^3 micro strain, with a yielding stress of 455 MPa (66 ksi), and then experienced a plastic failure. The test was ended at 8.8×10^4 micro strain, with the maximum stress of 759 MPa (110 ksi).
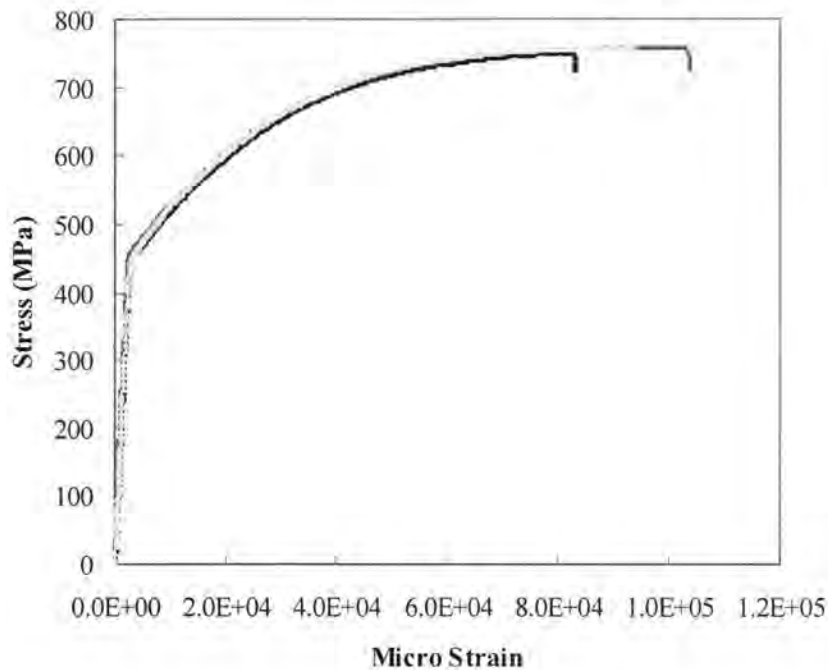

Figure 4.7 Stress-Strain of No.6 Steel Bars at Normal Temperature

4.2.6 Concrete Compressive Strength

Table 4.3 presents the concrete compressive strengths for the concrete cylinders cast during construction of the piers at SGES. There were two trucks of concrete used, whose symbols are "A" and "B". Six concrete cylinders were taken and left at the site to make sure they were cured at the same conditions as the concrete piers. These cylinders were broken on the same day of the lateral load testing, which is 8 months after pier installation. The compressive strengths ranged from 42.7 to 51.3 MPa (6.2 to 7.4 ksi). The mean compressive

strength for the test cylinders was 44.2 MPa (6.4 ksi) for truck "A" and 50.9 MPa (7.4 ksi) for truck "B", respectively.

Table 4.3 Concrete Compressive Strength

Sample No.	A1	A2	A3	B1	B2	B3
Compressive Strength (psi)	6185	6427	6614	7378	7304	7438
Average Strength (psi)		6409			7373	

4.2.7 Consolidation Test

Consolidation tests were conducted according to ASTM Standard D2435-96 *Standard Test Method for One-Dimensional Consolidation Properties of Soils* to investigate the preconsolidated pressures and overconsolidated ratio. The results are presented in Tables 4.4 and 4.5. From Tables 4.4 and 4.5, it is noted that the first Shelby tube (0-2.5ft) sample is heavily overconsolidated, with an OCR of 17.1 to 21.9. The soil below 2.5 ft is slightly overconsolidated, with an OCR ranging from 4.6 to 7.4.

Table 4.4 Summary of Consolidation Test Results - Boring #1

Depth (m)	OCR	σ_v'(kPa)	P_c'(kPa)	$C_v(10^{-3}$ cm^2/sec)
0.38	17.1	8	140	0.1-1.5
1.14	--	22.3	--	
1.91	--	31.2	--	
2.67	--	40.2	--	
3.43	--	49.1	--	

Note: -- Test not conducted.

Table 4.5 Summary of Consolidation Test Results - Boring #2

Depth(m)	OCR	$\sigma_v{}'$(kPa)	$P_c{}'$(kPa)	C_v(10^{-3} cm^2/sec)
0.30	21.9	6.4	140	0.1-1.4
0.38	19.4	8	155	0.1-0.7
1.14	7.4	21.8	160	0.1-0.7
1.91	--	30.3	--	
2.67	4.6	38.8	180	0.1-1.5
3.43	--	47.3	--	

Note: -- Test not conducted.

4.2.8 Consolidated-Undrained (CU) Triaxial Compression Test

Consolidated-Undrained Triaxial tests were conducted in general accordance to ASTM Standard D4767-95 *Test Method for Consolidated-Undrained Triaxial Compression Test for Cohesive Soils.* Six samples were taken from three bore holes at the site. Because the most severe loading conditions for pile foundations are short term loads, CU tests were conducted at different confining pressures of 10, 20, and 30 kPa to access the shear strengths of the soils. A loading rate of 0.05 inch (approximately 1% axial strain) per minute was used in performing the tests. This led to testing times of approximately 20 minutes because the tests were continued to 20% axial strain. Peak deviator stress was used as the failure criterion if the peak was reached at 10% axial strain or less. If the peak did not occur below 10% axial strain, the deviator stress at 10% axial strain was used as the failure criterion. Table 4.6 presents the tests results.

The strength envelopes for the two depths are shown in Figure 4.8. It is evident from Figure 4.8 that at the confining pressures at which the soils were tested the soils exhibited both cohesion and friction angle at the first 0.61 m (2 feet), while only exhibited friction angle at the depth of 0.91-1.22 m (3-4 feet).

The stress paths are presented in Figure 4.9. During the compression, the pore pressure increased and then decreased to below the original value. It shows that the soils are overconsolidated: contracted (pore pressure increased) at the beginning of compression and then dilated (pore pressure decreased). The stress strain curves of CU tests are included in Appendix B.

Table 4.6 CU Triaxial Tests

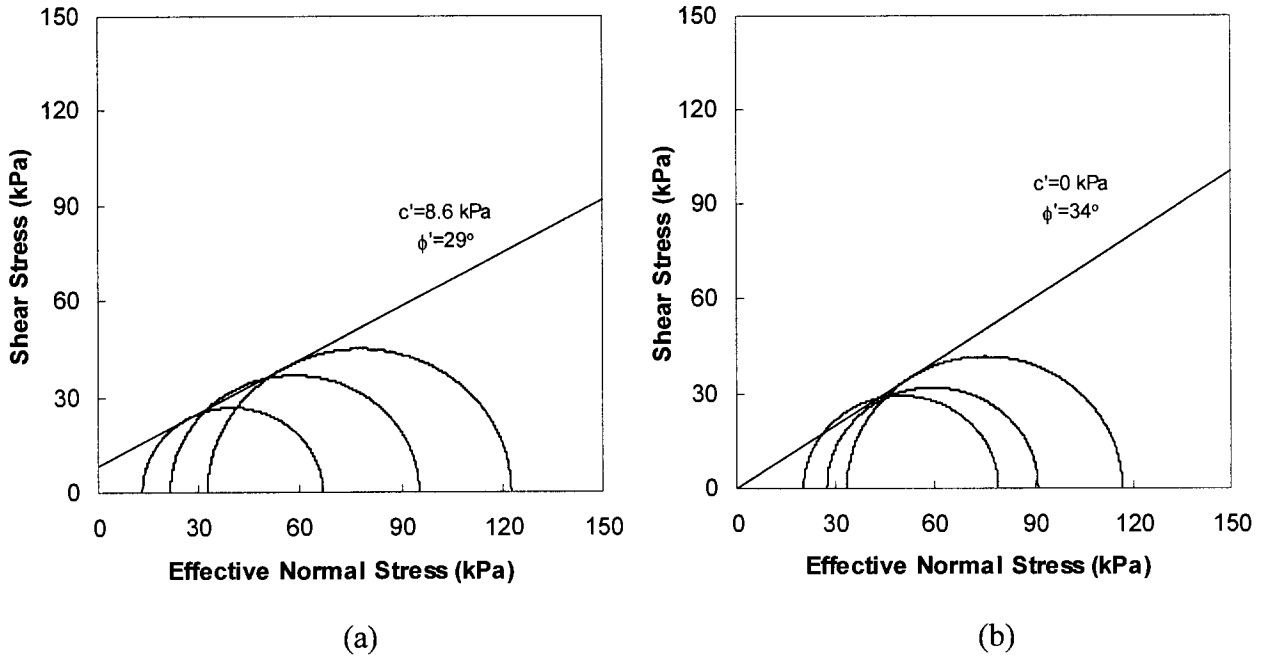| Depth m, (ft)	Bore hole #1		
	σ_3 (kPa)	$(\sigma_1-\sigma_3)_f$ (kPa)	C_u (kPa)
0.30-0.61 (1-2)	10	53.4	26.7
0.91-1.22 (3-4)	10	58.7	29.4
	Bore hole #2		
	σ_3 (kPa)	$(\sigma_1-\sigma_3)_f$ (kPa)	C_u (kPa)
0.30-0.61 (1-2)	20	73.6	36.8
0.91-1.22 (3-4)	20	63.9	32.0
	Bore hole #3		
	σ_3 (kPa)	$(\sigma_1-\sigma_3)_f$ (kPa)	C_u (kPa)
0.30-0.61 (1-2)	30	90	45
0.91-1.22 (3-4)	30	83.4	41.7
	c(kPa)	$\phi(^0)$	Averaged Undrained Shear Strength C_u (kPa)
0.30-0.61 (1-2)	8.6	29	36.2
0.91-1.22 (3-4)	0	34	34.3

Figure 4.8 Strength Envelope of CU Tests (a) Depth = 0.3-0.61 m (1-2 ft) (b) Depth = 0.91-1.22m (3-4 ft)
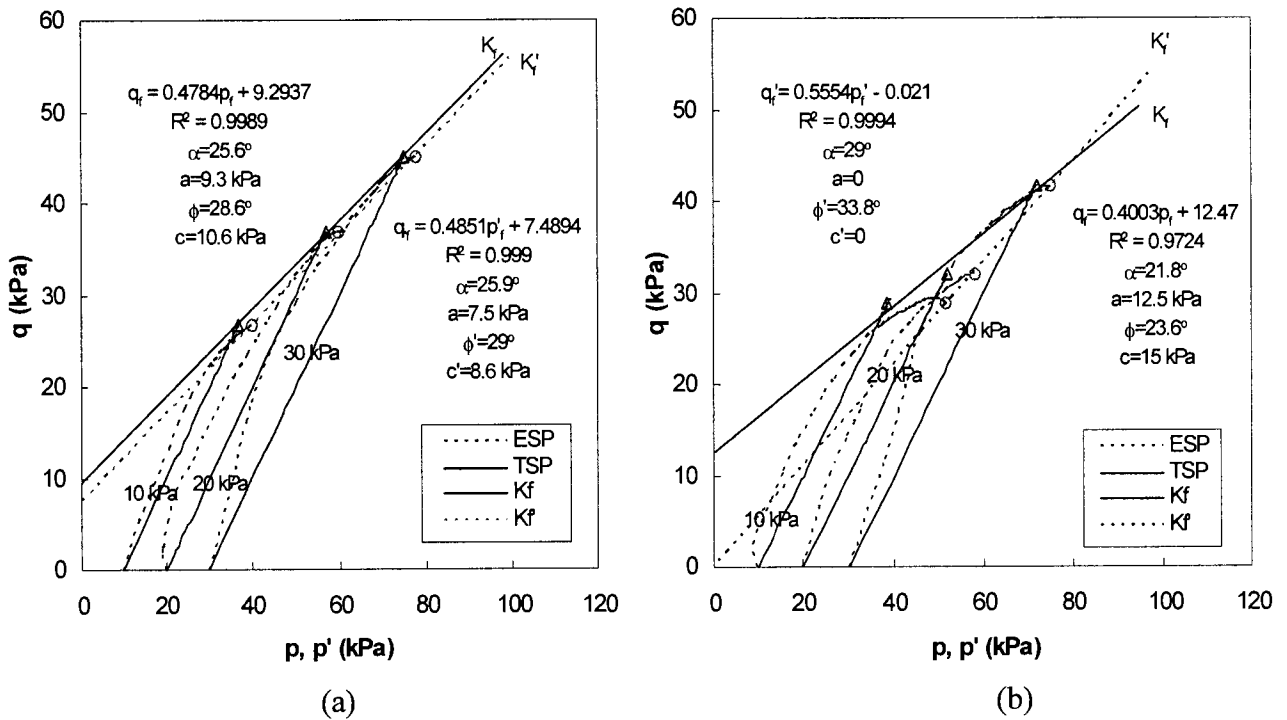

Figure 4.9 Stress Path of CU Tests (a) Depth = 0.3-0.61 m (1-2 ft) (b) Depth = 0.91-1.22m (3-4 ft)

4.3 In Situ Tests

4.3.1 Flat Dilatometer Test (DMT)

Dilatometer test was conducted in accordance with recommendation of ASTM Subcommittee D18.02.10 as presented by Schmertmann (1982). One DMT was performed at the site to a depth 9.45 m (31 feet) below the ground surface. DMT readings were recorded every 0.30 m (1feet) to yield semi-continuous profiles.

Two pressure readings were recorded from the simple control console during the test: 1) the A-Reading, the pressure required to just lift the diaphragm from the blade surface, and 2) the B-Reading, the pressure causing the diaphragm to expand 1mm from the face of the blade into the soil. The C-Reading, which corresponds to the pressure at which the diaphragm regains contact with the blade face, was not recorded. These pressure readings, once adjusted for membrane thickness, yielded corrected pressures of P_0, P_1, and P_2. Marchetti (1980) suggested that the values of P_0 and P_1 could be used in empirical correlations to define soil properties including, the Material Index, I_D, the Lateral Stress Index, K_D, and the Dilatometer Modulus, E_D. These parameters were determined using the following equations defined by Marchetti (1980):

$$I_D = (P_1-P_0)/(P_0-u_0) \qquad [4.1]$$

$$K_D = (P_0-u_0)/ \sigma_{ov}' \qquad [4.2]$$

$$E_D = 34.6 * (P_1-P_0) \qquad [4.3]$$

in which:

P_0, P_1 = pressures taken during the DMT (kPa)

u_0 = in situ pore pressure (kPa),

σ_{ov}' = effective overburden stress (kPa).

As proposed by Marchetti (1980), and presented in Table 4.7, the dilatometer material index, I_D, can be used to directly correlate the DMT results to a soil type, thus generating a stratigraphic profile. The horizontal stress index, K_D, related to the at rest lateral earth pressure coefficient, K_0, can be used to determine the overconsolidation ratio, OCR and the shear strength, s_u, in clays. The dilatometer modulus, E_D, is related to the stiffness of the soil during expansion.

Table 4.7 Soil Identification Using DMT ID Value (Marchetti 1980)

Sensitive Clays	Clay		Silt			Sand	
		Silty	Clayey		Sandy	Silty	
I_D Values	0.1	0.35	0.6	0.9	1.2	1.8	3.3

Figure 4.10 presents the DMT test pressure profile and correlated modulus profile. The pressures in the upper 7.62 m (25 feet) range from approximately 23 to 2167 kPa. In general, the P_1 values are greater than the P_0 values. Test results indicate an increasing pattern. A hard soil layer was encountered at approximately 7.62 m (25 feet). Raw data of the DMT test are included in Appendix B.
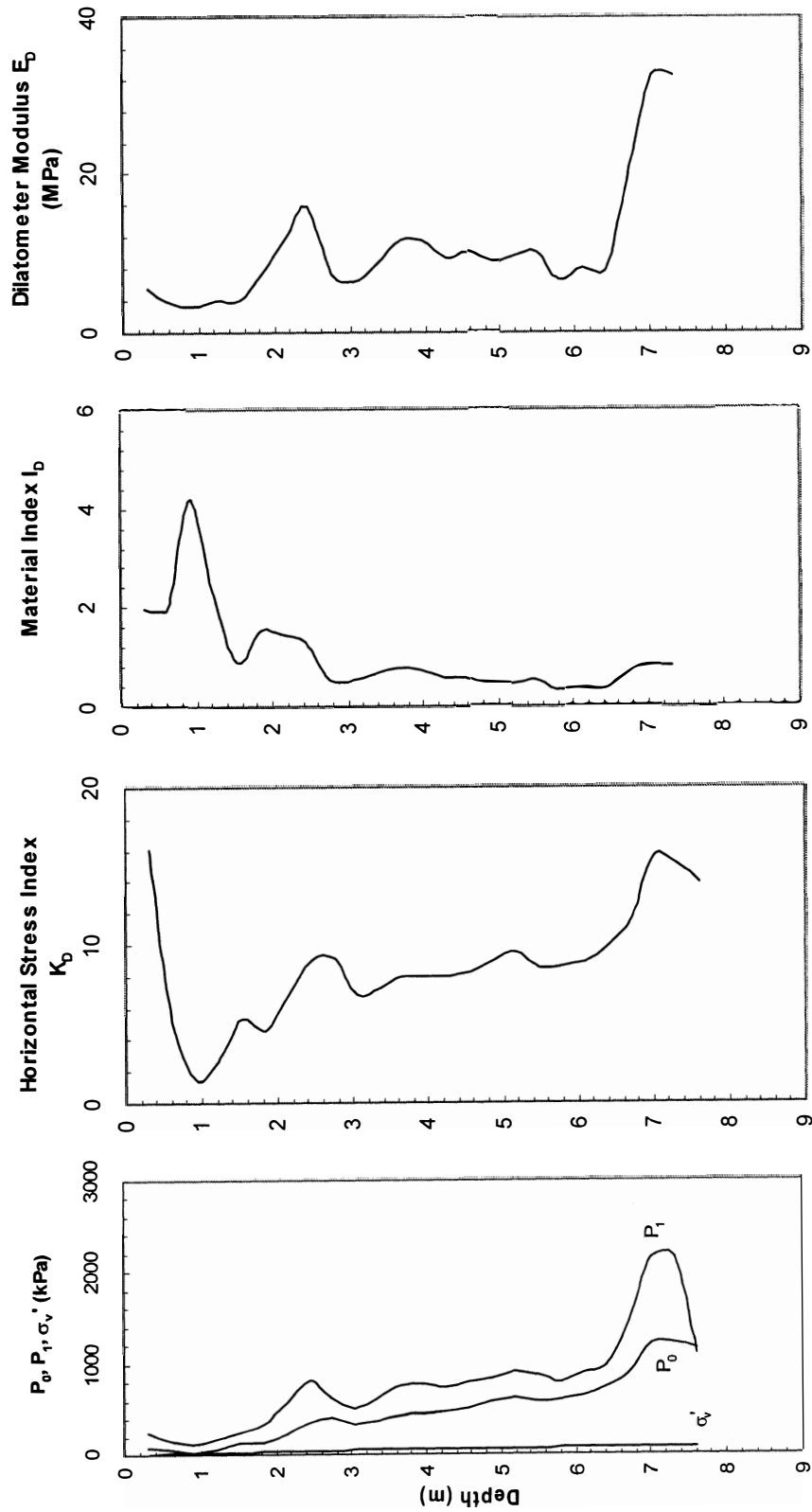
Figure 4.10 DMT Test

4.3.2 Cone Penetration Test (CPT)

Cone Penetration Tests were performed according to ASTM Standard D3441-86 *Standard Method for Deep, Quasi-Static, Cone and Friction Cone Penetration Tests of Soil.* Two CPT profiles were conducted at the site approximately 10.67m (35 feet), 32 m (105 feet) from the piers test area. CPTs were performed from the ground surface to a depth of 10.15 m (33 feet) and 8.15 m (27 feet) to yield semi-continuous profiles of tip and sleeve resistance of the soil on the cone penetrometer and geotechnical parameters such as shear strength and friction angle were obtained from empirical correlations.

The cone penetrometer was advanced vertically at a rate of 2 cm/sec (approximately 15 sec/ft) from a level drill rig. AW rods were threaded on the friction reducer which was threaded onto the cone penetrometer. The electrical wires were threaded through the AW rods to allow contact with lap-top computer which records tip resistance, sleeve friction resistance, and pore water pressure measurements. The computer program was started as the CPT was advanced into the subsurface in order for semi-continuous measurements to be obtained throughout the profile. Two CPT tests profiles are presented in Figures 4.11 and 4.12.

The first plot is depth vs. cone tip resistance. Two profiles both show that the cone tip resistance slightly increases with depth until at about 8 m (26 feet) with exception that CPT2 encountered a stiffer layer at approximately 3 m (10 feet). This indicates that the subsurface material at the first 8.0 m (26 feet) is a fairly uniform deposit and is relatively soft. At 8 m (26 feet) below the ground surface, the cone tip resistance jumps up from 5430 kPa to 27050 kPa, indicating a very stiffer layer exists, which is consistent with DMT profile.

The second plot is depth vs. sleeve resistance, which is similar to the first plot. Again, higher values indicate greater difficulty in penetration, and in these profiles, it appears that there are two distinct areas where the sleeve resistance was high, at 3.0 and at 8.0 m (10 and 26 feet) below the ground surface.

The third plot is a profile of the friction ratio varying with depth. The friction ratio show a larger variation on the top 2 m (6.6 feet) and below 8 m (26 feet), ranging from 0.1 to 14%. Between 2 m (6.6 feet) and 8 m (26 feet), the friction ratio slightly decreases with depth, ranging from 0.66 to 4.33%. The CPT data are included in Appendix B.
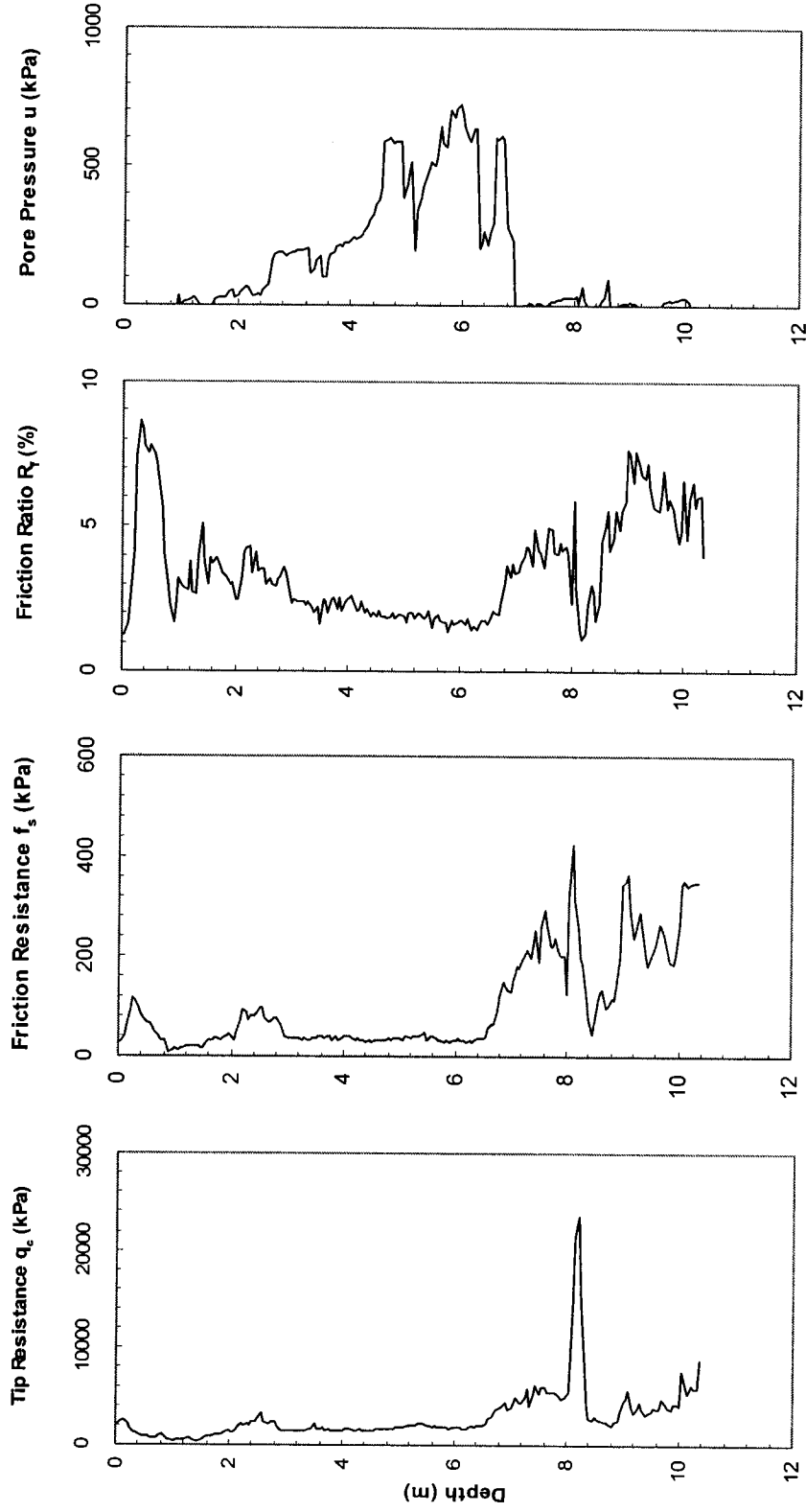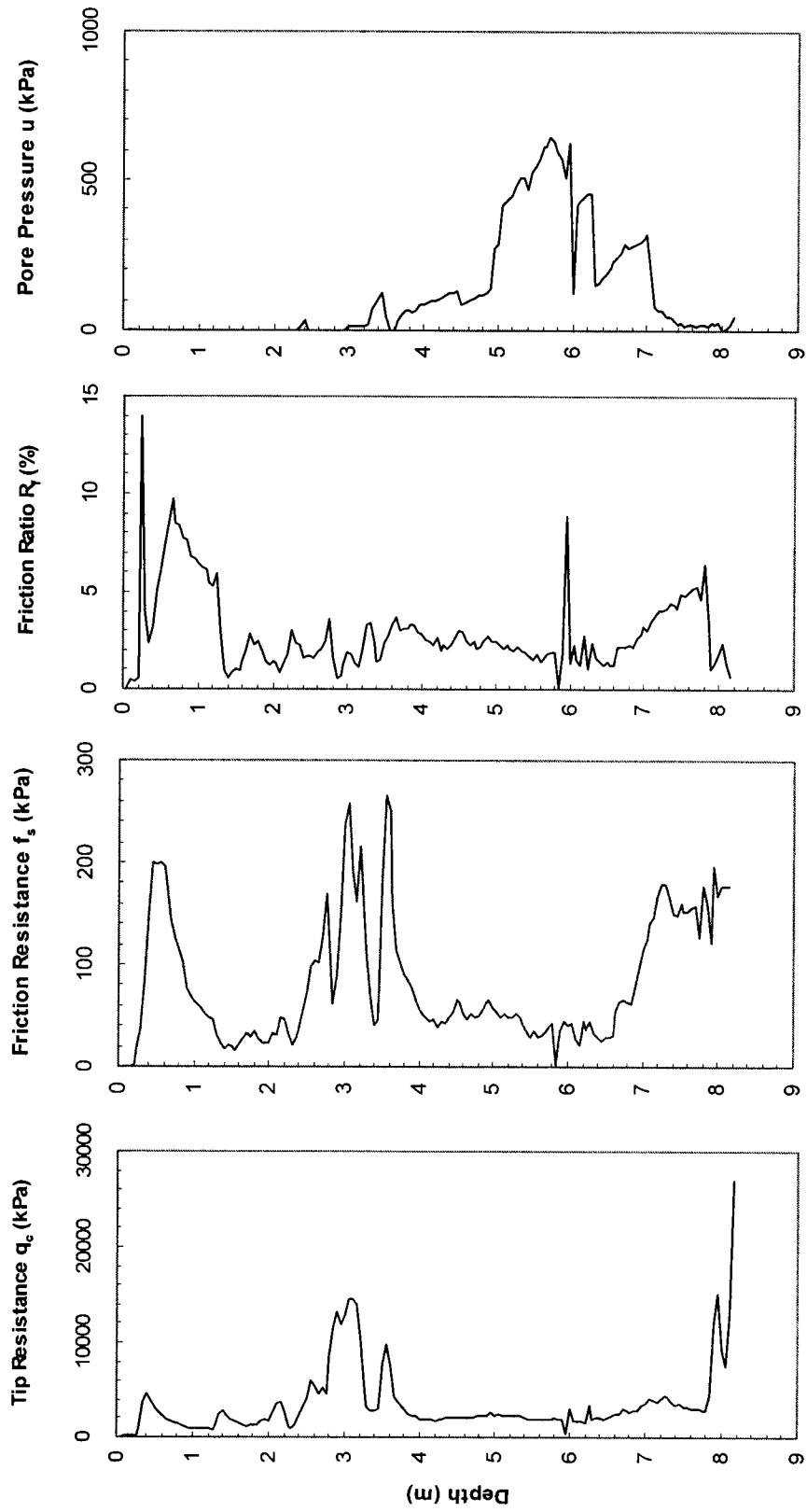
Figure 4.11 CPT Test No.1

Figure 4.12 CPT Test No.2

4.3.3 Standard Penetration Tests (SPT)

Standard penetration tests were performed according to ASTM 1586. These tests involved driving the split-spoon samples 0.46 m (18 inches) into the bottom of the borehole with a 63.5 kg (140 lbs) hammer falling 0.76 m (30 inches). Blow counts were recorded for each 7.5 cm (3 inches) depth interval, and the total number of blows of the final 0.30 m (12 inches) was designated the Standard Penetration Resistance or N value. As shown in Figure 4.13, the profiles of four borings are similar. The blow counts decrease with depth at the first 1.5 m (5 feet), and then increase to a depth of about 3 m (10 feet). Below 3 m (10 feet) the blow counts are relatively constant, with a slight variation. The SPT test results are included in Appendix B.
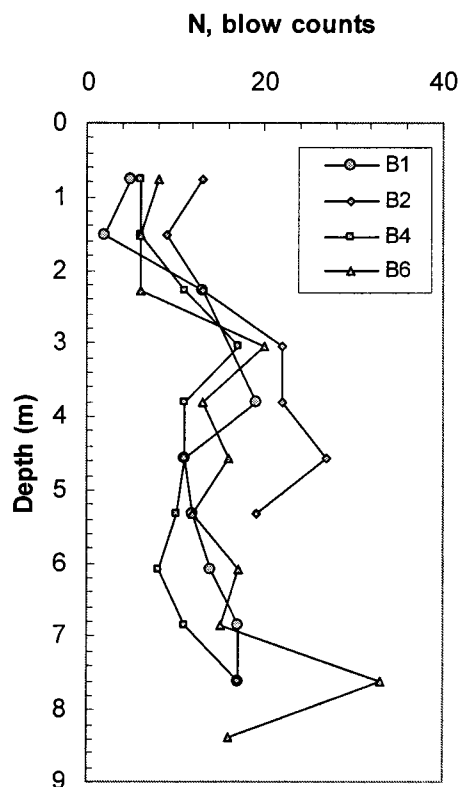
Figure 4.13 SPT Tests Blow Counts N vs. Depth

4.3.4 Open-Standpipe Piezometer Installation and Monitoring

An open-standpipe piezometer was installed at the site to monitor groundwater fluctuations in the upper 3.05 m (10 feet) of the subsurface. A borehole was drilled to approximately 3.2 m (10.5 feet) below the ground surface. The piezometer consisted of approximately 2.87 m (9.4 feet) of solid-wall PVC riser pipe connected to a lower section of 0.30m (1.0ft) of slotted PVC. Filter sand was placed in the bottom 152.4 mm (6 inch) of the borehole before the piezometer was inserted. Once the piezometer was placed in the borehole, the filter sand pack was continued 152.4 mm (6 inch) above the slotted screen. The remaining annular space was backfilled with Pure Gold medium bentonite chips up to the ground surface.

Approximately 0.61 m (2 feet) of riser piper remained above the sealed borehole and was covered with a vented cap.

Fluctuations in ground water levels were recorded at the time of pier construction, lateral load testing, and in situ testing using a water level indicator.

Figure 4.14 illustrates the fluctuations in the piezometric surface over the year. Between the months of November 2002 and June 2003, the piezometric surface gradually increased, ranging from 0.3 to 1.22 m (1 to 4 feet) below ground surface. While from June 2003, the piezometric surface decreased with time. These variations in groundwater levels are most likely indicative of precipitation and snow events during the winter and spring months. It should be noted that the ground water level was consistent for all lateral load tests performed on the piers. Data for open-standpipe piezometer monitoring are included in Appendix B.
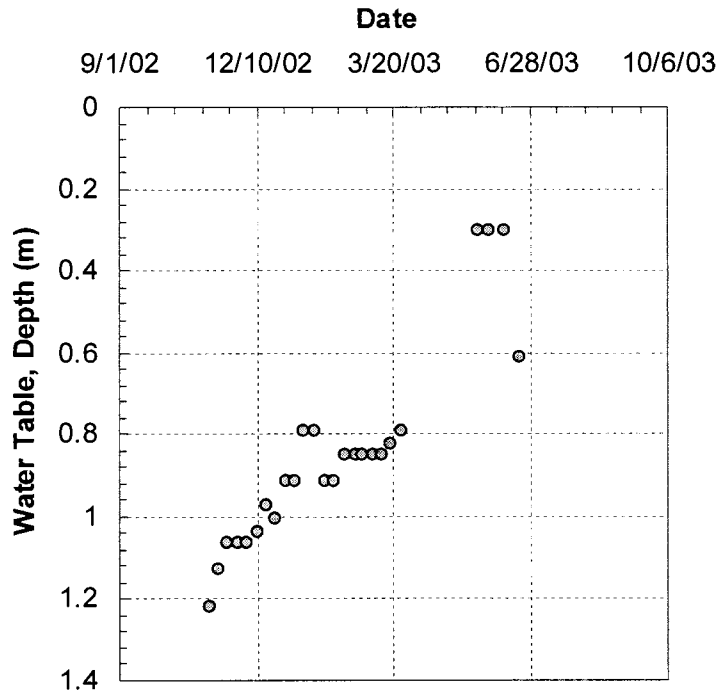
Figure 4.14 Variations of Water Table

4.3.5 Thermocouple Installation and Monitoring

A series of thermocouples was installed at each test site to monitor changes in subsurface temperatures. Thermocouples were installed in general accordance with instructions provided by the manufacturer, Omega Engineering, Inc. Soil temperature was monitored at SGES at 0.15, 0.30, 0.46, 0.76, 0.91, 1.07, 1.22, 1.52, 1.83, 2.44, 3.05, and 6.1 m (0.5, 1, 2, 3, 4, 6, 8, 10, 15, and 20 feet) below the ground surface.

Prior to installation, thermocouple connectors were constructed and connected to thermocouple wire. The wire was cut so that each thermocouple would extend down to the desired monitoring depth. Each connector was labeled and was then secured in a cluster. A 50.8 mm (2 inch) diameter auger was used to drill 6.1 m (20 feet) below the ground surface.

After augering, the thermocouple cluster was suspended in the borehole and the hole was backfilled with the removed soil cutting to the ground surface.

Figure 4.15 presents the results of thermocouple monitoring at the SGES. Soil temperatures ranges from -3.2 to 18.9 ^{0}C (26.2 to 66.1 ^{0}F), while ambient temperatures ranges from -8.9 to 28.9 ^{0}C (16 to 84 ^{0}F). In the fall and winter months, the soil temperature gradually increases with depth. It appears that this trend does not change significantly during the times that there was snow cover over the thermocouple cluster. The maximum frozen depth in winter is about 0.49 m (1.6 feet). In the warmer months, the soil temperature gradually decreases with increasing depth. In general, it appears that no matter what the ambient temperatures are at the site, the soil temperatures approach a general range between 3.9 and 14.6 ^{0}C(39 and 58.2 ^{0}F) below the depth of 1.22 m (4 feet). Thermocouple monitoring data are included in Appendix B.
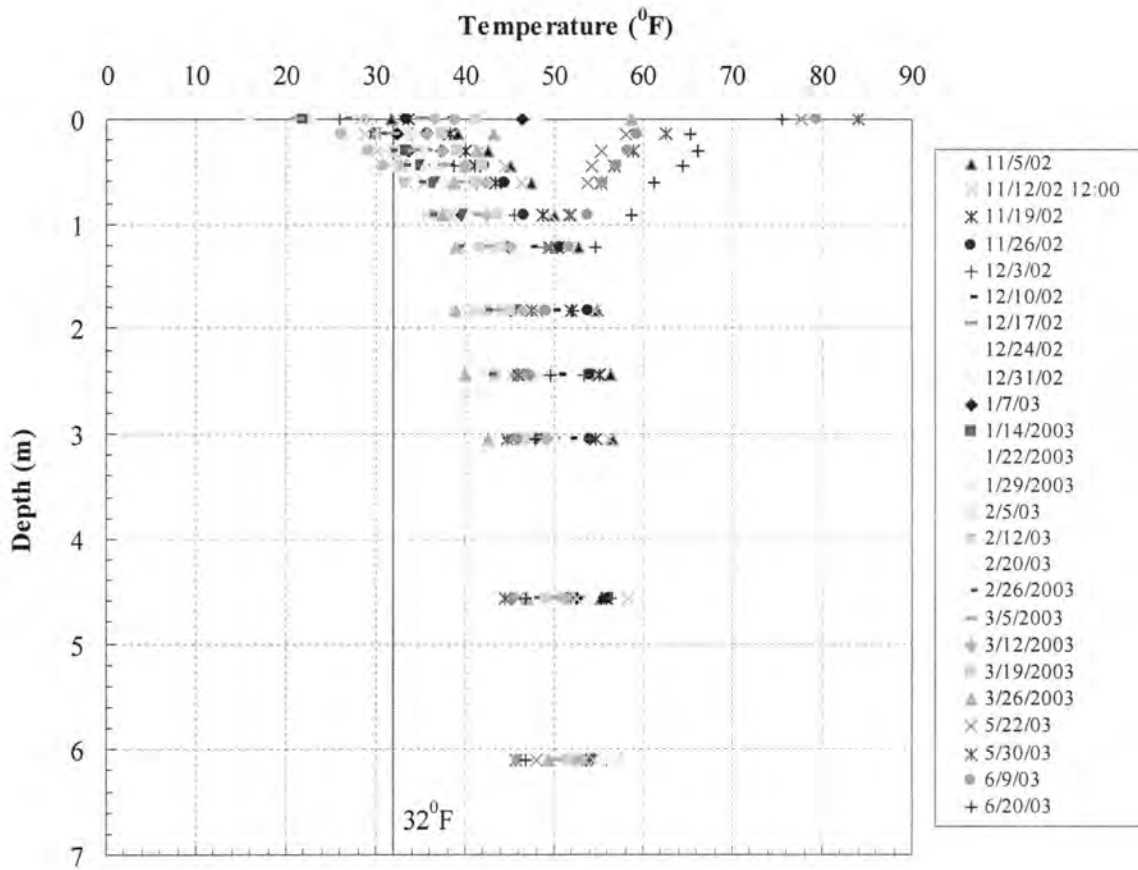
Figure 4.15 Thermocouple Readings (from 11/5/02 to 6/20/03)

CHAPTER 5: LATERAL LOAD TESTING

5.1 Introduction

Lateral load tests were conducted on twelve intermediate CIDH concrete piers to investigate the load-displacement behavior of piers embedded in glacial till. The pier geometry was designed for analyzing the influence of scale effects. The interpreted ultimate lateral load capacity, Q_{ult}, was arbitrarily defined as the load which produces a lateral ground line pier head displacement, s, equals to 10% of the pier diameter, D. In addition, the effect of defining ultimate pier capacity as the load occurring at a displacement equal to a percentage of pier diameter (e.g. s = 20%D), an absolute pier displacement, or an absolute pier rotation was also investigated. Load displacement relationship was analyzed in normalized form. The ultimate strength method and the p-y method were applied to lateral load test results to predict pier behavior. A comparison was made between predicted and measured results.

5.2 Pier Construction

Twelve piers were constructed at the SGES. All piers were constructed in pairs to serve as reactions to each other during load testing as shown in Figure 5.1. The proposed pier dimensions were 0.30, 0.46, 0.61, and 0.91m (12, 18, 24, and 36 inches) diameters with lengths of 1.52, 2.29, and 3.05 m (5, 7.5 and 10 feet) for each diameter. This design gave length/diameter ratios ranging from 1.7 to 10. Piers were fabricated by identical construction methods, essentially in three steps: (a) drill hole to pier tip elevation, (b) install steel reinforcement, and (c) free fall the concrete.

A utility post-hole auger operated from a drilling truck was used to drill the hole to the desired depth. A sonotube form was placed at the surface of the borehole to allow the pier to continue approximately 0.15 m (6 inch) above the ground surface. Concrete was placed in each of the holes and allowed to cure for a minimum of 30 days. The drill holes were left open for less than one hour prior to placement of concrete and steel reinforcing rods.

During the installations, cement concrete was batched and mixed at the site. Concrete cylinders were taken during casting, and compression tests on these cylinders were conducted on the same day as the load test. Cylinders were left at the site during this period. Photographs of pier installation are presented in Figure 5.2. The characteristics of piers are presented in Table 5.1.
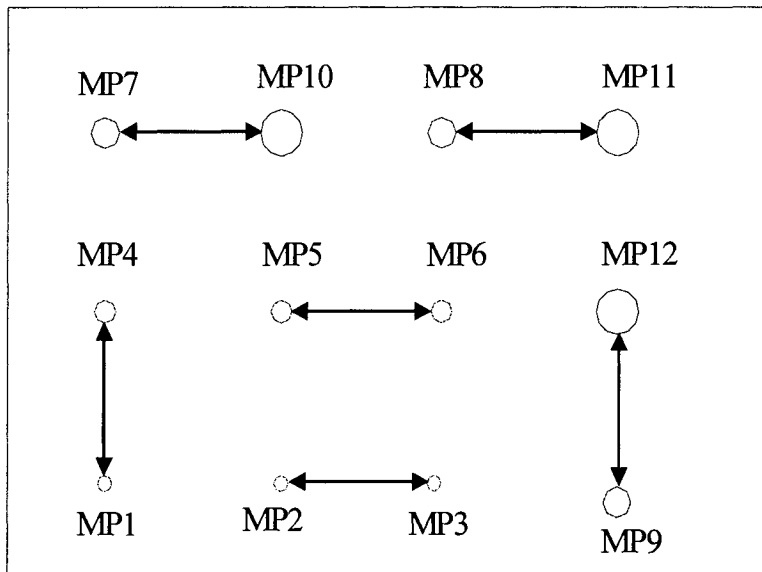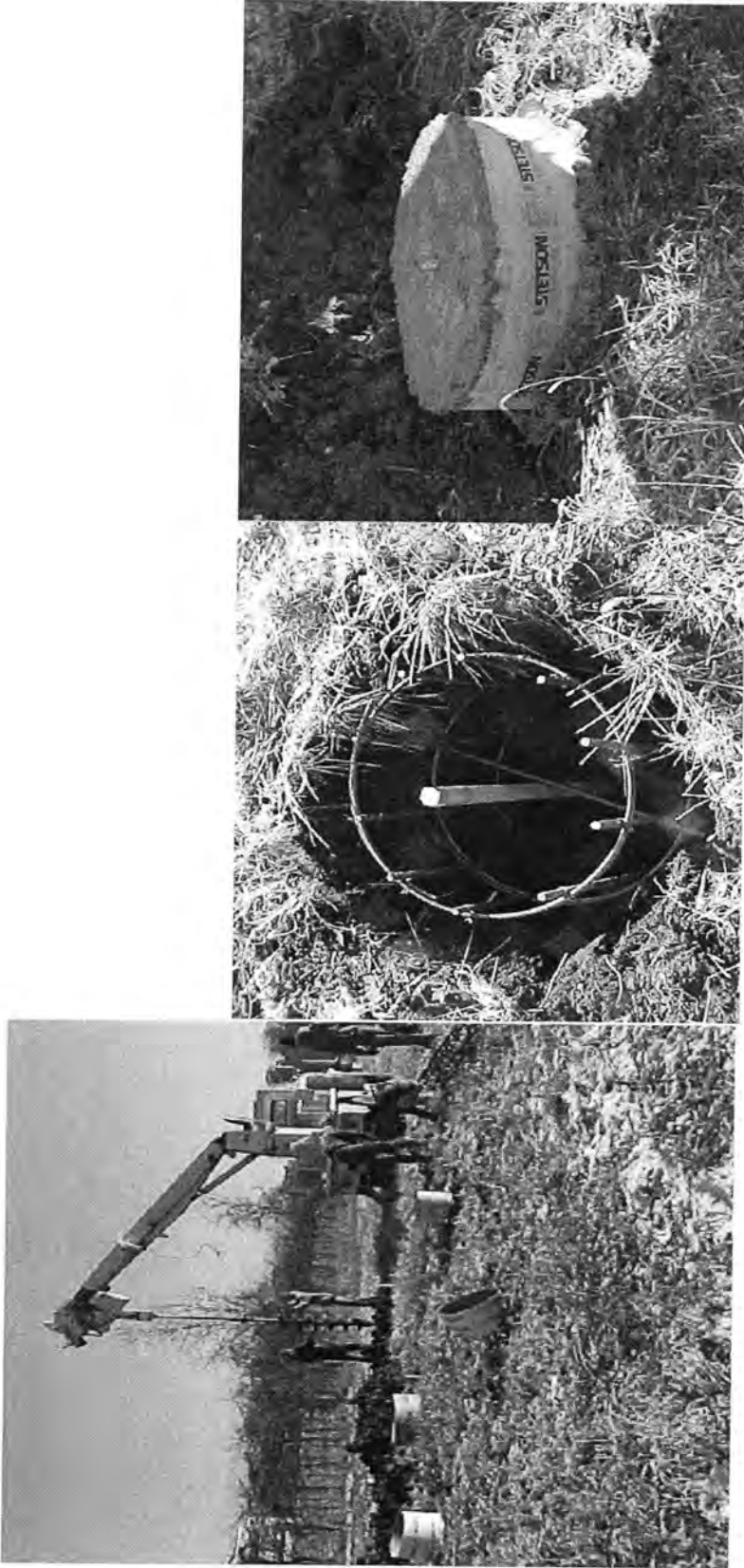

Figure 5.1 Plan View of Pier Testing

(a)

(b)

(c)

Figure 5.2 Photographs of Piers Construction (a) Utility Post-hole Auger (b) Reinforcing Cage with Inclinometer Tube (c) A Completed Pier

Table 5.1 Characteristics of the Piers at SGES

Pier	Length m(in.)	Diameter m(in.)	Reinforcing Bars	Hoop	Cage Diameter m(in.)	Date installed
MP1	1.5 (59)	0.32 (12.5)	5 No.6	6 No.2	0.15 (6)	11/21/02
MP2	2.29 (90)	0.32 (12.6)	5 No.6	8 No.2	0.15 (6)	11/21/02
MP3	3.15 (124)	0.32 (12.5)	5 No.6	10 No.2	0.15 (6)	11/21/02
MP4	1.63 (64)	0.47 (18.7)	7 No.6	6 No.2	0.3 (12)	11/12/02
MP5	2.29 (90)	0.5 (19.5)	7 No.6	8 No.2	0.3 (12)	11/12/02
MP6	3.12 (123)	0.46 (18)	7 No.6	10 No.2	0.3 (12)	11/12/02
MP7	1.6 (63)	0.6 (23.8)	8 No.6	6 No.2	0.46 (18)	11/12/02
MP8	2.44 (96)	0.6 (23.7)	8 No.6	8 No.2	0.46 (18)	11/12/02
MP9	3.18 (125)	0.62 (24.5)	8 No.6	10 No.2	0.46 (18)	11/12/02
MP10	1.6 (63)	0.96 (37.8)	9 No.6	6 No.2	0.76 (30)	11/12/02
MP11	2.31 (91)	0.96 (37.7)	9 No.6	8 No.2	0.76 (30)	11/12/02
MP12	3.1 (122)	0.94 (37)	9 No.6	10 No.2	0.76 (30)	11/12/02

5.3 Lateral Load Testing

Lateral load tests were conducted on each pair of piers on 21 July, 2003, 8 months after installation. The testing was completed on 12 August 2003. The lateral load tests were performed in close conformance with ASTM D3966-90 (ASTM 1995) *Standard Test Method for Piles under Lateral Loads*. Lateral loads were applied at the ground surface, and two piers were tested simultaneously by placing the 448 kN (100kips) hydraulic cylinder and a 224 kN (50 kips) load cell between them. Curved load plates were placed on the inside of each test pile to increase stability of the load test frame. Loads were applied incrementally in the range of approximately 5 to 10% of the estimated ultimate capacity. Each load increment was maintained for at least 15 minutes. Free rotation was allowed at the pier head at the ground surface.

Deformation measurements were made using two rulers attached to independent reference beams placed on the backside of each of the piers inline with the applied load.

Pier inclination was measured by inclinometer. The digitilt inclinometer model 50306 used during the load tests was provided by Iowa DOT, which is for measurement of progressive changes in angle of inclination of the guide casing.

A photograph and schematic of the test arrangement are presented in Figures 5.3 and 5.4, respectively.

(a)

(b)

(c)

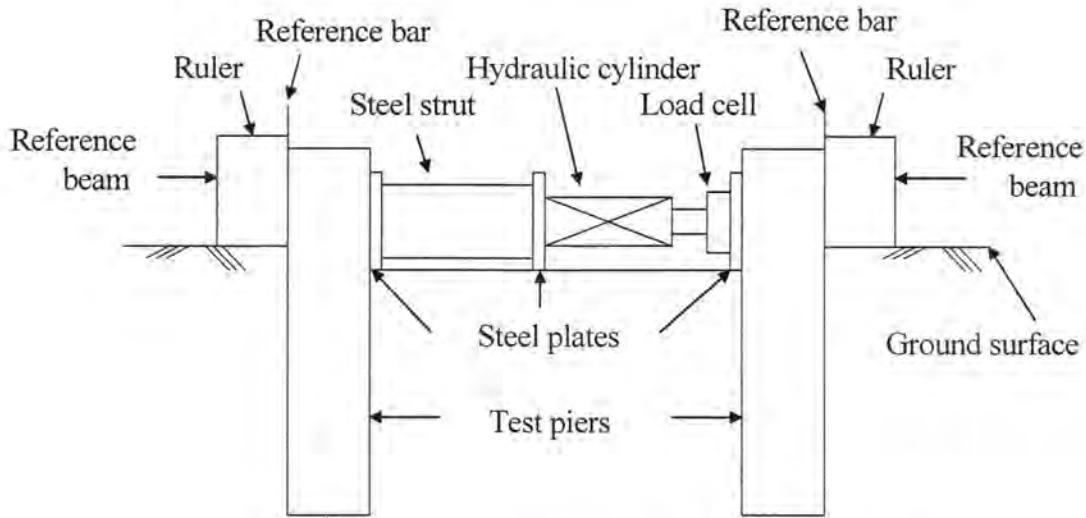**Figure 5.3 Photographs of Lateral Load Testing (a) Load Test Arrangement (b) Displacement Measurement (c) Inclinometer Measurement**

Figure 5.4 Schematic of Load Test Arrangement

5.4 Behavior of Laterally Loaded Piers

The demarcation between rigid and flexible behavior of the laterally loaded piers has been proposed by different researchers (Broms 1964, Woodward *et al.* 1972, Briaud 1997, Bierschwale *et al.* 1981, McCorkle 1969, and Reese *et al.* 2000) as presented in Tables 2.1. Six methods were used for the specific classification for all piers installed at the SGES as shown in Table 5.2. The presented methods are referred to as Methods 1 through 6.

Table 5.2 Laterally Loaded Pier Behavior Classification by Different Methods

Piers	L(m)	D(m)	L/D	$I\ (m^4)$	K(kPa)	R (m)	L/R	1	2	3	4	5	6
MP1	1.52	0.30	5	4.24E-04	2685	1.99	0.77	R	R	R	R	R	R
MP2	2.29	0.30	8	4.24E-04	5447	1.67	1.37	R	R	S	S	R	R
MP3	3.05	0.30	10	4.24E-04	7496	1.54	1.98	S	R	S	S	S	F
MP4	1.52	0.46	3.33	2.14E-03	4028	2.70	0.57	R	R	R	R	R	R
MP5	2.29	0.46	5	2.14E-03	8171	2.26	1.01	R	R	S	R	R	R
MP6	3.05	0.46	6.67	2.14E-03	11244	2.09	1.46	R	R	S	S	R	R
MP7	1.52	0.61	2.5	6.78E-03	5370	3.35	0.46	R	R	R	R	R	R
MP8	2.29	0.61	3.8	6.78E-03	10894	2.80	0.82	R	R	R	R	R	R
MP9	3.05	0.61	5	6.78E-03	14992	2.59	1.18	R	R	S	R	R	R
MP10	1.52	0.91	1.7	3.43E-02	8055	4.54	0.34	R	R	R	R	R	R
MP11	2.29	0.91	2.5	3.43E-02	16341	3.80	0.60	R	R	R	R	R	R
MP12	3.05	0.91	3	3.43E-02	22487	3.51	0.87	R	R	R	R	R	R

Note: R: Rigid, S: Semi-Rigid, F: Flexible

The soil lateral subgrade modulus K was obtained from DMT test. As proposed by Gabr and Borden (1988), K is given by the following equation:

$$K = \frac{(P_0 - \sigma_h)D}{0.00685}$$

[5.1]

in which:

P_0 = DMT A-reading (kPa),

σ_h = in situ lateral at rest pressure at depth z(kPa),

D = pier diameter (m).

0.00685 m = half thickness of dilatometer blade.

Average K values from ground surface to the bottom of the pier were used in the analyses. The moment of inertia of pile I was obtained by $\pi D^4/64$. The elastic modulus of pier was taken as 2.48×10^7 kPa (3.6×10^6 psi). The stiffness factor R, as defined in Equation 2.1, can then be calculated. Thus the classification based on Methods 1, 2 and 3 is determined.

Methods 4 and 5 are based on the geometry of the pier, i.e., L/D ratio.

For Method 6, a series of run was conducted using the LPILE program. Different loads were used to examine the critical length for each pier diameter. The critical length/diameter as a function of loading is presented in Figures 5.5 to 5.8. Table 5.3 lists the averaged critical lengths for each diameter. From Table 5.3, all the piers can be classified as rigid except MP3 (L=3.05 m, D = 0.3 m).
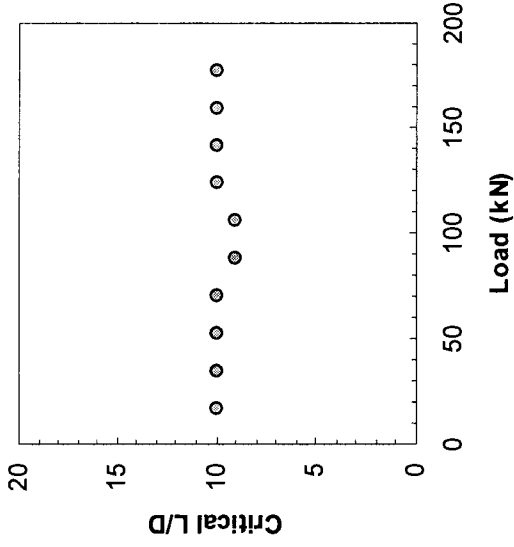
Figure 5.5 Critical L/D as a Function of Load (D = 0.91 m)   **Figure 5.6 Critical L/D as a Function of Load (D = 0.61 m)**
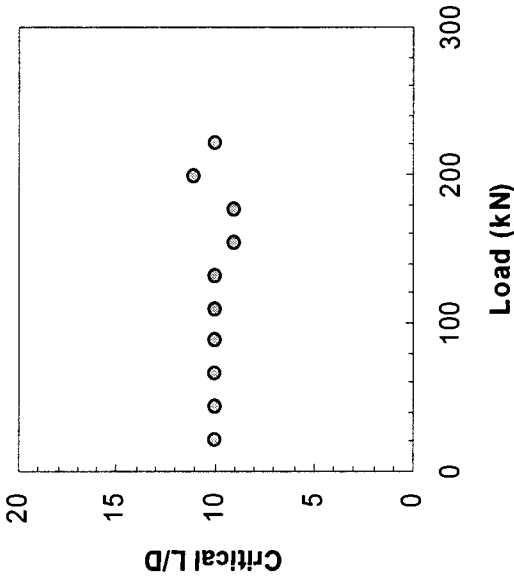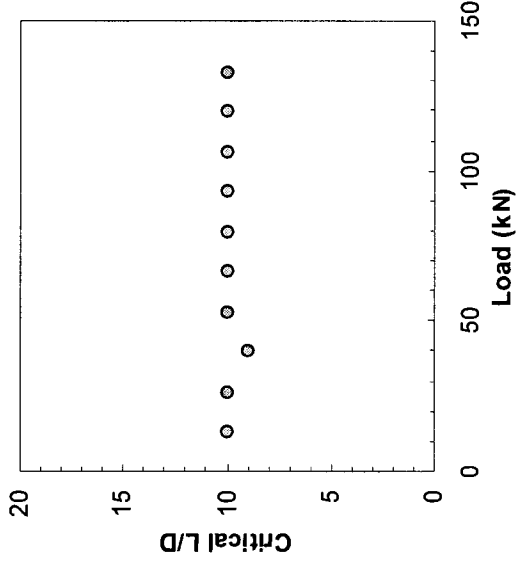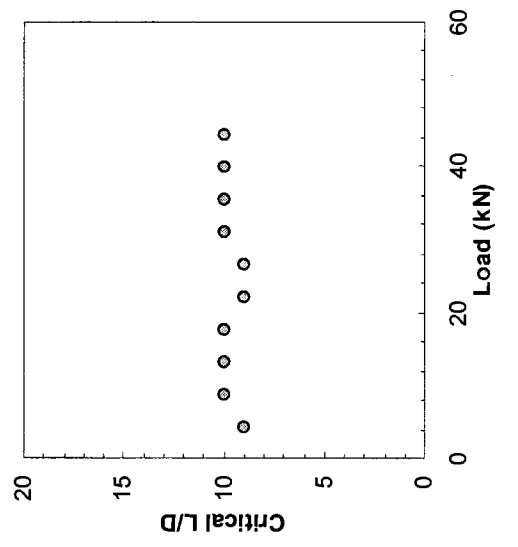
Figure 5.7 Critical L/D as a Function of Load (D = 0.46 m)   **Figure 5.8 Critical L/D as a Function of Load (D = 0.3 m)**

Table 5.3 Critical Length of the Piers Based on LPILE Analyses

D, m (in.)	L_{crit}, m (ft)	L_{crit}/D
0.30 (12)	3.05 (10)	10
0.46 (18)	4.57 (15)	10
0.61 (24)	6.1 (20)	10
0.91 (36)	8.69 (28.5)	9.5

5.5 Nondimensional Expression of Load Test Results

5.5.1 Normalized Results Based on 10% Method

The ultimate lateral load, Q_{ult}, maximum lateral load, Q_{max}, and maximum displacement, s_{max}, for the tests piers at SGES are presented in Table 5.4, in which the "ultimate" was interpreted as the load corresponding to a ground line pier head deflection equal to 10%D. MP6, MP10, MP11, and MP12 were retested because they did not reach the 10%D displacement before their reaction pier failed at the initial load test. Concrete blocks were lined in between two piers to serve as additional reaction during the retesting of those four piers. Load-deflection curves for each test are presented in Figure 5.9.

Table 5.4 Lateral Load Capacity of Piers at SGES

| Pier	Length m (ft)	Diameter m (in.)	Q_{ult} kN (kips) s/D=10%	Q_{max} kN (kips)	s_{max}/D (%)
MP1	1.52 (5)	0.305 (12)	36 (8.1)	57.8 (13)	52.8%
MP2	2.29 (7.5)	0.305 (12)	43.6 (9.8)	71.2 (16)	37.4%
MP3	3.05 (10)	0.305 (12)	51.2 (11.5)	71.2 (16)	24.6%
MP4	1.52 (5)	0.457 (18)	56 (12.6)	57.8 (13)	10.7%
MP5	2.29 (7.5)	0.457 (18)	62.3 (14)	84.5 (19)	35.1%
MP6	3.05 (10)	0.457 (18)	115.6 (26)	124.5 (28)	12.3%
MP7	1.52 (5)	0.61 (24)	59.2 (13.3)	75.6 (17)	26.5%
MP8	2.29 (7.5)	0.61 (24)	117.9 (26.5)	142.4 (32)	23.5%
MP9	3.05 (10)	0.61 (24)	166.8 (37.5)	186.8 (42)	13.6%
MP10	1.52 (5)	0.914 (36)	129 (29)	133 (30)	12%
MP11	2.29 (7.5)	0.914 (36)	151.2 (34)	151.2 (34)	14.4%
MP12	3.05 (10)	0.914 (36)	235.7 (53)	235.7 (53)	10.9%
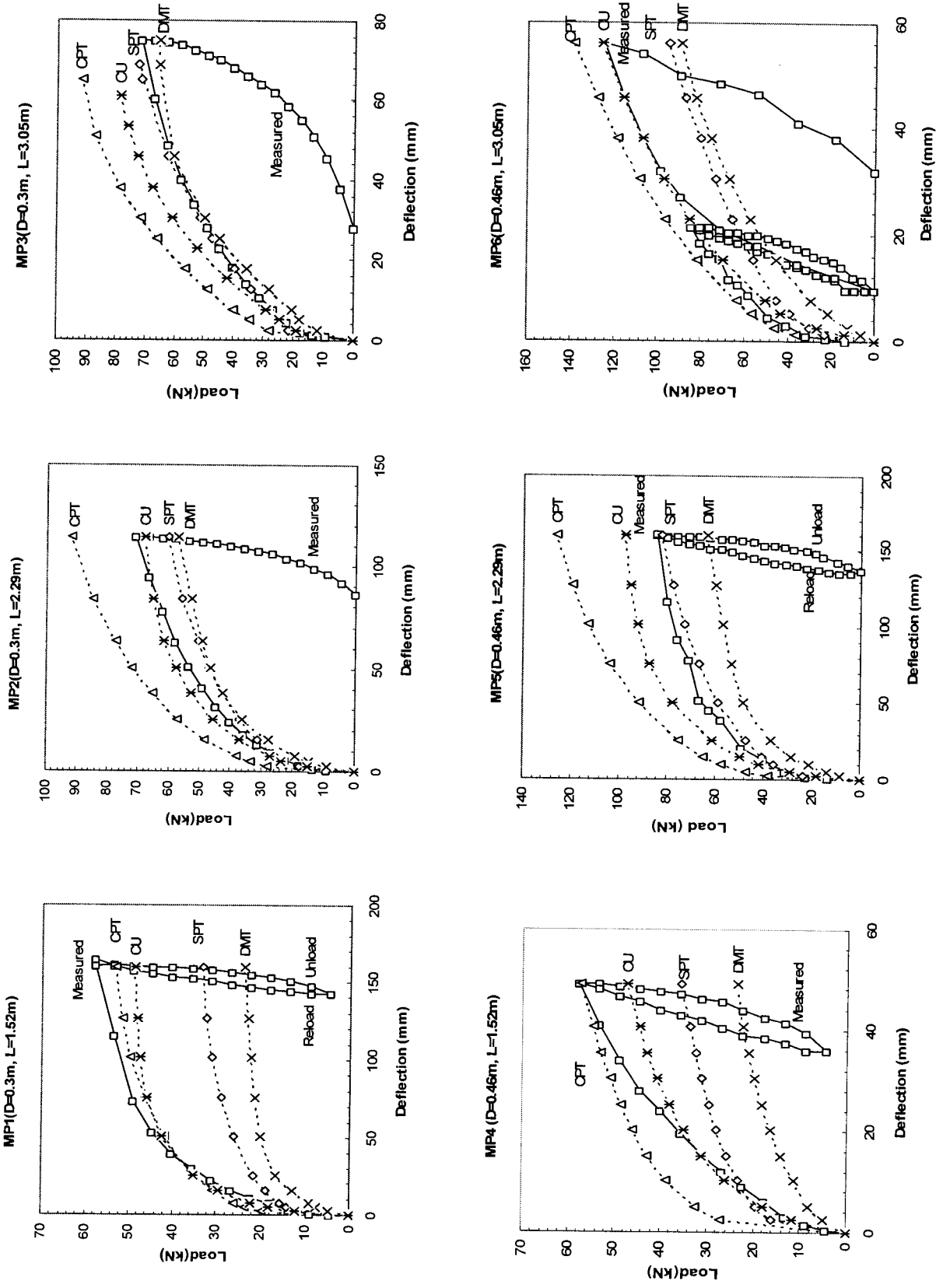
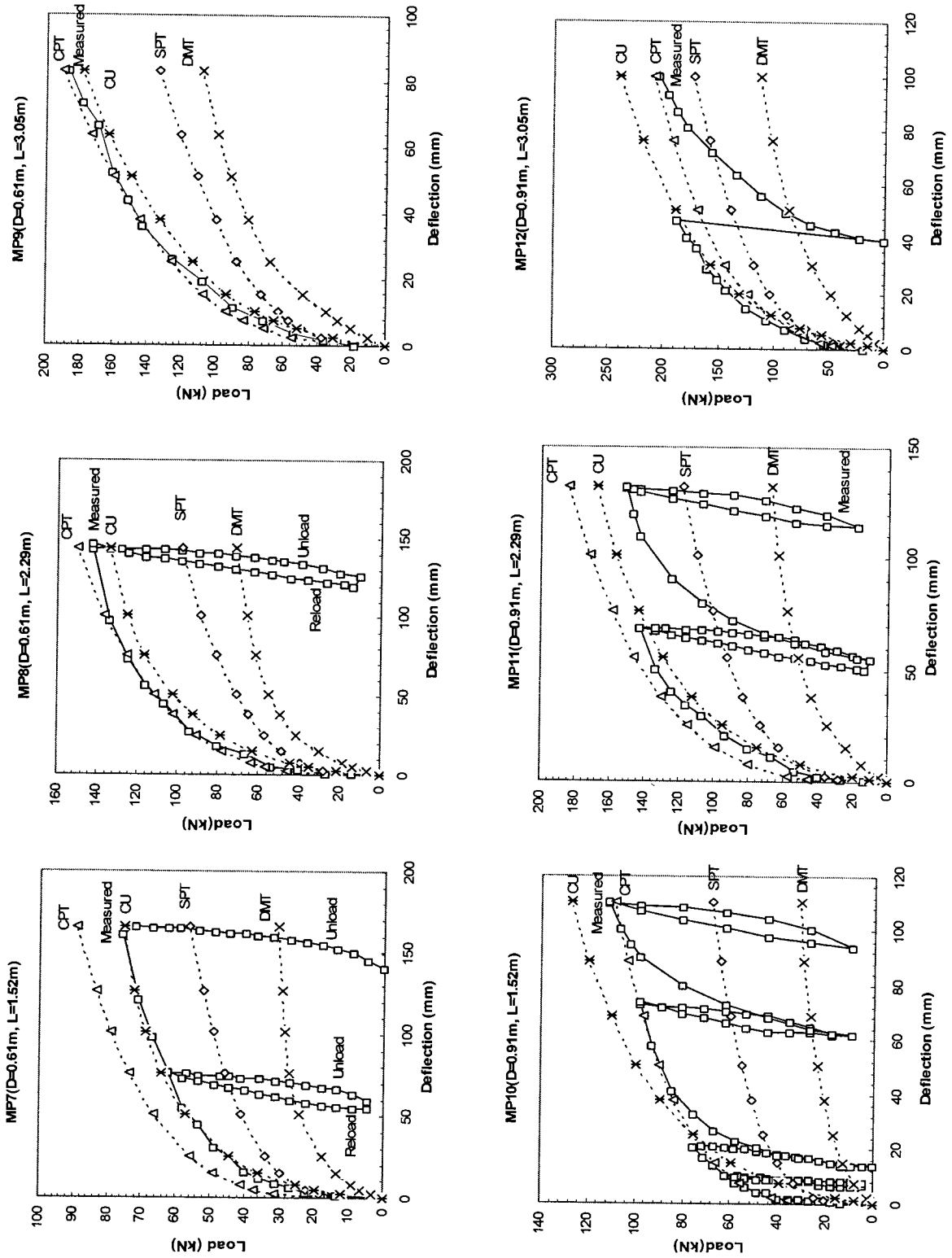**Figure 5.9 Load-Displacement Curves of 12 Piers at SGES**

Figure 5.9 (Continued)

The load-displacement behavior of piers may be expressed in nondimensional terms by normalizing the load by the interpreted ultimate lateral load capacity, Q_{ult} (Q at s/D=10%), and normalizing the displacement, s, by 10% of pier diameter, s_f. This normalizing technique has been used previously as discussed in Section 2.5. The normalized results of all piers are presented in Figure 5.10 for Q_{ult} at s/D=10%.
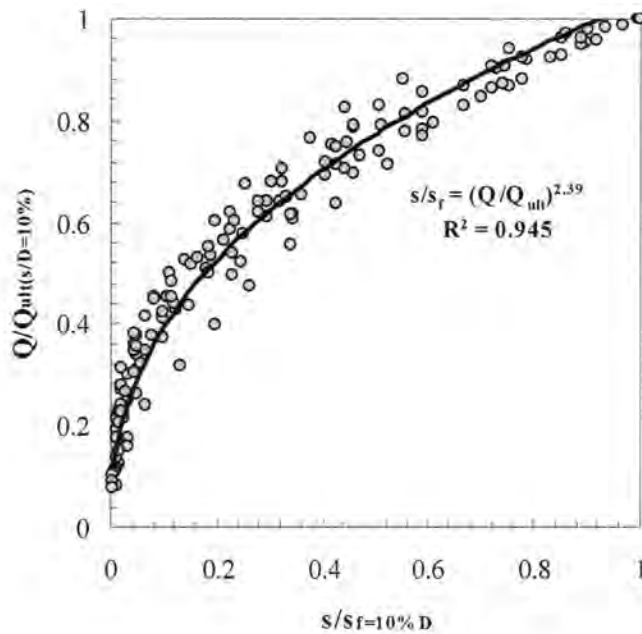

The curve is labeled with:

$$s/s_f = (Q/Q_{ult})^{2.39}$$
$$R^2 = 0.945$$

y-axis: $Q/Q_{ult(s/D=10\%)}$

x-axis: $s/s_{f=10\% D}$

Figure 5.10 Normalized Load-Displacement Results for All Test Piers (s_f/D=10%)

A study by Dearth (2002) showed that the lateral load-displacement behavior of drilled shafts could be described as a simple power function:

$$\frac{s}{s_f} = \left(\frac{Q}{Q_{ult}}\right)^x \qquad [5.2]$$

in which:

s = settlement at any load, Q

s_f = settlement at the failure load, Q_{ult}

x = an exponent

To use this model, a 2-parameter power function $y(x) = ax^b$ is fit through load test results plotted as normalized load versus normalized displacement. However, the normalized model requires the use of power function $x(y) = (y/a)^{1/b}$, in which the coefficient $1/a$ is assumed to be approximately 1 (a=1.0) and therefore the inverse of b (1/b) can be represented by the exponent, x.

Figure 5.10 presents the normalized load test results, taking the value of s_f as s = 10%D, where Q/Q_{ult} varies from 0 to 1 and s/s_f varies from 0 to 1. Using the simple power function model from Equation [5.2], the test results give the average curve:

$$\frac{s}{s_f} = \left(\frac{Q}{Q_{ult}}\right)^{2.39} \qquad\qquad [5.3]$$

For design purposes, the results presented in Figure 5.10 indicate that at a factor of safety of 2 (i.e., Q/Q_{ult} = 0.5), the average relative settlement s/s_f is approximately 0.2, which corresponds to an s/D of approximately 2%. The R^2 = 0.945 indicates a good trend exists for the relationship between normalized load and displacement.

Table 5.5 summarizes the normalized model parameters used to determine the average curve defined in Equation [5.2]. The exponent, equation coefficient, and R^2 value for all piers represented as a single population are presented. For comparison, the results of drilled shafts tests by Dearth (2002) at DOE and UMAF Site are also presented. It can be seen from Table 5.5 that the exponent of SGES is higher than the other two sites, indicating that the soil in SGES is softer than DOE and UMAF Sites. The average DMT modulus E_D at

the upper 3 m soil layer of SGES, DOE, and UMAF is 6.9, 14.6, and 14.3 MPa, respectively. The other test results are also presented for comparison.

In addition, the average exponent, x, for the simple power function model for all piles was determined by calculating the mean and standard deviation of x for each individual normalized load test result. Table 5.6 presents the normalized model parameters for each normalized load test conducted at the SGES. The mean value of x, 2.38, with standard deviation, 0.3, compares very well with the exponent 2.39 from Figure 5.10, where the all load test results were modeled as a single population.

Table 5.6 also presents the "coefficient" for the normalized model expressed in terms of y. As expected, the coefficient is very close to one (0.92) and exhibits minimal variability with a standard deviation equal to 0.08. It appears that grouping all test results at a single site as a single population adequately represents the normalized behavior of laterally loaded piers.

Table 5.5 Comparison of Normalized Model Parameters of Different Sites, where $s_f/D=10\%$

Site	R^2	Coefficient	Exponent, x	DMT* E_D (kPa)	PMT*	
					P_L (kPa)	S_u (kPa)
SGES	0.945	0.92	2.39	6900	--	--
DOE	0.980	1.04	1.71	14600	759	97
UMAF	0.971	1.03	2.07	14300	677	89

Site	CPT*		SPT*	BST*		CU*		Unconfined*			USCS classification
	q_c (kPa)	E_s (kPa)	N	c (kPa)	ϕ	c (kPa)	ϕ	q_u (kPa)	e_{50}	S_u (kPa)	
SGES	1338	4014	11	--	--	2	32	118	0.027	59	CL, ML, SC
DOE	2450	7350	--	0.5	32	--	--	--	--	--	CL-ML
UMAF	--	--	--	1.2	36	--	--	--	--	--	CL

Note: -- Test not performed.

* Averaged values from ground surface to 3 m (10 feet) deep.

Table 5.6 Normalized Model Parameters for Individual Load Test Results at SGES, where $s_f/D=10\%$

Pier	R^2	Coefficient	Exponent, x
MP1	0.98	0.96	2.13
MP2	1	1	2.57
MP3	0.977	0.99	2.18
MP4	0.998	0.971	1.8
MP5	0.998	0.998	2.99
MP6	0.961	1.034	2.53
MP7	0.981	0.878	2.686
MP8	0.969	0.845	2.428
MP9	0.992	0.855	2.203
MP10	0.953	0.902	2.569
MP11	0.977	0.762	2.306
MP12	0.975	0.805	2.169
Average		**0.92**	**2.38**
Standard Deviation		**0.08**	**0.30**

5.5.2 Influence of Definition of "Ultimate" Lateral Load Capacity

Work by Dearth (2002) showed that the power function model is independent of the definition of "ultimate" lateral load capacity. Dearth (2002) stated that the pier capacity can also be defined as the displacement equal to 2.5, 5, and 20% of pier diameter, an absolute deflection of 25.4mm (1.0in.), and absolute rotation about the pile base of 1 and 2 degrees. The normalizing technique was applied by normalizing the lateral load Q by the interpreted "ultimate" load (e.g., $Q_{s=20\%D}$), and normalizing the displacement s by "ultimate" displacement (e.g. 20%D). It was found that at DOE and UMAF Site, the exponent of power function is 1.71 and 2.07, respectively.

Pier behavior at SGES Site was analyzed as a single population for simplicity as it does not appear to have a significant impact of normalized model. Load-displacements results expressed in nondimensional terms for multiple definitions of lateral load capacity can be described by the same general curve. Table 5.7 summarizes the normalized model

parameters for 7 definitions of pier capacity. The mean "coefficient" of the normalized model for all definitions of ultimate capacity is 0.91 ± 0.02. The mean exponent is 2.37 ± 0.13. The normalized model works very well for all presented definitions of lateral load capacity at SGES Site. Normalized results for each definition of ultimate pier capacity are presented in Appendix C.

Figure 5.11 graphically illustrates the results summarized in Table 5.7. Both Figure 5.11 and Table 5.7 clearly indicate that the definition of "ultimate" pier capacity does not affect the normalized load-displacement results. Therefore, for all suggested definitions of "ultimate" capacity, the load-displacement behavior of piers at the SGES Site can be described by the simple expression:

$$\frac{s}{s_f} = \left(\frac{Q}{Q_{ult}}\right)^{2.39}$$

Table 5.7 Influence of Definition of "Ultimate" Lateral Load Capacity of Normalized Model Parameters

Failure Criterion	R^2	Coefficient	Exponent, x
Q at s/D=2.5%	0.928	0.9	2.2
Q at s/D=5%	0.937	0.93	2.31
Q at s/D=10%	0.945	0.92	2.45
Q at s/D=20%	0.949	0.9	2.57
Q at s=25.4mm (1in.)	0.933	0.92	2.25
Q at 1^0 rotation	0.946	0.92	2.3
Q at 2^0 rotation	0.957	0.868	2.49
Mean		**0.91**	**2.37**
Standard Deviation		**0.02**	**0.13**
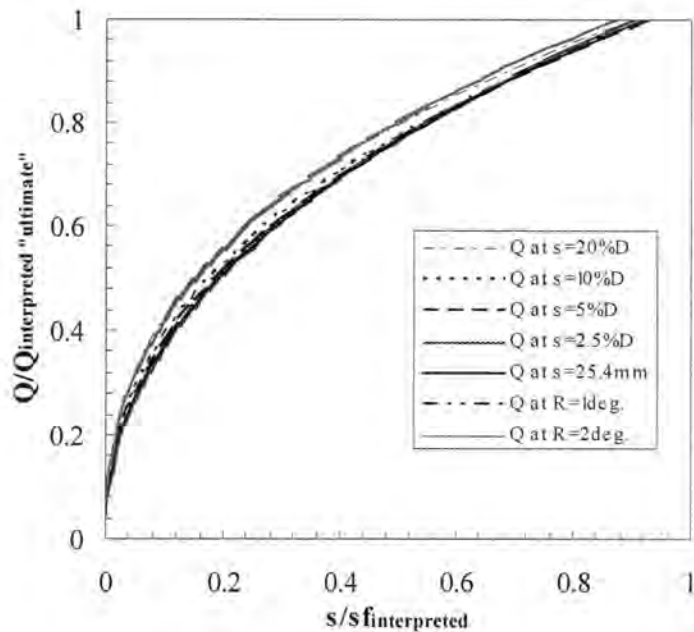
Figure 5.11 Influence of Definition of "Ultimate" Pier Capacity on Normalized Load-Displacement Behavior at SGES

5.6.3 Influence of Undrained Shear Strength of Soil

Given the exponent of nondimensional form, the load-displacement behavior of a pier can be predicted. However, the exponent depends on the soil strength, as indicated by Table 5.5. Three different sites give different exponents. To evaluate the influence of undrained shear strength on the exponent, a study was conducted, as shown in Figure 5.12.

This study shows that the exponent ranges from 1.7 to 3. For a constant e_{50}, the exponent decreases as the undrained shear strength S_u increases. However, when the S_u is greater than about 110 kPa (16psi), the additional increase of S_u has very little effect on the exponent. The undrained strengths and exponents of SGES, DOE, and UMAF Sites are included in this figure.

For SGES Site, the unconfined compression tests results (q_u) were used to obtain the undrained shear strength S_u ($S_u=q_u/2$). For DOE and UMAF Sites, the undrained shear strengths were obtained by using the empirical correlation proposed by Baguelin *et al.* (1978):

$$S_u = 0.67 \, p_L^{0.75} \tag{5.4}$$

As indicated in Table 5.5, the undrained shear strengths of SGES, DOE and UMAF Sites are 59, 89, and 97 kPa, respectively.
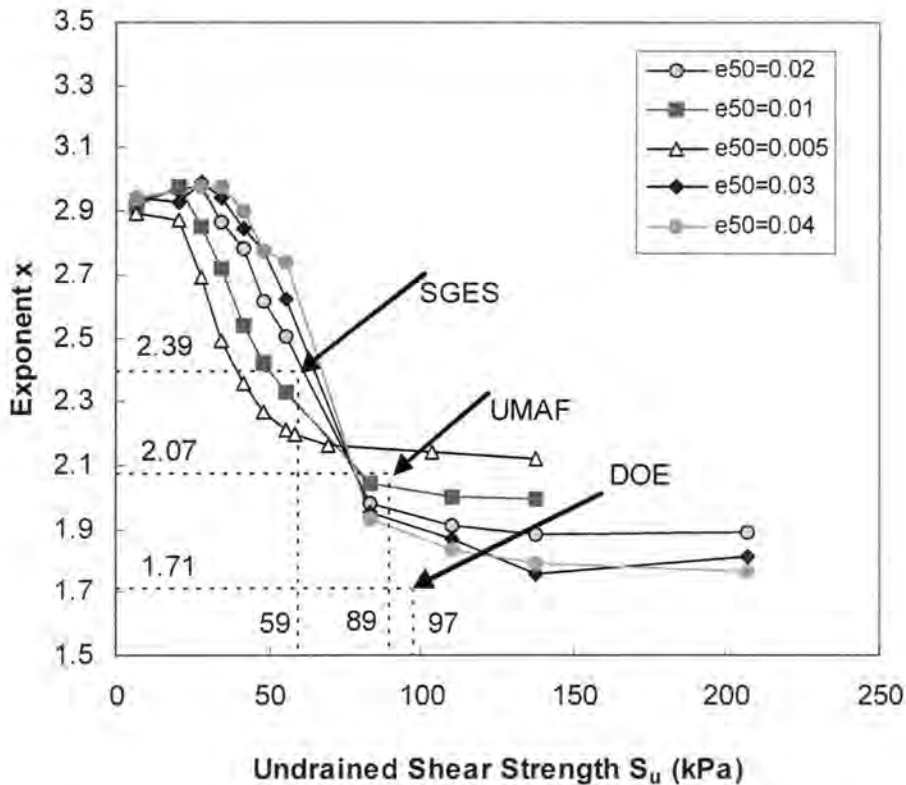
Figure 5.12 Effect of Undrained Shear Strength and e_{50} on Exponent

5.6 Base Shear Effect

By using the LTBASE program, the base shear was calculated for each pier and compared with the ultimate pier capacity. To investigate the base shear effect as a function of

L/D ratio, the base shear is normalized by Q_{ult} (s_f=10%D). Figure 5.12 presents the normalized results. When L/D increases, base shear/Q_{ult} decreases rapidly. From Figure 5.13 it can be seen that base shear is less than 10%Q_{ult} when L/D is greater than about 7, indicating the base shear is insignificant for MP2 (L = 2.29 m, D = 0.305 m) and MP3 (L = 3.05 m, D = 0.305 m).
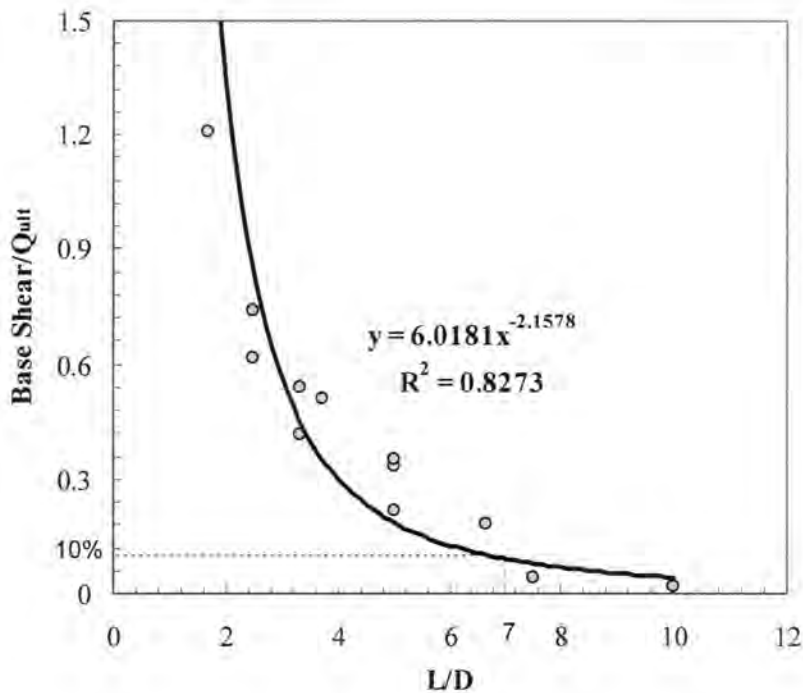
Figure 5.13 Normalized Results of Base Shear

5.7 Predicting Load-Displacement Behavior and Ultimate Lateral Capacity

At present, there are a number of different methods for predicting the lateral load-displacement behavior of piers and ultimate lateral load capacity, which may be defined in many ways. This investigation compares measured and predicted behavior and capacities for laterally loaded piers at SGES Site. Prediction methods discussed herein include: ultimate

strength method, in situ test methods, Consolidated-Undrained (CU) method and commercially available computer software, LPILE and LTBASE.

5.7.1 Ultimate Strength Method

As previously discussed in Section 2.4.1, Broms' (1964) theory can be used to estimate the ultimate lateral load capacity Q_{ult} of the pier. For rigid pier embedded in the soils, using the requirements of moment equilibrium at the base of the pier, together with the distribution of soil resistance shown in Figures 2.4 and 2.5, the following expressions for Q_{ult} can be derived:

For cohesive soil:

$$Q_{ult} = \frac{9C_u D(L - 1.5D)^2}{2(e + L)}$$
[5.3]

For cohesionless soil:

$$Q_{ult} = \frac{\gamma DL^3 K_p}{2(e + L)}$$
[5.4]

in which:

Q_{ult} = ultimate load capacity (force)

D = pier diameter (length)

L = embedded pier length (length)

e = load eccentricity (length)

C_u = undrained shear strength of soil.

K_p = Rankine passive earth pressure coefficient = $\tan^2(45+\phi/2)$, and

ϕ = angle of internal friction.

For cohesive soils, it was found that when L/D is less than 4, the Q_{ult} calculated by Equation [5.3] may underestimate the pier load capacity because the top 1.5D soil resistance was ignored. Instead, the coefficient 9 is replaced by a shape factor, N_p, defined as:

$$N_p = 3 + \frac{\sigma_v'}{C_u} + J(\frac{z}{D})$$

[5.5]

in which:

σ'_v = effective overburden stress at depth z, and

J = empirical coefficient, 0.5 for soft clays and 0.25 for stiff clays.

The predicted and measured lateral load capacity Q_{ult} for twelve piers is presented in Table 5.8. The soil was assumed to be cohesionless and Equation [5.4] was used. To apply Equation [5.4], load eccentricity e was taken as zero. Based on the CU triaxial tests results, the unit weight γ and friction angle ϕ was taken as 19 kN/m^3, and 34^0, respectively.

From Table 5.8 it can be seen that the overall prediction is very close to the measured Q_{ult}. The average $Q_{predicted}/Q_{measured}$ is 1.05, with a deviation of 0.36. Broms' (1964) method tends to underpredict the measured value when L/D is small. For cohesionless soil, the soil resistance is assumed to increase linearly. Thus, the upper soil is much softer than the deeper soil.

Table 5.8 Summary of Measured and Predicted Ultimate Loads Based on Broms' (1964) Theory on Cohesionless Soil

Piers	L (m)	D (m)	L/D	$Q_{Measured}$ $(s_f=10\%D)$ (kN)	$Q_{predicted}$ (kN)	$Q_{predicted}/$ $Q_{measured}$
MP1	1.52	0.30	5	36	23.8	0.66
MP2	2.29	0.30	7.5	43.6	53.5	1.23
MP3	3.05	0.30	10	51.2	95.2	1.86
MP4	1.52	0.46	3.33	56	35.7	0.64
MP5	2.29	0.46	5	62.3	80.3	1.29
MP6	3.05	0.46	6.67	115.6	142.7	1.23
MP7	1.52	0.61	2.5	59.2	47.6	0.80
MP8	2.29	0.61	3.8	117.9	107.0	0.91
MP9	3.05	0.61	5	166.8	190.3	1.14
MP10	1.52	0.91	1.67	129	71.4	0.55
MP11	2.29	0.91	2.5	151.2	160.6	1.06
MP12	3.05	0.91	3.33	235.2	285.5	1.21
Average						**1.05**
Standard Deviation						**0.36**

5.7.2 Nonlinear Subgrade Reaction Method (p-y Method)

One of the greatest difficulties in predicting the lateral load-displacement behavior of piers is in estimating the nonlinear p-y relationship of the soil. Previous investigations have suggested the use of a variety of in situ tests to analyze the lateral load behavior of drilled shafts, as discussed previously in Section 2.4.2.5. CPT, SPT, and DMT tests were performed at SGES to use with the most common methods for predicting the lateral load behavior of the test piers. In addiction, CU triaxial tests were also performed to predict the lateral load behavior using LPILE computer software. The test procedures and results for the CPT, SPT, DMT and CU have been previously presented in Chapter 4.

The LPILE input parameters used to determine p-y curves based on the SPT and CPT tests results are previously summarized in Table 2.3. Tables 5.9 and 5.10 present these values.

Table 5.9 SPT Profile Used to Determine P-y Curves

Depth (m)	Layer	Soil type	Effective unit weight γ' (kN/m³)	p-y modulus k (kN/m³)	Undrained shear strength s_u (kPa)	Soil strain ε_{50}	friction angle ϕ (°)
0-0.76	1	Stiff Clay (above GWT)	19.9	135717	48.6	0.007	--
0.76-1.52	2	Soft Clay (below GWT)	10.1	--	35	0.01	--
1.52-2.29	3	Sand (below GWT)	10.1	16286	--	--	30.3
2.29-3.05	4	Sand (below GWT)	10.1	16286	--	--	33.1

Note: Ground water table (GWT) = 0.76 m

    --: Not Required

Table 5.10 CPT Profile Used to Determine P-y Curves

Depth (m)	Layer	Soil type	Effective unit weight γ' (kN/m³)	p-y modulus k (kN/m³)	Undrained shear strength s_u (kPa)	Soil strain ε_{50}	friction angle ϕ (°)
0-0.76	1	Stiff Clay (above GWT)	19.9	135717	81.8	0.007	--
0.76-1.52	2	Stiff Clay (above GWT)	19.9	--	37.8	0.007	--
1.52-2.29	3	Sand (below GWT)	10.1	16286	--	--	33
2.29-3.05	4	Sand (below GWT)	10.1	16286	--	--	33.6

Note: GWT = 1.52 m

    --: Not Required

As previously discussed in Section 2.4, the DMT method proposed by Robertson *et al.* (1989) and CU triaxil test method proposed by McClelland and Focht (1958) was also used to predict the lateral load-displacement behavior.

P-y curves were generated every 0.76 m (2.5 feet) interval along the length of pier. All the p-y curves are included in Appendix C.

Figure 5.14 presents an example of p-y curves for pier with D = 0.61m, L = 1.52m at the depth of 0.76m. Figure 5.15 presents the comparison between measured load-deflection curve and predicted curves. Table 5.11 presents lateral load capacity predictions and measured results at s/D=10% using the in situ test and CU test methods.
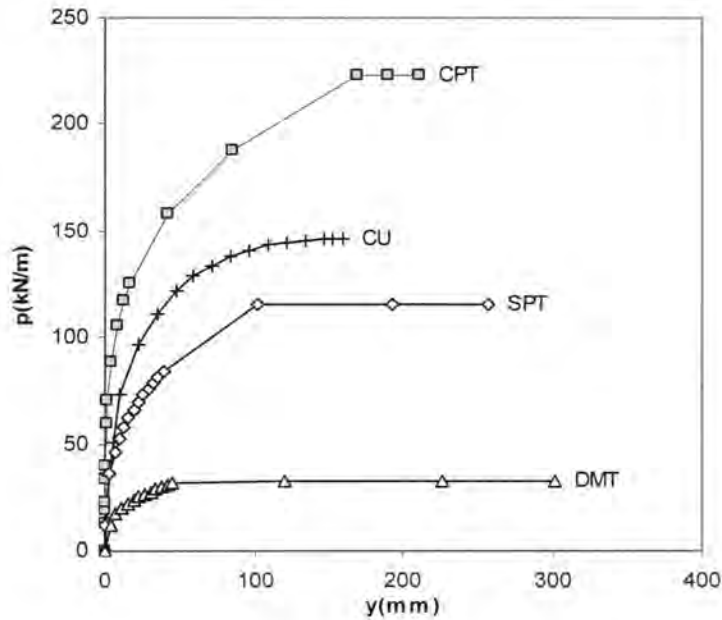
Figure 5.14 P-y Curves for MP7 (D = 0.61m, L = 1.52m) at Depth of 0.76m
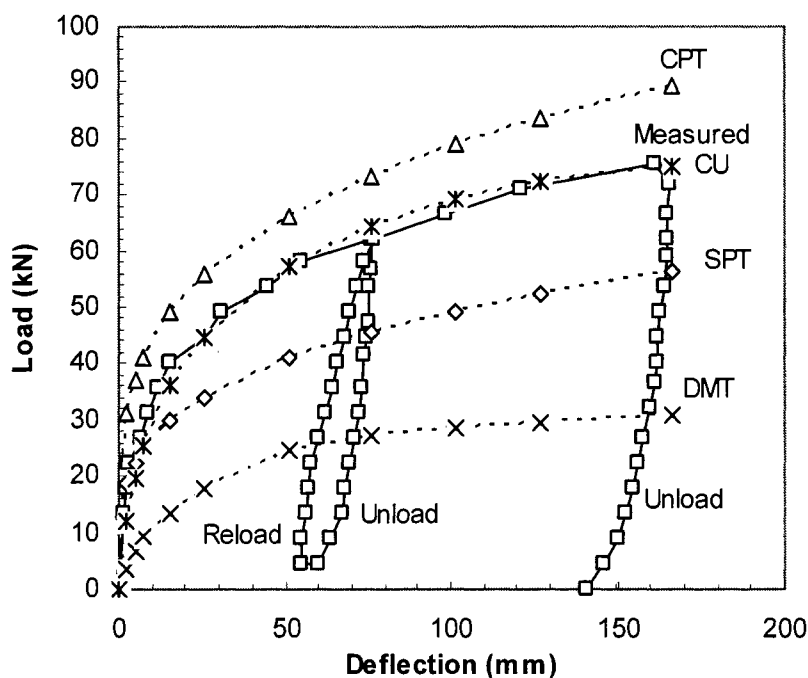
Figure 5.15 Measured vs. Predicted Load-Deflection Curves for MP7 (D = 0.61m, L = 1.52m)

Table 5.11 Comparison of Load Capacity between Measured and Predicted by In Situ Tests and CU Triaxial Tests

Pile	$Q_{s=10\%D}$ (kN)					$Q_{predicted}/Q_{measured}$			
	DMT	SPT	CPT	CU	Measured	DMT	SPT	CPT	CU
MP1	18.0	20.0	36.0	36.0	36	0.50	0.56	1.00	1.00
MP2	38.7	38.7	60.0	48.9	43.6	0.89	0.89	1.38	1.12
MP3	49.9	51.3	71.3	60.6	51.2	0.97	1.00	1.39	1.18
MP4	23.1	34.7	56.0	48.9	56	0.41	0.62	1.00	0.87
MP5	46.3	56.5	89.0	74.3	62.3	0.74	0.91	1.43	1.19
MP6	82.0	86.8	127.3	115.5	115.6	0.71	0.75	1.10	1.00
MP7	25.8	42.7	68.9	59.6	59.2	0.44	0.72	1.16	1.01
MP8	57.4	75.6	117.9	107.6	117.9	0.49	0.64	1.00	0.91
MP9	97.9	118.3	169.0	160.1	166.8	0.59	0.71	1.01	0.96
MP10	29.8	64.5	104.5	121.0	129	0.23	0.50	0.81	0.94
MP11	62.3	106.8	166.8	151.2	151.2	0.41	0.71	1.10	1.00
MP12	109.0	169.0	201.0	231.3	235.7	0.46	0.72	0.85	0.98
Average						**0.57**	**0.73**	**1.10**	**1.01**
Standard Deviation						**0.22**	**0.15**	**0.2**	**0.1**

As shown in Figures 5.14, 5.15 and Table 5.11, p-y curves developed by different tests methods exhibit large variation. The DMT, SPT and CPT methods did not predict the pier capacity very well. The mean ratio of predicted to measured capacity at s/D=10% was 0.57 ± 0.22, 0.73 ± 0.15, and 1.1 ± 0.2, respectively. On the other hand, CU tests predicted the load capacity very well, the mean ratio of predicted to measured capacity at s/D=10% was 1.01 ± 0.1.

DMT method is limited by its dependence on empirical correlations of the dilatometer modulus for all soils, of the undrained shear strength for cohesive soils, and of the effective friction angle for cohesionless soils. For the Robertson *et al.* (1989) method, p_u and y_{50} are very sensitive to soil type. It is hard to differentiate whether it is cohesive or cohesionless as the soil may have both cohesion and friction angle. DMT predictions are also sensitive to empirical coefficients F_c and F_ϕ, for which suggestions of both are very vague. Similarly, the CPT and SPT methods also are limited by their dependence on the empirical correlations to obtain cohesion and friction angle. The friction angle obtained from CPT profile tends to be too high. Currently, there is no approach available that correlates the CPT and SPT profiles directly to p-y curves. The undrained shear strength and friction angles obtained by CU triaxial tests are more accurate to represent the soil properties.

5.8 Inclinometer Tests

To observe the distribution of horizontal movements along the piers, an inclinometer tube was installed in the center of each pier except those with diameter of 0.3 m (12 inches), since they are too small to be installed. The deflection was measured by digitilt inclinometer

model 50306, which has a precision of 0.5mm approximately. Inclinometer measurements were carried out before, during, and at the end of load test.

Figure 5.16 shows the inclinometer test results for MP7 (D = 0.61m, L=1.52m). The pier deflection was measured at depth of 0.52, 0.82, and 1.13 m (1.7, 2.7, and 3.7 feet) when the loading was 44.5, 53.4, 62.3, and 76.6 kN (10, 12, 14, and 17 kips). A trend line was plotted and extended both to the base and the ground surface. At the ground surface, the deflection agreed well with the lateral deflection measured by the rulers during the load tests. It can be seen from Figure 5.16 that the pier rotated as a unit with respect to a point close to its toe, which is typical for rigid pier. All piers behaved rigidly. Other inclinometer test results are presented in Figure 5.17.
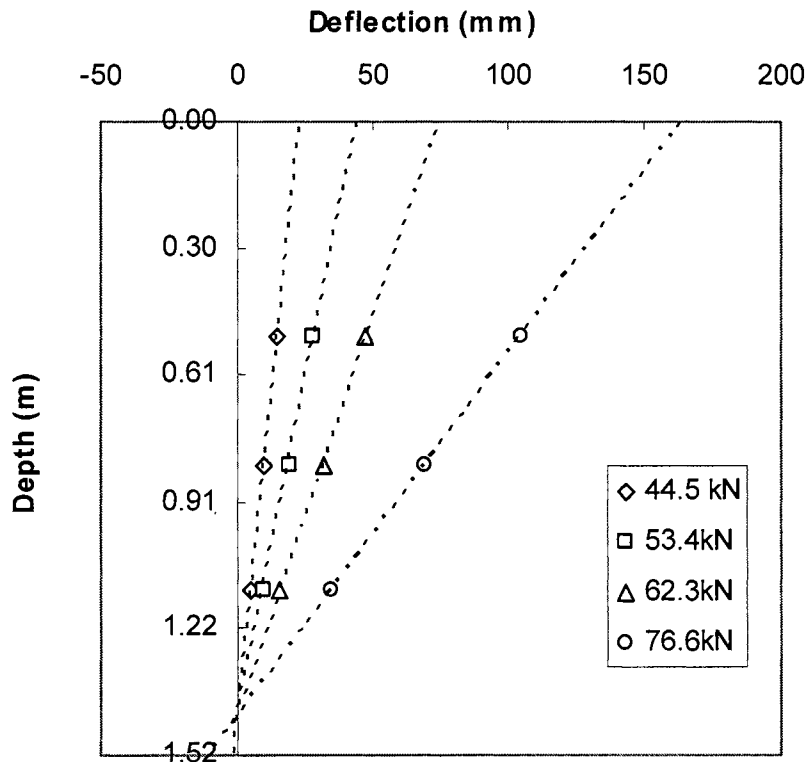
Figure 5.16 Inclinometer Test Results for MP7 (D = 0.61m, L = 1.52 m)
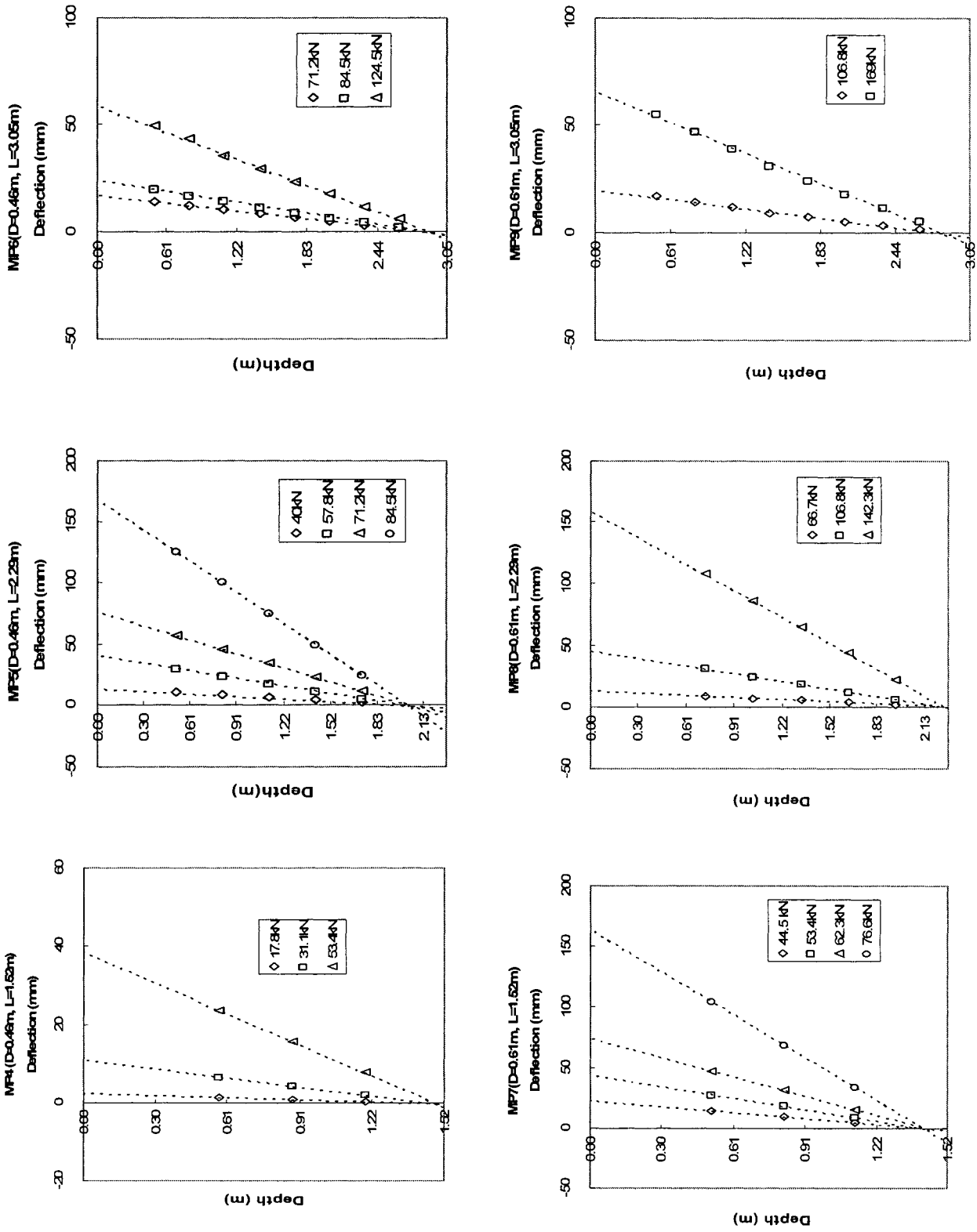
Figure 5.17 Inclination Curves of 12 Piers at SGES
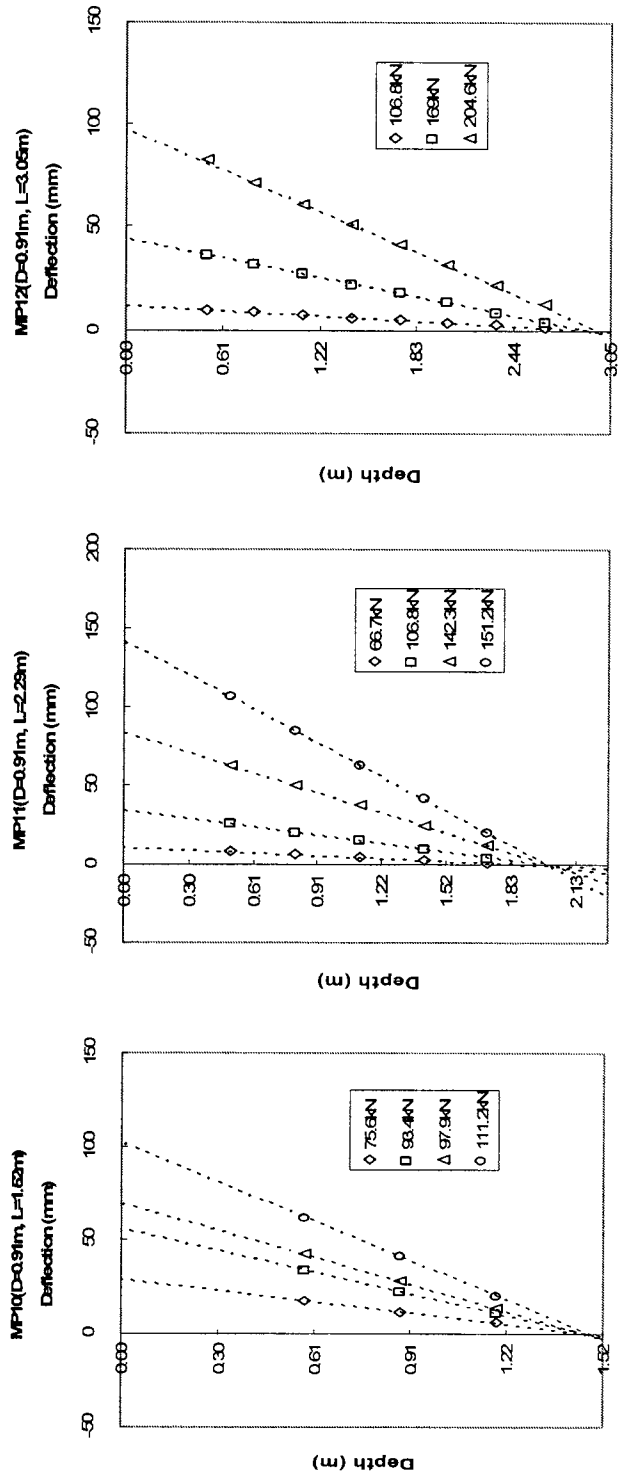
Figure 5.17 (Continued)

CONCLUSIONS

The major conclusions derived from this research are:

Parametric Study

- Pier behavior depends on pier geometry, pier material, embedment soil.

- When L/D is less than or equals to 4, a pier is classified as rigid by all methods and it is independent of embedment soil.

- Pier yields or breaks at smaller displacement in stiff clay, intermediate in sand, and larger in soft clay.

- In the same soil, pier with larger diameter yields or breaks at smaller s_f/D.

- The general lateral load-displacement of piers embedded in stiff clay can be described by a single simple power function model defined as:

$$\frac{s}{s_f} = \left(\frac{Q}{Q_{ult}}\right)^4$$

The exponent is similar to the p-y curve ($y/y_{50} = (p/p_u)^{1/4}$) exponent of stiff clay and it is independent of the definition of Q_{ult} (s_f/D=1%, 2%, 5%, 10%, 20%)

- The general lateral load-displacement of piers embedded in soft clay can be described by a single simple power function model defined as:

$$\frac{s}{s_f} = \left(\frac{Q}{Q_{ult}}\right)^3$$

The exponent is similar to the p-y curve ($y/y_{50} = (p/p_u)^{1/3}$) exponent of soft clay and it is independent of the definition of Q_{ult} (s_f/D=1%, 2%, 5%, 10%, 20%).

- The general lateral load-displacement of piers embedded in sand can also be described by a single power function model defined as:

$$\frac{s}{s_f} = (\frac{Q}{Q_{ult}})^{1.39 - 3.42}$$

in which the exponent varies from 1.39 to 3.42 and depends on the definition of Q_{ult} (at $s_f/D=1\%, 2\%, 5\%, 10\%, 20\%$).

- In soft clay, piers always behave as rigid and it is hard to reach breaking moment. In stiff clay, however, piers can yield or break at the displacement less than 10%D.

- The base shear effect is significant when the pile length-diameter ratio is small. However, when length-diameter ratio increases to about 5 in sand, 13 in clay, the base shear is less than 10% of Q_{ult}. The base shear can be neglected.

- Due to base shear effect, ultimate loads Q_{ult} calculated by LTBASE was higher than calculated by LPILE. When L/D is greater than 4, Q_{ult} calculated by LPILE is about 95%-100% as that by LTBASE.

Lateral Load Tests and Inclinometer Tests

- From inclinometer test results, all piers embedded in the SGES exhibited rigid behavior. The soil in SGES is relatively soft as compared to DOE and UMAF Sites at the University of Massachusetts Campus. Pier behavior depends on relative stiffness of pier and embedment soil. There is no common criterion which is applicable to all pier material and soil type. For all methods presented in Table 2.1, the numerical solution provided by Reese *et al.* (2000) (Figure 2.2) may be a good tool to predict the pier behavior.

- The simple power function suggested by Lutenegger *et al.* (1998) can be used to normalize the lateral load-displacement piers and the form of normalized results is independent of the definition of Q_{ult}.

- The load displacement behavior of all piers at the SGES can be defined as:

$$\frac{s}{s_f} = (\frac{Q}{Q_{ult}})^{2.39}$$

in which s_f is the interpreted failure displacement, and Q_{ult} is the load at s_f.

As compared with $\frac{s}{s_f} = (\frac{Q}{Q_{ult}})^{1.71}$ at DOE Site and $\frac{s}{s_f} = (\frac{Q}{Q_{ult}})^{2.07}$ at UMAF Site,

the exponent of SGES Site is larger than the other two, indicating that the soil at SGES

Site is softer.

- The exponent of nondimensional form depends on soil undrained shear strength. The

exponent increases as undrained shear strength decreases. However, undrained shear

strength has little effect on the exponent when it is greater than about 110 kPa (16 psi).

- Broms' (1964) method on cohesionless soil tends to underestimate the ultimate lateral

load capacity when the pier length is small (5 ft), and overestimate when the length is

large (7.5 ft and 10 ft). Broms' (1964) method on cohesive soil can't be used when L/D

is small (L/D $\leq$ 4), since the upper 1.5D soil resistance is ignored.

- The DMT method proposed by Robertson *et al.* (1989) underestimated the ultimate

capacity and poorly predicted the load displacement curves. p_u and y_{50} are sensitive to

the assumption of whether the soil is cohesive or cohesionless. The difference can be 5

times. Also, the suggestions of empirical coefficients F_c and F_ϕ are not clear.

- There is no direct correlation between CPT or SPT profile and p-y curve. P-y curves

were generated by LPILE program. The input parameters were obtained from some

empirical correlation between undrained shear strength, friction angle and CPT tip

resistance, SPT blow count. CPT and SPT prediction is not recommended.

- CU triaxial method predicted the load-displacement well. Skempton (1951) and McClelland and Focht (1958) method correlates the CU stress-strain curve directly to p-y curve, which may be more accurate to represent the soil condition.

- Prediction by LTBASE showed that the base shear effect becomes insignificant (base shear/Q_{ult} ≤10%) when L/D ≥ 7 at SGES Site.

Recommendations for Future Research

- Perform DMT tests, PMT tests and CU triaxial tests to simulate the p-y curves.

- In addition to lateral loads tests on virgin soil conditions, perform the lateral load tests on "rehabilitated" piers to evaluate some repair options.

REFERENCES

Aas, G., S. Lacasse, T. Lunne, and K. Hoeg. 1986. Use of In Situ Tests for Foundation Design on Clay. In *Use of In Situ Tests in Geotechnical Engineering* (S. P. Clemence, ed.), Geotechnical Special Publication 6, American Society of Civil Engineers, New York, pp.1-30.

Alizadeh, M. and Davisson, M.T., 1970. "Lateral Load Tests on Piles-Arkansas River Project." *Journal of the Soil Mechanics and Foundations Division, ASCE,* Vol. 96, No. SM5, pp. 1583-1603.

ASTM Standard D3966, 1995. "Standard Test Method for Piles Under Lateral Loads".

Baqulein, F., Jézéquel, J.F., and Shields, D.H., 1978. "The Pressuremeter and Foundation Engineering." *Trans Tech Publications, Gower Publishing Co., Brookfield*, VT, p.617.

Baguelin, F., Jezequel, J.F., and Shields, D.H., 1978. *The Pressuremeter and Foundation Engineering,* Trans Tech Publications, Clausthal-Zellerfeld, W. Germany.

Bierschwale, M.W., Coyle, H.M., Bartoskewitz, R.E., 1981. "Lateral Load Tests on Drilled Shafts Founded in Clay". In M.W. O'Neill (ed.), *Drilled Piers and Caissons*, New York: ASCE, pp. 98-113.

Borden, R.H. and Gabr, M.A., 1987. "LTBASE: Lateral Pier Analysis Including Base and Slope Effects." *Research Report No. HRP 86-5.* Center for Transportation Engineering Studies, North Carolina State University, Raleigh.

Briaud, J.-L., Smith, T.D. and Meyer, B.J., 1984. "Laterally Loaded Piles and the Pressuremeter: Comparison of Existing Methods." *Laterally Loaded Deep Foundations; Analysis and Performance, ASTM* STP No. 835, pp.97-111.

Briaud, J.-L., 1989. "The Pressuremeter Test for Highway Applications." U.S. Department of Transportation, Federal Highway Administration, No. FHWA-IP-89-008.

Briaud, J. L., and Gibbens, R. M. 1994. " Tests and prediction results for five large spread footings on sand." *Proceedings, FHWA Spread Footing Prediction Symposium,* Geotechnical Special Publication. No. 41, ASCE, New York, N.Y., 92-128.

Briaud, J.-L., 1997. "SALLOP: Simple Approach for Lateral Loads on Piles." *Journal of Geotechnical and Geoenvironmental Engineering, ASCE,* Vol. 123, No. 10, pp. 958-964.

Broms, Bengt B., March 1964. "Lateral Resistance of Piles in Cohesive Soils, *"Journal of the Soil Mechanics and Foundation Division, ASCE,* Vol. 90, No. SM2, pp. 27-63.

Broms, Bengt B., May 1964. "Lateral Resistance of Piles in Cohesionless Soils, *"Journal of the Soil Mechanics and Foundation Division, ASCE*, Vol. 90, No. SM3, pp. 123-157.

Bruce, D. A., Bruce, M. E. C., and Traylor, R. P. 1999. "High capacity micropiles- Basic principles and case histories." Geo-Engineering for Underground Facilities, G. Fernande and R. A. Bauer eds., Geotechnical Special Publication No. 90, ASCE, Reston, Virginia. 188-199.

Davisson, M. T., and Gill, H. L., May 1963. "Laterally Loaded Piles in a Layered Soil System," *Journal of the Soil Mechanics and Foundation Division, ASCE*, Vol. 89, No. SM3, Proc. Paper 3509, pp. 63-94

Dearth, A.E., 2002. Behavior of Laterally Loaded Rigid Drilled Shafts.

DeBeer, E.E., 1970. Experimental Determination of the Shape Factors and the Bearing Capacity Factors of Sand. Geotechnique, Vol. 20, No. 4, pp. 387-411.

Douglas, D.J., and Davis, E. H., 1964. " The Movement of Buried Footings Due to Moment and Horizontal Load and the Movement of Anchor Plates," *Geotechnique*, Vol. 14, London, England, pp. 115-132.

Electrical Power Research Institute (EPRI)., 1990. *Manual on estimating soil properties for foundation design*, Cornell Univ., Ithaca, N.Y.

Gabr, M.A. and Borden, R.H., 1988. "Analysis of Load Deflection Response of Laterally Loaded Piers Using DMT." *Proceedings of the First International Sysposium on Penetration Testing*, ISOPT-1, pp. 513-520.

Gabr, M.A., Lune, T., and Powell, J.J., 1994. "P-y Analysis of Laterally Loaded Piles in Clay Using DMT. " *Journal of Geotechnical Engineering, ASCE*, Vol. 120, No.5, pp.816-837.

Gazioglu, S.M. and O'Neill, M.W., 1984. "Evaluation of p-y relationships in cohesive soils. " *Proc., Analysis and Design of Pile Foundations, ASCE Technical Council on Codes and Standards, ASCE National Convention*, J. Meyers, ed., New York, 192-213.

Gill, H. L., and Demars, K.R., 1970. "Displacement of Laterally Loaded Structures in Nonlinearly Responsive Soils," *Technical Report R670*, Naval Civil Engineering Laboratory, Port Hueneume, Calif., pp.1-59.

Girija Vallabhan, C.V., and Fariborz Alikhanlou, 1982. "Short Rigid Piers in Clays," *Journal of the Geotechnical Engineering Division, Proceedings of the American Society of Civil Engineers, ASCE, Vol. 108, No.GT10.*

Hansen, J.B. , 1961. "The Ultimate Resistance of Rigid Piles Against Transverse Forces, " *Bulletin 12*, Danish Geotechnical Institute, Copenhagen, Denmark.

Huang, A.B., Lutenegger, A.J., Islam, M.Z., and Miller, G.A., 1989. "Analysis of Laterally Loaded Drilled Shafts Using In Situ Tests Results." *Transportation Research Record*, No. 1235, pp.60-68.

Hirany, A. and Kulhawy, F.H., 1989. "Interpretation of Load Tests on Drilled Shafts, Part 3: Lateral and Moment." In F.H. Kulhawy (ed.), *Foundation Engineering: Current Principles and Practices, ASCE*, pp. 1160-1172.

IWM99 (1999), Proceedings of Second International Workshop on Micropiles, Yamaguchi University, Ube City, Japan.

Jamiolkowski, M. and Garassino, A., 1977. Soil Modulus for Laterally Loaded Piles. *Proc., Special Session No. 10, 9th International Conference on Soil Mechanics and Foundation Engineering,* Tokyo, Japan, pp. 43-57.

Laefer, D. F. 1999. "Geotechnical procedures for at-risk and in-distress structures." The Use of and Need for Preservation Standards in Architectural Conservation, L. B. Sickels Taves ed., ASTM STP 1355, ASTM, West Conshohochen, PA, 211-225.

Lutenegger, A.J., 1988. "Current Status of the Marchetti Dilatometer Test." *Proceedings of Penetration Testing 1988,* ISOPT-1, pp.137-156.

Lutenegger A.J. and Miller, G.A., 1993. "Behavior of Laterally Loaded Drilled Shafts in Stiff Soil." *Proceedings of the 3rd International Conference on Case Histories in Geotechnical Engineering,* Vol. 1, pp. 147-152.

Lutenegger, A.J., and Adams, M.T., 1998. Bearing Capacity of Footings on Compacted Sand. Proceedings of the 4th International Conference on Case Histories in Geotechnical Engineering, pp. 1216-1224.

Lutenegger, A.J., 2003. Load-Settlement Behavior of Shallow Foundations, 27th Annual ASCE Geotechnical Conference.

Lytton, Robert L., May 1975. "Design Charts for Minor Service Structure Foundations," *Research Report No. 506-1F,* Texas Transportation Institute, Texas A&M University, College Station.

Marchetti, S., 1980. "In-Situ Tests by Flat Dilatometer," *ASCE Journal of the Geotechnical Engineering Division,* Vol. 106, No. GT3, pp.299-321.

Mascardi, C. A. 1982. "Design criteria and performance of micropiles." Recent Developments in Ground Improvement Techniques, A. A. Balkema, Rotterdam, 439-450.

Matlock, Hudson, and Reese, Lymon C. , October 1960. " Generalized Solutions for Laterally Loaded Piles," *Journal of the Soil Mechanics and Foundation Division, ASCE*, Vol. 86, No. SM5, Part I, Proc. Paper 2626, pp. 63-91.

Matlock, H., 1970. "Correlations for Design of Laterally Loaded Piles in Soft Clay," *Preprints*, Second Annual Offshore Technology Conference, American Institute of Mining, Mettallurgical, Petroleum Engineering, Vol. I, No. OTC 1204, Houston, Tex., pp. I-577-588.

Mayne, P.W. and Kulhawy, F.H., 1991. "Load-Displacement Behavior of Laterally Loaded Rigid Drilled Shafts in Clay." *Proc., 4th International Deep Foundations Inst. Conference*, pp. 409-413.

Mayne, P. W., Kulhawy, F.H., and Trautmann, C.H., 1995. "Laboratory Modelling of Laterally Loaded Drilled Shafts in Clay." *Journal of Geotechnical Engineering, ASCE*.

McClelland, B., and Focht, J. A., Jr., 1956. "Soil Modulus for Laterally Loaded Piles," *Journal of the Soil Mechanics and Foundation Division, ASCE*, Vol. 82, No. SM4, Proc. Paper 1081, Oct., pp. 1-22

McClelland, B., and Focht, J.A., 1958. " Soil modulus for laterally loaded piles. " *Trans., ASCE*, Vol. 123, Paper No. 2954, 1049-1086.

McCorkle, B. L., 1969. "Side-Bearing Pier Foundations." *Civil Engineering, ASCE*, Vol. 39, No. 5, pp. 65-66.

McNulty, J.F., 1956. "Thrust Loading on Piles." *Journal of Soil Mechanics and Foundations Division. ASCE,* 82(SM2), pp. 940-1 to 25.

Murchison, J.M. and O'Neill M.W., Oct. 1984. "Evaluation of p-y Relationships in Cohesionless Soils," *Proceedings of ASCE Symposium on Analysis and Design of Pile Foundations*.

Parker, P.Jr. and Reese, L.C., 1970. "Experimental and Analytical Studies of Behavior of Single Piles in Sand Under Lateral and Axial Loading." *RE. Report 117-2, Center for Highway Research*, University of Texas at Austin.

Peck, R.B., Hanson, W.E., and Thornburn, T.H., 1974. *Foundation engineering*, Wiley, New York.

Poulos, H.G., May, 1971. "Behavior of Laterally Loaded Piles; I-single Piles, " *Journal of the Soil Mechanics and Foundations Division, ASCE*, Vol.97, No. SM5, Proc. Paper 8092, pp. 711-731.

Reese, L.C., William, R. C, and Koop, F.D., 1974. "Analysis of Laterally Loaded Piles in Sand," Sixth Annual Offshore Technology Conference.

Reese, L.C., and Welch, R.C., July, 1975. "Lateral Loading of Deep Foundations in Stiff Clay, "*Journal of the Geotechnical Engineering Division, ASCE*, Vol. 101, No. GT7, Proc. Paper 11456, pp. 633-649.

Reese, L.C. and J.D. Allen. 1977. *Drilled Shaft Design and Construction Guidelines Manual*, Vol. 2, *Structural Analysis and Design for Lateral Loading*. U.S. Department of Transportation Offices of Research and Development Implementation Division HDV-22, Washington, D.C., 227 pp.

Reese, L.C., Wang, S.T., 1997. LPILE Plus 3.0 Technical Manual, Ensoft, Inc.

Reese, L.C., Wang, S.T., 2000. LPILE Plus 4.0 Technical Manual, Ensoft, Inc.

Robertson, P.K., and Campanella, R.G., 1983. "Interpretation of cone penetration tests: Parts 1 and 2." *Can. Geotech. J.*, 20(4), 718-745.

Robertson, P.K., Campanella, R.G., Brown, P.T., Grof, I., and Hughes, J.M., 1985. "Design of Axially and Laterally Loaded Piles Using In Situ Tests : A Case History," *Canadian Geotechnical Journal*, Vol. 22, No.4, pp. 518-527.

Robertson, P.K., Davies, M.P., Campanella, R.G., 1989. "Design of Laterally Loaded Driven Piles Using the Flat Dilatometer." *Geotechnical Testing journal, ASCE,* Vol. 149, No 89, pp. 30-38.

Rollins, K., Mikesell, R. Clayton, R., and Keane, E., 1994. Uplift Load Tests on Drilled Shafts in Gravels to Evaluate Side Friction. Proceedings of the International Conference on Design and Construction of Deep Foundations, U.S. Federal Highway Administration, Vol. 3, pp. 1717-1731.

Schmertmann, J.H., 1982. "A Method for determining the Friction Angle in Sands from the Marchetti Dilatometer Test," *Proceedings, II European Symposium on Penetration Testing*, ESOPT II, Vol. 2, pp. 853-861.

Skempton, A.W., 1951. "The Bearing Capacity of Clays," *Proceedings,* Building Research Congress, Division I, Building Research Congress, London.

Taylor, G. E., Gularte, F. B., and Gularte, G. G. (1998). "Seismic retrofit of Fourth Street& Riverside Viaducts with micropiles." Soil Improvement for Big Digs, A. Maher and D. S. Yang eds., Geotechnical Special Publication No. 81, ASCE, Reston, Virginia, 313-325.

Terzaghi, K., 1955. "Evaluation of coefficients of subgrade reaction." *Geotechnique,* London, 5(4), 297-326.

Terzaghi, K., and Peck, R.B., 1968. *Soil mechanics in engineering practice*, 2nd Ed., Wiley, New York.

Trautmann, C.H. and Kulhawy, F.H., 1988. Uplift Load-Displacement Behavior of Spread Foundations. Journal of Geotechnical Engineering, ASCE, Vol. 114, No. 2, pp. 168-184.

Welch, R. C., and Reese, L. C., 1972 "Laterally Loaded Behavior of Drilled Shafts," Research Report No. 3-5-65-89, Center for Highway Research, The University of Texas at Austin.

Woodward, R.J., Gardner, W.S., Greer, D.M., 1972. *Drilled Pier Foundations,* McGraw-Hill Publishing Co., Inc., New York, N.Y., pp.64-67.

Zelenko, B. H., Bruce, D. A., Schoenwolf, D. A., and Traylor, R. P. (1998). "Micropiles applications for seismic retrofit preserves historic structure in old San Juan, Puerto Rico." Grouts and Grouting, L. Johnsen and D. Berry eds., Geotechnical Special Publication No. 80, ASCE, Reston, Virginia, 43-62.

APPENDIX A: PARAMETRIC STUDY

Appendix A1: Piers Displacement, Shear and Moment Curves in Sand (LPILE and LTBASE)
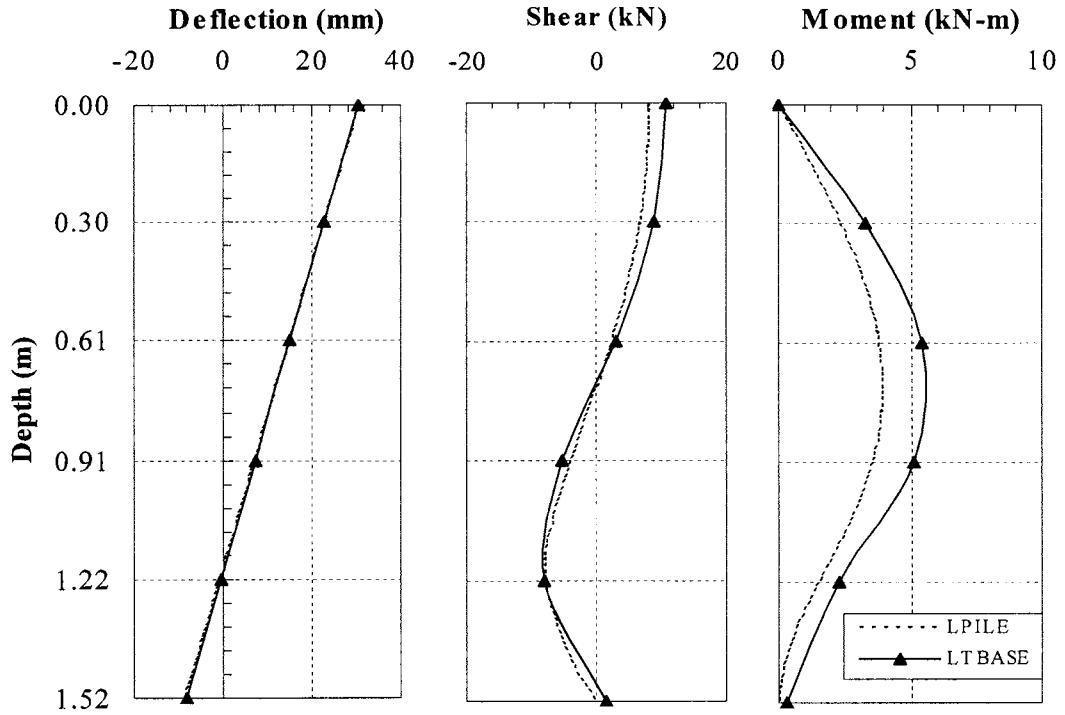
Displacement, Shear and Moment Curves in Sand (D = 0.3m, L=1.52m)
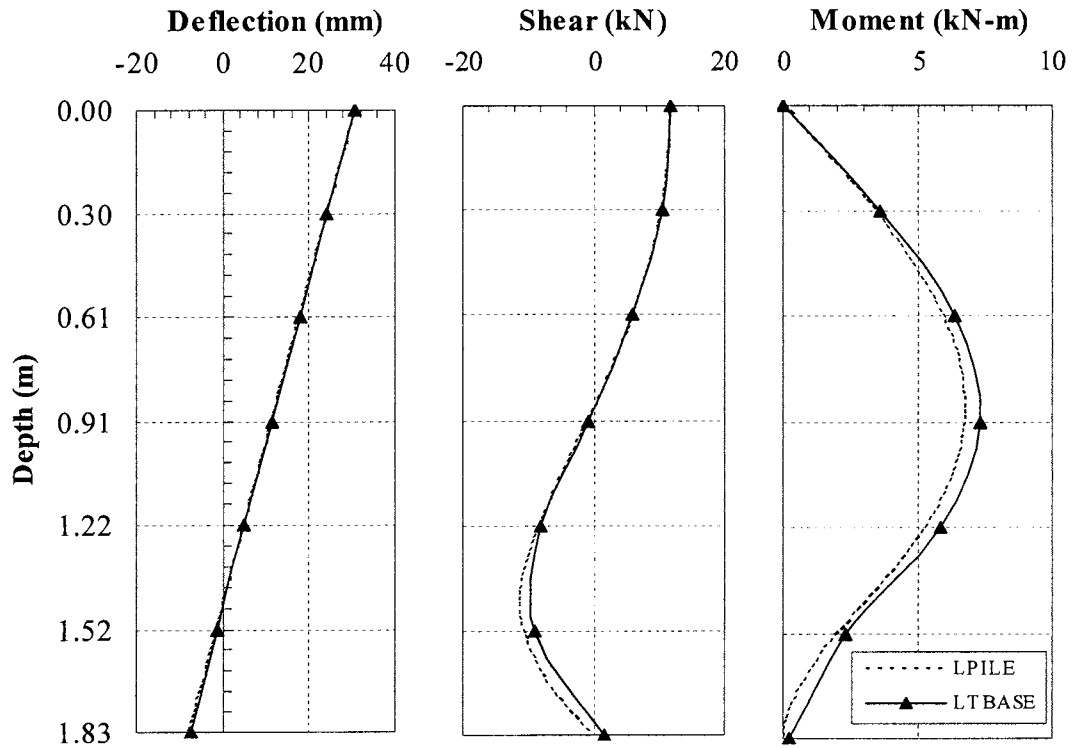
Displacement, Shear and Moment Curves in Sand (D = 0.3m, L=1.83m)
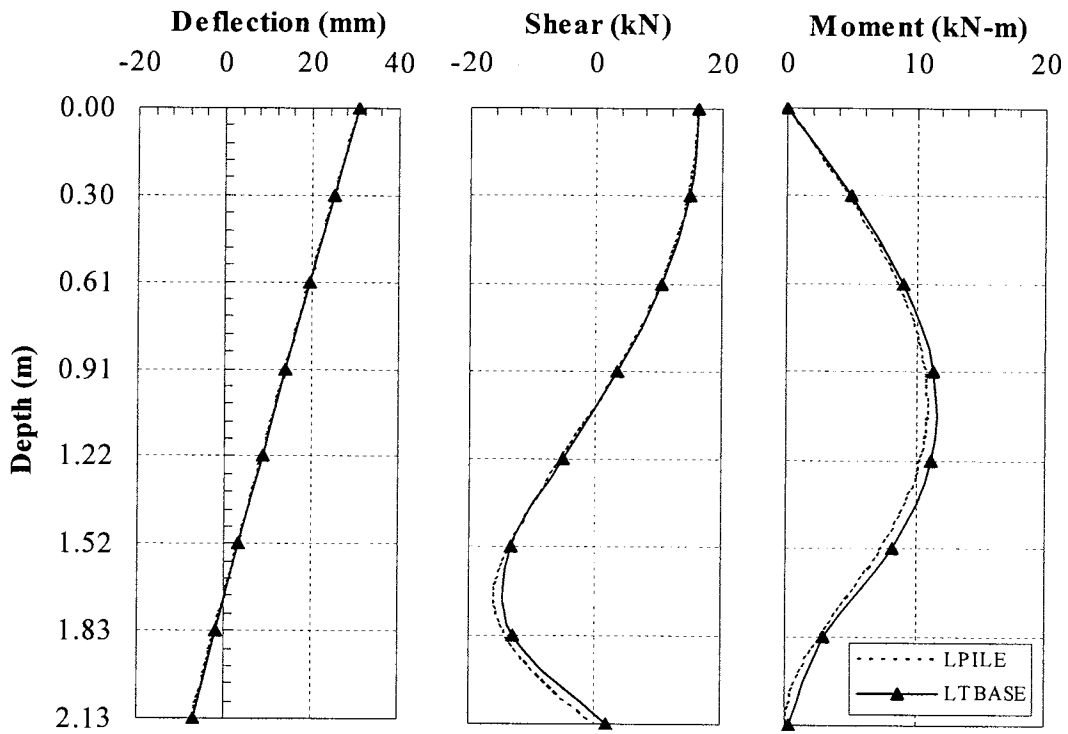
Displacement, Shear and Moment Curves in Sand (D = 0.3m, L=2.13m)
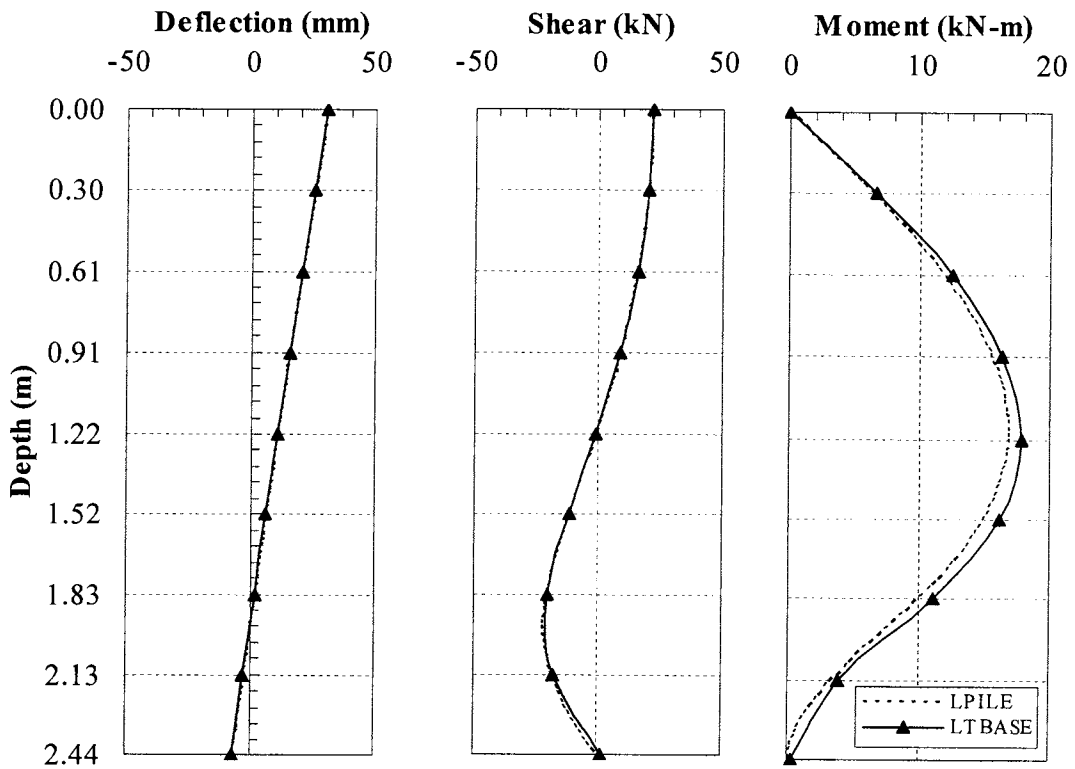
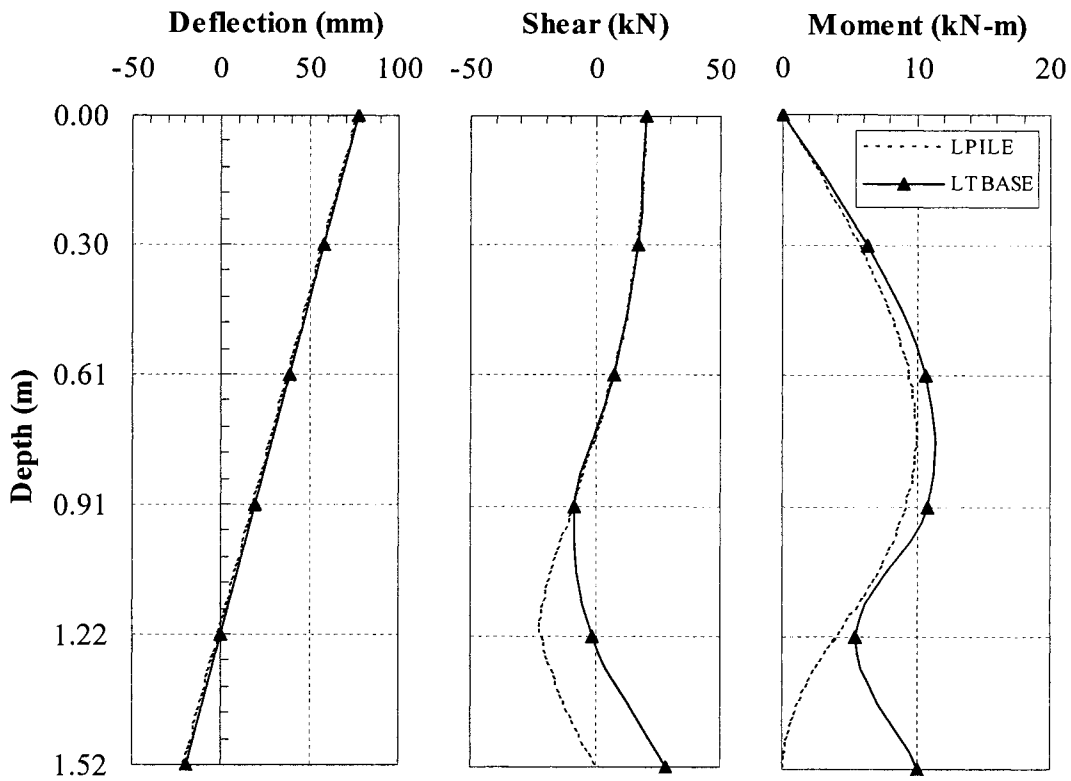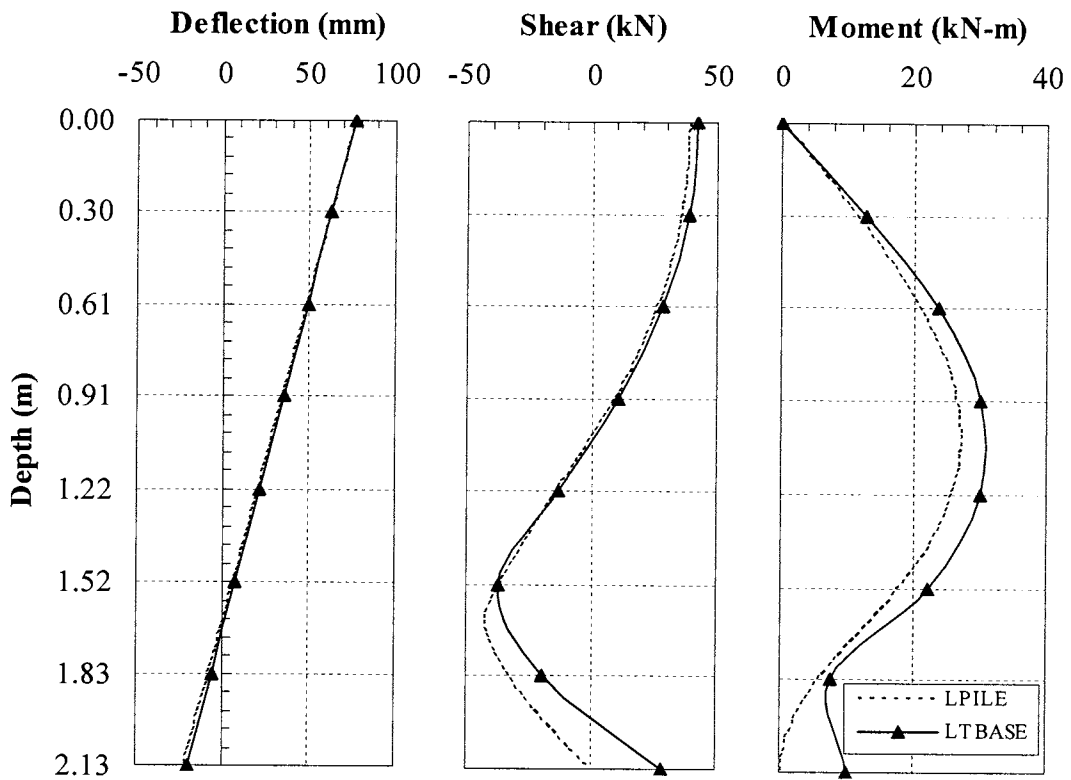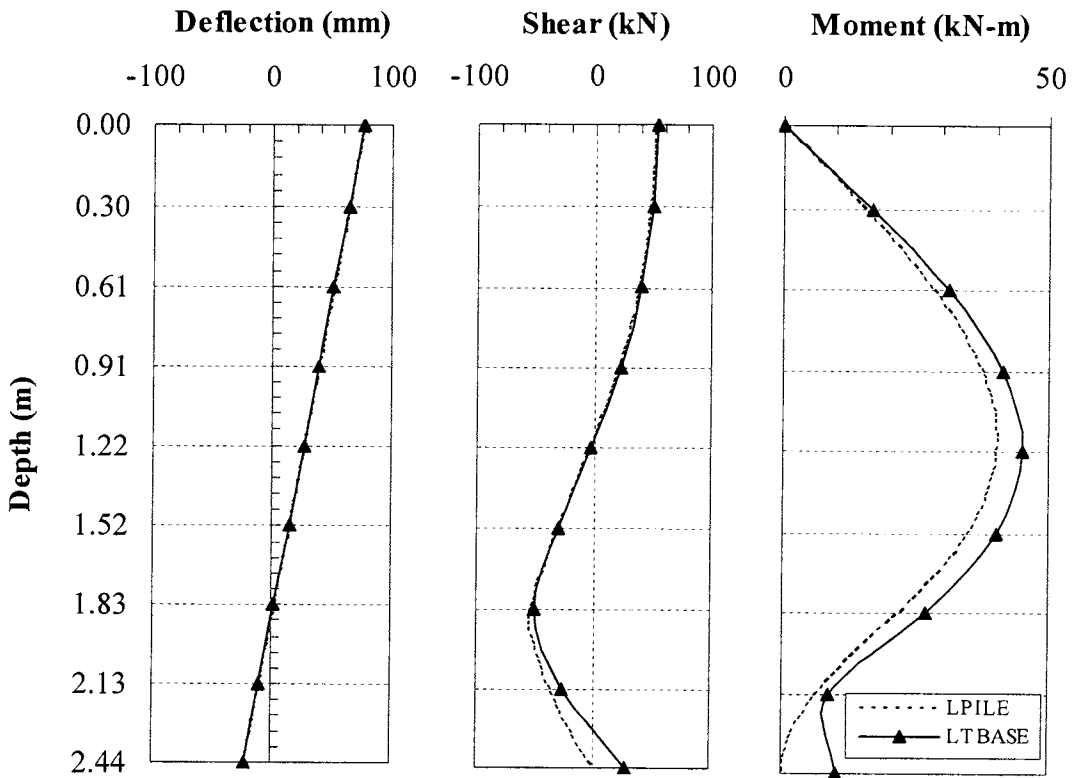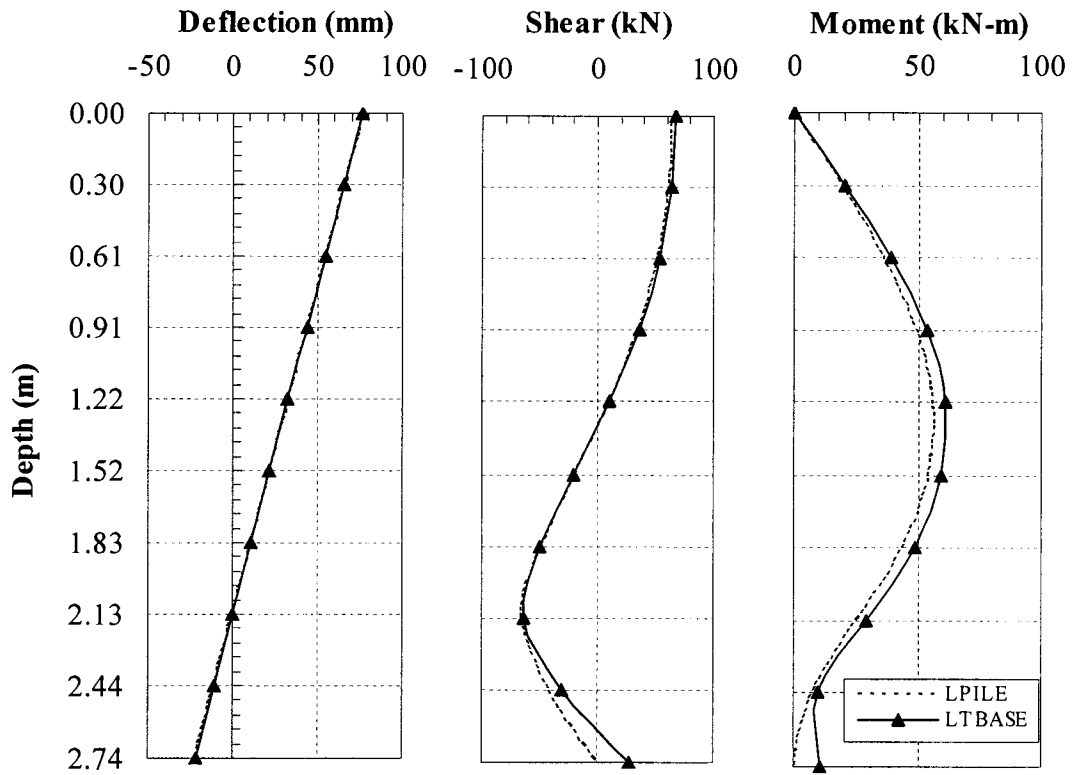**Displacement, Shear and Moment Curves in Sand (D = 0.3m, L=2.44m)**
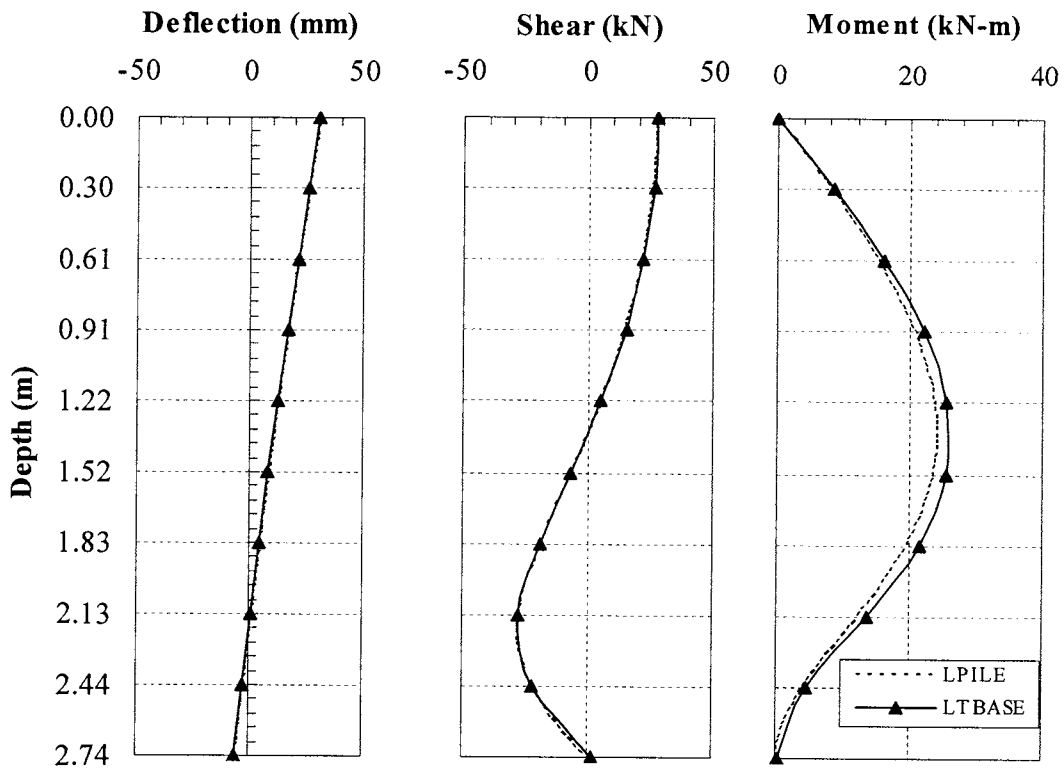
Displacement, Shear and Moment Curves in Sand (D = 0.3m, L=2.74m)
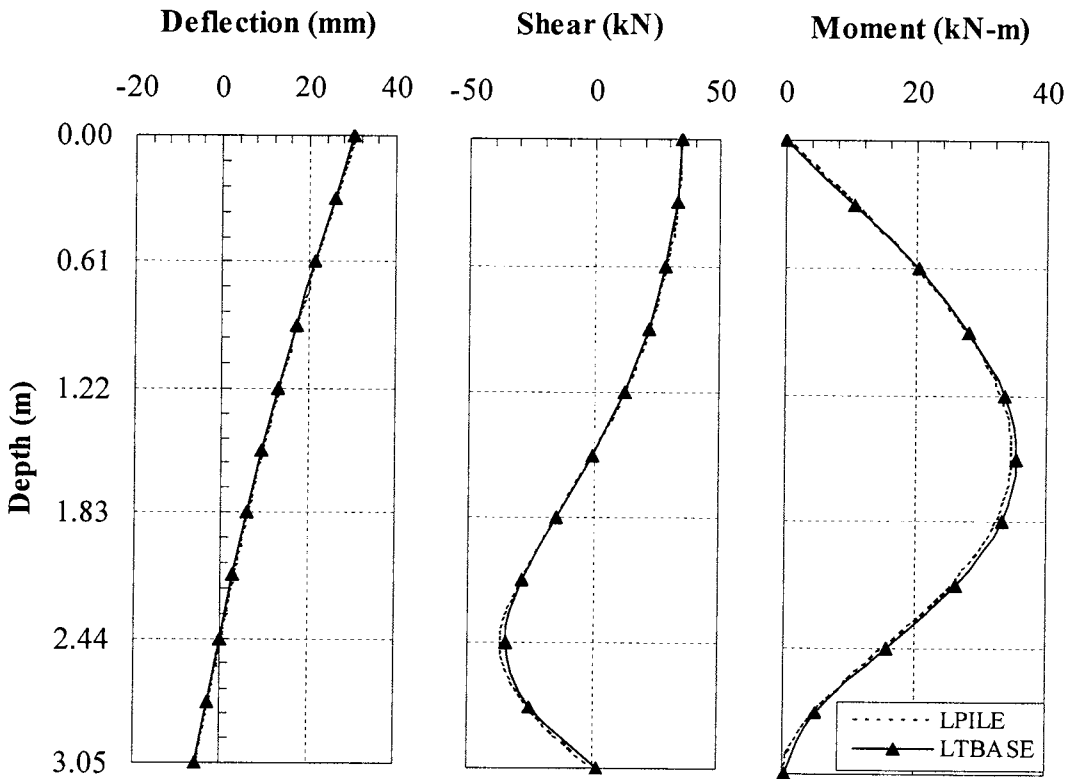
Displacement, Shear and Moment Curves in Sand (D = 0.3m, L=3.05m)
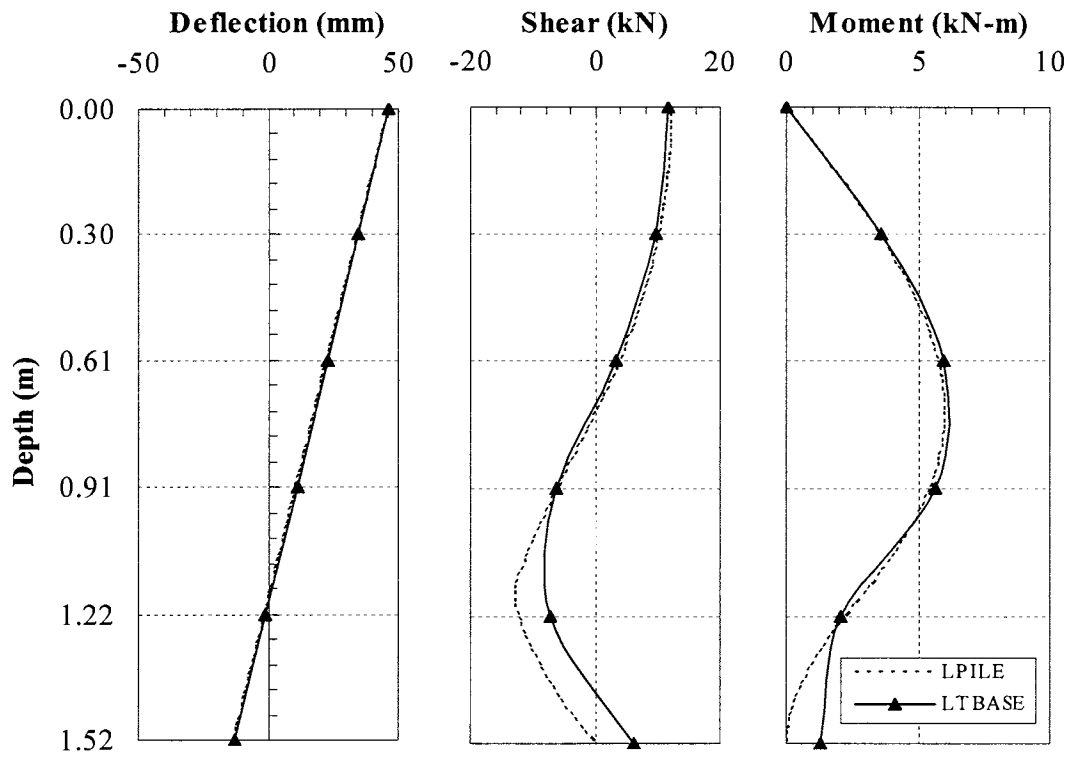
Displacement, Shear and Moment Curves in Sand (D = 0.46m, L=1.52m)
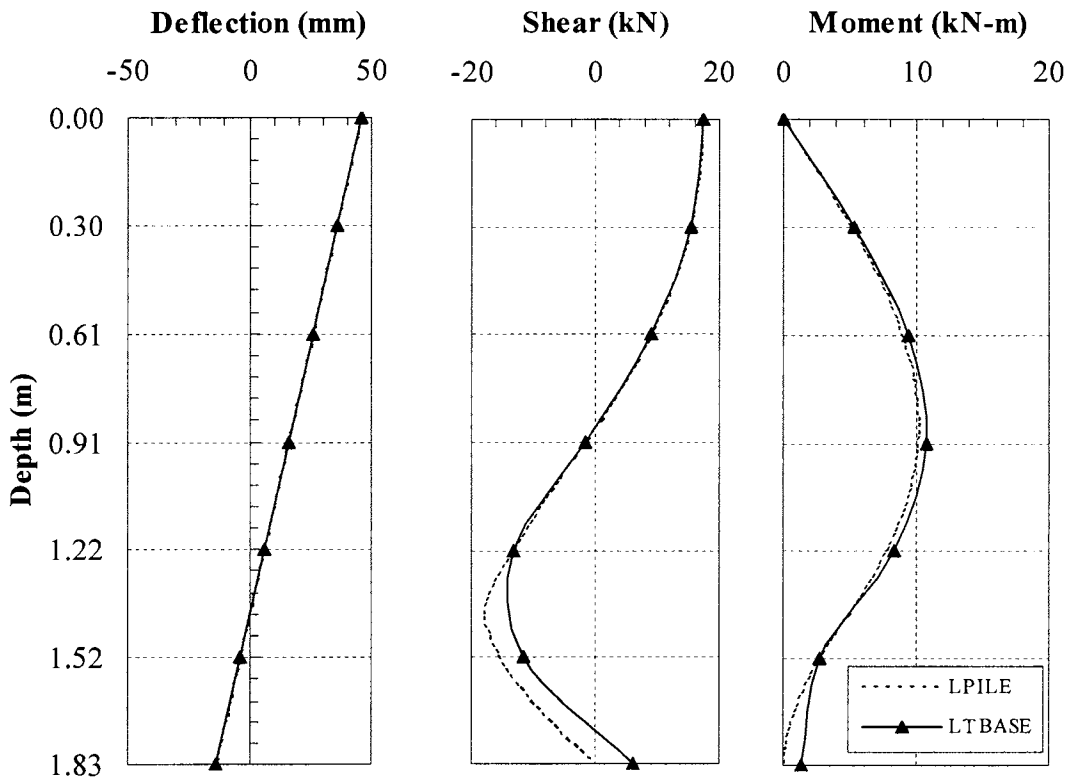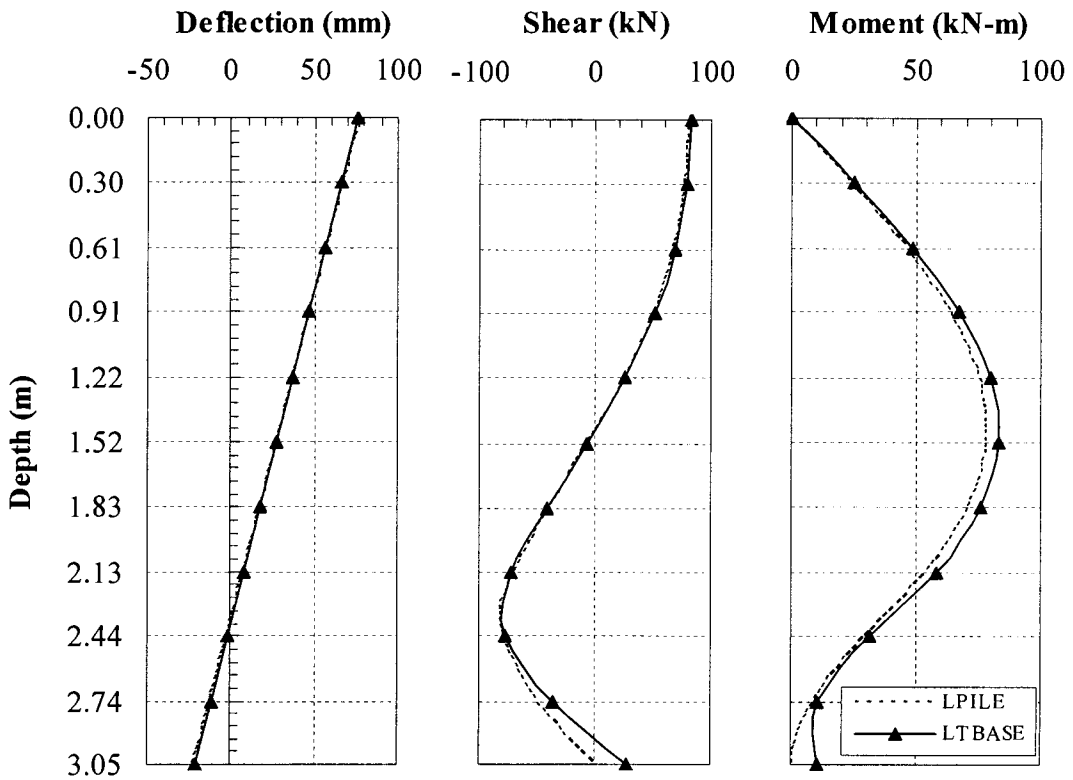

Displacement, Shear and Moment Curves in Sand (D = 0.46m, L=1.83m)
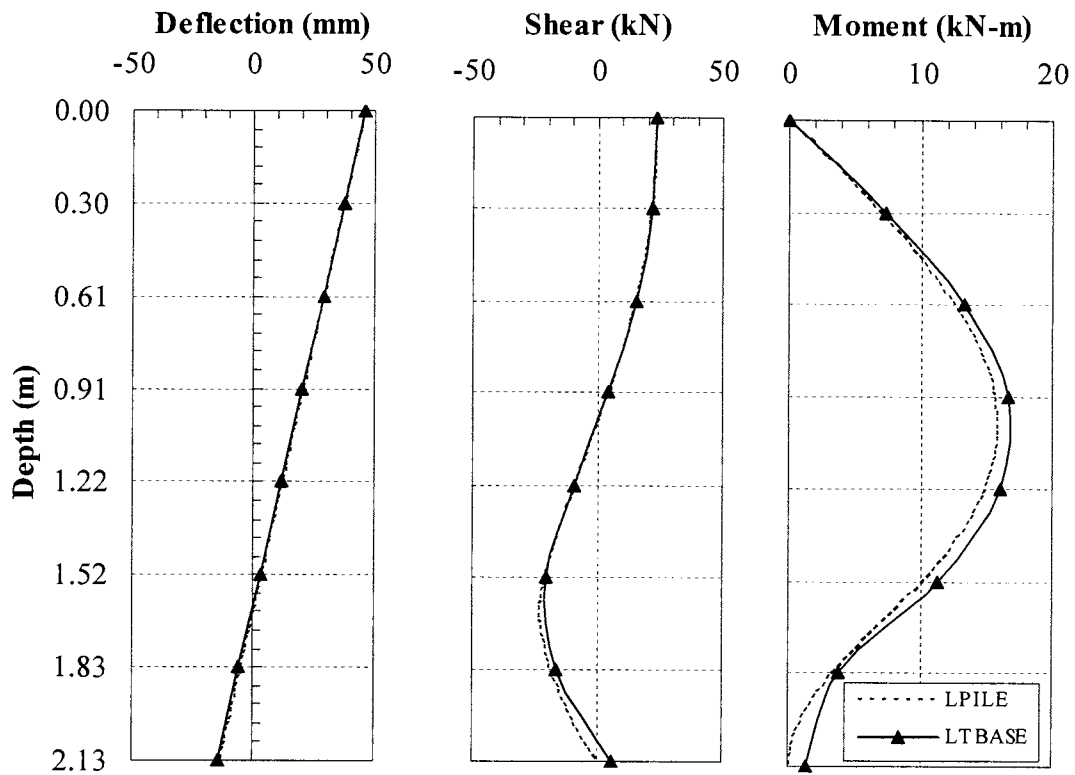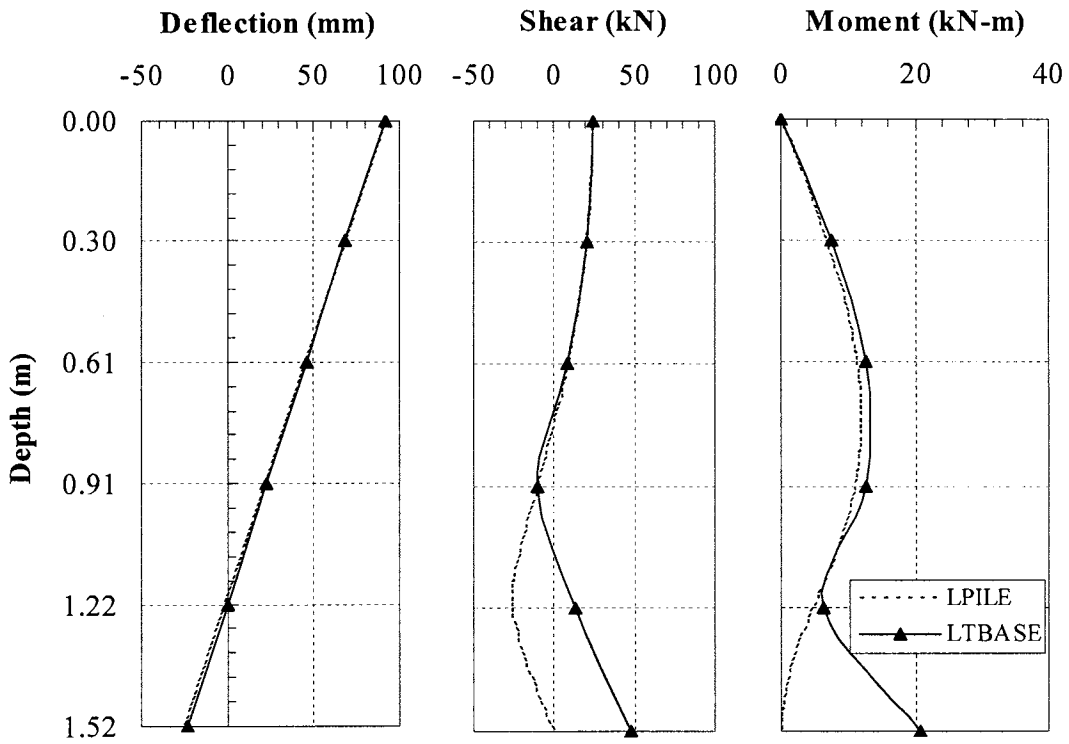
Displacement, Shear and Moment Curves in Sand (D = 0.46m, L=2.13m)
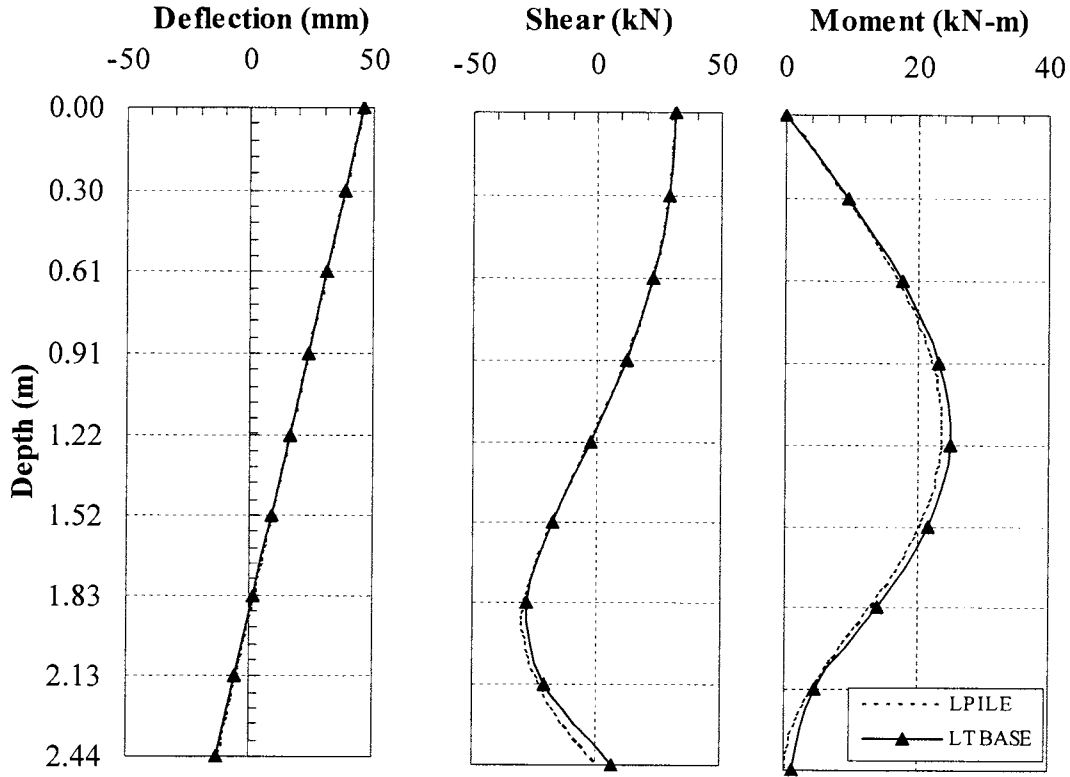
Displacement, Shear and Moment Curves in Sand (D = 0.46m, L=2.44m)
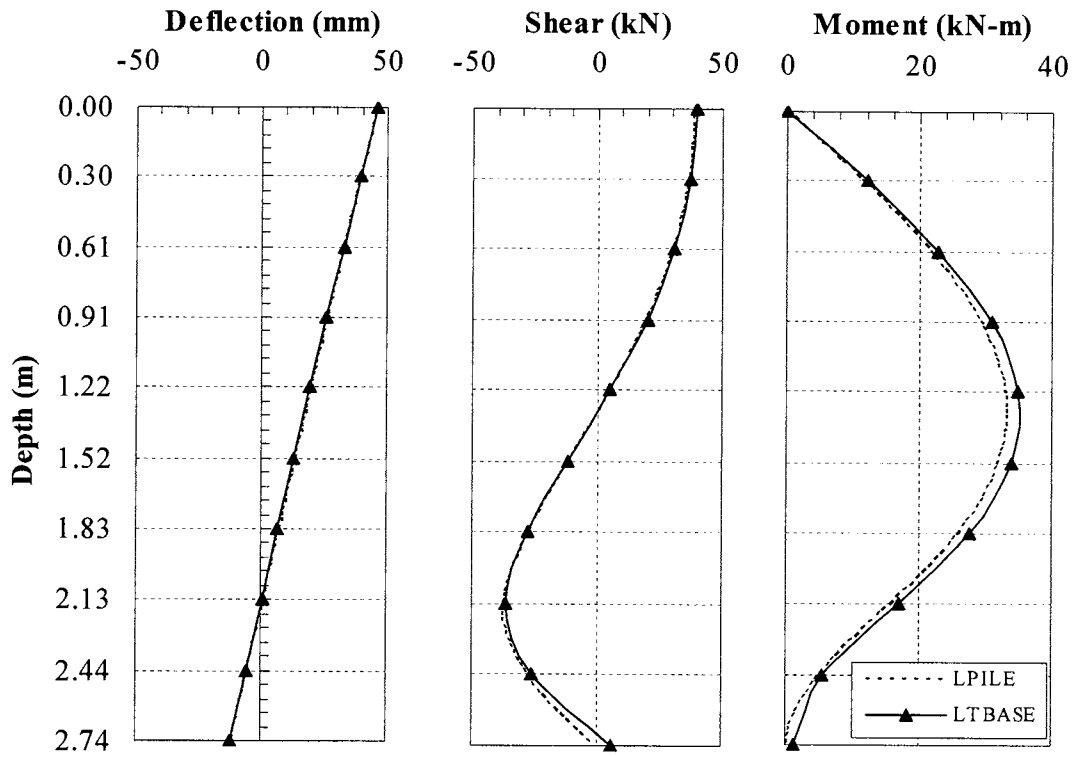
Displacement, Shear and Moment Curves in Sand (D = 0.46m, L=2.74m)
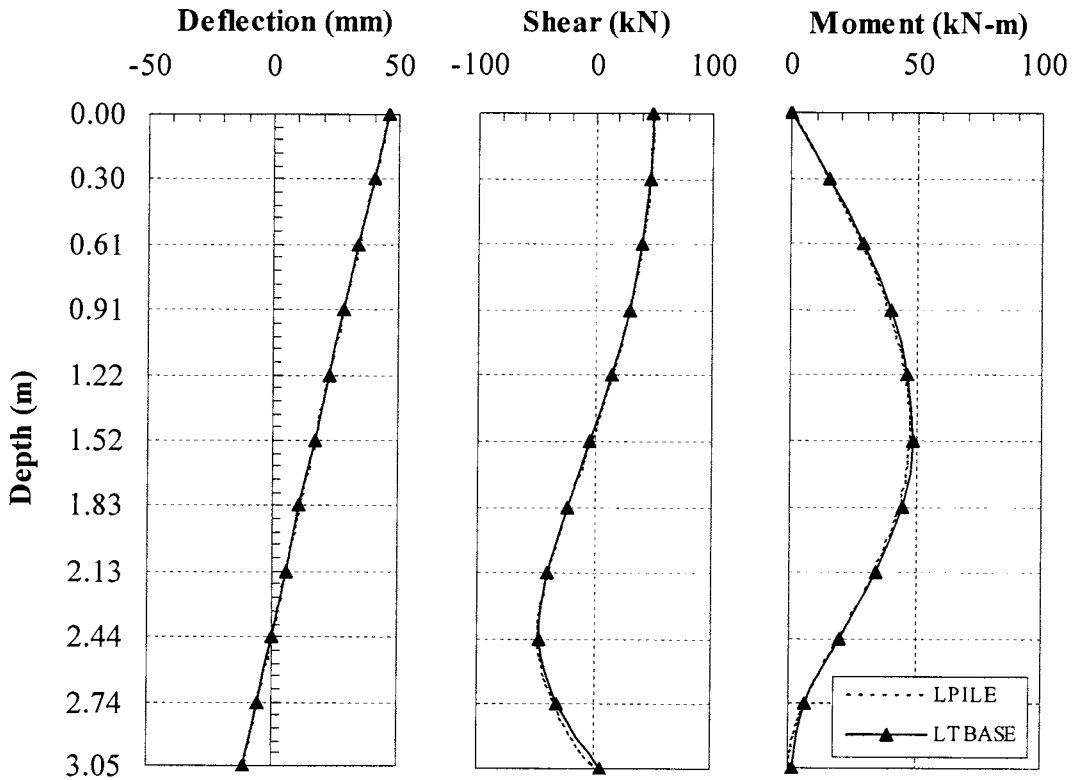
Displacement, Shear and Moment Curves in Sand (D = 0.46m, L=3.05m)
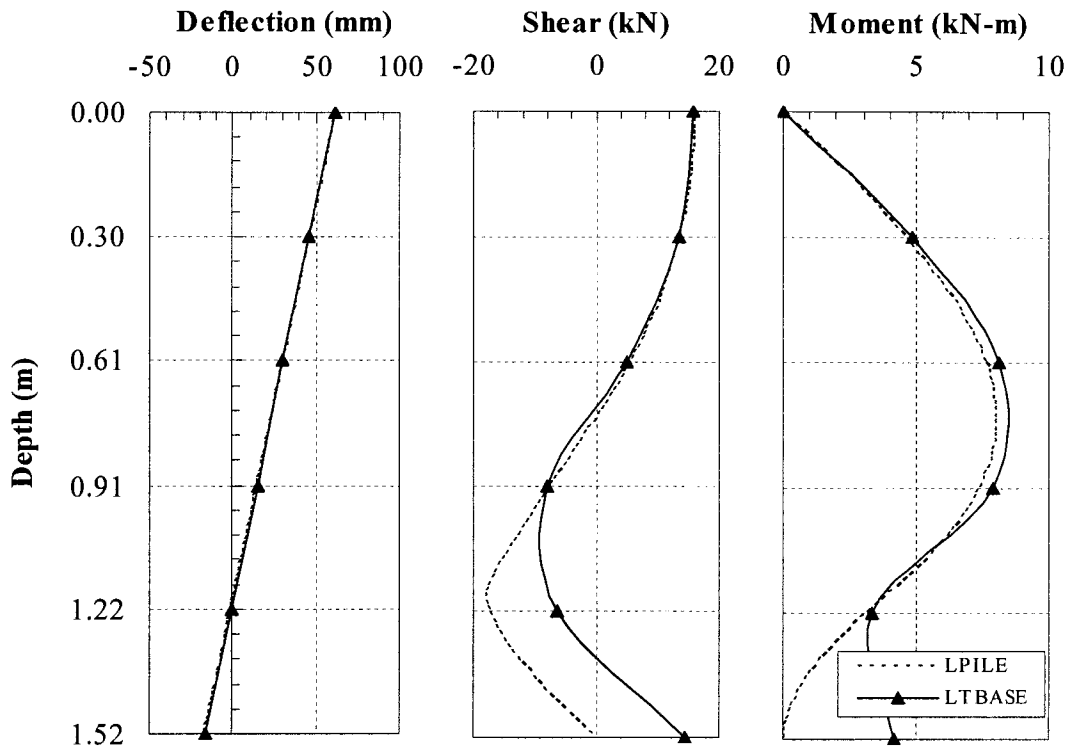
Displacement, Shear and Moment Curves in Sand (D = 0.61m, L=1.52m)
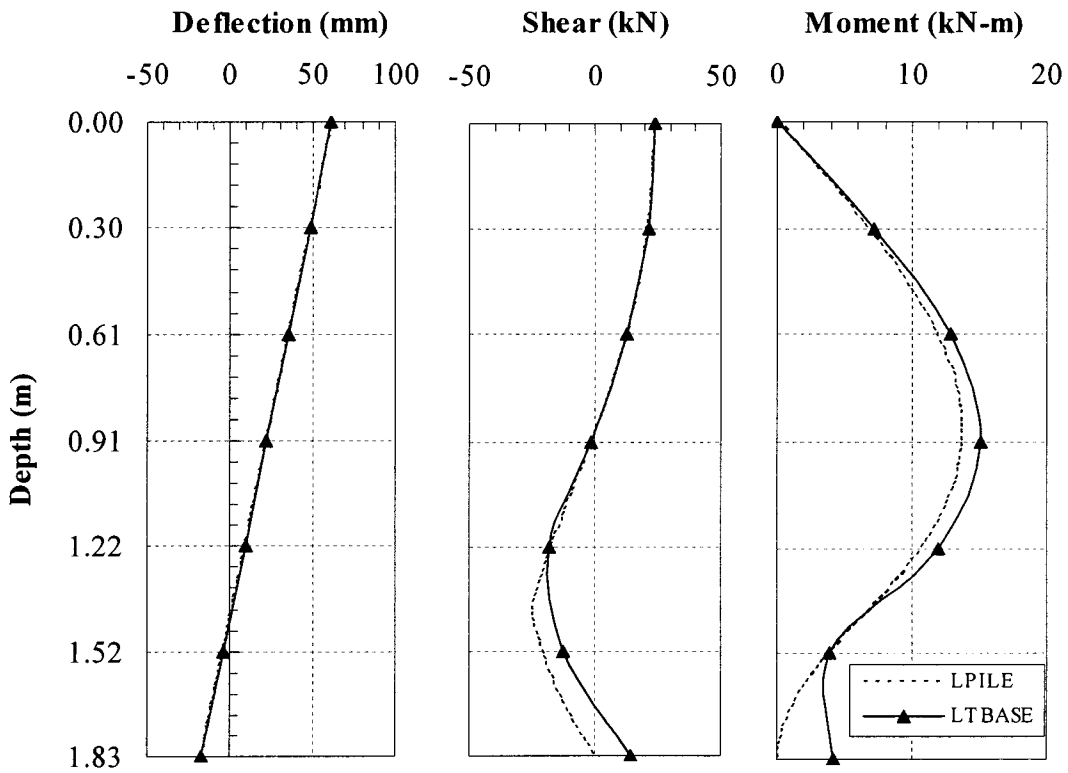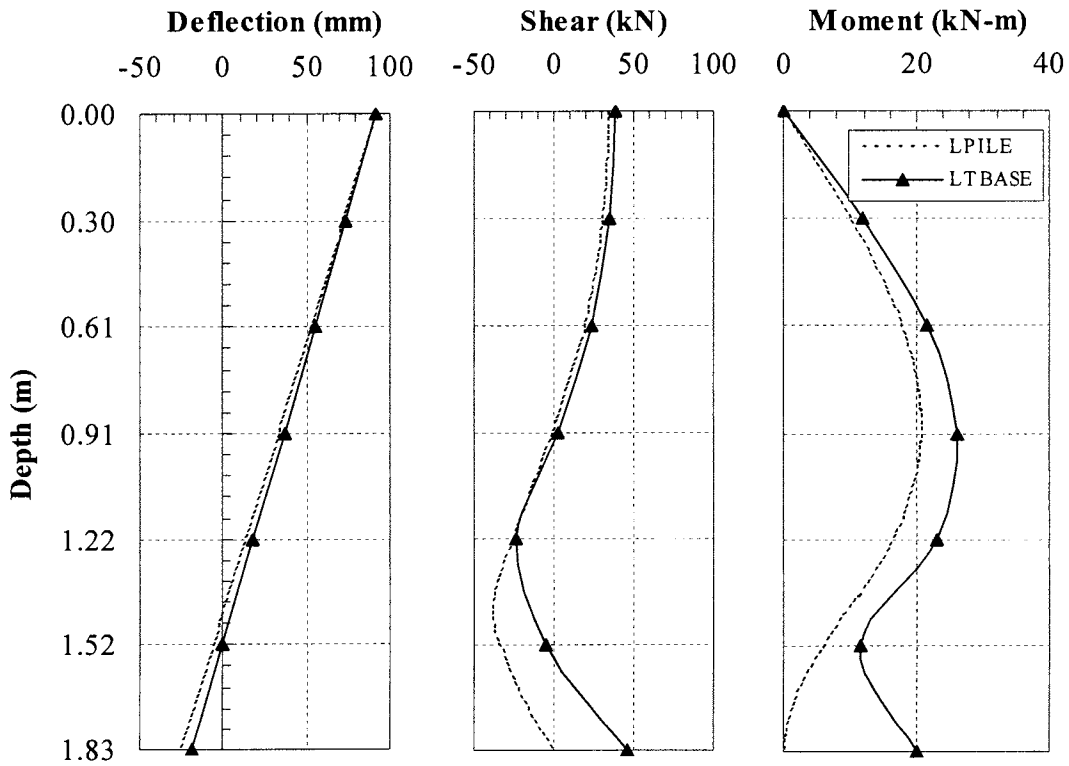
Displacement, Shear and Moment Curves in Sand (D = 0.61m, L=1.83m)
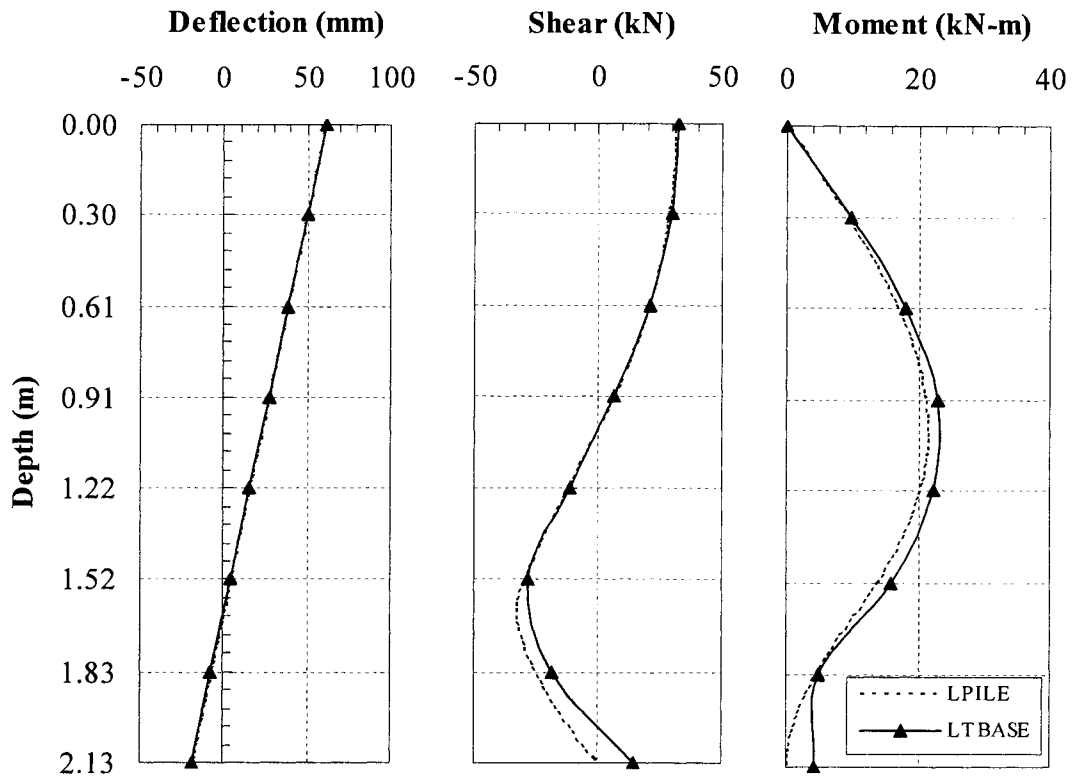
Displacement, Shear and Moment Curves in Sand (D = 0.61m, L=2.13m)
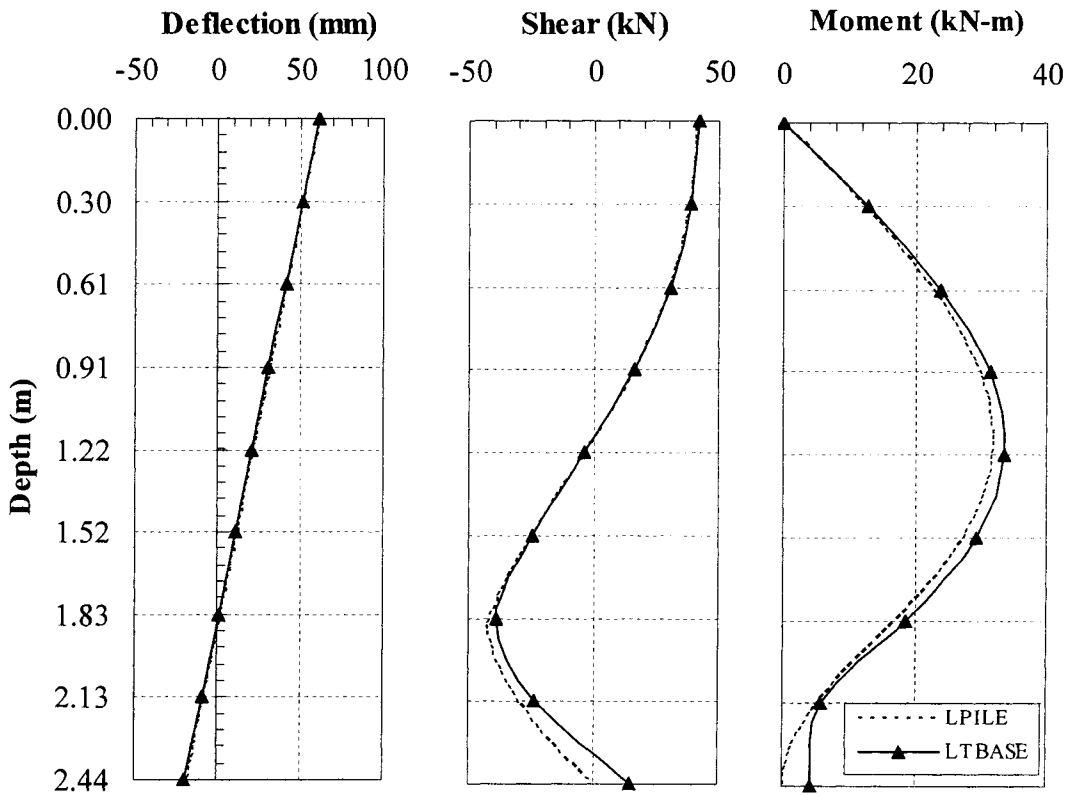
Displacement, Shear and Moment Curves in Sand (D = 0.61m, L=2.44m)
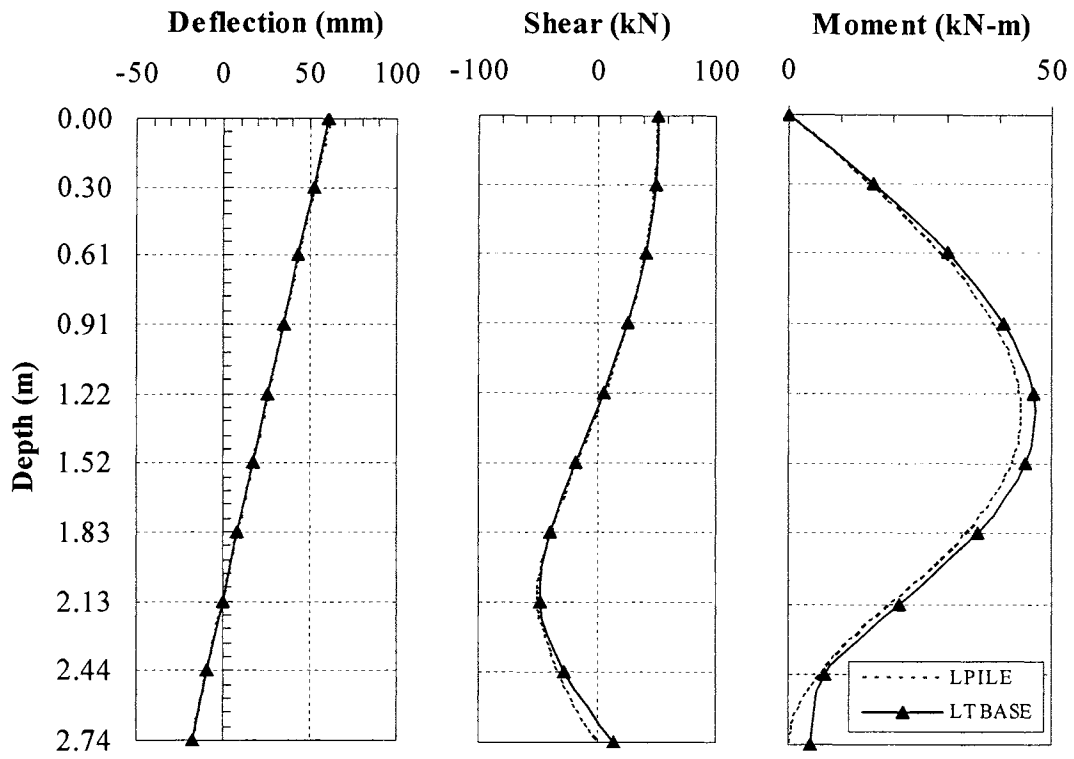
Displacement, Shear and Moment Curves in Sand (D = 0.61m, L=2.44m)
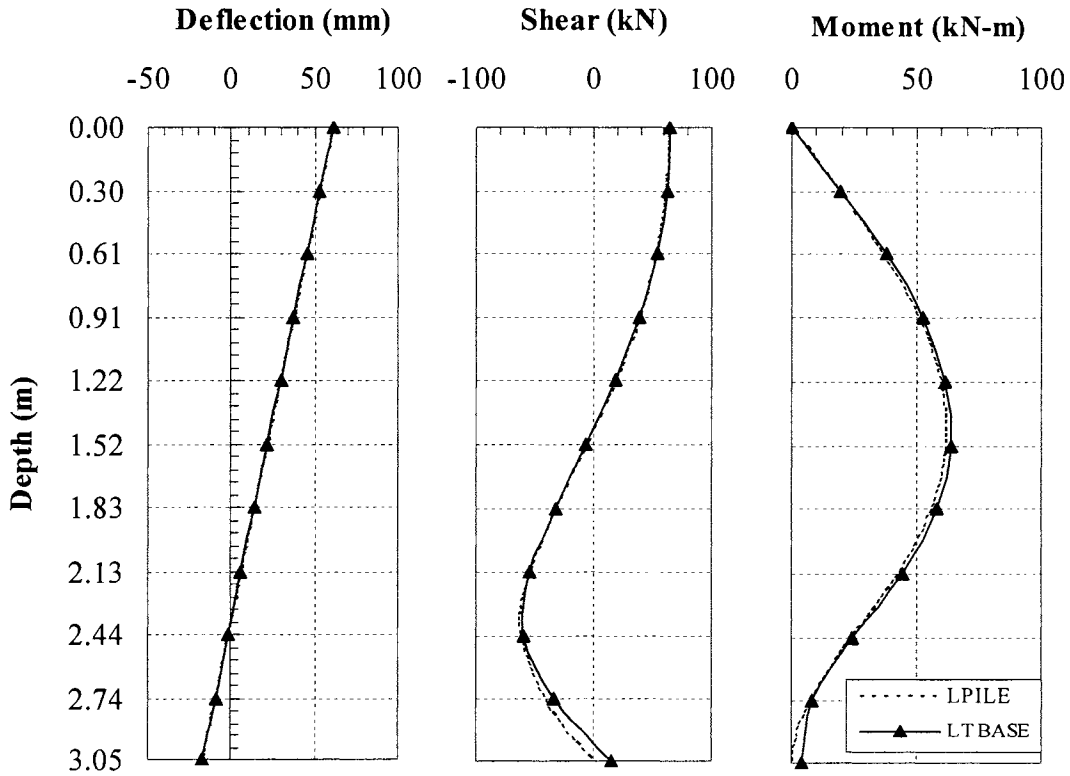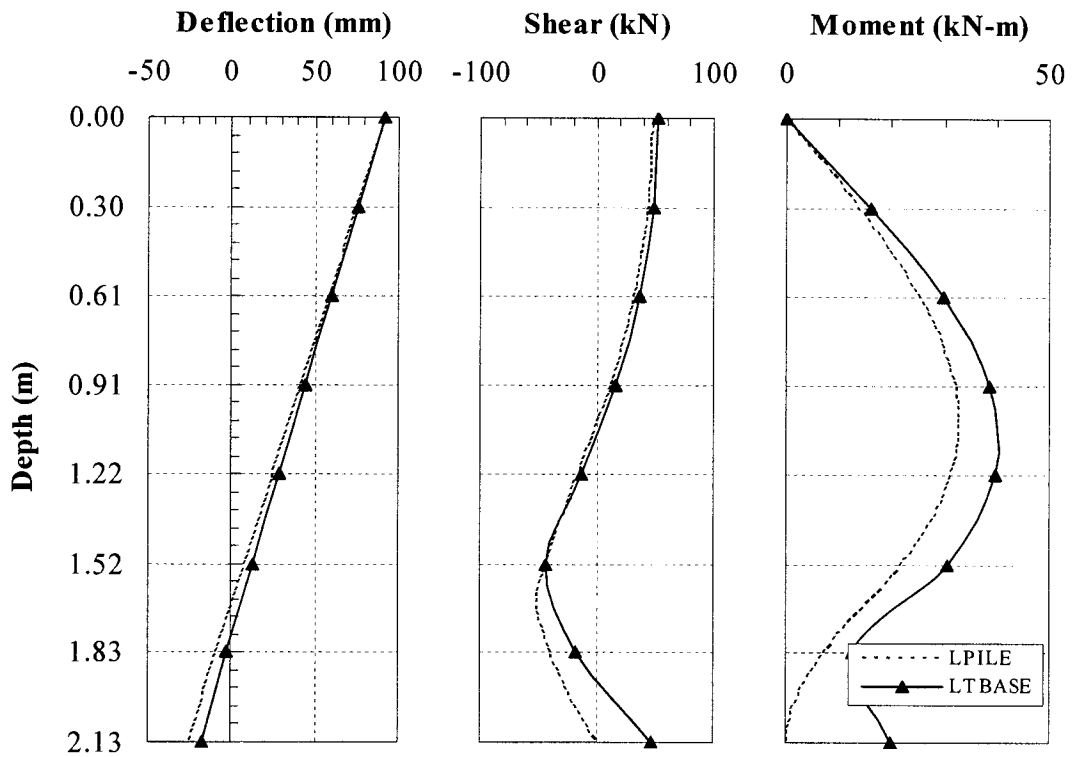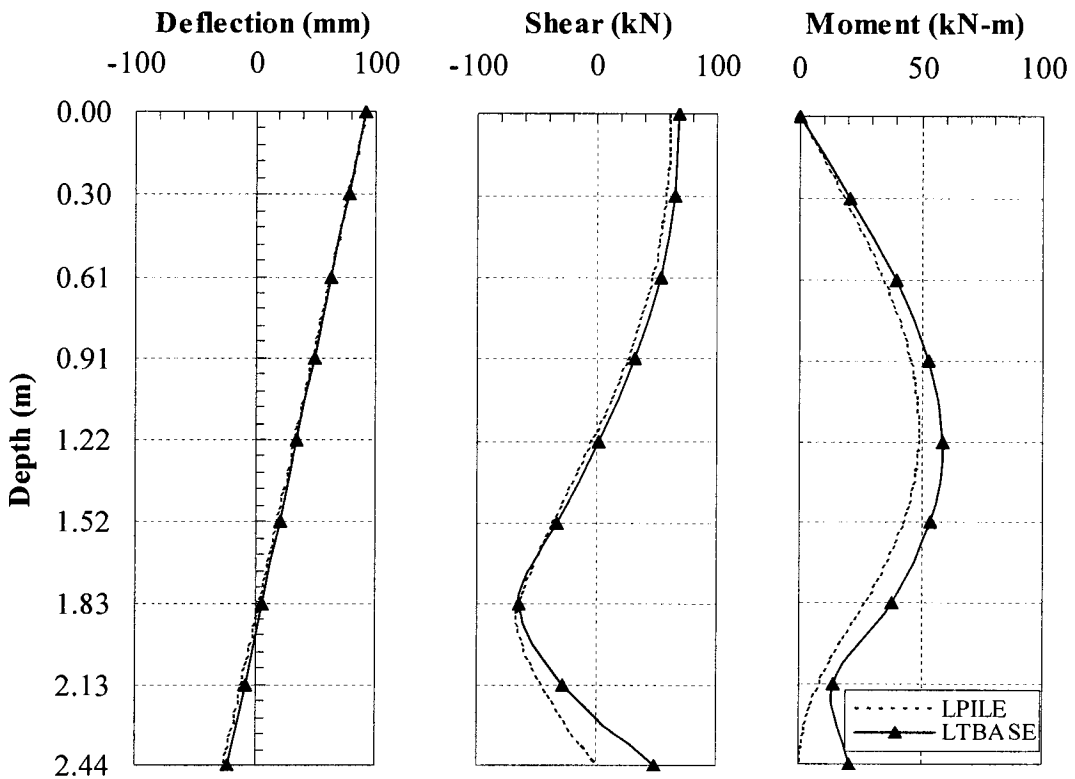

Displacement, Shear and Moment Curves in Sand (D = 0.61m, L=3.05m)

Displacement, Shear and Moment Curves in Sand (D = 0.76m, L=1.52m)
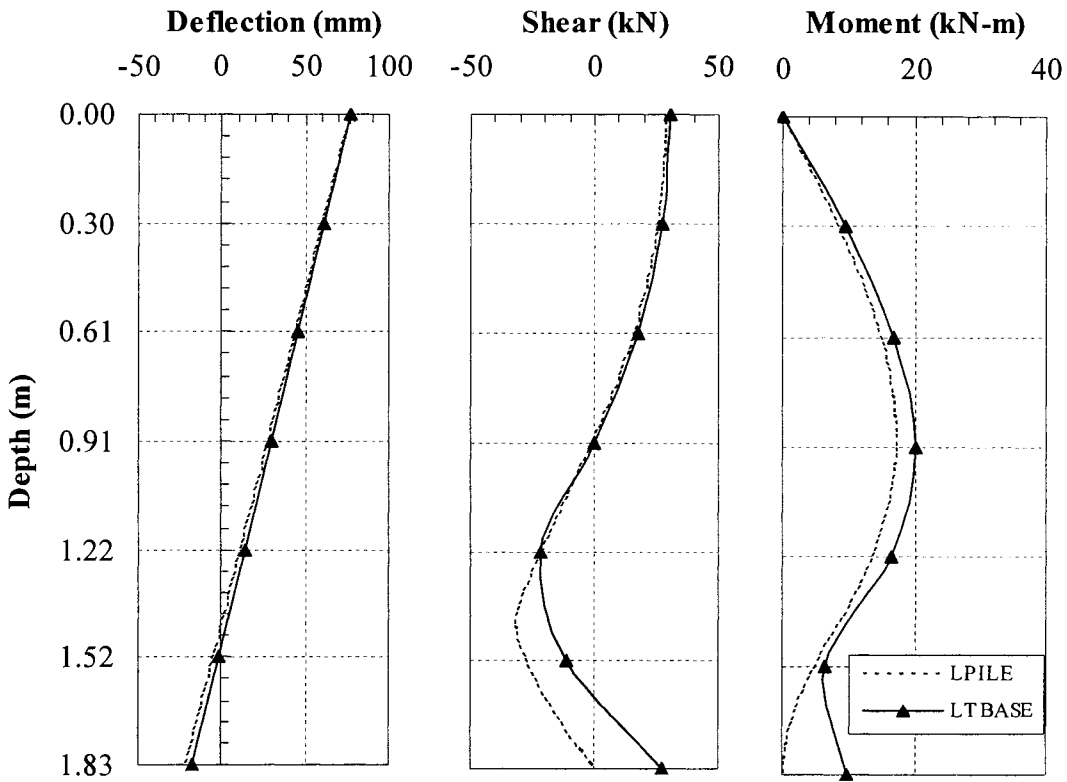
Displacement, Shear and Moment Curves in Sand (D = 0.76m, L=1.83m)

Deflection (mm)

Shear (kN)

Moment (kN-m)

Displacement, Shear and Moment Curves in Sand (D = 0.76m, L=2.13m)

Deflection (mm)

Shear (kN)

Moment (kN-m)

Displacement, Shear and Moment Curves in Sand (D = 0.76m, L=2.44m)

Displacement, Shear and Moment Curves in Sand (D = 0.76m, L=2.74m)

Displacement, Shear and Moment Curves in Sand (D = 0.76m, L=3.05m)

Displacement, Shear and Moment Curves in Sand (D = 0.91m, L=1.52m)

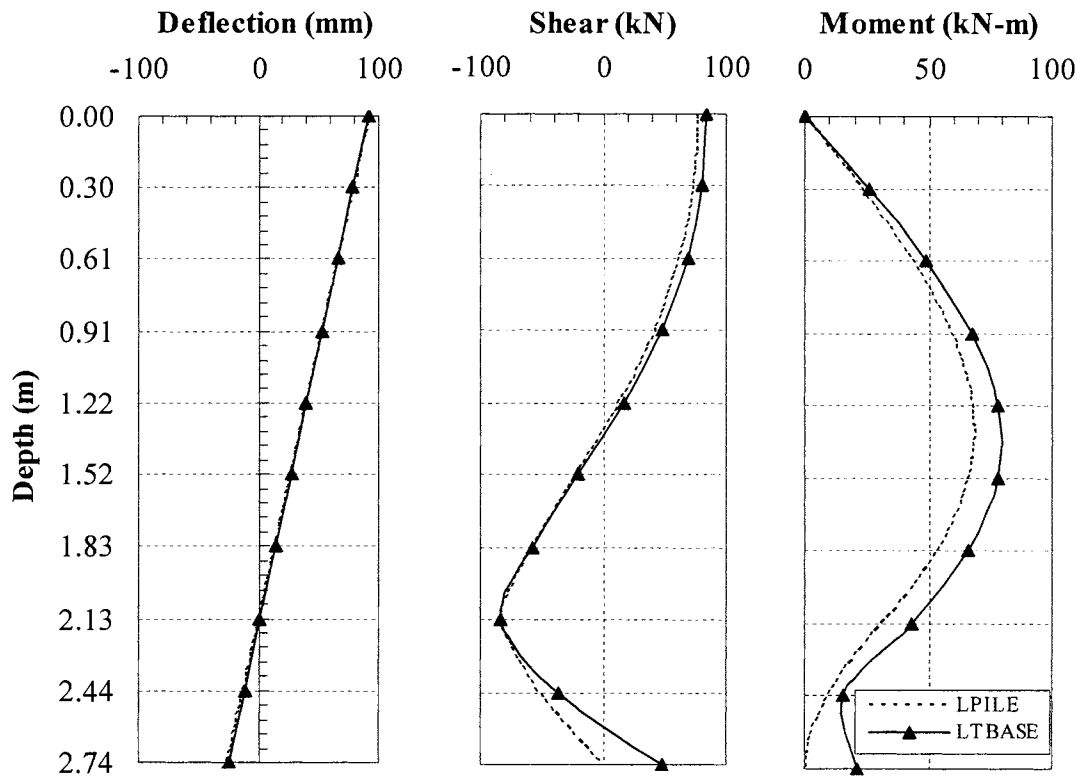
Displacement, Shear and Moment Curves in Sand (D = 0.91m, L=1.83m)

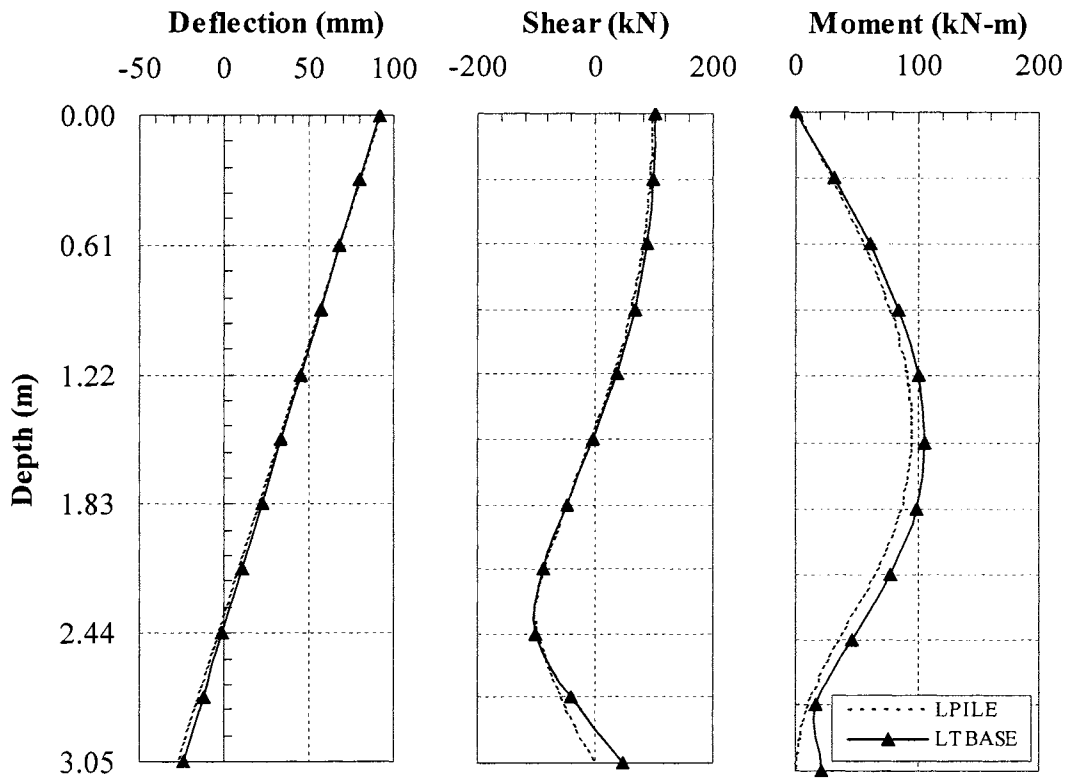**Displacement, Shear and Moment Curves in Sand (D = 0.91m, L=2.13m)**

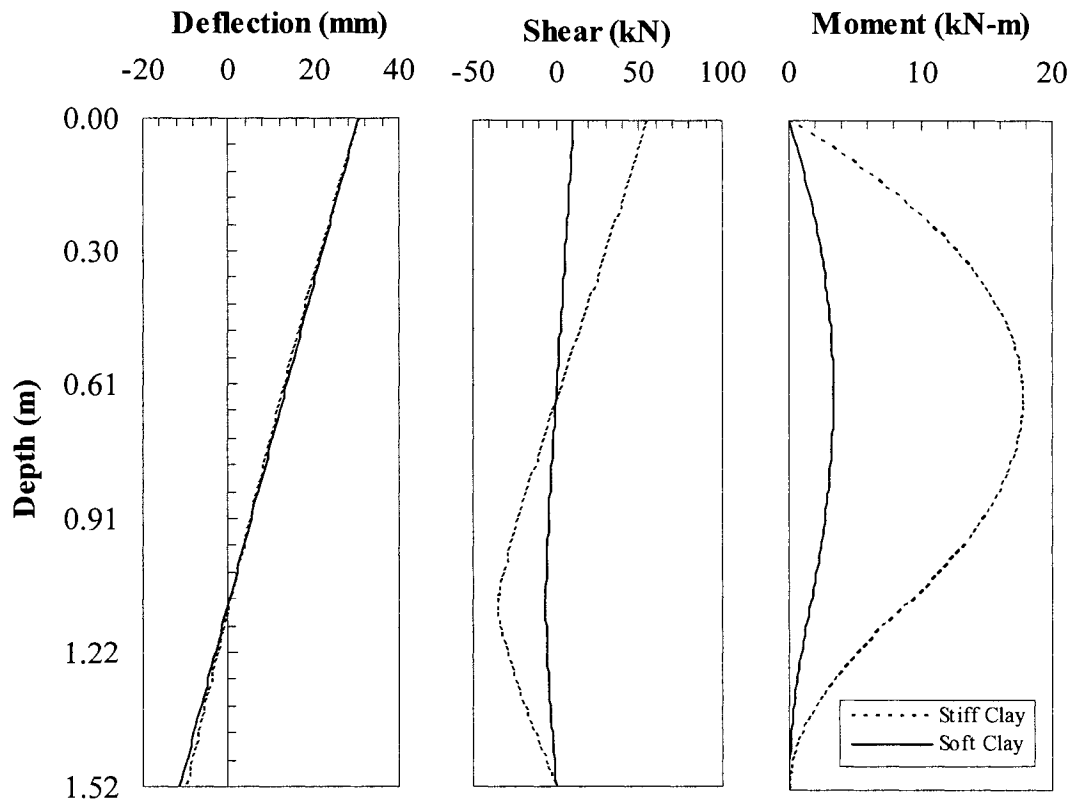**Displacement, Shear and Moment Curves in Sand (D = 0.91m, L=2.44m)**

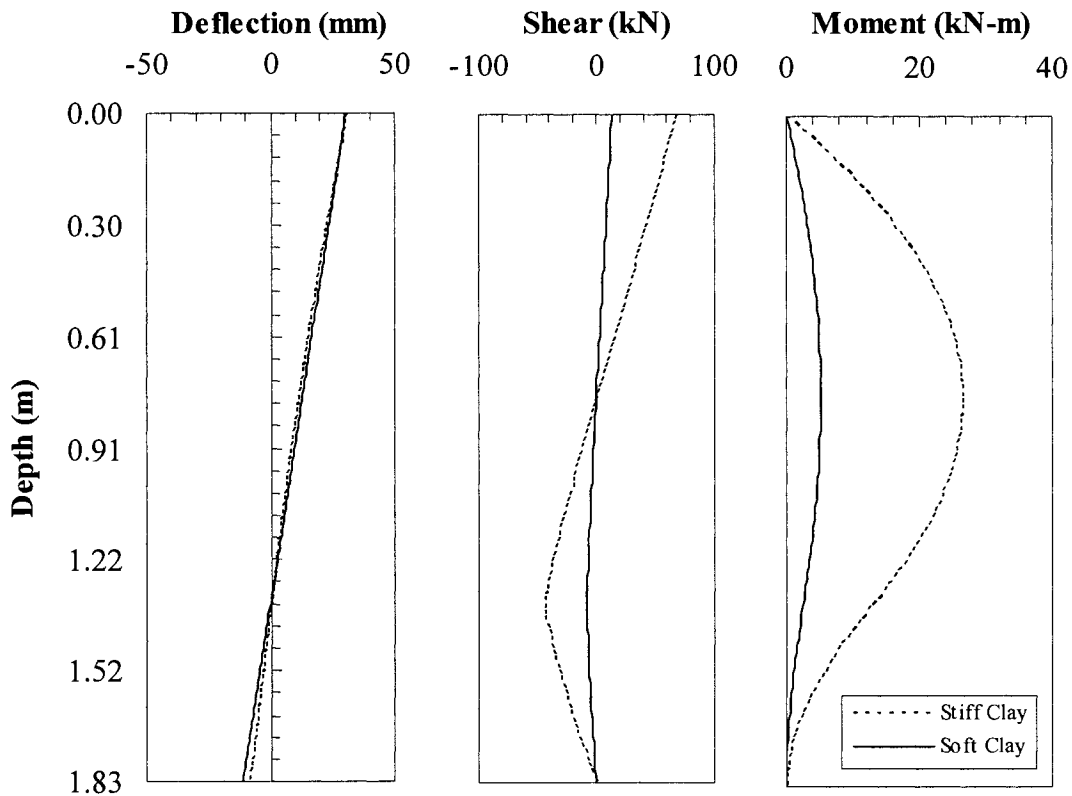Displacement, Shear and Moment Curves in Sand (D = 0.91m, L=2.74m)

Displacement, Shear and Moment Curves in Sand (D = 0.91m, L=3.05m)

Appendix A2: Pier Displacement, Shear and Moment Curves in Soft Clay and Stiff Clay
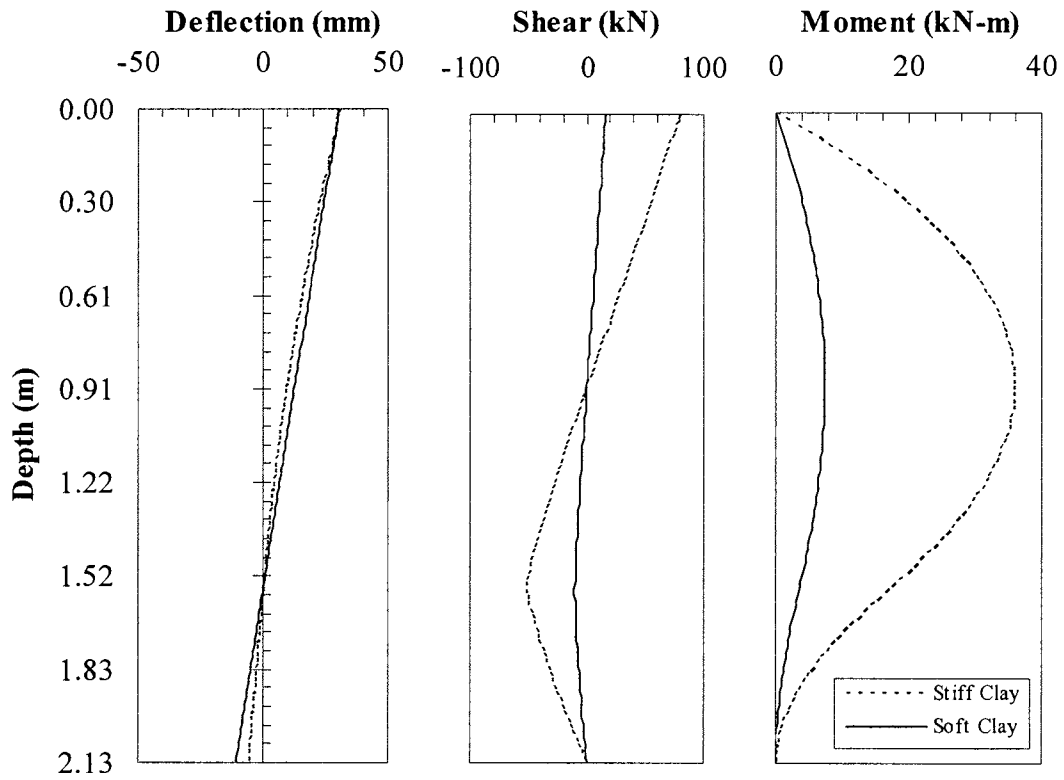
(LPILE)

Displacement, Shear and Moment Curves in Soft, Stiff Clay (D = 0.3m, L=1.52m)

Displacement, Shear and Moment Curves in Soft, Stiff Clay (D = 0.3m, L=1.83m)

Displacement, Shear and Moment Curves in Soft, Stiff Clay (D = 0.3m, L=2.13m)

Displacement, Shear and Moment Curves in Soft, Stiff Clay (D = 0.3m, L=2.44m)

Displacement, Shear and Moment Curves in Soft, Stiff Clay (D = 0.3m, L=2.74m)

Displacement, Shear and Moment Curves in Soft, Stiff Clay (D = 0.3m, L=3.05m)

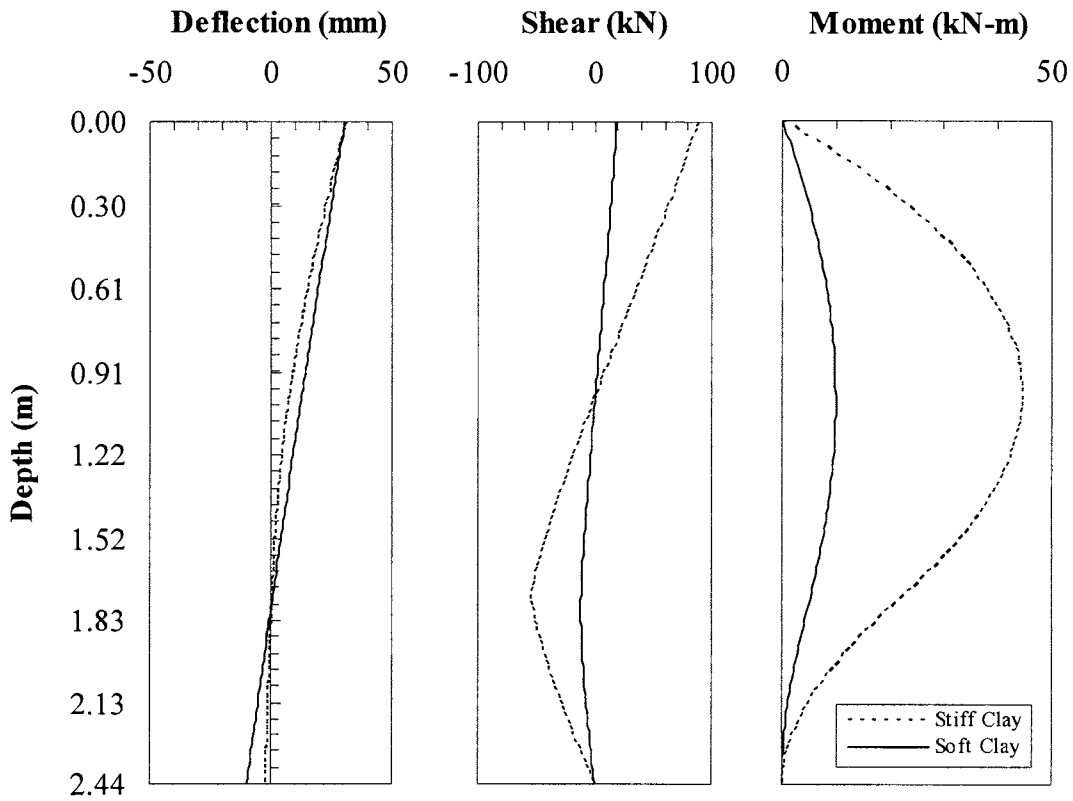**Displacement, Shear and Moment Curves in Soft, Stiff Clay (D = 0.46m, L=1.52m)**

Displacement, Shear and Moment Curves in Soft, Stiff Clay (D = 0.46m, L=1.83m)

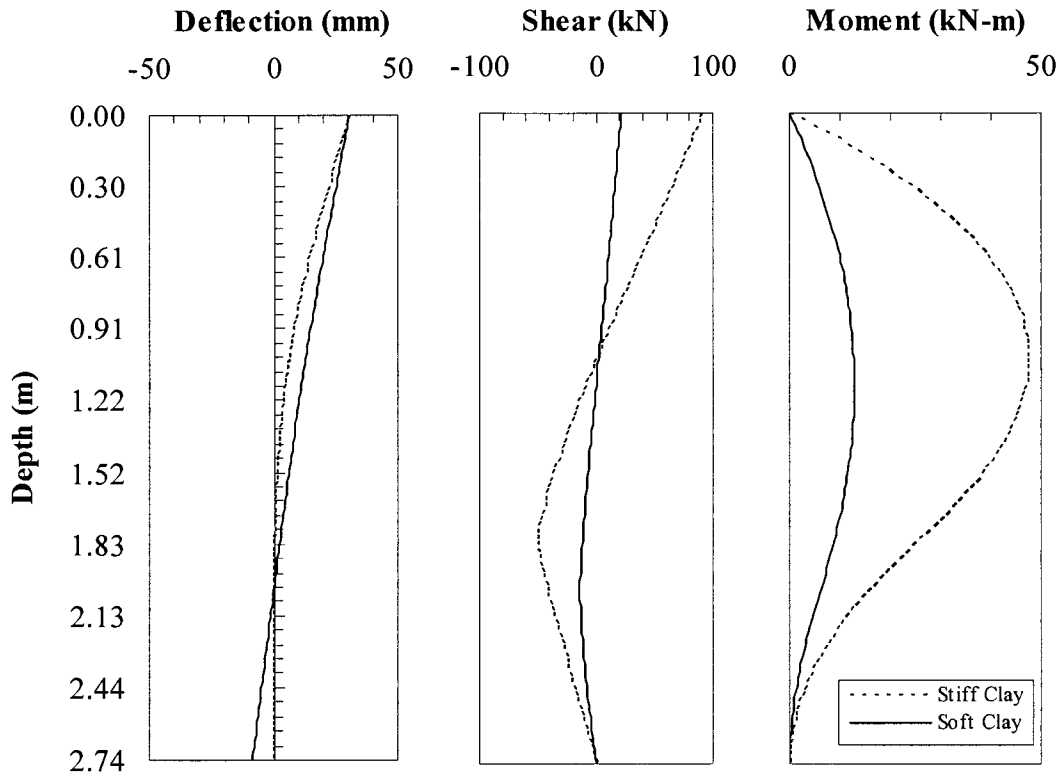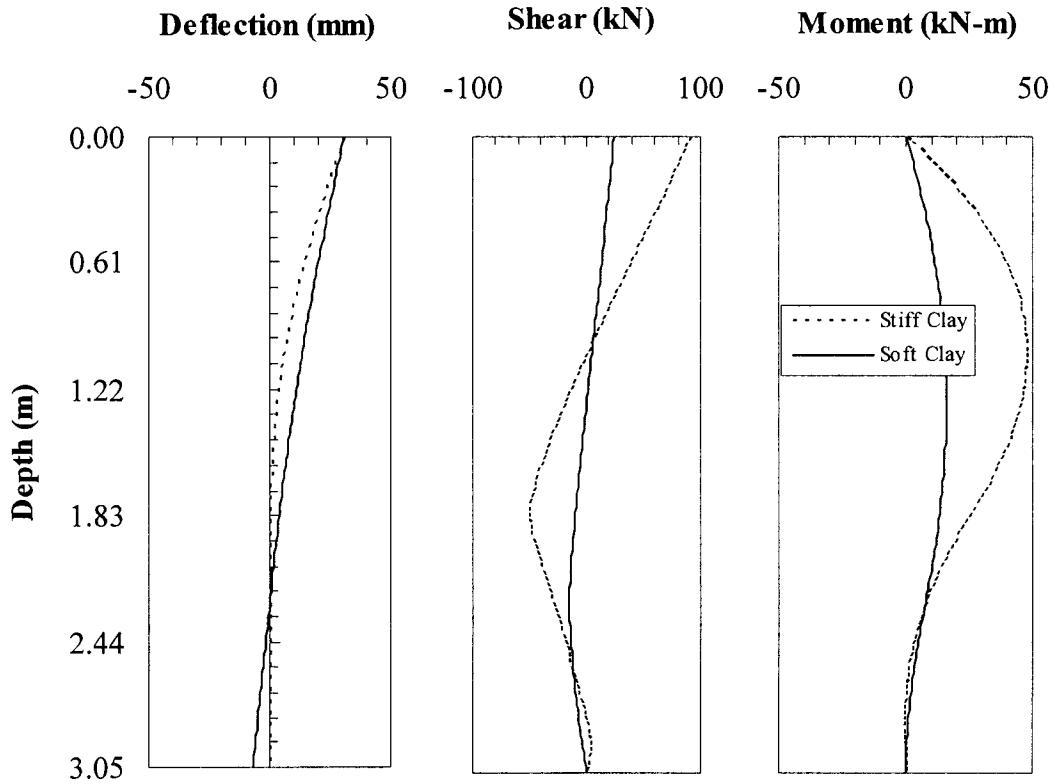**Displacement, Shear and Moment Curves in Soft, Stiff Clay (D = 0.46m, L=2.13m)**

Displacement, Shear and Moment Curves in Soft, Stiff Clay (D = 0.46m, L=2.44m)

Deflection (mm) **Shear (kN)** **Moment (kN-m)**

-50 0 50   -200 0 200   0 50 100

Depth (m): 0.00, 0.30, 0.61, 0.91, 1.22, 1.52, 1.83, 2.13, 2.44, 2.74

Stiff Clay
Soft Clay

Displacement, Shear and Moment Curves in Soft, Stiff Clay (D = 0.46m, L=2.74m)

Deflection (mm) **Shear (kN)** **Moment (kN-m)**

-50 0 50   -200 0 200   0 100 200

Depth (m): 0.00, 0.30, 0.61, 0.91, 1.22, 1.52, 1.83, 2.13, 2.44, 2.74, 3.05

Stiff Clay
Soft Clay

Displacement, Shear and Moment Curves in Soft, Stiff Clay (D = 0.46m, L=3.05m)

Displacement, Shear and Moment Curves in Soft, Stiff Clay (D = 0.61m, L=1.52m)

Displacement, Shear and Moment Curves in Soft, Stiff Clay (D = 0.61m, L=1.83m)

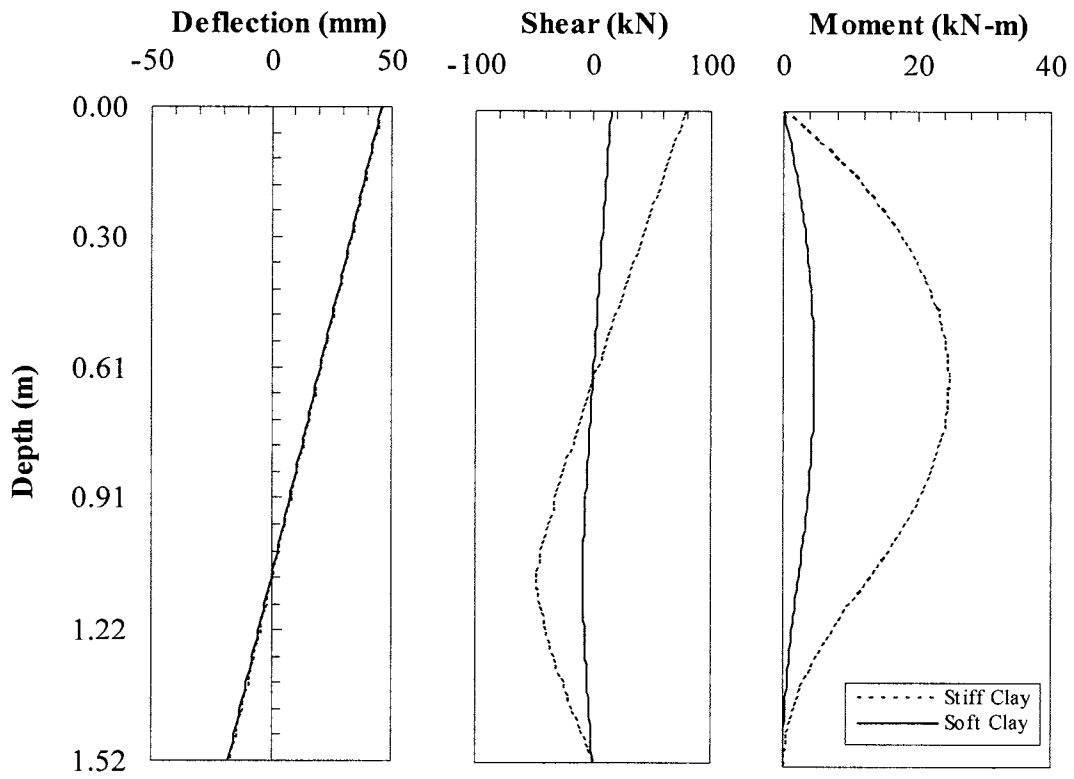**Displacement, Shear and Moment Curves in Soft, Stiff Clay (D = 0.61m, L=2.13m)**

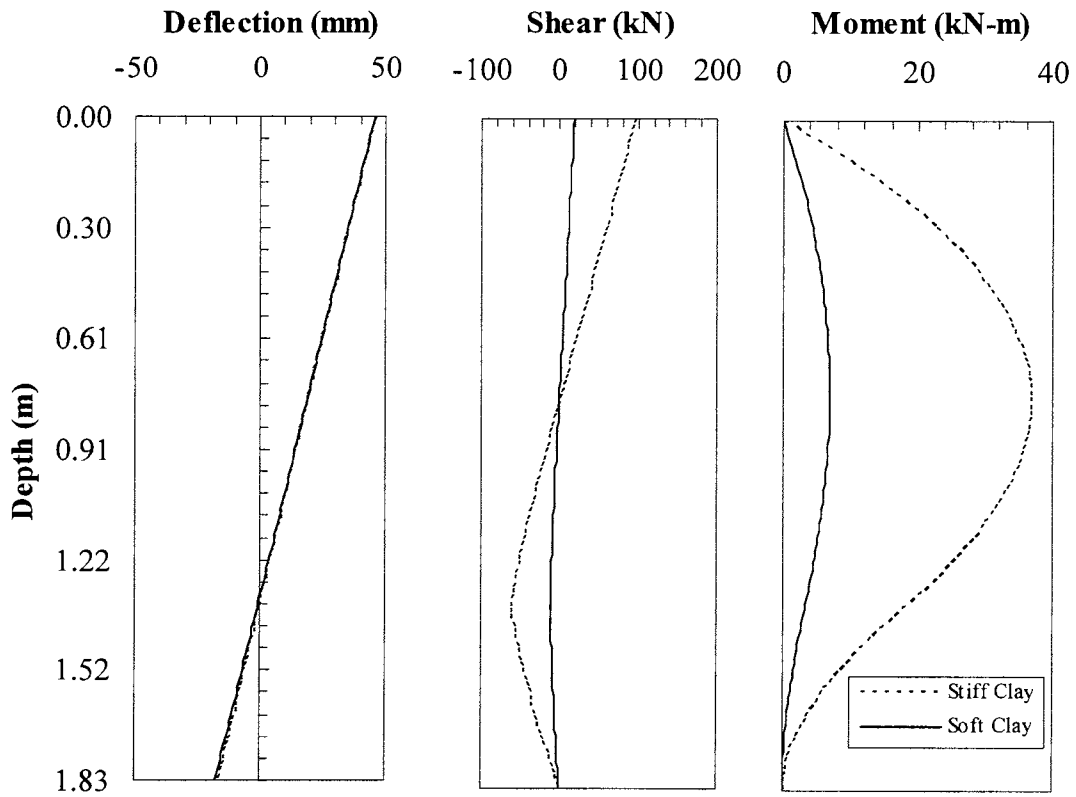**Displacement, Shear and Moment Curves in Soft, Stiff Clay (D = 0.61m, L=2.44m)**

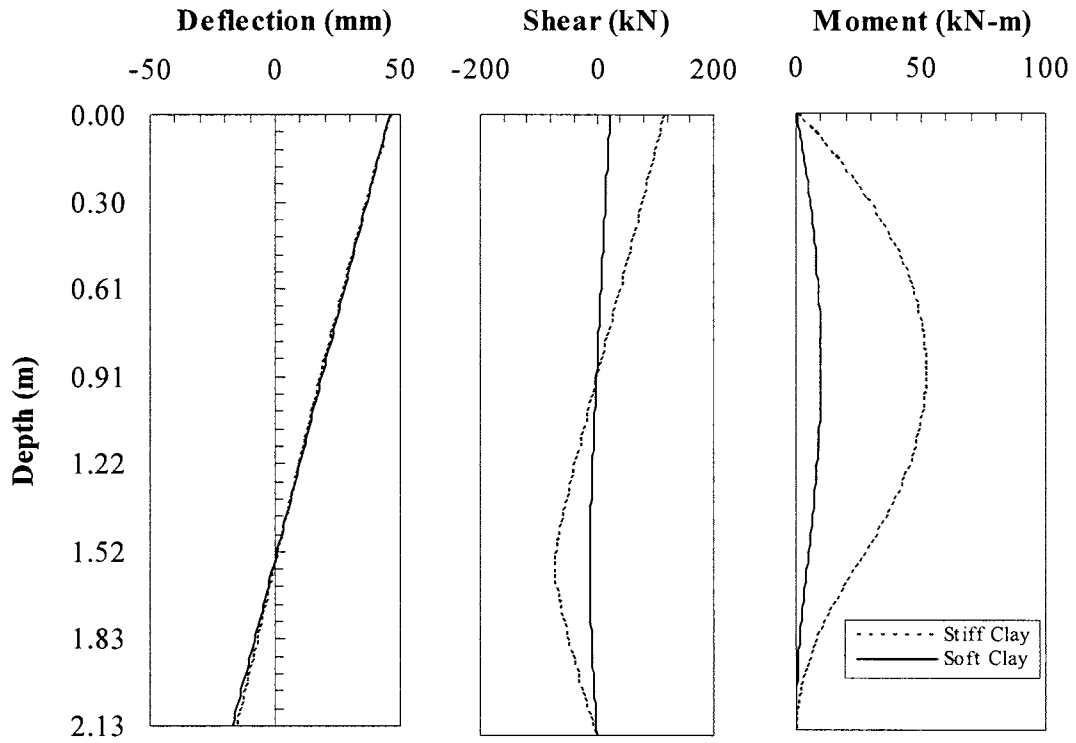Displacement, Shear and Moment Curves in Soft, Stiff Clay (D = 0.61m, L=2.74m)

Displacement, Shear and Moment Curves in Soft, Stiff Clay (D = 0.61m, L=3.05m)
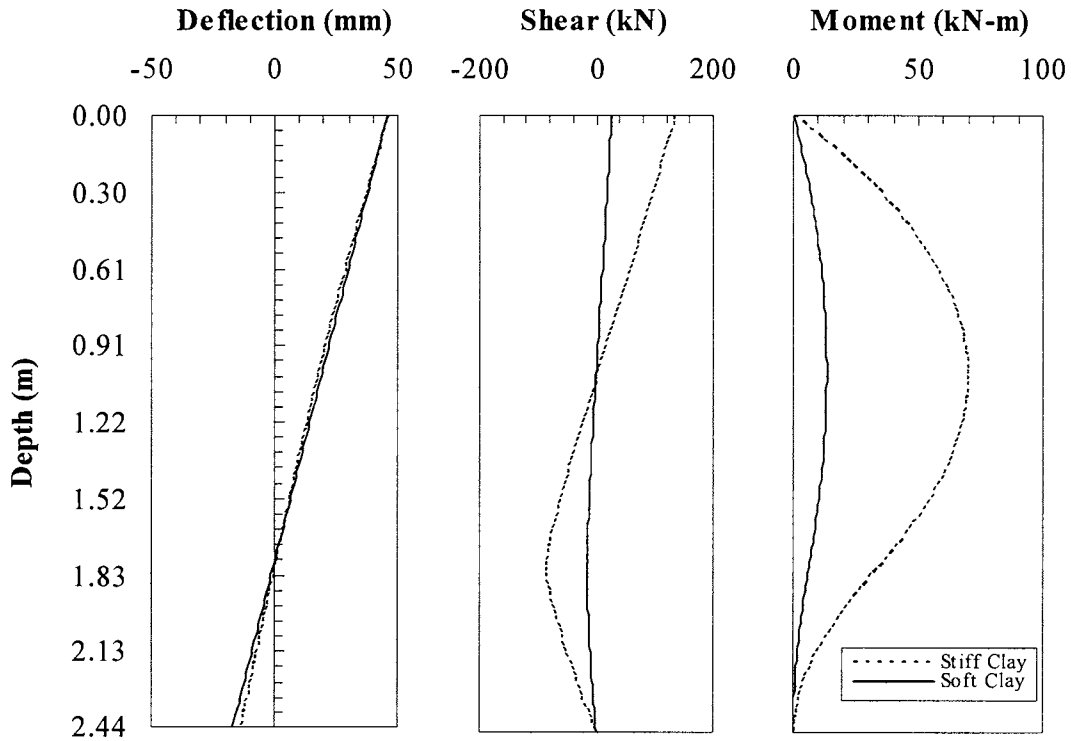
Displacement, Shear and Moment Curves in Soft, Stiff Clay (D = 0.76m, L=1.52m)
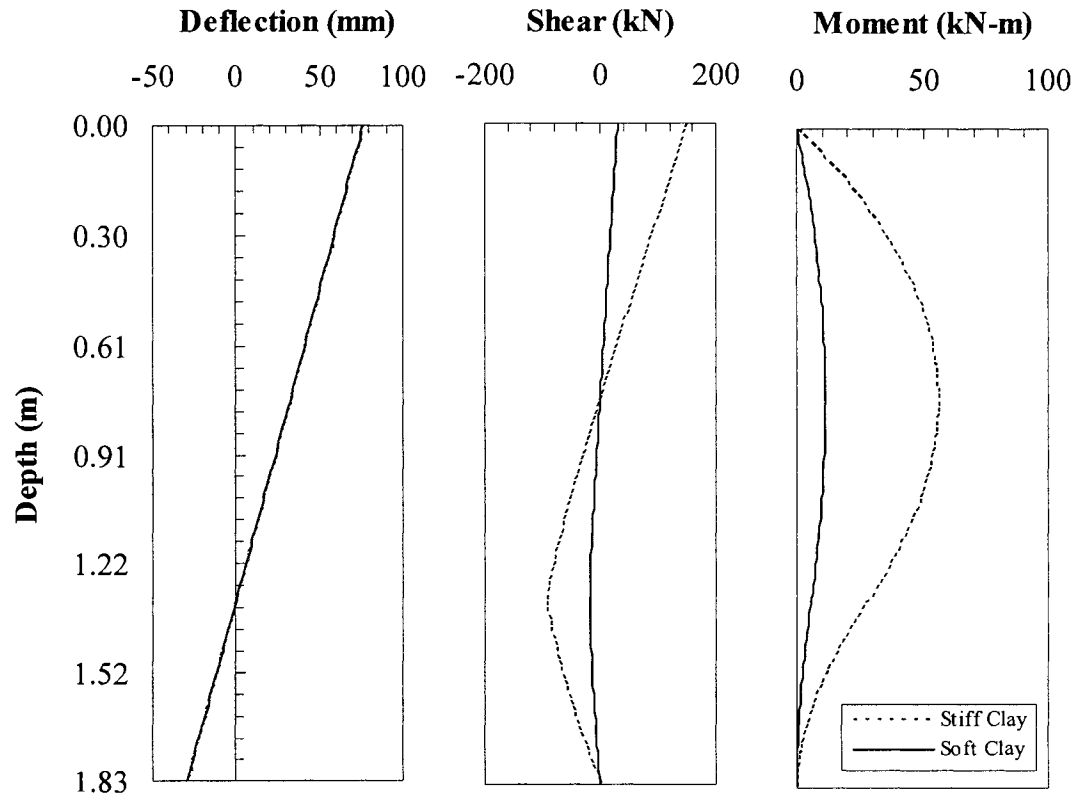
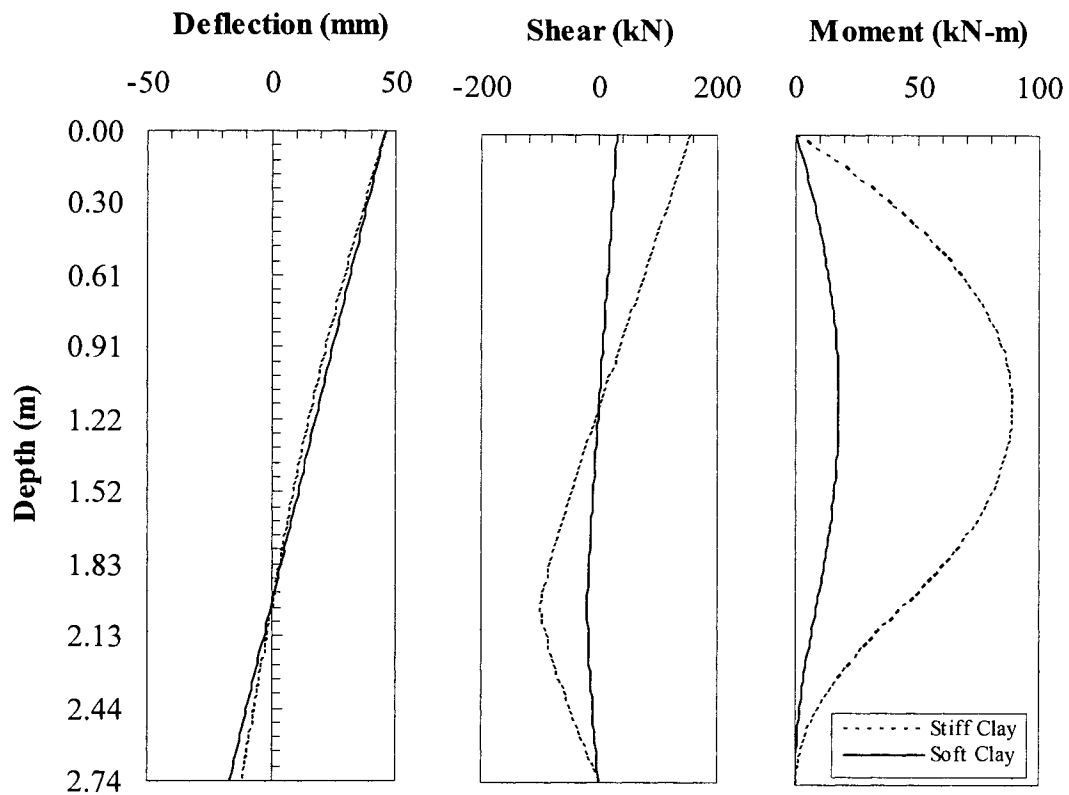**Displacement, Shear and Moment Curves in Soft, Stiff Clay (D = 0.76m, L=1.83m)**
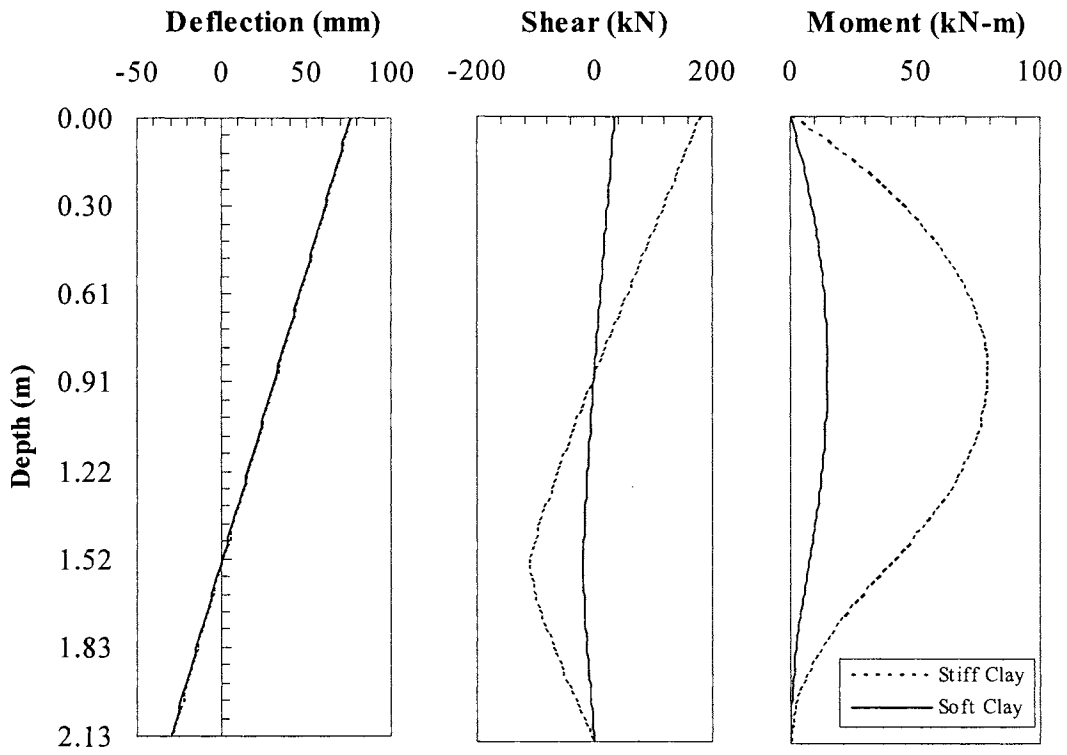
Displacement, Shear and Moment Curves in Soft, Stiff Clay (D = 0.76m, L=2.13m)
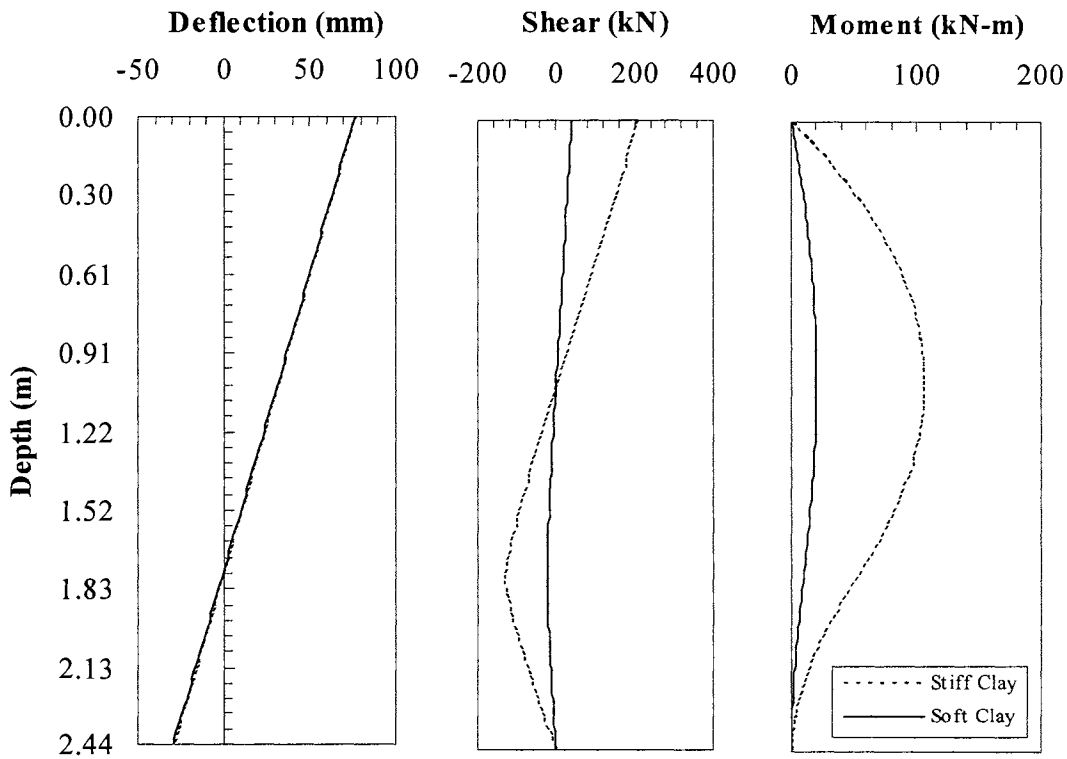
Displacement, Shear and Moment Curves in Soft, Stiff Clay (D = 0.76m, L=2.44m)
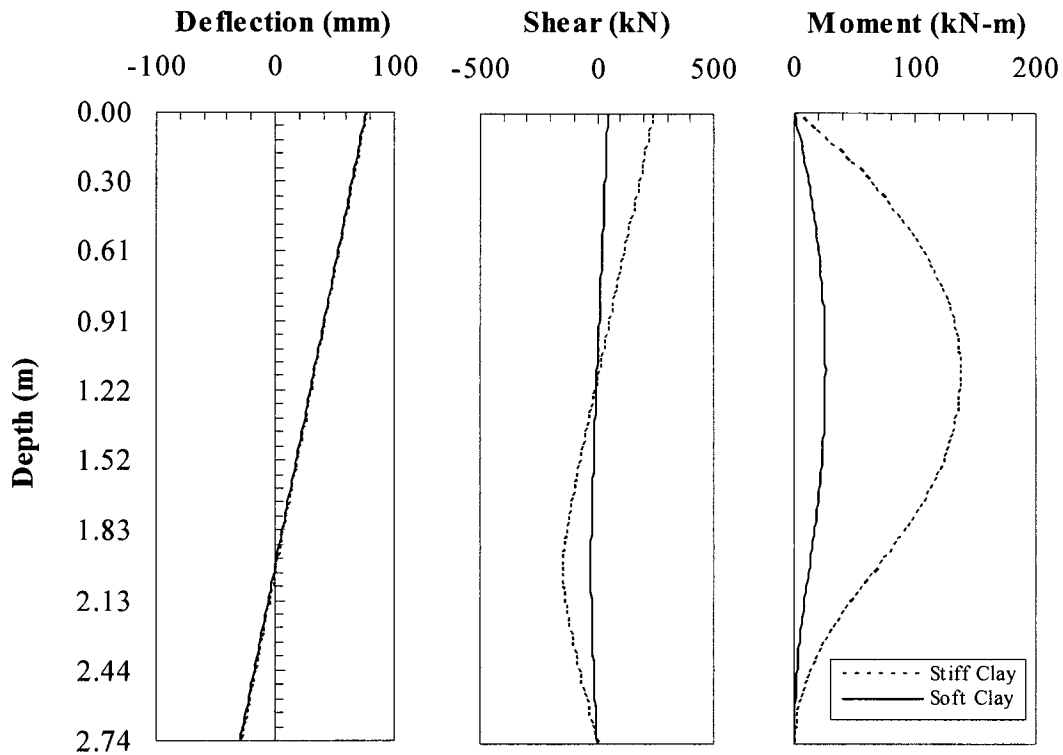
Displacement, Shear and Moment Curves in Soft, Stiff Clay (D = 0.76m, L=2.74m)
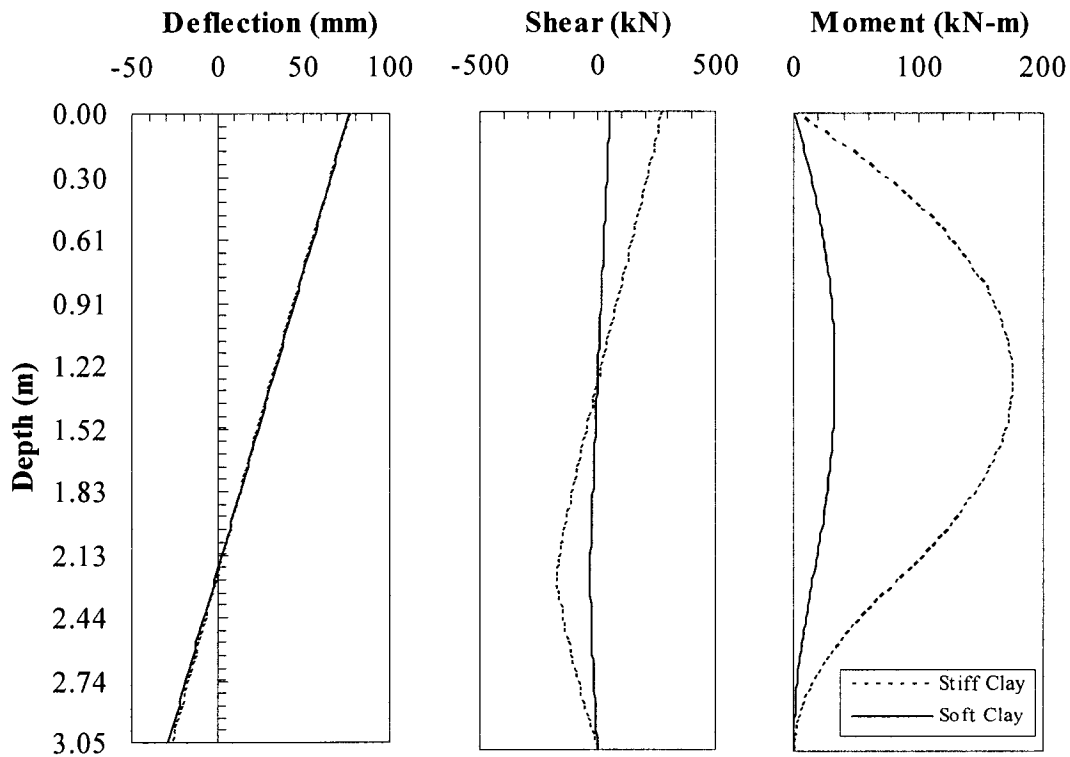
Displacement, Shear and Moment Curves in Soft, Stiff Clay (D = 0.76m, L=3.05m)
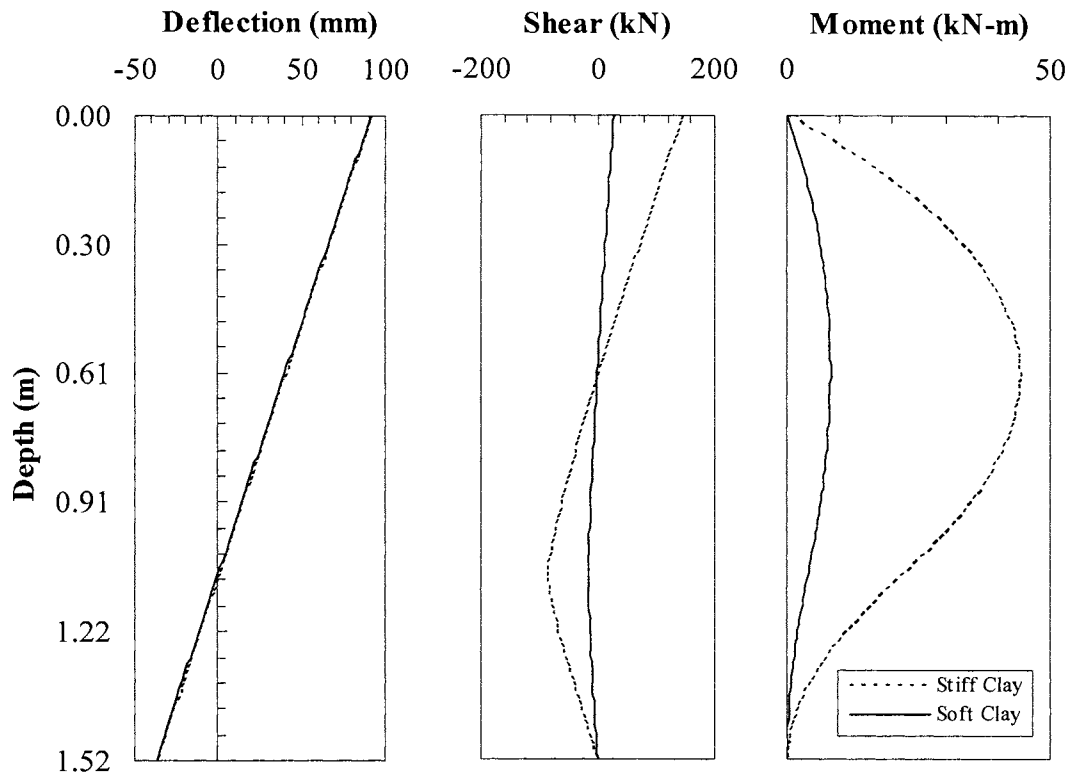
Displacement, Shear and Moment Curves in Soft, Stiff Clay (D = 0.91m, L=1.52m)
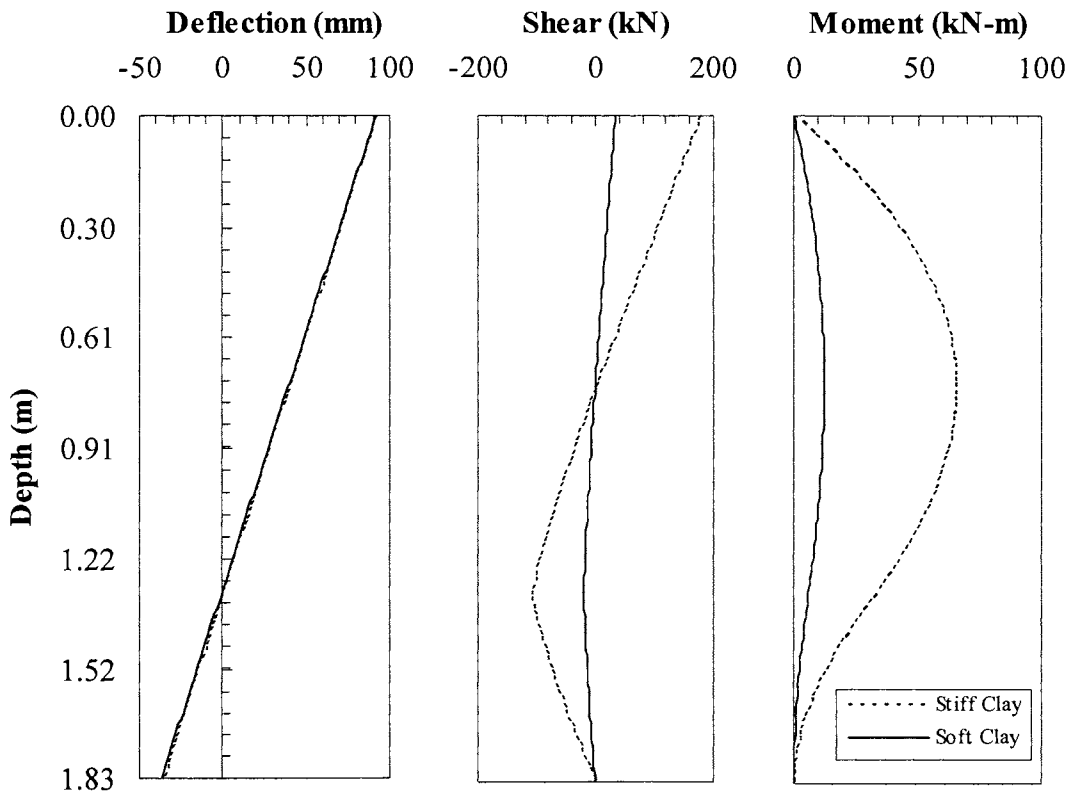
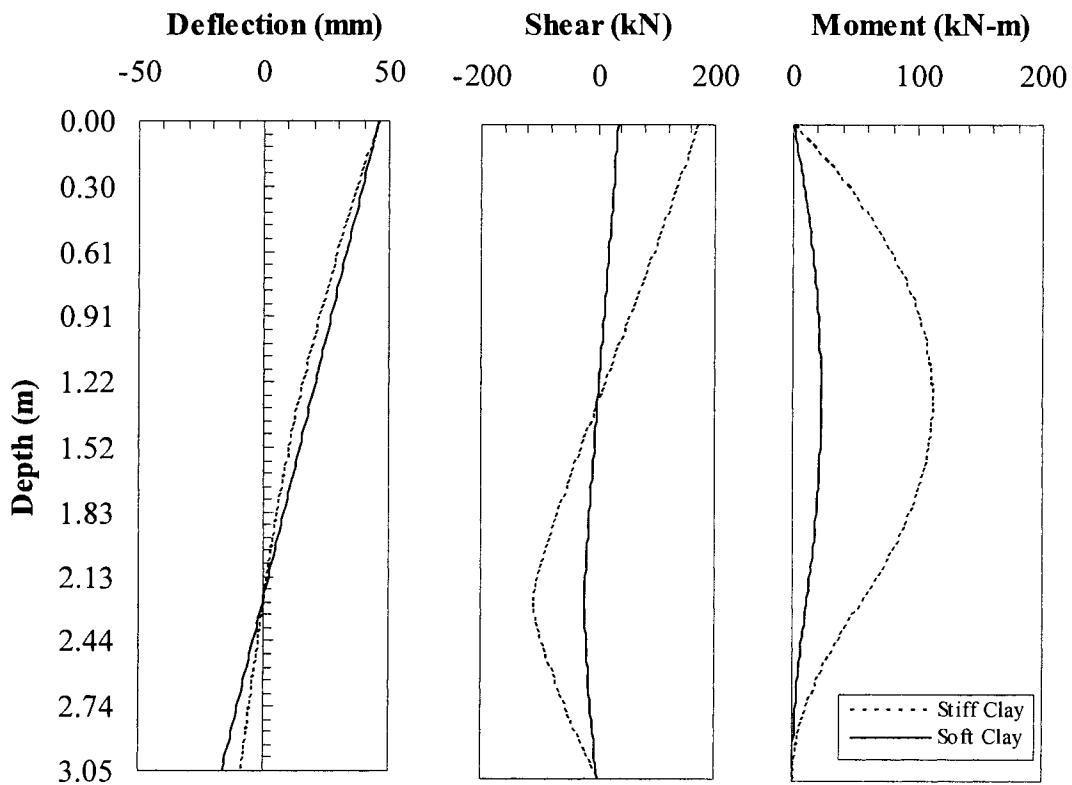**Displacement, Shear and Moment Curves in Soft, Stiff Clay (D = 0.91m, L=1.83m)**
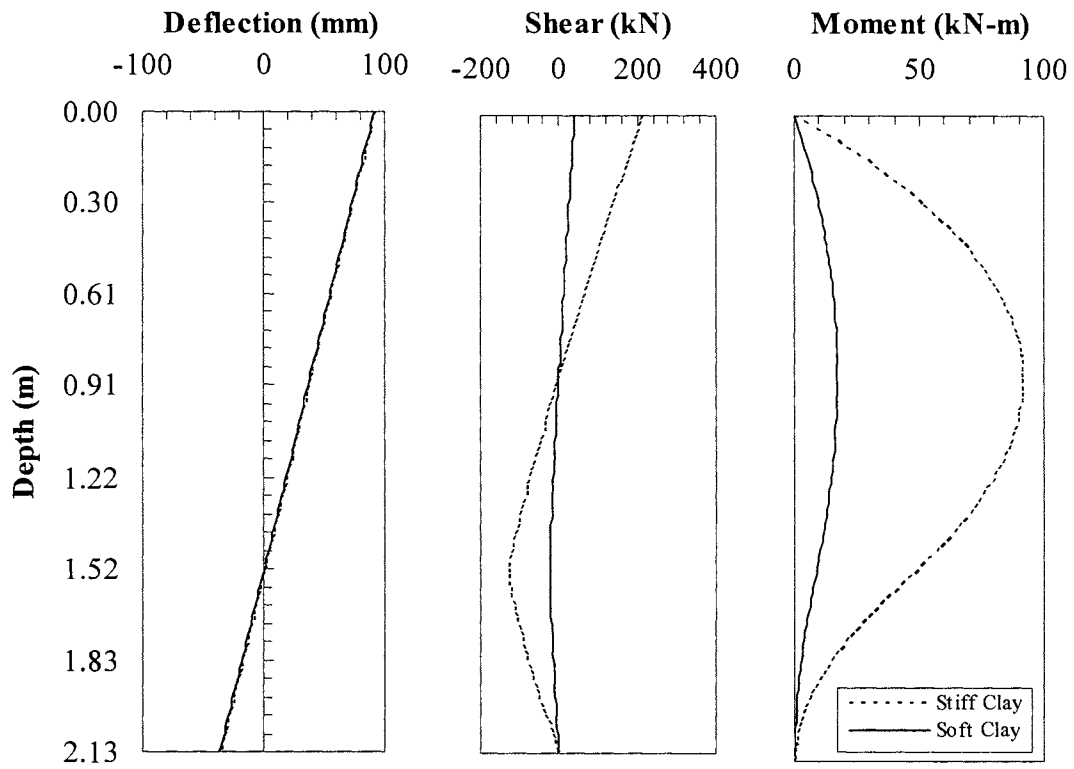
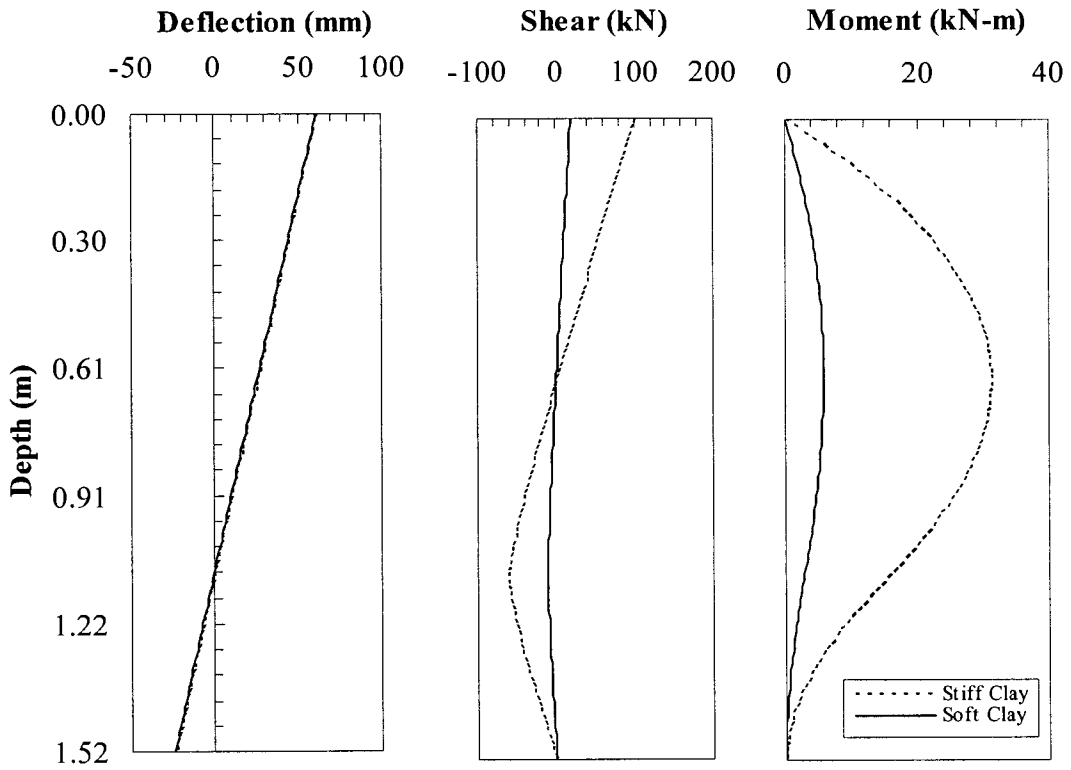**Displacement, Shear and Moment Curves in Soft, Stiff Clay (D = 0.91m, L=2.13m)**
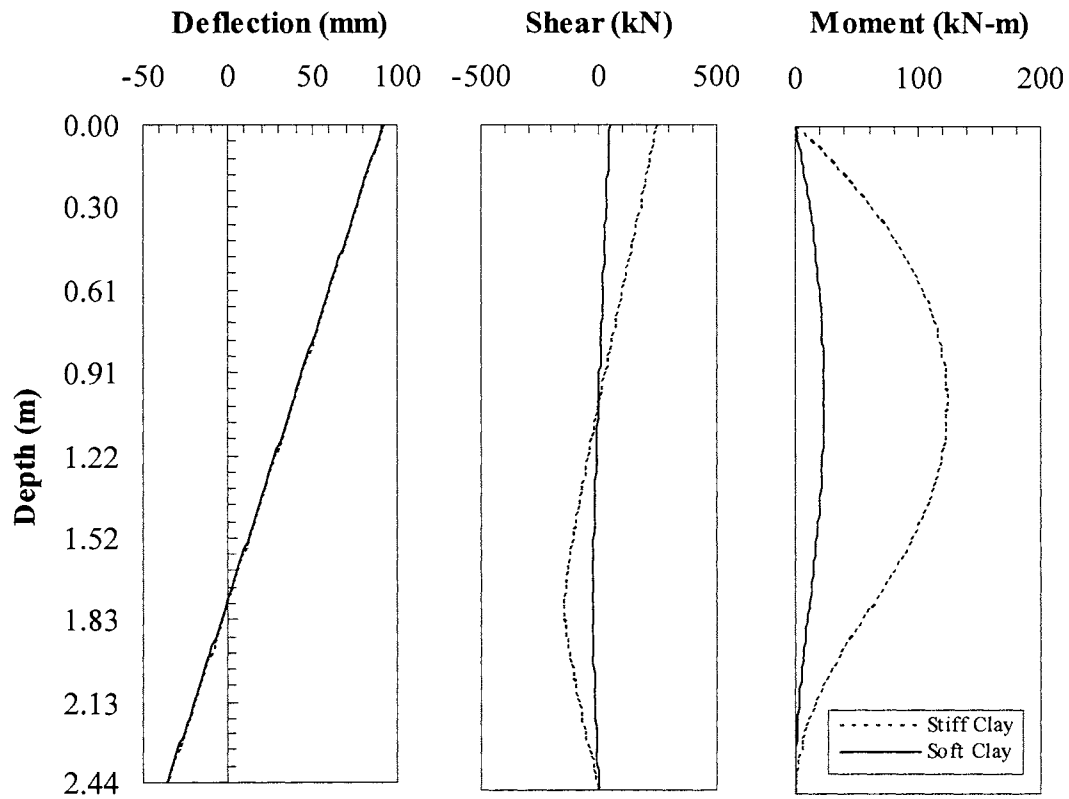
Displacement, Shear and Moment Curves in Soft, Stiff Clay (D = 0.91m, L=2.44m)
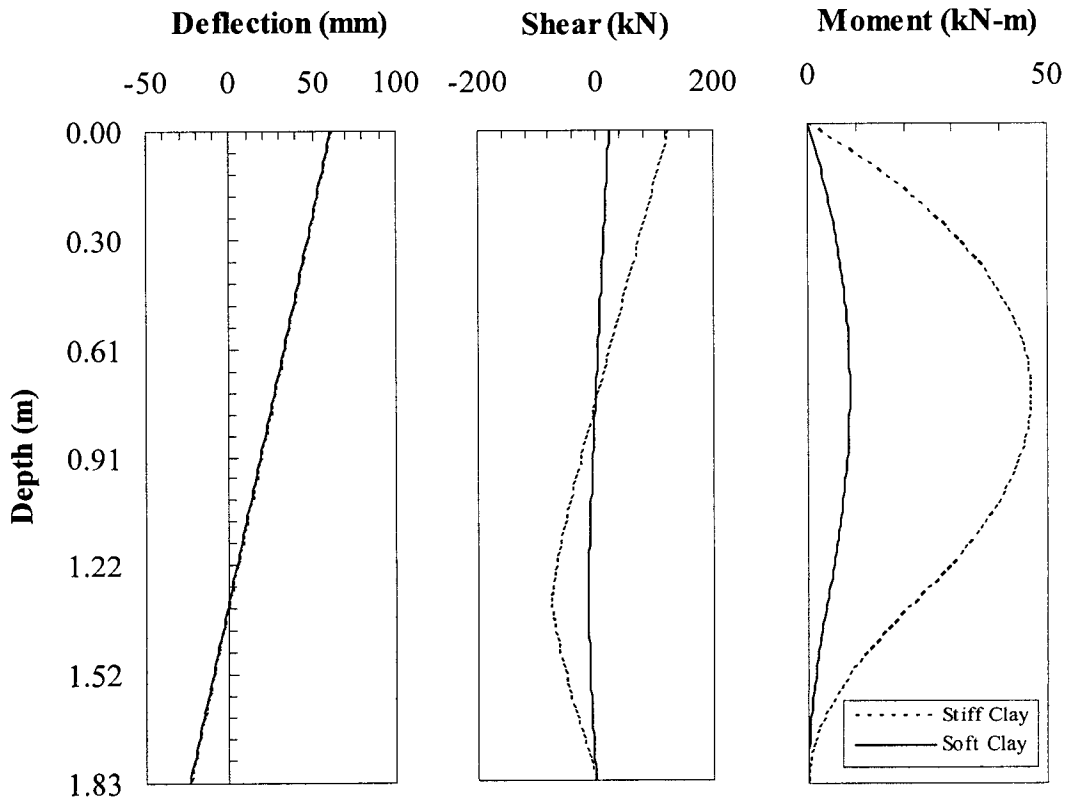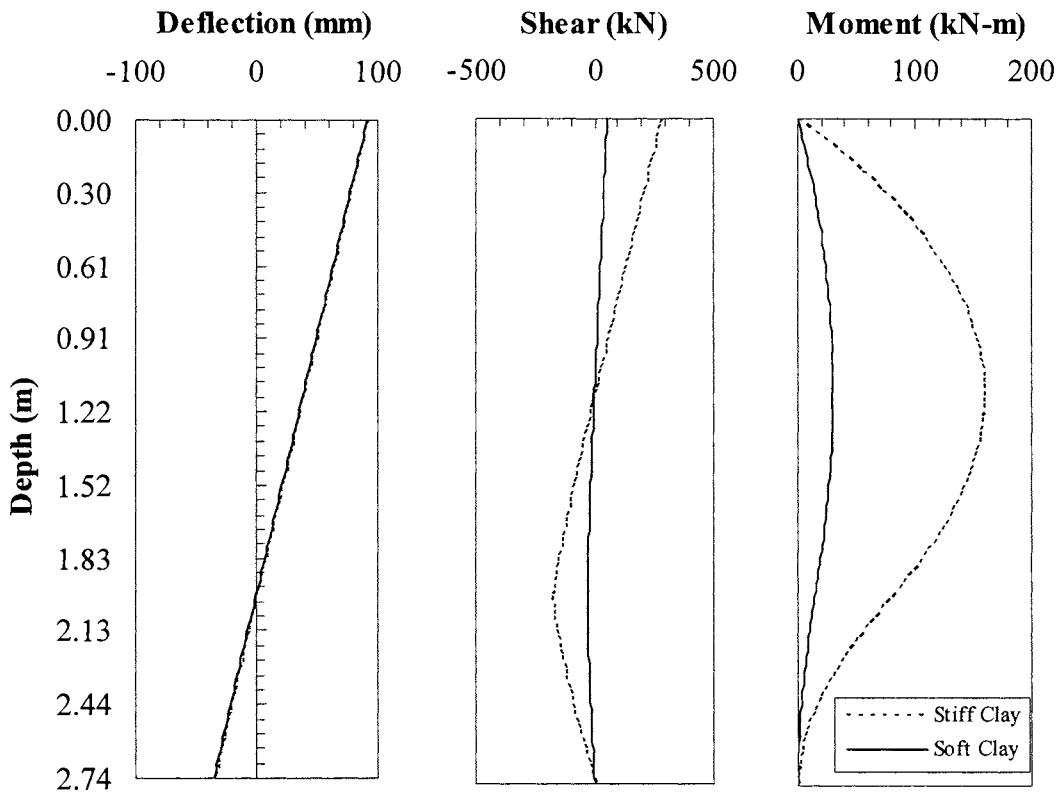
Displacement, Shear and Moment Curves in Soft, Stiff Clay (D = 0.91m, L=2.74m)

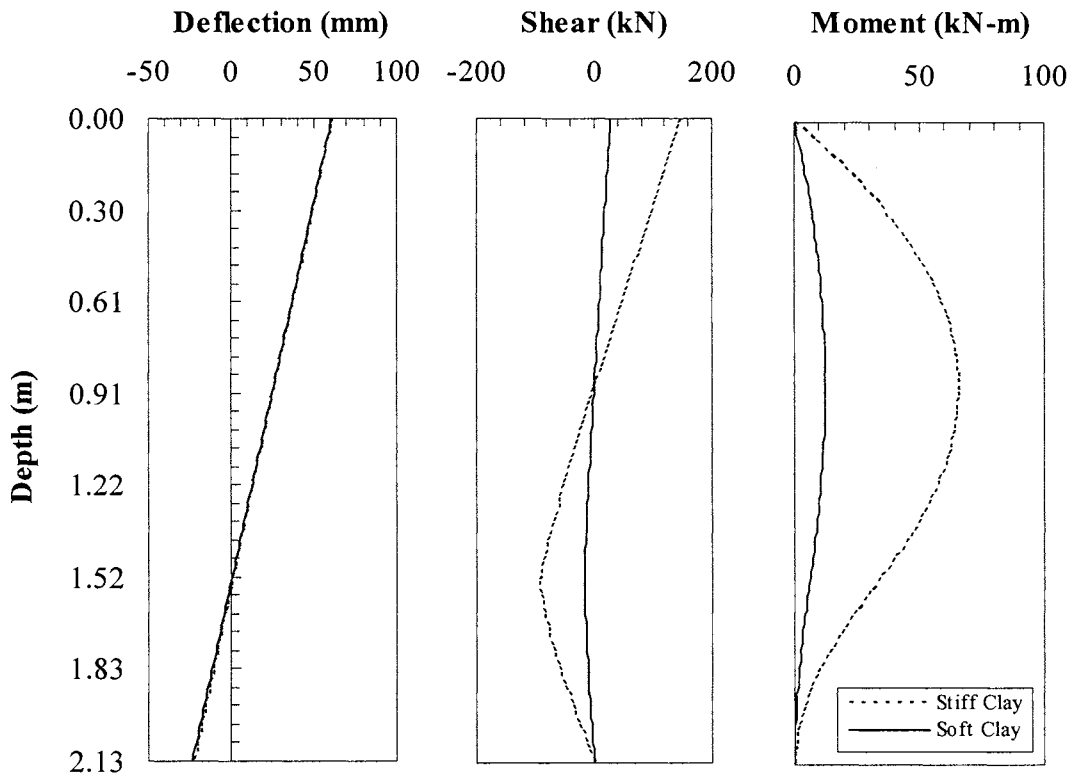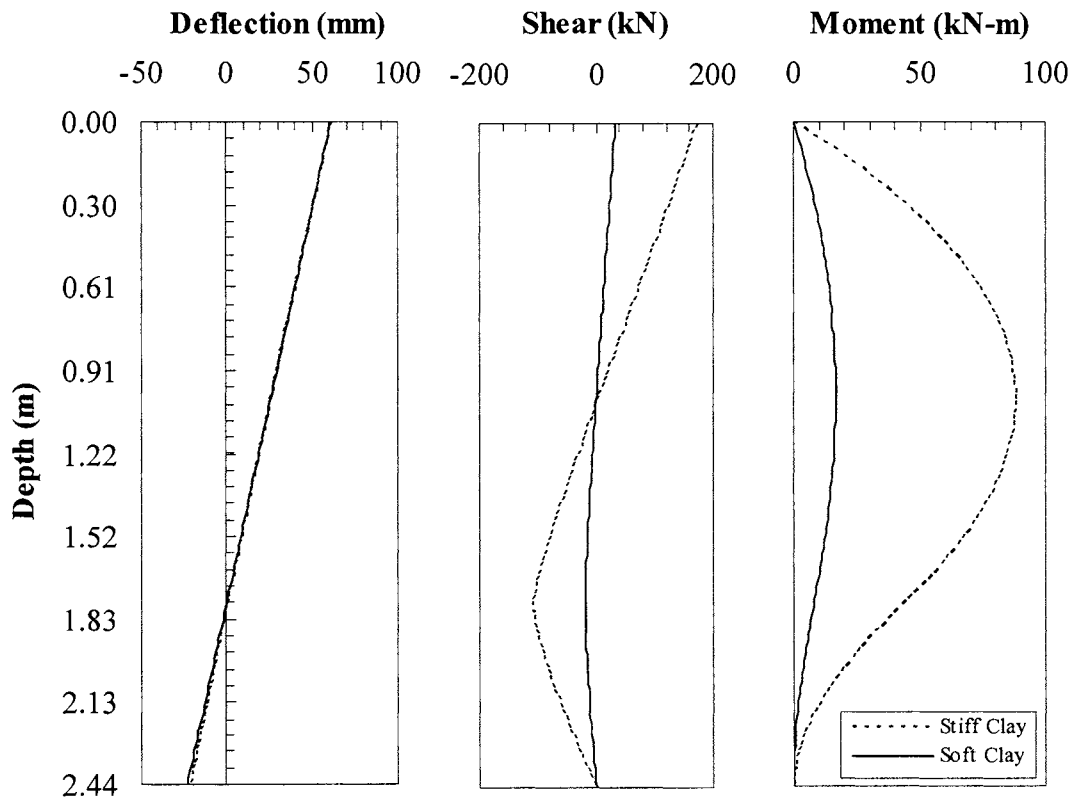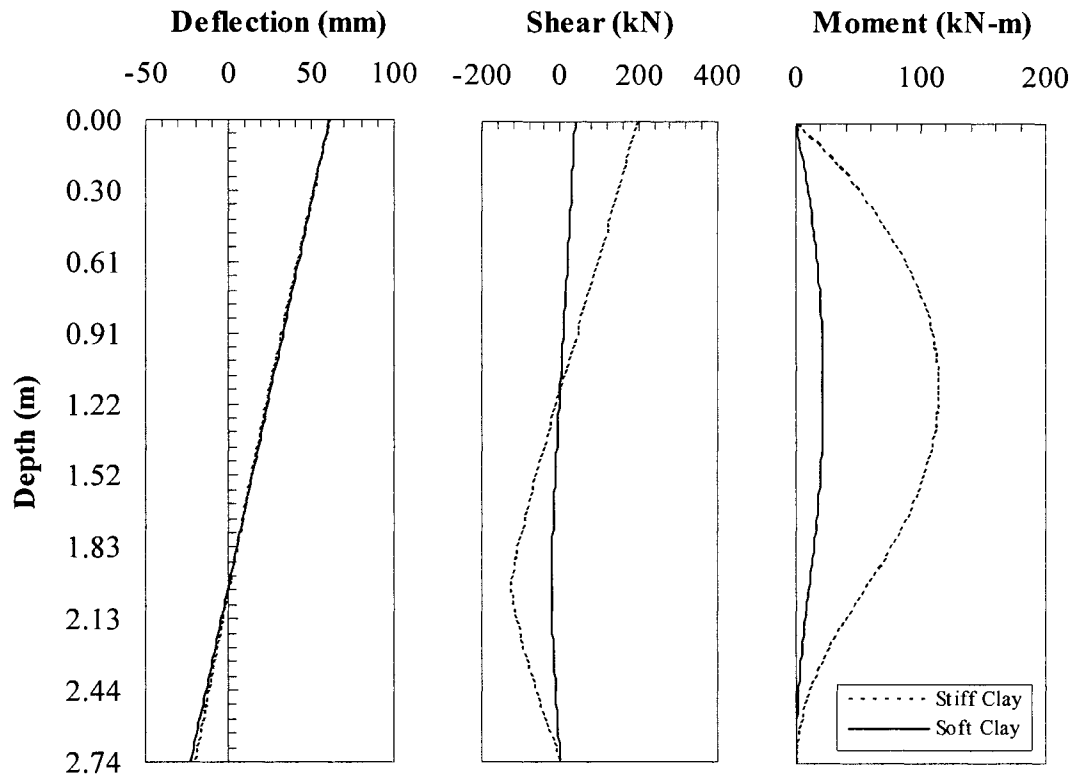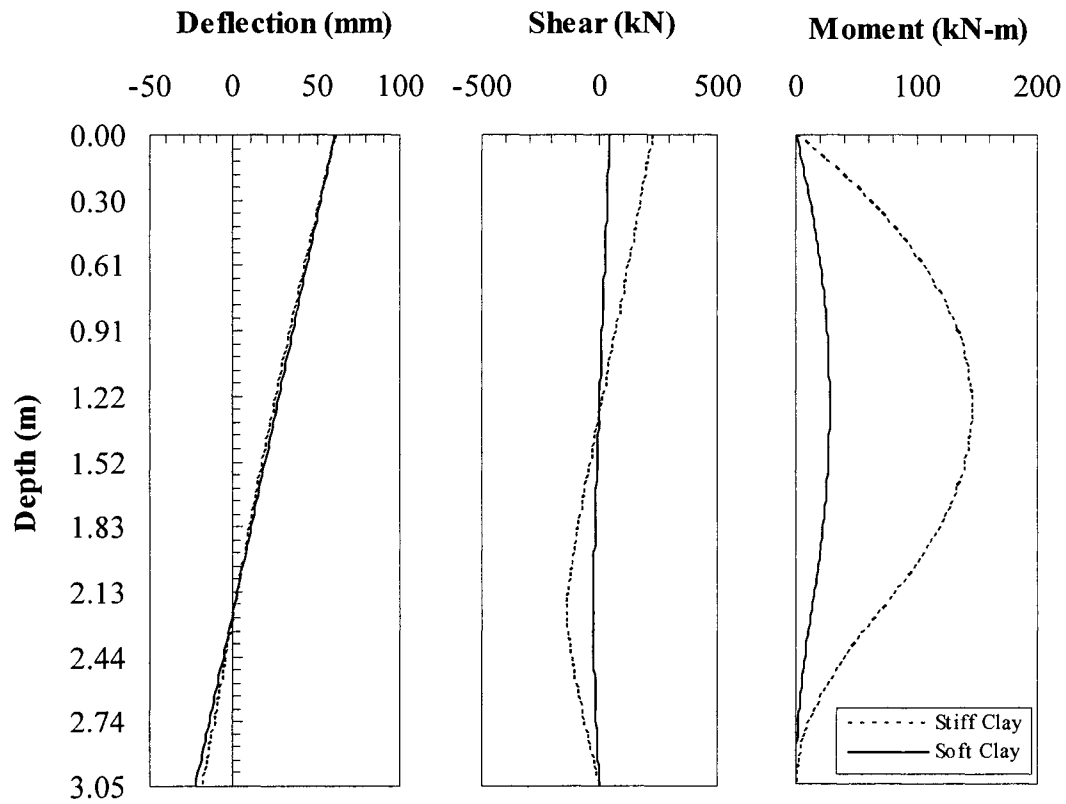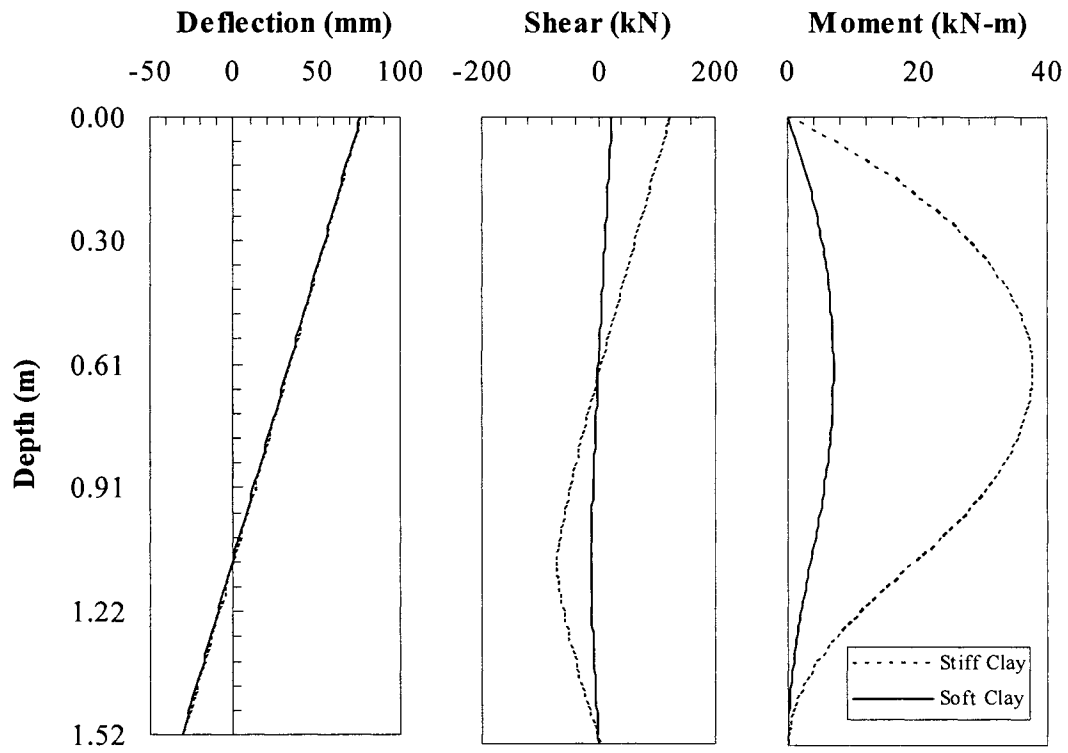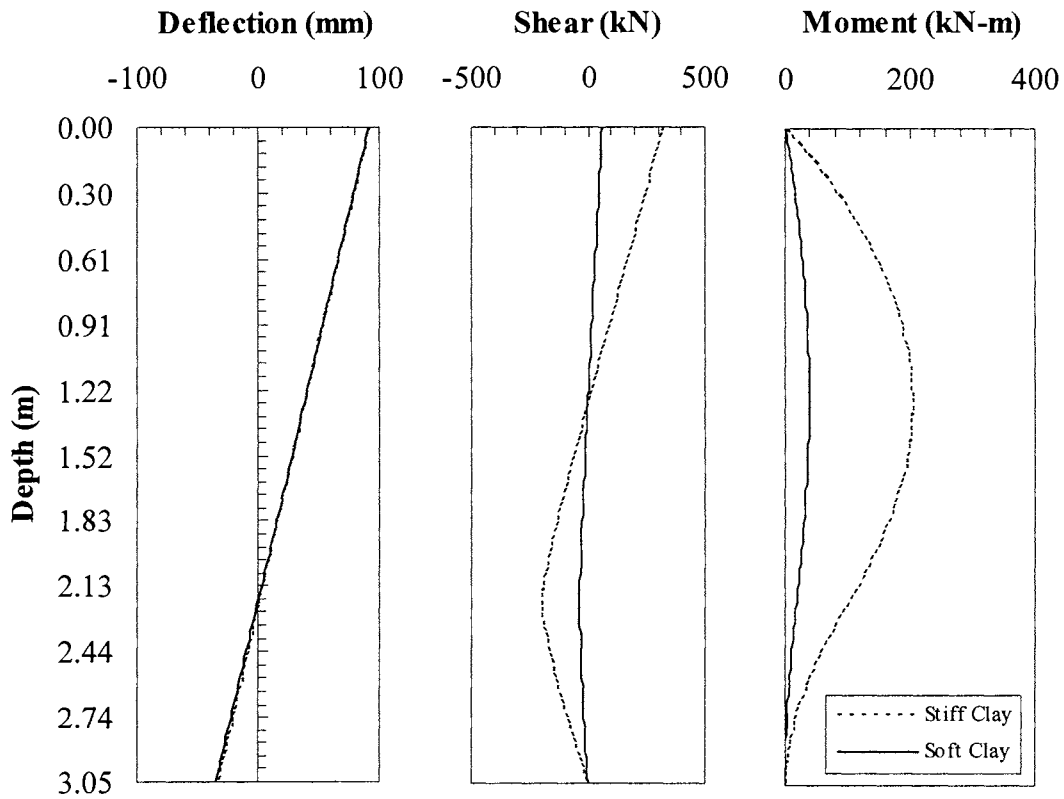**Displacement, Shear and Moment Curves in Soft, Stiff Clay (D = 0.91m, L=3.05m)**

Appendix B: Laboratory and In Situ Tests

Appendix B1: Laboratory Tests Results

Boring #1 Ground Water Table GWT = 3 ft

Depth (ft)	Sample No.		Sample length (in.)	Water Content (%)	γ_d (pcf)	Unconfined compression strength q_u (kPa)	Strain at q_u (%)
2.08	1-1		10	11.9	--	--	--
4.58	1-2		10	24.1	--	--	--
6.33		1-3-1	5.6	22	113.6	90	15
6.80	1-3	1-3-2	5.6	15.7	119	102	9
7.27		1-3-3	5.6	16.2	117.2	154	6
8.91		1-4-1	5	16.8	--	--	--
9.33	1-4	1-4-2	5	18.8	--	--	--
9.77		1-4-3	5.6	11.9	122.6	280	3.57
11.41		1-5-1	5	14.3	--	--	--
11.85	1-5	1-5-2	5.6	12	119.4	149	2.86
12.29		1-5-3	5	11.3	--	--	--

Depth (ft)	OCR	σ'_v(kPa)	P'_c(kPa)	LL(%)	PL(%)	PI(%)	Gs	Unified Soil Classification
1.25	17.1	8	140	31.6	22.7	8.8	2.65	CL
3.75	--	22	--	31.4	20	11.4	--	CL
6.25	--	31	--	25	18	7	--	CL
8.75	--	40	--	26	17	9	2.72	CL
11.25	--	49	--	24.4	19	5.4	--	CL

Boring #2 GWT = 3 ft

Depth (ft)	Sample No.		Sample length (in.)	Water Content (%)	γ_d (pcf)	Unconfined compression strength q_u (kPa)	strain at q_u (%)
2.08	2-1		10	26.9	--	--	--
2.73		2-2-1	5.6	20.9	110.5	32	8
2.97	2-2	2-2-2	5.6	24.1	106.6	70	10
3.20		2-2-3	5.6	26.9	104.1	100	8
3.98		2-2-4	13.2	21.7	--	--	--
5.63	2-3	2-3-1	15	21	--	--	--
6.88		2-3-2	15	14.9	--	--	--
8.96		2-4-1	5	18.8	--	--	--
9.38	2-4	2-4-2	5	17.9	--	--	--
9.79		2-4-3	5	14.5	--	--	--
11.83	2-5	2-5-1	5	23.1	--	--	--
12.27		2-5-2	5.6	19.7	113	112	18

Depth (ft)	OCR	σ'_v(kPa)	P'_c(kPa)	LL(%)	PL(%)	PI (%)	Gs	Unified soil Classification
1	21.9	6.4	140	40	26.7	13.3	2.66	CL
1.25	19.4	8	155	40	26.7	13.3	2.66	CL
3.75	7.4	22	160	25.6	19	6.6	2.72	CL
6.25	--	30	--	25	15	10	--	SC
8.75	4.6	39	180	23.4	17	6.4	2.68	SC
11.25	--	47	--	24.6	18	6.6	--	CL

Grain Size Distribution
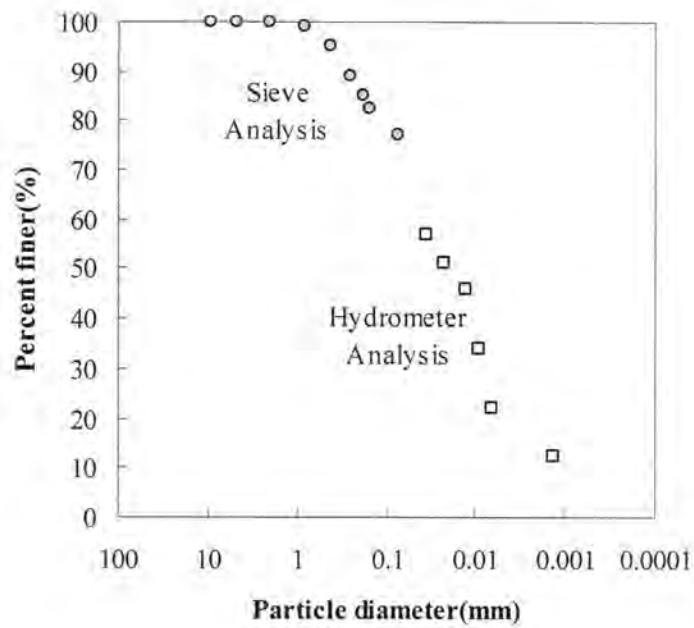
Grain-Size Distribution at 0-2.5 ft (Boring 1)
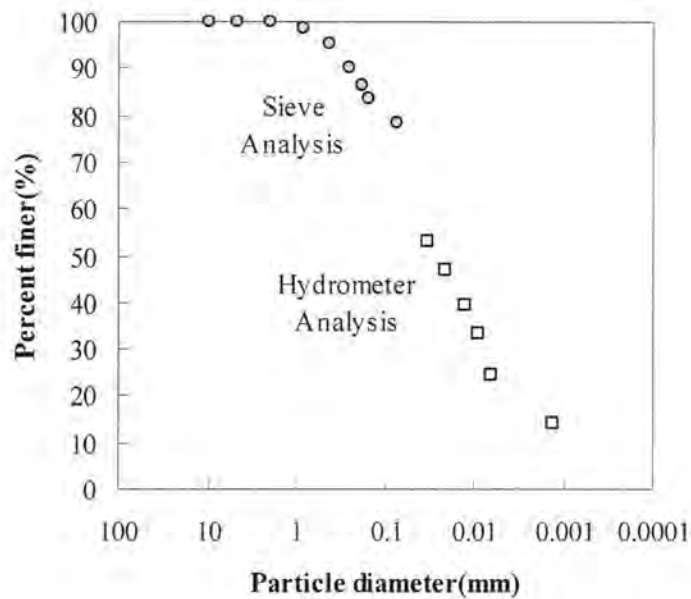
Grain-Size Distribution at 2.5-5 ft (Boring 1)
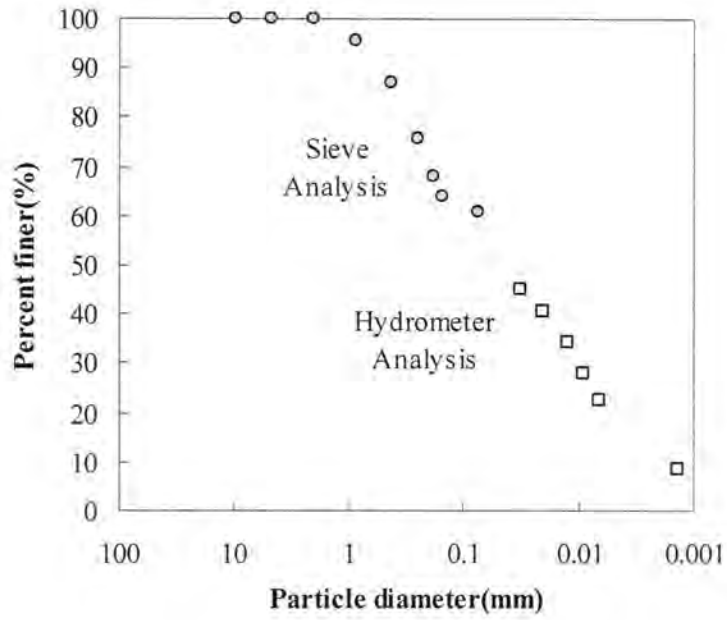
Grain-Size Distribution at 5-7.5 ft (Boring 1)
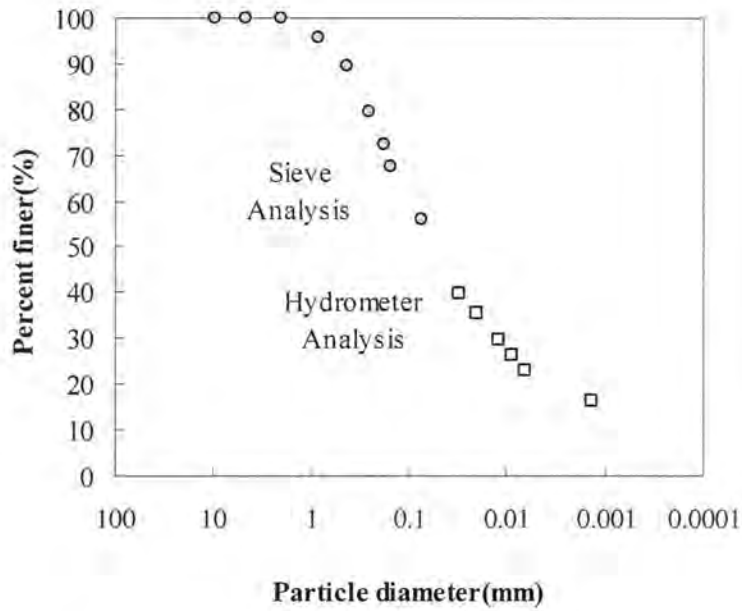
Grain-Size Distribution at 7.5-10 ft (Boring 1)
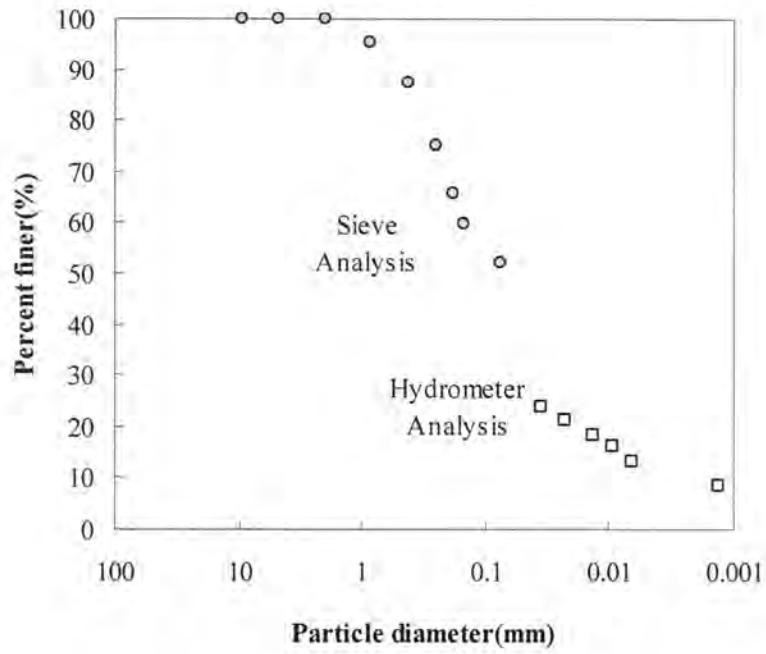
Grain-Size Distribution at 10-12.5 ft (Boring 1)
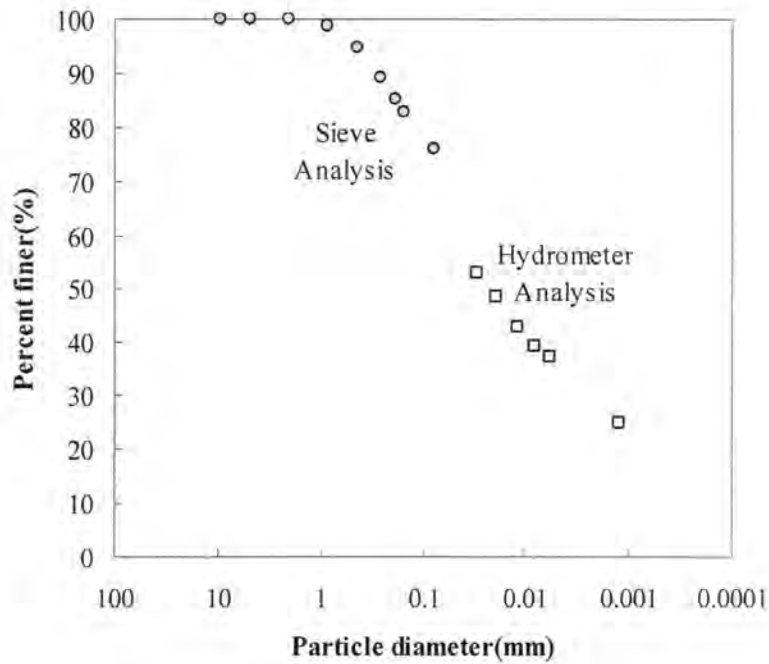
Grain-Size Distribution at 0-2.5 ft (Boring 2)
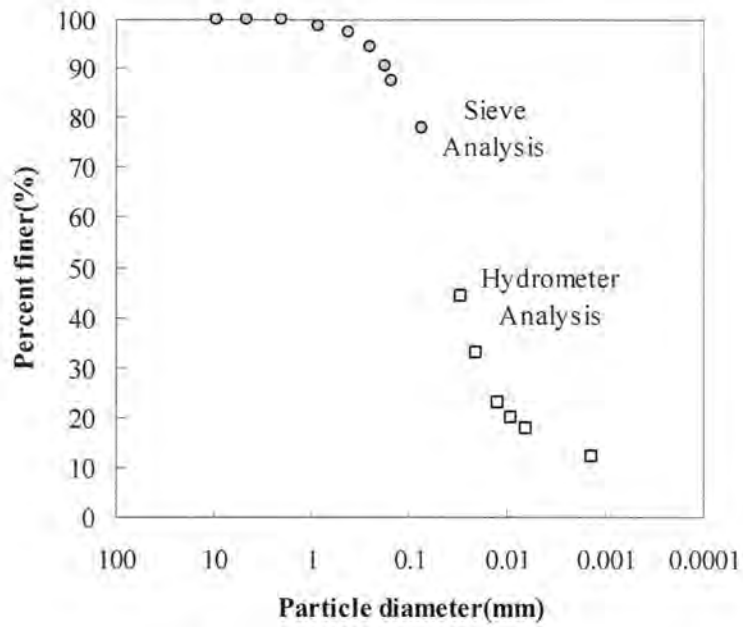
Grain-Size Distribution at 2.5-5 ft (Boring 2)
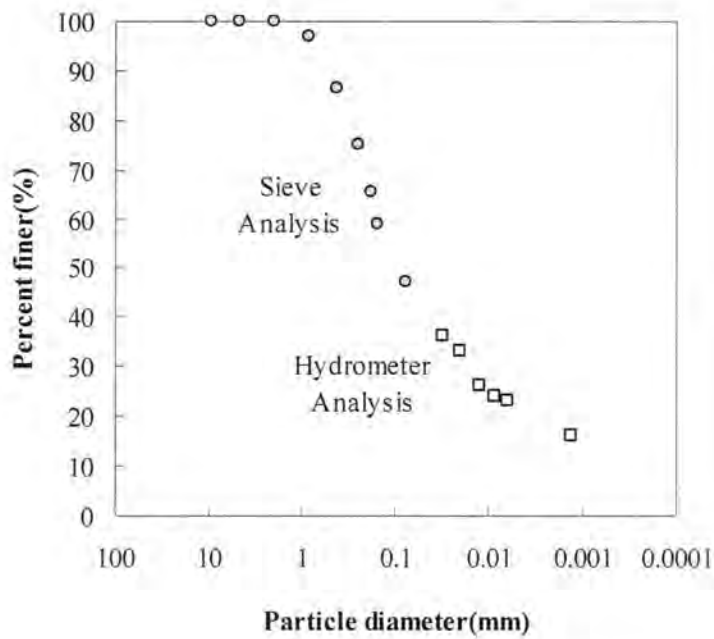
Grain-Size Distribution at 5-7.5 ft (Boring 2)
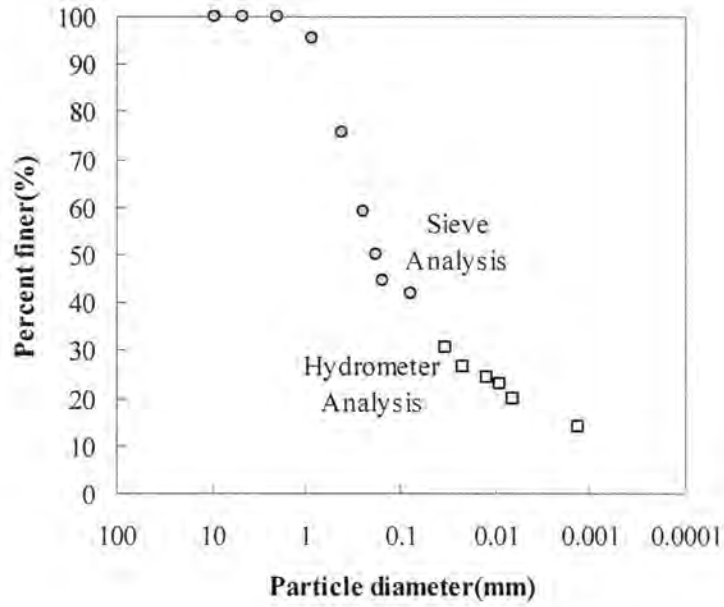
Grain-Size Distribution at 7.5-10 ft (Boring 2)
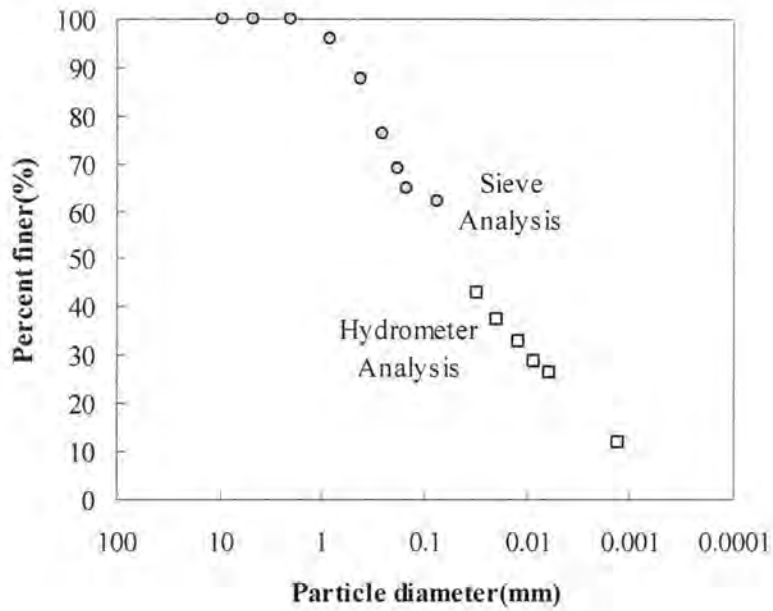
Grain-Size Distribution at 10-12.5 ft (Boring 2)

Unconfined Compression Tests Stress-Strain Curves
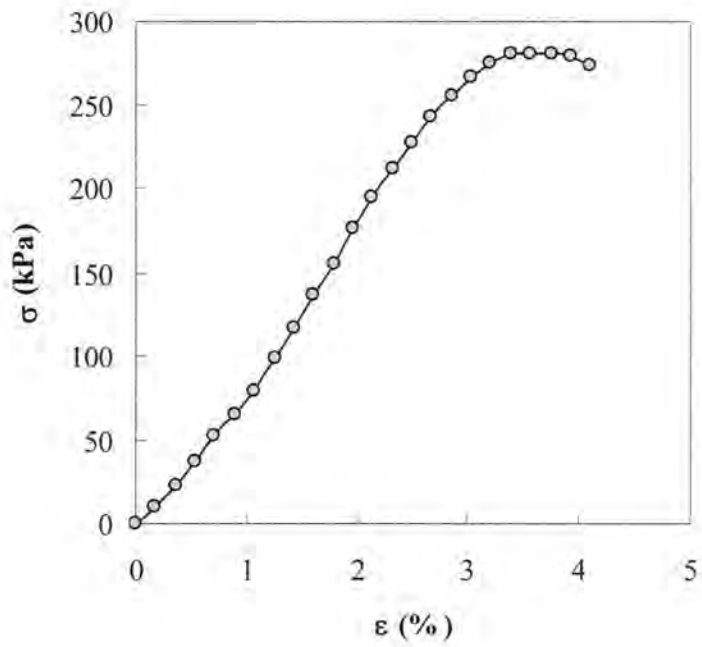
Stress-Strain Curve at Depth 9.8 ft (Boring 1)
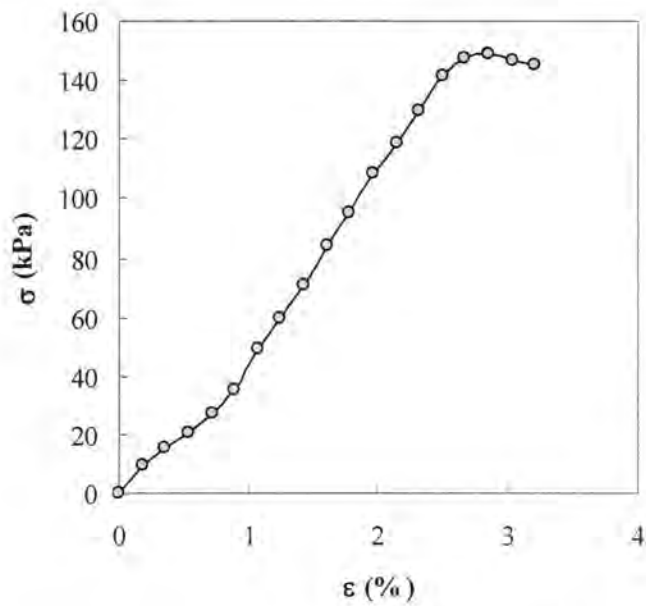
Stress-Strain Curve at Depth 11.9 ft (Boring 1)
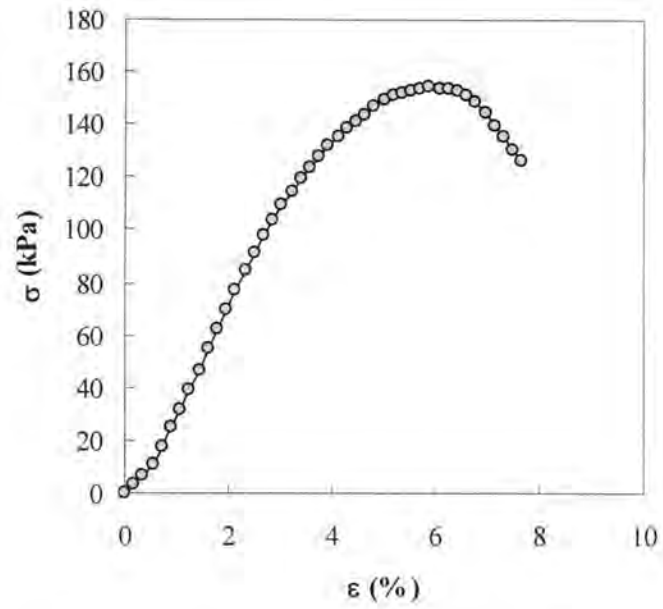
Stress-Strain Curve at Depth 7.3 ft (Boring 1)
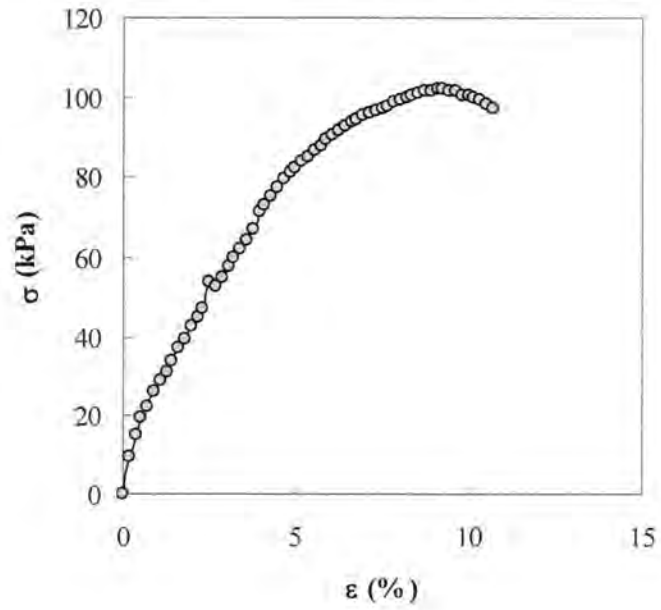
Stress-Strain Curve at Depth 6.8 ft (Boring 1)
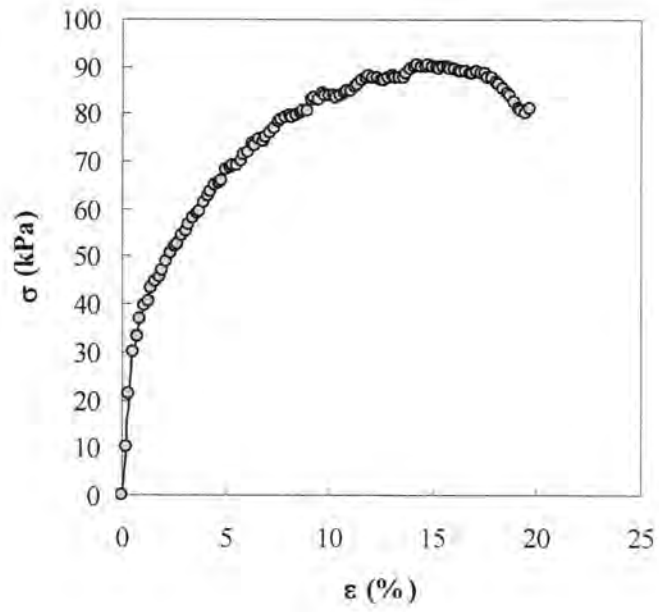
Stress-Strain Curve at Depth 6.3 ft (Boring 1)
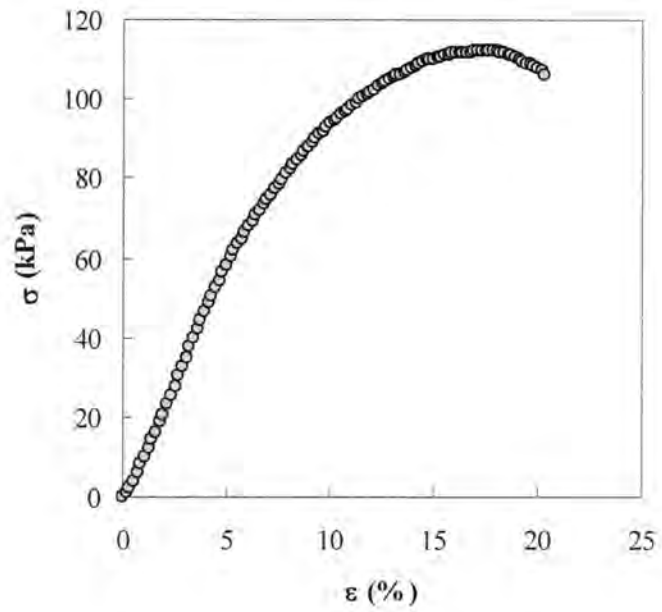
Stress-Strain Curve at Depth 12.3 ft (Boring 2)
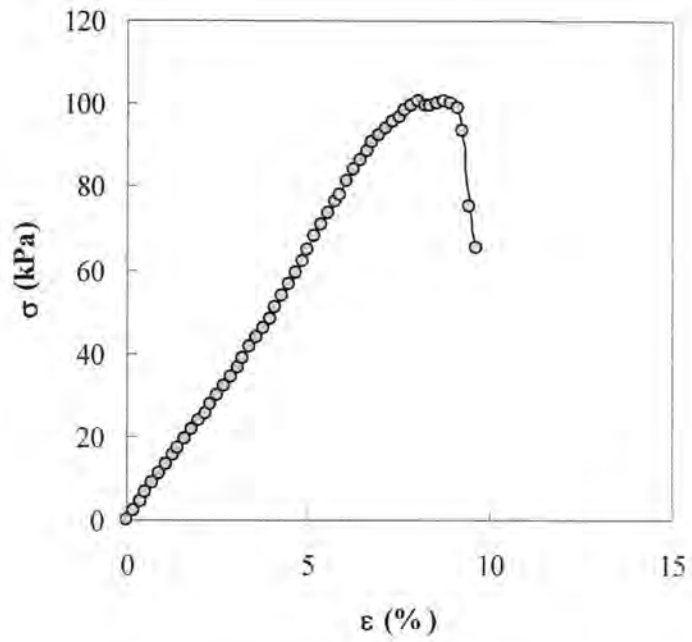
Stress-Strain Curve at Depth 3.2 ft (Boring 2)
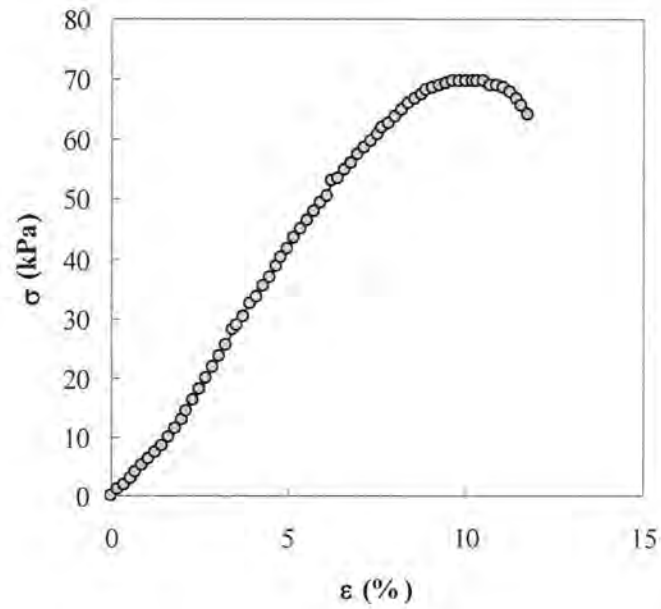
Stress-Strain Curve at Depth 3 ft (Boring 2)
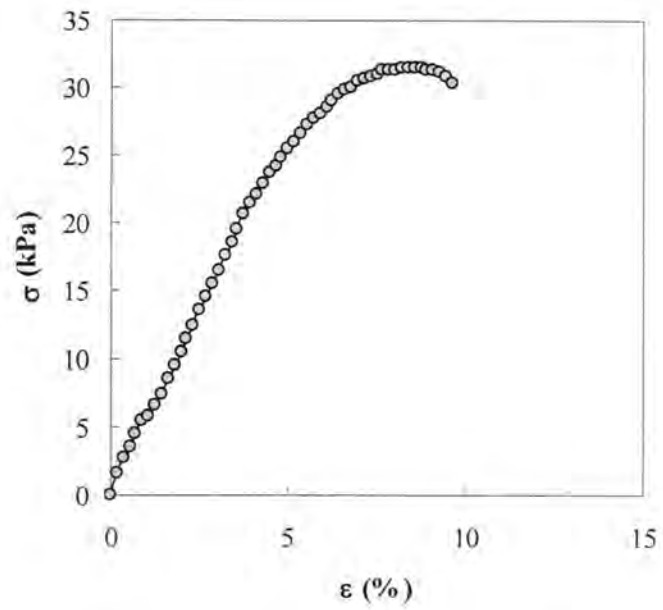
Stress-Strain Curve at Depth 2.7 ft (Boring 2)

CU Triaxial Tests Stress-Strain Curves
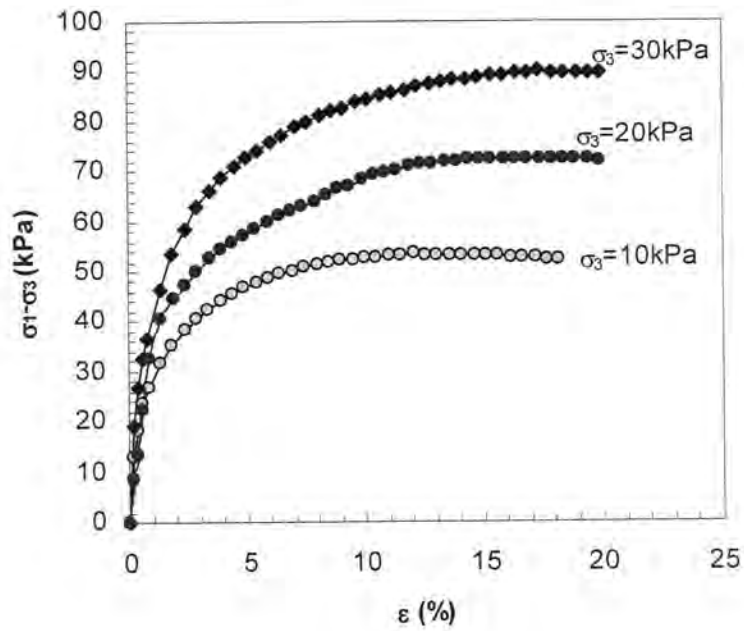
Stress-Strain Curve at Depth 1-2 ft
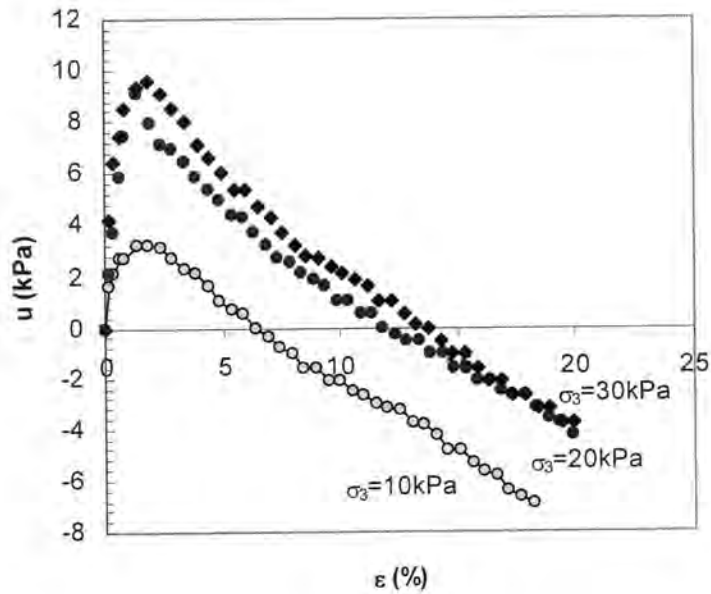
Pore Water Pressure vs. Strain Curve at Depth 1-2 ft
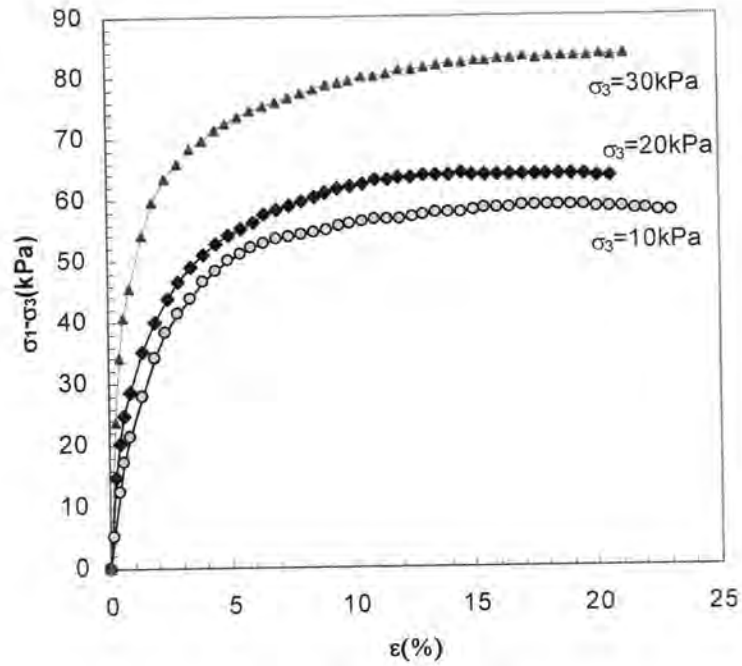
Stress-Strain Curves at Depth 3-4 ft
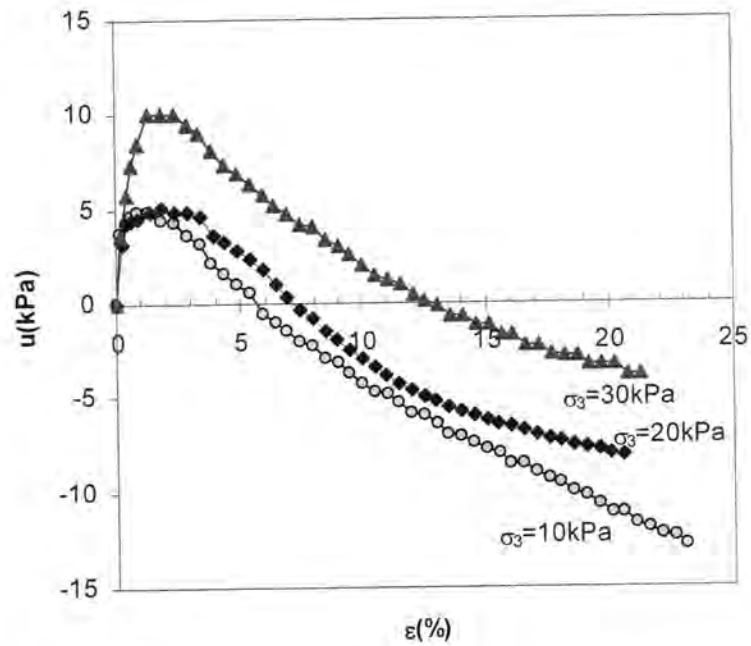
Pore Water Pressure vs. Strain Curve at Depth 3-4 ft

Appendix B2: In Situ Tests Results

DMT Test

Depth (m)	A-Reading (bar)	B-Reading (bar)	P_0 (kPa)	p_1 (kPa)	p_2 (kPa)	$\Delta p = p_1-p_0$ (kPa)
0.305	1.7	4	80.61	240.32		159.7
0.61	1.4	3.2	52.73	159.20		106.5
0.914	1.1	2.8	22.82	118.64		95.82
1.219	1.4	3.3	52.22	169.34		117.1
1.524	2.2	4.1	133.34	250.46		117.1
1.829	2.3	5.1	138.92	351.86		212.9
2.134	3.3	7.3	234.23	574.94		340.7
2.438	4.6	9.7	360.48	818.30		457.8
2.743	5	7.8	412.70	625.64		212.9
3.048	4.3	6.8	343.24	524.24		181
3.353	4.7	7.8	380.76	625.64		244.9
3.658	5.3	9.2	437.54	767.60	-84.16	330.1
3.962	5.5	9.4	457.82	787.88	-84.16	330.1
4.267	5.7	9	481.14	747.32	-84.16	266.2
4.572	6	9.5	510.55	798.02	-84.16	287.5
4.877	6.7	9.9	583.05	838.58	-84.16	255.5
5.182	7.2	11	632.74	909.56	-84.16	276.8
5.486	6.8	10	591.67	879.14		287.5
5.791	7	9.6	616.51	808.16	-84.16	191.6
6.096	7.4	10	655.04	889.28	-84.16	234.2
6.401	8.3	11	746.81	970.40		223.6
6.706	10	16	903.47	1457.12		553.6
7.01	13	23	1229.98	2166.92		936.9
7.315	13	23	1229.98	2166.92		936.9
7.62	12	13	1166.10	1102.22		-63.88
7.925					-84.16	
8.23						
8.534						
8.839	11	17	981.55	1599.08		617.5
9.144	11	19	992.71	1801.88		809.2
9.449	11	20	990.68	1842.44	-84.16	851.8

(continued)

Depth (m)	Vertical Effective Stress (bar)	u_0 (bar)	Material Index I_d	Classification	Horizontal Stress Index K_d	Dilatometer Modulus E_d (MPa)	Pore Pressure Index U_d
0.305	0.0496	0	1.981	sand	16.035	5.542	
0.61	0.0992	0	2.019	sand	5.244	3.695	
0.914	0.1487	0	4.200	sand	1.513	3.325	
1.219	0.1983	0	2.243	sand	2.597	4.064	
1.524	0.2479	0	0.878	silty sand	5.305	4.064	
1.829	0.2975	0	1.533	n/a	4.605	7.389	
2.134	0.3471	0	1.455	sand	6.656	11.822	
2.438	0.3966	0	1.270	silty sand	8.963	15.886	
2.743	0.4462	0	0.516	sandy silt	9.121	7.389	
3.048	0.4958	0	0.527	sandy silt	6.827	6.281	
3.353	0.5159	0.0295	0.648	silt	7.221	8.497	
3.658	0.5360	0.0590	0.765	clayey silt	7.940	11.453	-0.2089
3.962	0.5561	0.0884	0.735	clayey silt	7.959	11.453	-0.2075
4.267	0.5763	0.1179	0.567	silty clay	8.030	9.236	-0.2049
4.572	0.5964	0.1474	0.580	silty clay	8.196	9.975	-0.2
4.877	0.6165	0.1769	0.452	clayey silt	9.040	8.867	-0.1807
5.182	0.6366	0.2064	0.452	clayey silt	9.478	9.606	-0.1718
5.486	0.6567	0.2358	0.506	silty clay	8.526	9.975	
5.791	0.6768	0.2653	0.325	silty clay	8.591	6.650	-0.1884
6.096	0.6970	0.2948	0.375	clayey silt	8.846	8.128	-0.1824
6.401	0.7171	0.3243	0.313	clayey silt	9.819	7.758	
6.706	0.7372	0.3537	0.638	sandy silt	11.607	19.211	
7.01	0.7573	0.3832	0.787	clayey silt	15.511	32.512	
7.315	0.7774	0.4127	0.789	clay	15.072	32.512	
7.62	0.7975	0.4422		clay	13.865		
7.925	0.8176	0.4717		silty clay			
8.23	0.8378	0.5011		silty clay			
8.534	0.8579	0.5306		silty clay			
8.839	0.8780	0.5601	0.668	clayey silt	10.387	21.428	
9.144	0.8981	0.5896	0.867	clayey silt	10.244	28.078	
9.449	0.9182	0.6191	0.918	clayey silt	9.966	29.556	-0.1584

CPT Tests No.1

Depth (m)	q_c (MPa)	f_s (kPa)	Pore Pressure (kPa)	R_f (%)	Depth (m)	q_c (MPa)	f_s (kPa)	Pore Pressure (kPa)	R_f (%)
0.05	2.12	27	-1.8	1.27	1.95	1.39	42.8	29.2	3.07
0.1	2.47	40.9	-2.6	1.66	2	1.37	34.4	36.9	2.50
0.15	2.56	60.6	-2.4	2.37	2.05	1.32	32.7	47.5	2.46
0.2	2.2	91.2	-1.1	4.15	2.1	1.41	46.3	58.9	3.26
0.25	1.59	117.4	-10.5	7.39	2.15	1.72	70.9	69.7	4.09
0.3	1.28	110.4	-25.5	8.66	2.2	2.12	90.3	62.9	4.23
0.35	1.18	97.9	-28.4	8.34	2.25	2.03	88.3	34.9	4.33
0.4	1.06	82.4	-24	7.81	2.3	2.12	71.9	35.5	3.38
0.45	0.94	70.3	-22.5	7.51	2.35	1.92	79.4	37.6	4.12
0.5	0.88	68	-21.1	7.76	2.4	2.35	80.9	35.8	3.43
0.55	0.84	63	-19.1	7.53	2.45	2.35	82.8	52.4	3.51
0.6	0.78	55.8	-16.9	7.18	2.5	2.7	96.6	66.7	3.56
0.65	0.74	49	-13.6	6.65	2.55	3.16	94.6	73.2	2.98
0.7	0.73	41.1	-11.9	5.65	2.6	2.38	77.8	163.8	3.22
0.75	0.83	33.8	-7.4	4.08	2.65	2.2	67.7	179.5	3.03
0.8	1.01	30.2	-7.2	2.99	2.7	2.2	66.4	186.5	2.97
0.85	0.82	18.8	-4.8	2.30	2.75	2.38	77.9	192.2	3.22
0.9	0.59	9.9	-3.8	1.68	2.8	2.26	74.9	191.9	3.26
0.95	0.46	10.8	36.6	2.31	2.85	1.76	64.3	178.3	3.58
1	0.44	14.2	2.9	3.22	2.9	1.43	50	182.4	3.41
1.05	0.46	13.6	11.4	2.94	2.95	1.46	40	190.4	2.67
1.1	0.52	14.9	16.4	2.85	3	1.49	35.8	190.1	2.34
1.15	0.55	15.4	20.7	2.78	3.05	1.46	37.4	196.6	2.49
1.2	0.56	21.5	26	3.80	3.1	1.47	36.6	196.9	2.42
1.25	0.73	20.4	29.9	2.77	3.15	1.51	37.9	196.4	2.45
1.3	0.76	20.2	5.2	2.65	3.2	1.43	35.7	201	2.43
1.35	0.52	20.6	-13.5	3.98	3.25	1.44	33.7	205.4	2.28
1.4	0.39	19.8	-12.5	5.11	3.3	1.46	35.5	113.5	2.39
1.45	0.43	16.3	-9.8	3.81	3.35	1.41	31.9	126	2.22
1.5	0.53	15.9	-5	3.01	3.4	1.53	32.1	159.2	2.06
1.55	0.71	27.9	-0.6	3.93	3.45	1.58	36.3	176.2	2.25
1.6	0.82	30.9	23.6	3.75	3.5	2.22	37.3	102.9	1.66
1.65	0.84	33.2	25.7	3.93	3.55	1.53	38	99.8	2.45
1.7	0.97	37.3	29.2	3.82	3.6	1.61	40	163.7	2.43
1.75	1	34.1	29.9	3.39	3.65	1.74	36.3	183.3	2.04
1.8	0.99	33.3	31	3.34	3.7	1.52	38.9	187.4	2.50
1.85	1.07	35.1	44.8	3.25	3.75	1.55	40.7	207.7	2.56
1.9	1.29	39.5	51.5	3.04	3.8	1.5	33.6	214.5	2.18

(continued)

Depth (m)	q_c (MPa)	f_s (kPa)	Pore Pressure (kPa)	R_f (%)	Depth (m)	q_c (MPa)	f_s (kPa)	Pore Pressure (kPa)	R_f (%)
3.85	1.45	38	212.1	2.55	5.85	1.75	33.1	674.5	1.76
3.9	1.49	31.6	221.3	2.06	5.9	1.65	29.4	706.2	1.64
3.95	1.46	36.2	225.3	2.41	5.95	1.75	32.8	723.1	1.73
4	1.5	38.4	231.4	2.48	6	1.78	33.5	686.4	1.75
4.05	1.55	41.4	241.9	2.59	6.05	1.84	34.5	640.4	1.75
4.1	1.63	40.6	239.7	2.42	6.1	1.71	30.5	601.4	1.67
4.15	1.63	34.6	243.9	2.06	6.15	1.61	31.1	588.2	1.80
4.2	1.47	32.6	249.2	2.14	6.2	1.69	26.3	636.1	1.45
4.25	1.44	35.8	261.6	2.40	6.25	1.87	31.5	638	1.58
4.3	1.53	31.9	286.2	2.01	6.3	1.97	28.6	200.9	1.42
4.35	1.46	33.2	302.1	2.18	6.35	1.84	30.3	226.1	1.61
4.4	1.51	29.6	326.1	1.88	6.4	1.96	36	263.7	1.79
4.45	1.47	31.4	356.1	2.04	6.45	1.96	35.3	213.7	1.76
4.5	1.5	29.4	381.7	1.87	6.5	2.02	34.5	257.4	1.67
4.55	1.47	32.9	417.9	2.12	6.55	2.13	41.6	294.5	1.90
4.6	1.59	32.4	588.8	1.90	6.6	2.64	56.9	603.4	2.06
4.65	1.57	31.8	594.2	1.88	6.65	2.96	62.7	595.2	2.04
4.7	1.62	32.3	602.7	1.86	6.7	3.21	65.2	605.9	1.96
4.75	1.62	32.9	582	1.89	6.75	3.65	92.3	592.6	2.45
4.8	1.65	36.3	588.2	2.05	6.8	3.82	119.7	276.2	3.09
4.85	1.66	32	588.2	1.80	6.85	4.01	149.5	261.5	3.68
4.9	1.64	34.9	585.6	1.99	6.9	4.27	141.3	229.3	3.27
4.95	1.77	36.6	388	1.98	6.95	3.58	133.7	-13.9	3.74
5	1.81	35.6	431.9	1.88	7	3.82	129.8	-8.7	3.40
5.05	1.85	32.8	476.7	1.69	7.05	4.33	150.9	-4.5	3.49
5.1	1.77	38.1	513.1	2.03	7.1	4.86	181	-1.2	3.72
5.15	1.99	40.7	198.4	2.01	7.15	4.35	174.7	0.7	4.02
5.2	1.89	36.3	335.9	1.85	7.2	4.4	188.4	3.6	4.28
5.25	1.98	41.2	382.6	2.00	7.25	4.78	204.1	5.3	4.27
5.3	2.04	41.3	428.6	1.94	7.3	5.77	212.8	-4.7	3.69
5.35	2.19	41.7	463.8	1.83	7.35	4.01	195.4	4.2	4.87
5.4	2.12	42.7	484.5	1.93	7.4	5.25	219.3	10.1	4.18
5.45	2.13	46	513.7	2.06	7.45	6.16	251.8	0.1	4.09
5.5	2.02	32.3	502.1	1.52	7.5	5.2	188.2	2	3.62
5.55	2.04	39.2	529.9	1.83	7.55	5.95	258.6	5.4	4.35
5.6	1.87	39.6	645	1.98	7.6	5.89	292	12.1	4.96
5.65	1.98	37.3	584.1	1.78	7.65	5.42	264.5	13.1	4.88
5.7	1.75	32	569.2	1.72	7.7	5.35	219	19.6	4.09
5.75	1.73	32.1	658.7	1.72	7.75	5.44	221.2	21.6	4.06
5.8	1.84	27.6	705.2	1.39	7.8	5.35	237.1	26	4.43

(continued)

Depth (m)	q_c (MPa)	f_s (kPa)	Pore Pressure (kPa)	R_f (%)	Depth (m)	q_c (MPa)	f_s (kPa)	Pore Pressure (kPa)	R_f (%)
7.85	4.98	209.6	24	4.20	9.15	3.85	291.5	-5.8	7.57
7.9	4.63	201.1	25.1	4.34	9.2	3.3	234.3	-7.3	7.10
7.95	4.92	199.7	29.3	4.05	9.25	3.73	253.4	-5.5	6.80
8	5.17	123	29.6	2.38	9.3	4.32	287.5	-5.4	6.66
8.05	5.43	319.1	35.9	5.87	9.35	3.61	259.2	-7.6	7.18
8.1	14.86	422.9	5.3	2.85	9.4	3.12	199.8	-5.4	6.41
8.15	21.31	312.8	65.3	1.47	9.45	3.15	180	-4.2	5.72
8.2	23.59	255.8	17.4	1.08	9.5	3.46	193.5	-4.3	5.59
8.25	14.67	195.8	-3.5	1.33	9.55	3.83	212.7	-2.9	5.55
8.3	7.96	182.2	-36.9	2.29	9.6	3.67	225.5	12.9	6.14
8.35	4.05	120.6	-17.1	2.98	9.65	3.84	265.9	14.9	6.92
8.4	2.75	75.2	-10.8	2.74	9.7	4.6	257.4	18.7	5.59
8.45	2.5	44.6	-3.7	1.78	9.75	4.08	243.5	14.9	5.96
8.5	2.81	66	19.1	2.35	9.8	3.71	209.1	18.9	5.63
8.55	2.56	115.5	28.1	4.50	9.85	3.66	186.2	20.5	5.08
8.6	2.56	129.9	92.1	5.04	9.9	4.1	182.2	25.4	4.44
8.65	2.4	133.5	-0.8	5.56	9.95	4.15	201.1	27.9	4.84
8.7	2.29	96.4	-0.2	4.21	10	4.02	265.8	29.2	6.60
8.75	2.2	100.4	0.8	4.56	10.05	7.51	345	12.8	4.59
8.8	2.05	114.3	1.1	5.58	10.1	5.96	352.6	-49.5	5.93
8.85	2.3	113.3	4.5	4.92	10.15	5.2	338.2	-52.8	6.52
8.9	2.55	141	6.2	5.53	10.2	6.04	343.4	-52.7	5.70
8.95	3.36	198	9.4	5.89	10.25	5.79	347.2	-51	6.01
9	4.5	343.4	10.7	7.63	10.3	5.74	347.2	-50.5	6.06
9.05	4.66	351	6.5	7.53	10.35	8.72	347.2	-48.1	3.99
9.1	5.52	362.3	9	6.56					

CPT Test No.2

Depth (m)	q_c (MPa)	f_s (kPa)	Pore Pressure (kPa)	R_f (%)	Depth (m)	q_c (MPa)	f_s (kPa)	Pore Pressure (kPa)	R_f (%)
0.05	0	-0.1	0.8	0.11	2.05	2.61	33.4	-3.4	1.28
0.1	0.2	0.9	0.1	0.45	2.1	3.62	31.1	-27.3	0.86
0.15	0.17	0.7	-0.2	0.41	2.15	3.7	49	-27.2	1.33
0.2	0.25	1.3	-1.1	0.52	2.2	2.55	46.8	-20.8	1.84
0.25	0.13	18.2	1.5	13.97	2.25	1.04	31.3	-16.5	3.02
0.3	0.92	36.7	0.6	3.99	2.3	0.93	21.8	-2.1	2.35
0.35	3.77	87.3	-1.6	2.32	2.35	1.3	29	14.4	2.23
0.4	4.68	149.9	-0.6	3.20	2.4	2.21	36.5	31.3	1.65
0.45	3.92	199.1	-7.6	5.08	2.45	3.26	54.7	-5	1.68
0.5	3.25	198.7	-6.9	6.12	2.5	4.12	70.7	-32.6	1.72
0.55	2.68	200.7	-6.6	7.49	2.55	6.07	97.5	-19	1.61
0.6	2.28	195.3	-33.9	8.59	2.6	5.52	103.2	-18.9	1.87
0.65	1.85	179.6	-28.5	9.74	2.65	4.81	101.3	-7.1	2.11
0.7	1.69	143.5	-24.7	8.52	2.7	5.25	126.8	-25.2	2.42
0.75	1.51	126.3	-20.2	8.39	2.75	4.78	169.9	-36.8	3.56
0.8	1.49	115.3	-25.9	7.77	2.8	8.41	137.3	-45.2	1.63
0.85	1.32	101.1	-20.3	7.68	2.85	11.48	61.3	-39.2	0.53
0.9	1.15	77.3	-20.5	6.75	2.9	13.29	88.7	-2.8	0.67
0.95	1.03	68.6	-13.6	6.68	2.95	11.95	148.9	2.7	1.25
1	0.98	62.5	-12.3	6.39	3	12.83	237	11.8	1.85
1.05	0.96	59.4	-7.2	6.20	3.05	14.52	257.1	12.8	1.77
1.1	0.95	58.1	-11.4	6.13	3.1	14.5	189.6	13.6	1.31
1.15	0.95	52.1	-5.6	5.49	3.15	14.05	161.8	15.9	1.15
1.2	0.91	48.1	-8.4	5.30	3.2	10.21	216	15.5	2.11
1.25	0.77	45.8	-8.9	5.96	3.25	5.38	179.9	22.6	3.34
1.3	1.09	31.6	-6.5	2.90	3.3	3.29	111.3	69	3.37
1.35	2.47	23.4	-9	0.95	3.35	2.87	71.1	92.3	2.46
1.4	2.79	16.6	-16.7	0.60	3.4	2.9	40.4	107.1	1.38
1.45	2.29	20.3	-18.1	0.89	3.45	2.93	45.5	123.2	1.54
1.5	1.89	19.7	-14.1	1.04	3.5	7.69	183.9	48	2.39
1.55	1.69	16.2	-11.5	0.96	3.55	9.82	264.6	-2.7	2.69
1.6	1.42	20.5	-9.7	1.45	3.6	7.66	250.8	-6.4	3.27
1.65	1.33	26.4	-15.3	1.99	3.65	4.37	161.7	30.8	3.70
1.7	1.16	32.4	-34.7	2.81	3.7	3.7	112.6	52.2	3.03
1.75	1.25	28.3	-30.2	2.27	3.75	3.23	101.9	61.9	3.14
1.8	1.39	34.5	-33.8	2.49	3.8	2.95	91.2	63.6	3.08
1.85	1.32	26.2	-18.3	1.99	3.85	2.53	84.5	61.3	3.32
1.9	1.64	22.5	-18.1	1.37	3.9	2.31	77.3	64.7	3.33
1.95	1.85	23.2	-9.1	1.26	3.95	2.21	64.5	81.6	2.90
2	1.61	23.1	-5.3	1.44	4	1.98	56.4	83.4	2.82

(continued)

Depth (m)	q_c (MPa)	f_s (kPa)	Pore Pressure (kPa)	R_f (%)	Depth (m)	q_c (MPa)	f_s (kPa)	Pore Pressure (kPa)	R_f (%)
4.05	1.96	49.6	90	2.51	6.05	1.78	42.2	413	2.27
4.1	1.95	48.6	98	2.47	6.1	1.64	26.2	425.9	1.52
4.15	1.95	44.4	100.3	2.25	6.15	1.65	21.7	444.4	1.25
4.2	1.73	45.5	104.3	2.60	6.2	1.49	43.3	452.5	2.74
4.25	1.85	37.8	111.5	2.02	6.25	3.42	36.7	454.5	1.05
4.3	1.96	44.9	115.1	2.26	6.3	1.88	44.3	148.5	2.32
4.35	2	42.2	122.4	2.08	6.35	2.02	32.4	158.6	1.58
4.4	2.09	48	122.9	2.27	6.4	2.01	28.5	177.2	1.39
4.45	2.05	54.8	130.1	2.64	6.45	1.98	24.9	188.7	1.23
4.5	2.15	65.3	87.6	3.01	6.5	2.06	29.7	208.3	1.41
4.55	2.15	62.5	93.2	2.88	6.55	2.32	29.1	225.1	1.23
4.6	2.13	52.2	100.3	2.43	6.6	2.36	30.5	242.6	1.27
4.65	2.03	46.1	101.6	2.25	6.65	2.45	54.3	250.4	2.17
4.7	2.07	51.3	111.4	2.45	6.7	2.93	64.4	284.3	2.16
4.75	2.28	47.5	116.5	2.06	6.75	2.91	65.4	271.4	2.21
4.8	2.26	49.4	118.9	2.16	6.8	2.73	62.8	279	2.25
4.85	2.2	56.1	126.3	2.52	6.85	2.78	62.1	286.9	2.19
4.9	2.28	64	134.3	2.77	6.9	2.92	79.1	294.6	2.66
4.95	2.62	66.1	273.7	2.47	6.95	3.4	96.5	305.5	2.79
5	2.34	58.2	285.5	2.43	7	3.56	116.1	318.1	3.20
5.05	2.36	54.8	416.2	2.24	7.05	4.16	125.4	201.4	2.99
5.1	2.23	48.6	425.9	2.10	7.1	3.97	139.5	76.7	3.50
5.15	2.22	51.7	444	2.24	7.15	3.83	146.2	63.8	3.80
5.2	2.23	47.7	447.7	2.06	7.2	4.12	166.6	64.3	4.03
5.25	2.31	47.7	479	1.98	7.25	4.46	179.5	45.6	4.02
5.3	2.32	52.2	505.8	2.16	7.3	4.28	178.4	45.2	4.16
5.35	2.32	47.9	504.9	1.98	7.35	3.72	165.3	32.1	4.44
5.4	2.16	42.1	470.3	1.87	7.4	3.49	150.9	22.5	4.32
5.45	1.91	35	526.4	1.74	7.45	3.55	147.5	24	4.15
5.5	1.8	29.3	545.2	1.53	7.5	3.29	160.5	13.9	4.87
5.55	1.83	34	572.9	1.75	7.55	3.2	152.7	17	4.77
5.6	1.92	29	608.3	1.42	7.6	3.04	152.6	17.4	5.01
5.65	1.93	30.7	612.4	1.50	7.65	2.97	155.4	15.4	5.23
5.7	1.86	35.4	639.9	1.78	7.7	2.98	157.2	19.2	5.27
5.75	1.96	40.3	627.3	1.93	7.75	2.77	127.1	18.4	4.58
5.8	2.11	43	590.9	1.93	7.8	2.76	176.1	15.6	6.37
5.85	1.94	-1.2	570.6	0.06	7.85	4.45	158.5	25	3.56
5.9	1.82	33.8	509.4	1.76	7.9	11.87	121.9	21.9	1.03
5.95	0.38	44.7	624.7	8.85	7.95	15.06	196.7	24.8	1.31
6	2.94	40.1	121.2	1.35	8	9.24	167.1	3.1	1.81

(continued)

Depth (m)	q_c (MPa)	f_s (kPa)	Pore Pressure (kPa)	R_f (%)	Depth (m)	q_c (MPa)	f_s (kPa)	Pore Pressure (kPa)	R_f (%)
8.05	7.55	177.1	8.3	2.35	8.15	27.05	177.1	48.7	0.65
8.1	13.05	177.1	22.1	1.36					

SPT Tests

SPT Test No.1

Sample	Depth (m)	C_R	SPT N (blows/ft)	SPT N_{60} (blows/ft)
1	0.76	0.75	5	4
2	1.52	0.75	2	2
3	2.29	0.75	13	10
5	3.81	0.75	19	14
6	4.57	0.85	11	9
7	5.33	0.85	12	10
8	6.10	0.95	14	13
9	6.86	0.95	17	16
10	7.62	0.95	17	16

SPT Test No.2

Sample	Depth (m)	C_R	SPT N (blows/ft)	SPT N_{60} (blows/ft)
1	0.76	0.75	13	10
2	1.52	0.75	9	7
3	2.29	0.75	13	10
4	3.05	0.75	22	17
5	3.81	0.75	22	17
6	4.57	0.85	27	23
7	5.33	0.85	19	16

SPT Test No.3

Sample	Depth (m)	C_R	SPT N (blows/ft)	SPT N_{60} (blows/ft)
1	0.76	0.75	6	5
2	1.52	0.75	6	5
3	2.29	0.75	11	8
4	3.05	0.75	17	13
5	3.81	0.75	11	8
6	4.57	0.85	11	9
7	5.33	0.85	10	9
8	6.10	0.95	8	8
9	6.86	0.95	11	10
10	7.62	0.95	17	16

SPT Test No.4

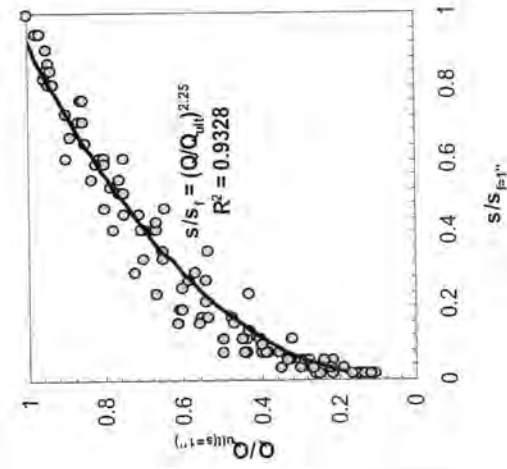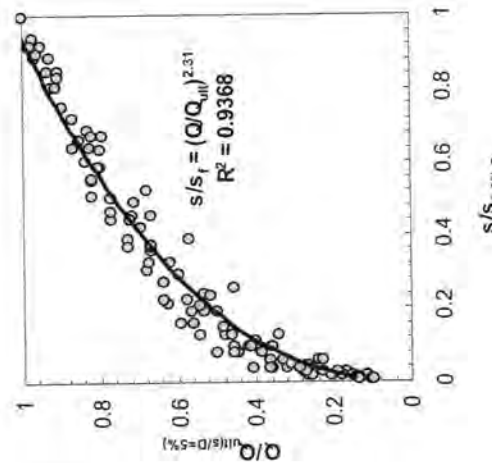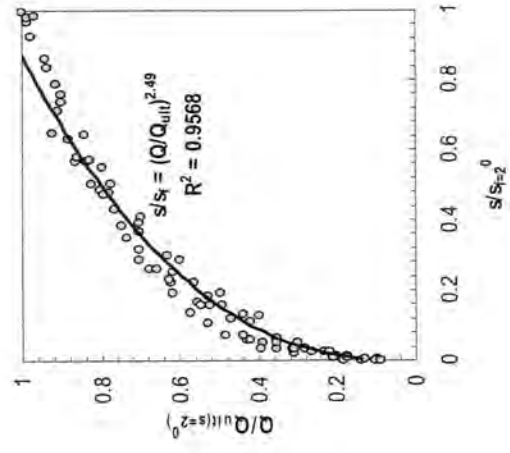| Sample	Depth (m)	C_R	SPT N (blows/ft)	SPT N_{60} (blows/ft)
1	0.76	0.75	8	6
2	1.52	0.75	6	5
3	2.29	0.75	6	5
4	3.05	0.75	20	15
5	3.81	0.75	13	10
6	4.57	0.85	16	14
7	5.33	0.85	12	10
8	6.10	0.95	17	16
9	6.86	0.95	15	14
10	7.62	0.95	33	31
11	8.38	0.95	16	15

Torvane and Pocket Penetrometer Tests No.1

Sample	Depth (ft)		Midpoint (ft)	Midpoint (m)	Torvane s_u (kg/cm^2)	Torvane s_u (kPa)	Pocket Penetrometer q_u (kg/cm^2)	Pocket Penetrometer q_u (kPa)
1	1.5	3.5	2.5	0.76	0.15	14.7	0	0.0
2	4	6	5	1.52	0.25	24.5	0	0.0
3	6.5	8.5	7.5	2.29	0.45	44.1	1.5	147.1
4	9	11	10	3.05	0.65	63.7	1.5	147.1
5	12	14	13	3.96	0.75	73.5	1	98.1
6	15	17	16	4.88	0.975	95.6	1.5	147.1
7	19	21	20	6.10	NA	NA	NA	NA
8	23	25	24	7.32	1	98.1	5.5	539.4

Torvane and Pocket Penetrometer Tests No.2

Sample	Depth (ft)		Midpoint (ft)	Midpoint (m)	Torvane s_u (kg/cm^2)	Torvane s_u (kPa)	Pocket Penetrometer q_u (kg/cm^2)	Pocket Penetrometer q_u (kPa)
1	1.5	3.5	2.5	0.76	0.575	56.4	0.6	58.8
2	4	6	5	1.52	0.55	53.9	0.25	24.5
3	6.5	8.5	7.5	2.29	0.3	29.4	4.5	441.3
4	9	11	10	3.05	0.6	58.8	2.5	245.2
5	12	14	13	3.96	0.875	85.8	4	392.3
6	15	17	16	4.88	0.75	73.5	2.25	220.6
8	23	25	24	7.32	1.0	98.1	--	--
10	29	31	30	9.14	0.625	61.3	0.75	73.5

Appendix C: Field Lateral Load Tests Normalized Load-Displacement Results

$s/s_f = (Q/Q_{ult})^{2.49}$

$R^2 = 0.9568$

ACKNOWLEDGEMENTS